

Optical Behaviour of Selected XBLs

PhD Thesis

of

Bidzina Kapanadze

Submitted to the Dissertation Council of Ilia State University
in Partial Fulfillment of the Requirements for the Degree of

Doctor of Physics

Supervisor: Professor Giorgi Javakhishvili

Ilia State University,
School of Graduate Studies,
Tbilisi, Georgia

December 21, 2009

Contents

Abstract	8
1 Introduction	10
1.1 Active galactic nuclei	10
1.2 Blazar Population	11
1.3 Blazar Structure	13
1.3.1 Blazar Model	13
1.3.2 Blazar Jets	14
1.3.3 Jet Magnetic Fields	17
1.3.4 Blazar Accretion Discs	18
1.4 Blazar Emission Mechanisms	20
1.5 Blazar Variability	23
1.5.1 Variability Patterns	23
1.5.2 Shock Waves in Blazar Jets	25
1.5.3 Quasi-periodical flares in blazars	29
1.6 Motivation and Objectives	30
2 Observational Background	34
2.1 X-ray Observations	34
2.2 Optical Observations	37
2.3 Radio Observations	43
2.4 Infrared Observations	45
2.5 Gamma-ray observations	46
3 Observations and Data Reduction	49
3.1 Observational Conditions and Telescope	49
3.2 Devices	49
3.3 Observations	52
3.4 Image Processing	53
3.5 Variability Investigation	58
4 Results	68
4.1 1ES 0229+200	68
4.2 1ES 0323+022	71
4.3 1ES 0414+009	76

4.4	1ES 0502+675.....	80
4.5	1ES 0647+250	85
4.6	1ES 0806+524	88
4.7	1ES 1028+511	92
4.8	1ES 1426+428	96
4.9	1ES 1517+6	100
4.10	1ES 1959+650	104
4.11	1ES 2344+514	114
5	Summary and Future Investigations	119
5.1	Long-term Variability	119
5.2	Short-term Bursts	123
5.3	Intra-day Variability	125
5.4	Microvariability	126
	Bibliography	128
	Acknowledgements	135
Appendix A	Charts and Comparison Stars	136
A1	1ES 0229+200	136
A2	1ES 0323+022	137
A3	1ES 0414+009	138
A4	1ES 0502+675.....	139
A5	1ES 0647+250	140
A6	1ES 0806+524	141
A7	1ES 1028+511	142
A8	1ES 1426+428	143
A9	1ES 1517+656.....	144
A10	1ES 1959+650	145
A11	1ES 2344+514	146
Appendix B	Observational Data	147
B1	<i>R</i> band Data of 1ES 0229+200.....	147
B2.1	<i>R</i> band Data of 1ES 0323+022.....	150
B2.2	Color Indices of 1ES 0323+022 derived from Abastumani and Torino observations	154
B2.3	Color Indices of 1ES 0323+022 derived from Jannuzi et al. (1993) observations	155
B3.1	<i>R</i> band Data of 1ES 0414+009	156

B3.2	Color Indices of 1ES 0414+009	159
B4.1	<i>R</i> band Data of 1ES 0502+675	160
B4.2	Color Indices of 1ES 0502+675	166
B5.1	<i>R</i> band Data of 1ES 0647+250	167
B5.2	Color Indices of 1ES 0647+250	170
B6.1	<i>R</i> band Data of 1ES 0806+524	171
B6.2	Color Indices of 1ES 0806+524	179
B7.1	<i>R</i> band Data of 1ES 1028+511	180
B7.2	Color Indices of 1ES 1028+511	186
B8	<i>R</i> band Data of 1ES 1426+428	187
B9.1	<i>R</i> band Data of 1ES 1517+656	194
B9.2	Color Indices of 1ES 1517+656	198
B10.1	<i>R</i> band Data of 1ES 1959+650	199
B10.2	Color Indices of 1ES 1959+650	246
B11.1	<i>R</i> band Data of 1ES 2344+514	248
B11.2	Color Indices of 1ES 2344+514	261

List of Tables

Table 1.1	List of target objects.....	31
Table 2.2	characteristics of host galaxies of the sample	41
Table 3.1	CCD <i>ST-6</i> characteristics.....	50
Table 3.2	CCD <i>APOGEE6</i> specifications.....	51
Table 4.1	Short-term busts in 1ES 0229+200.....	70
Table 4.2	Intraday changes in 1ES 0229+200.....	70
Table 4.3	Short-term busts in 1ES 0323+022.....	75
Table 4.4	Intraday changes in 1ES 0323+022.....	75
Table 4.5	Long-term variability in 1ES 0414+009.....	78
Table 4.6	Short-term busts in 1ES 0414+009.....	80
Table 4.7	Intraday changes in 1ES 0414+009.....	80
Table 4.8	Long-term variability in 1ES 0502+675.....	82
Table 4.9	Short-term bursts in 1ES 0502+675.....	84
Table 4.10	Intraday changes in 1ES 0502+675.....	85
Table 4.11	Long-term variability in 1ES 0647+250.....	87
Table 4.12	Long-term variability in 1ES 0806+524.....	89
Table 4.13	Short-term bursts in 1ES 0806+524.....	91
Table 4.14	Intraday changes in 1ES 0806+524.....	91
Table 4.15	Long-term variability in 1ES 1028+511.....	93
Table 4.16	Short-term busts in 1ES 1028+511.....	95
Table 4.17	Intraday changes in 1ES 1028+511.....	96
Table 4.18	Long-term variability in 1ES 1426+428.....	98
Table 4.19	Short-term busts in 1ES 1426+428.....	99
Table 4.20	Long-term variability in 1ES 1517+656.....	101
Table 4.21	Short-term bursts in 1ES 1517+656.....	102
Table 4.22	Intraday changes in 1ES 1517+656.....	103
Table 4.23	Long-term variability in 1ES 1959+650	107
Table 4.24	Short-term bursts in 1ES 1959+650.....	109
Table 4.25	Intraday changes in 1ES 1959+650.....	110
Table 4.26	Results of intranight optical observations for 1ES 1959+650.....	112
Table 4.27	Short-term bursts in 1ES 2344+514.....	117
Table 4.28	Intraday changes in 1ES 2344+514.....	117
Table 4.29	Results of intranight optical observations for 1ES 2344+514.....	118
Table 5.1	Summary of long-term variations.....	119
Table 5.2	Summary of short-term bursts.....	123
Table 5.3	Summary of intraday changes.....	126

List of Figures

Figure 1.1	Blazar sketch	13
Figure 1.2	Spine+sheath geometry in blazar jet	16
Figure 1.3	Sketch of helical jet	18
Figure 1.4	M87 CXO image with 8 GHz contours	26
Figure 1.5	Sketch of a shock in relativistic jet	27
Figure 2.1	Optical spectrum of 1ES 1959+650	39
Figure 2.2	Image and de Vaucleurs profile of the host galaxy of 1ES 2344+514 obtained by <i>HST</i>	41
Figure 3.1	Spectral response curve of <i>ST-6</i> camera	49
Figure 3.2	Spectral Response curve APOGEE6 camera	52
Figure 3.3	Skech of ideal structure Function	63
Figure 4.1	Historical <i>R</i> band light-curves of 1ES 0229+200	69
Figure 4.2	Short-term busts in 1ES 0229+200	69
Figure 4.3	Historical <i>R</i> band light-curves of 1ES 0323+022	71
Figure 4.4	Structure function of 1ES 0323+022	72
Figure 4.5	<i>V</i> band light curve constructed on basis of Jannuzzi et al. (1993) data...	72
Figure 4.6	<i>V-R</i> values for 1ES 0323+022	73
Figure 4.7	Colour indices of 1ES 0323+022 derived from Jannuzzi et al. (1993)....	74
Figure 4.8	<i>B-R</i> values of 1ES 0323+022 derived from Villata et al. (2000)	74
Figure 4.9	Short-term bursts in 1ES 0323+022	74
Figure 4.10	Example of intarnight optical observations of Bai et al. (1998).	76
Figure 4.11	Historical <i>R</i> band light-curves of 1ES 0414+009	77
Figure 4.12	Structure function of 1ES 0414+009	78
Figure 4.13	<i>V-R</i> values for 1ES 0414+009	78
Figure 4.14	Short-term bursts in 1ES 0414+009	79
Figure 4.15	Historical <i>R</i> band light curves of 1ES 0502+675	81
Figure 4.16	Structure function of 1ES 0502+675	83
Figure 4.17	<i>V-R</i> values for 1ES 0502+675	83
Figure 4.18	Short-term bursts in 1ES 502+675	83
Figure 4.19	Example of intraday changes in 1ES 0502+675	85
Figure 4.20	Historical <i>R</i> band light-curves of 1ES 0647+250	86
Figure 4.21	Two-peak maximum in the historical light curve of 1ES 0647+250	87
Figure 4.22	Figure 4.23: <i>V-R</i> values for 1ES 0647+250	87
Figure 4.23	Historical <i>R</i> band light-curves of 1ES 0806+524	88
Figure 4.24	Structure function of 1ES 0806+524	90
Figure 4.25	<i>V-R</i> values for 1ES 0806+524	90

Figure 4.26	Short-term bursts in 1ES 0806+524	90
Figure 4.27	Example of Intranight R band light curve of 1ES 0806+524	92
Figure 4.28	Historical <i>R</i> band light curve of 1ES 1028+511	93
Figure 4.29	Structure function of 1ES 1028+511	94
Figure 4.30	<i>V-R</i> values for 1ES 1028+511	95
Figure 4.31	Short-term bursts in 1ES 1028+511	95
Figure 4.32	Intranight R band light curve of 1ES 0806+524	96
Figure 4.33	Reference stars in the field of 1ES 1426+428	97
Figure 4.34	Historical <i>R</i> band light-curves of 1ES 1426+428	97
Figure 4.35	Structure function of 1ES 1426+428	99
Figure 4.36	Short-term bursts in 1ES 1426+428	99
Figure 4.37	Intranight R band light curve of 1ES 1426+428	100
Figure 4.38	Historical <i>R</i> band light curve of 1ES 1517+656	101
Figure 4.39	<i>V-R</i> values for 1ES 1517+656	102
Figure 4.40	Short-term bursts in 1ES 1517+656	102
Figure 4.41	Example of intraday changes in 1ES 1517+656	104
Figure 4.42	Intranight R band light curve of 1517+656	104
Figure 4.43	Historical <i>R</i> band light-curves of 1ES 1959+650	105
Figure 4.44	Two-peak maximum in the historical light curve of 1ES 1959+650 ...	108
Figure 4.45	Structure function of 1ES 1959+650	108
Figure 4.46	<i>V-R</i> values for 1ES 1959+650	108
Figure 4.47	<i>B-R</i> values for 1ES 1959+650	108
Figure 4.48	Short-term bursts in 1ES 1959+650	108
Figure 4.49	Examples of intraday changes in 1ES 1959+650	111
Figure 4.50	Intranight observations of 1ES 1959+650 during two different nights ...	113
Figure 4.51	Historical <i>R</i> band light-curves of 1ES 2344+514	115
Figure 4.52	Structure function of 1ES 2344+514	116
Figure 4.53	<i>V-R</i> values for 1ES 2344+514	116
Figure 4.54	Short-term bursts in 1ES 2344+514	116
Figure 4.55	Intranight behaviour of 1ES 2344+514	118
Figure 5.1	Correlation of characteristic timescales with redshifts	121
Figure 5.2	Correlation of overall variabilities with redshifts	121
Figure 5.3	Distributions of the slopes during flares and decays	122
Figure 5.4	Distributions of burst slopes during brightenings and decays	124
Figure 5.5	Statistics of burst amplitudes.....	125
Figure 5.6	Statistics of intraday flux changes during increases and decays.....	127

Abstract

Within the framework of this thesis, the optical behavior of eleven of X-ray selected blazars (XBLs) from the catalogue *Eisntein Slew Survey* (1ES 0229+200, 0323+022, 0414+009, 0502+675, 0647+250, 0806+524, 1028+511, 1426+428, 1517+656, 1959+650, 2344+511) is investigated. The research is mainly based on the observations performed at Georgian National Astrophysical Observatory (Abastumani, Georgia). In addition, the data from different publications and databases are also included.

As one of the most extreme active galactic nuclei (AGN) classes, blazars are prominent with their violent variability across the whole electromagnetic spectrum. This feature provides the scientists with a very effective tool to study blazar structure and sources of tremendous energies governed by the most powerful processes. To achieve this goal, blazars have been the targets of numerous ground- and satellite-based observations, and developing theoretical simulations. Along with other spectral bands, optical domain plays a very important role in understanding of blazar physics. In order to draw a statistical picture of blazar optical variability, we have to study the behavior of great number of these sources over different timescales. Despite the great progress in this regard, we are far from having a complete picture of blazar variability, especially for XBLs which remain as the least investigated objects among blazars in optical diapason.

Targeted on the research of optically less investigated sources, current thesis can put some contribution in understanding of the blazar phenomenon. We begin with Chapter 1 where the basics of blazar astrophysics are briefly presented. Here, blazar features and theoretical models, constructed to explain them, are briefly discussed. Along with the solved problems, it is pointed at the remained challenges. Finally, thesis motivation and objectives are presented. Chapter 2 comprises the history of the investigation of target objects. It is presented separately for different spectral diapasons and the observational campaigns are described in a chronological manner. Great number of ground- and satellite-based experiments clearly shows the importance of the target objects in developing our knowledge about active galactic nuclei.

Due the fact that the work carries mainly an experimental character, I have devoted a separate chapter (Chapter 3) to the description of observational technique, data processing and variability investigation methods applied during the research. Target charts and comparison stars are provided in Appendix A.

Detailed description of the obtained results comprising optical behavior of selected XBLs at different timescales (historical lightcurves, variability character, amplitudes, characteristic timescales, duty cycles, colour indices, correlation with brightness states etc.) is provided in Chapter 4. The results are presented by turns from long-term down to intranight timescales separately for each target object. Respective plots and tables are also

included. Long tables, comprising the monitoring data (observation time in Julian days, source brightness in stellar magnitudes and linear fluxes - corrected/non-corrected on host contribution and galactic absorption, observational uncertainties, differences between comparison stars in stellar magnitudes, colour indices) are provided for each source in Appendix B.

Optical behavior of target objects are summarized and statistically investigated separately for each kind of the timescale (long-term variability, short-term bursts, intraday and intranight behaviour) in Chapter 5. The existence of the correlation between variability patterns of the sample are examined. I have made also some conclusions concerning the mechanisms responsible for obtained results. In addition, the objectives for future investigations, based on the performed research, are also presented.

1 Introduction

In order a reader could understand the importance of current work, I give a brief description of blazar features and the challenges related to them. At the end of the chapter, the thesis motivation and objectives are presented.

1.1 Active Galactic Nuclei

Active galactic nuclei attracted considerable attention about 45 years ago in spite of the fact that the first AGN-related phenomena, although not recognized as such, were reported as early as 1908 (Fath 1908) and in the following decades, when observers discovered bright emission lines from nuclei of several galaxies (Slipher 1917, Humason 1932, Mayall 1934), and the first extragalactic jet in M87 was observed (Curtis 1918). The first systematic study of these objects was performed by Seyfert (Seyfert 1943) noticing that emission lines from the nuclei of six galaxies were unusually broadened (several 1000 km s^{-1}), but he suggested that this phenomenon was probably correlated with the physical properties of the nucleus, without any further interpretation.

In the 1950s and 1960s, the first radio sky surveys were completed and catalogues, like the Third Cambridge Catalogue, were published. In 1963, Schmidt (1963) recognized that the quasi-stellar object 3C 273 has a redshift of almost 0.16, it became immediately clear that it was an extragalactic object. Because it has had a stellar-like appearance at optical wavelengths, the source was named 3C273 and other objects of its class were named quasars (from Quasi-Stellar Objects or QSOs). At that time 3C273 was peculiar due to the fact that it emitted 100 times more light than a typical galaxy. It was suggested that extragalactic radio sources were mainly driven by gas accreted into a disc around super-massive black holes (Zeldovich 1964, Salpeter 1964, Lynden-Bell 1969).

A big step in the investigation of QSOs was made by developing of the aperture synthesis technique in 1970s. Very Long Baseline Interferometry (VLBI) allowed the astronomers to observe quasars at a resolution of several tenths of an arcsecond. These observations showed that the radio emission of quasars is often dominated by jet-like structures, connecting the central compact source with external structures (“radio lobes”), which are sometimes located at very large distances (of megaparsecs order) from the quasar.

Later, Blandford & Königl (1979) proposed that the radio emission from AGN is produced by a relativistic outflow of plasma along magnetic field lines. Their model, with numerous modifications, is still viable.

Currently, we know that quasars form one of the active galactic nuclei classes (along with Seyfert galaxies, blazars, radio galaxies). AGNs are characterized by the presence of the central compact region (with a size of the order of a parsec) emitting tremendous amounts of energy with a luminosity which, in many cases, exceeds the luminosity of a typical galaxy by a factor of 10^4 .

1.2. Blazar Population

Blazars are the most extreme class of Active Galactic Nuclei. The term “Blazar” was introduced three decades ago by Ed Speigel in order to denote the objects which are notable with following characteristics (Fan 2000):

1. strong radio sources;
2. smooth spectra (featureless or with very weak lines (equivalent width $\text{EW} < 5 \text{\AA}$) except for the occasional presence of strong quasar emission lines;
3. violent variability in all spectral diapasons;
4. strong and variable polarization especially in the optical range;

Blazars are identified as BL Lacertae objects and Flat Spectrum Radio Quasars (FSRQs). On their turn, FSRQs consist of (Fan 2005):

- optically violently variable quasars (OVVs) displaying variation amplitude of greater than 1.0 magnitude, have steep optical spectra and are associated with compact variable radio sources which have flat radio spectra at GHz frequencies;
- Highly polarized quasars (HPQs) have optical polarization more than 3% (Moore and Stockman 1981).
- Core dominated quasars (CDQs), which show ratio of the radio emissions from the core component to from the extended component being greater than unity ($L_{\text{core}}/L_{\text{ext}} > 1.0$).
- Superluminal motion sources (SMs) exhibiting the velocity of the radio-component leaving its parent component being greater than the speed of light (the prototype is 3C 279).

Broadband energy distribution of blazars are usually presented by means of spectral energy distribution (SED) plot (i.e. $\log \nu F_\nu$ values plotted versus $\log \nu$). It consists of two distinct, broad components: A low-energy component from radio through UV or X-rays, and a high-energy component from X-rays to γ -rays (Böttcher 2007).

Depending on the position of low-energy peak, one divides BL Lacertae objects into Radio selected BL Lacs (RBLs) and X – ray selected ones (XBLs) (Giommi, Ansari & Micol

1995). LBLs are intermediate between the FSRQs, which have much higher bolometric luminosities, and the XBLs, which are the least luminous among the blazars. The peak of their low-frequency component is located at *IR* or optical wavelengths, while high-frequency component peaks at several GeV, and the γ -ray output is of the order of or slightly higher than the level of the low-frequency emission. In the case of XBLs, these peaks occur at relatively higher UV/X-ray and GeV/TeV bands (Böttcher 2007).

The other criterion for BL Lacertae division is based on their X-ray (F_X) to radio flux (F_R) ratio. According to Wurtz (1994), an object may be called as “XBL-like” if

$$\log\left(\frac{F_X}{F_R}\right) \geq -5.5 \quad (1.1)$$

and “RBL-like”, otherwise, where the X-ray flux density has been taken at 1 keV and the radio flux density at 5 GHz (in Jy). Giommi & Padovani (1994) used, instead, the ratio of the flux in the 0.3-3.5 keV *Einstein* band (in cgs units) to the monochromatic flux at 5 GHz (in Jy). In that case, the dividing line between XBLs and RBLs is at

$$\log\left(\frac{F_X}{F_R}\right) = -11.3 \quad (1.2)$$

Nevertheless, these two methods are equivalent in practice (see Perlmann et al. 1996).

XBLs and RBLs have different $\alpha_{RO} - \alpha_{OX}$ spectral indices XBLs have a broad-band spectral index $\alpha_{RX} \leq 0.75$ and LBLs have $\alpha_{RX} > 0.75$, i.e. HBLs have flatter spectra relative to RBLs, Fan 1999) and possibly show different cosmological evolution (Morris et al. 1991). Additionally, XBLs seem to have weaker radio cores and extended emission and are less core dominated (Perlman & Stocke 1993). The averaged polarisation of XBLs (<5%) is lower than that of LBLs (>10%) (Fan 1999);

On the other hand, no differences have been found among the properties of their host galaxies (Wurtz et al., 1996) and their cluster environment at redshifts below $z = 0.65$ (Wurtz et al. 1997). Note that many BL Lacs have been found with intermediate types of SEDs (Wiita 2007). Ghisellini et al. (1993) proposed that XBLs and RBLs are intrinsically the same objects differing mainly by their average viewing angle of their jets to the observer (< 30° for XBLs and < 15° for RBLs).

Sambruna et al. (1996) studied the multifrequency spectral properties of BL Lac objects and explained the differences between XBLs and RBLs by a systematic change of the intrinsic physical parameters of the jet such that XBLs have higher magnetic fields/electron energies and smaller jet sizes than radio selected ones. Brinkmann et al. (1996) proposed that XBLs and RBLs are intrinsically different and either originate from different populations or have emission conditions with different physical parameters (e.g. accelerating jets in RBL and decelerating jets in XBLs or the later are intrinsically less beamed BL Lac objects).

It is notable that the bulk of the TeV emitting BL Lac sources belong to the XBLs (see e. g. Wagner 2008). If the blazar γ -ray emission is due to inverse Compton scattering, this fact confirms that the electron population in XBLs is dominated by higher Lorentz factors than in the case of radio-selected BL Lacertae objects.

Padovani & Giommi (1995) introduced an alternate classification scheme for BL Lacs. Namely, the so-called LBLs (low-energy sampled BL Lacs) and HBLs (high-energy sampled BL Lacs). Currently, both classification schemes are in use.

1.3 Blazar Structure

1.3.1 Blazar Model

Blazars are considered to be active galactic nuclei of bright ($M_R \sim -23.1$), large ($r_e \sim 7$ kpc) and fairly round ($\epsilon = 0.1-0.3$) elliptical galaxies (e.g. Scarpa et al. 2000, Nilsson et al. 2007), whose bulk properties do not differ significantly from the population of inactive giant ellipticals. It's generally accepted that one of blazar jet is pointed towards to the observer, so, in fact, we are able to observe only its nonthermal emission (see Fig. 1.1). The central engine is assumed to be a supergiant black hole with masses $\sim 10^7-10^8 M_\odot$ (e.g. Falomo et al. 2002). Relativistically hot, magnetized plasma, collimated into the jets, should flow outward with speeds up to at least $0.995c$ (Marscher 1996). Presumably, an oppositely directed jet should emanate from blazar nucleus, but it's invisible for us.

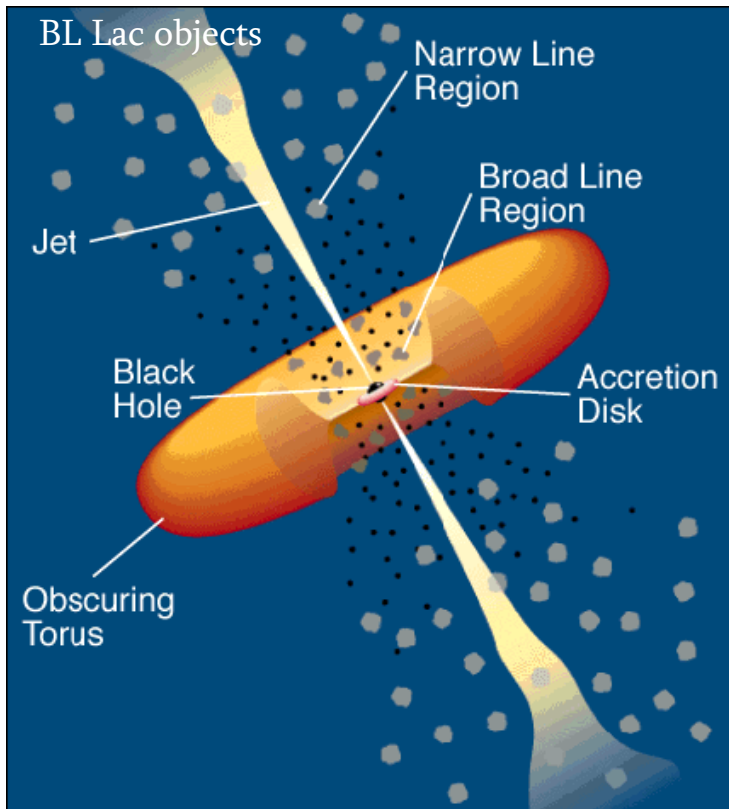


Figure 1.1: Blazar sketch (Sbarufatti 2003).

It is generally accepted that the blazar phenomenon is due to the anisotropic boosting of the radiation along jet direction which gives rise to an apparent enhanced luminosity at all wavelengths if the observer is located close to the direction of motion.

A distant observer measures an apparent transverse velocity

$$V_{obs} = \beta_{app} C \quad (1.3)$$

for any feature moving with a space velocity $V = \beta C$ at an angle θ to the line of sight towards the observer and

$$\beta_{app} = \frac{\beta \sin \theta}{1 - \beta \cos \theta} \quad (1.4)$$

(Blandford & Konigl 1979). This relation has a maximum

$$\beta_{app}^{max} = \Gamma \beta \quad (1.5)$$

for $\cos \theta = \beta$. Here,

$$\Gamma = \frac{1}{\sqrt{1 - \beta^2}} \quad (1.6)$$

is the Lorentz factor. Hence, $\beta_{app}^{max} > 1$ for $\beta > 0.5$. Consequently, the apparent transverse velocity becomes superluminal for large jet velocities (i.e., β close to 1) and sufficiently small θ angles. Let's define the Doppler factor as

$$\delta = \frac{1}{\Gamma(1 - \beta \cos \theta)} \quad (1.7)$$

Then the observed flux ($F_{\nu,obs}$) is apparently enhanced as follows (Marscher & Gear 1985)

$$F_{\nu,obs} = \delta^3 F_{\nu,em} \quad (1.8)$$

Thus, blazar fluxes and bulk velocities measured by the observer should be greatly boosted due to relativistic effects.

1.3.2 Blazar Jets

Even nowadays, no consensus has been achieved concerning the fundamental attributes of blazar jets such as their composition, formation, and collimation.

Just a few data about relativistic jets (LeVeque et al. 1997): a supersonic pressure-matched light jets consist of a supersonic beam of nearly constant diameter, which stays well collimated due to the presence of internal oblique shock waves and of plane and centered rarefaction waves. The beam ends in a contact discontinuity called the working surface, which separates ambient gas shocked by a leading bow shock from beam gas decelerated to the speed of the contact discontinuity by a trailing terminal shock configuration called a Mach disk. The Mach disk, the contact discontinuity and the intermediate beam cap gas form the head of the jet. The propagation speed of the working surface determines the velocity of the jet, i.e., its advance through the ambient medium. The jet velocity should not be

confused with the actual velocity of the material in the beam which is referred to as the beam flow velocity.

Part of the shocked, high pressure beam cap gas is deflected sideways and flows backward along the beam, feeding the cocoon. The deflection process involves the repeated formation of a strong vortex at the jet head, which is then shed off the beam cap and becomes part of the backflow in the cocoon. Simultaneously, a new vortex is generated. The backflow in the cocoon is supersonic except for the regions between the vortices. At the cocoon boundary the subsonic shear flow gives rise to Kelvin-Helmholtz instabilities, which eventually lead to a turbulent cocoon (LeVeque et al. 1997)

The beam should be confined by the pressure of the cocoon and the shocked ambient gas. However, the surface of the beam is not stable. According to Mizuta et al. (2004), oblique shocks appear within the beam, when the beam expands in lateral directions. This re-establishes pressure equilibrium between the beam and its surroundings and keeps it confined. When the beam is pinched for some reason, the gas tends to expand because of increased pressure caused by the compression. If the pressure outside is high enough to confine the beam, an oblique shock appears to prevent it from expansion.

Note that the only possibility to observe relativistic motions direct is given at radio wavelengths when motion close to the line of sight produces an apparent superluminal motion. High resolution interferometric radio images are able to measure such motions which are typically less than one milliarcsecond per year (Kellerman et al. 2003). This observations revealed one of the greatest challenges of blazar astrophysics – the crisis of Lorentz factor.

There is growing evidence from VLBI studies that pc scale jets in strong TeV BL Lacs move slowly (Edwards & Piner 2002; Giroletti et al. 2004). On the contrary, the bright and rapidly variable TeV emission implies that at the place where this emission originates, the jet should be highly relativistic. This is necessary to avoid the absorption of TeV photons by the IR radiation produced cospatially with the TeV emission (Ghisellini et al., 2005).

In order to reconcile very high Lorentz bulk factor needed for the observed TeV emission with the low ones observed for VLBI knots, Georganopoulos & Kazanas (2003) proposed that ultra-relativistic electrons with power law distribution are injected at the jet base that decelerates with the time because of radiatively cooling. The photons of highest frequencies originate via SSC mechanism preferentially near the jet base (~ 0.1 pc from jet apex) where the electrons are more energetic and the bulk Lorentz factor is greatest. As both the flow velocity and electron energy drop with distance (i.e. decreasing Γ), the emitted synchrotron spectrum shifts to lower energies (so-called “Stratified Jet Model”).

Gopal-Krishna et al. (2004) proposed another way to reconcile the very high bulk Lorentz factors needed for IC radiation with the low β_{app} seen in TeV blazar jets. Instead of assuming that the jets are cylindrical as was done in all previous models, they assumed that

jets should have small opening angles, ω (so-called “conical jet”). In that case the apparent transverse speeds peak at lower values and at significantly higher θ than for cylindrical jets.

Another explanation for above mentioned difference is following: blazar jets should consist of an ultra-fast “spine,” perhaps composed of electron-positrons pairs, surrounded by a slower (but still relativistic) “sheath” containing normal matter (e.g. Ghisellini et al. 2005). Laing & Bridle (2004) assume a gradual decline of flow velocity from the jet center to the outer parts of the jet: i.e. many layers with different velocities. Radio observations of transversely resolved jets (e.g. Swain, Bridle & Baum 1998), in fact, indicate a velocity gradient across the jet. Ghisellini et al. (2005) found that lateral velocity structure in compact jets would allow less extreme physical parameters to be used for explaining the rapid high-energy variability of TeV BL Lac objects. The spine gives rise to the γ -ray emission via IC while the sheath produce the radio knot emission.

Ghisellini et al. (2005) proposed that this structure exists even on the spatial scale of regions responsible for the gamma-ray emission. One component sees the (beamed) radiation produced by the other, and this enhances the inverse Compton emission of both components. In addition, this allows the magnetic field to be nearly in equipartition with the emitting particles. The inverse Compton emission of the spine is anisotropic in its frame, possibly producing the deceleration of the spine by the Compton rocket effect. The boundaries between jet layers of different velocity may accelerate particles (Stawarz & Ostrowski 2002) and are of special interest for jet stability considerations.

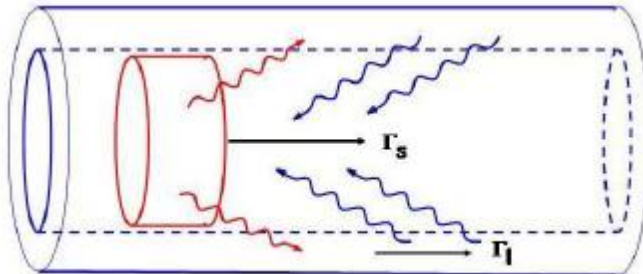


Figure 1.2: Spine+sheath geometry in blazar jet (Ghisellini et al. 2005)

Jets are believed to be launched from accreting supermassive black holes and powered by either the gravitational energy of accreting matter that moves toward the black hole or, in the Blandford-Znajek process (Blandford & Znajek 1977) by the rotational energy of a rotating black hole. In the first case, jets may either be launched purely electromagnetically (e.g. Blandford 1976), or as the result of magnetohydrodynamic processes at the inner regions of the accretion disk (e.g. Begelman, Blandford & Rees 1984;). In the Blandford-Znajek process, the black hole rotating in the magnetic field supported by the accretion disk gives rise to a Poynting flux.

Most models of jet formation face the σ -problem (σ is the ratio of electromagnetic energy density to particle energy density), namely that they predict a Poynting flux

dominated energy transport by a strongly magnetized or high- σ plasma, while pc-scale observations indicate that the jets consist of particle dominated, low- σ plasma (e.g. Krawczynski, Coppi & Aharonian 2002). Understanding the launching of jets may thus require the solution of two problems: the launching of a magnetically dominated outflow, and the conversion of such an outflow into a particle dominated jet. The latter transition is poorly understood, and requires more theoretical work.

Theorists are now concentrating on production of jets via differentially twisting magnetic fields tied to the ergosphere of the central BH (see e.g. Marscher 2006). One of the primary difficulties is to get enough particles across the field lines so that the jet is more than just Poynting flux. However, if at least some particles make it into the flow, this difficulty could be an advantage, since a high ratio of magnetic to rest-mass energy density at the base is needed to propel the jet to a high Lorentz factor farther out (Vlahakis & Königl 2004). Pair creation might be the dominant process that injects particles into the base of the jet. According to McKinney (2006), photons produced in accretion disk and corona are able to enter the jet and produce pairs in the case of the strong magnetic field.

One strong prediction of the magnetic launching models is that the geometry of the field should correspond to a helix (Marscher 2006). Despite the existence of indications that helical fields might be consistent with polarized intensity VLBI images (e.g. Gabuzda et al. 2004), there are models incorporating shocks propagating through a turbulent plasma with disordered field explaining a wider range of phenomena associated with jets (e.g. Marscher et al. 1992; Lister & Homan 2005). In addition, Sikora et al. (2005) consider various observational constraints and conclude that the region of helical magnetic field is restricted to distances from the central engine considerably less than the structures resolved on VLBI images.

Thus, the scientists have to solve many problems with respect to jet launching mechanisms and jet fine structure. Optical observations along those in other spectral bands can reveal many aspects necessary to solve these problems.

1.3.3 *Jet Magnetic Field*

VLBI polarization observations of radio-loud BL Lacs have shown a tendency for the polarization E vectors in the parsec-scale jets to be aligned with the local jet direction. Since the jet emission is believed to be optically thin, this implies that the corresponding magnetic B field should be transverse to the jet (e.g. Gabuzda, Pushkarev & Cawthorne 2000). This has usually been interpreted as evidence for relativistic shocks that enhance the B -field component in the plane of compression, perpendicular to the direction of propagation of the shock (Marscher 1996). The fact that the observed polarization vectors remain aligned with the jet over extensive sections of the jet, even in the presence of appreciable bending (e.g.

1ES 1803 + 784, Gabuzda 1999) and some individual VLBI features that display transverse \mathbf{B} -field structures are far from compact (against the expectation that energetic shocks should be relatively compact features, led Gabuzda, Murray & Cronin (2004) to the suggestion that the observed transverse \mathbf{B} fields in these sources are associated with the dominant toroidal component of the intrinsic jet \mathbf{B} fields (see fig. 1.3), in which case maintenance of the transverse field orientation as the jets curve would be natural. The suggestion of helical magnetic fields is in favour of magnetic launching models (Marscher 2006). But there are models incorporating shocks propagating through a turbulent plasma with disordered field explaining a wider range of phenomena associated with jets (e.g. Marscher et al. 1992; Lister & Homan 2005). In addition, Sikora et al. (2005) consider various observational constraints and conclude that the region of helical magnetic field is restricted to distances from the central engine considerably less than that of the structure resolved on VLBI images.

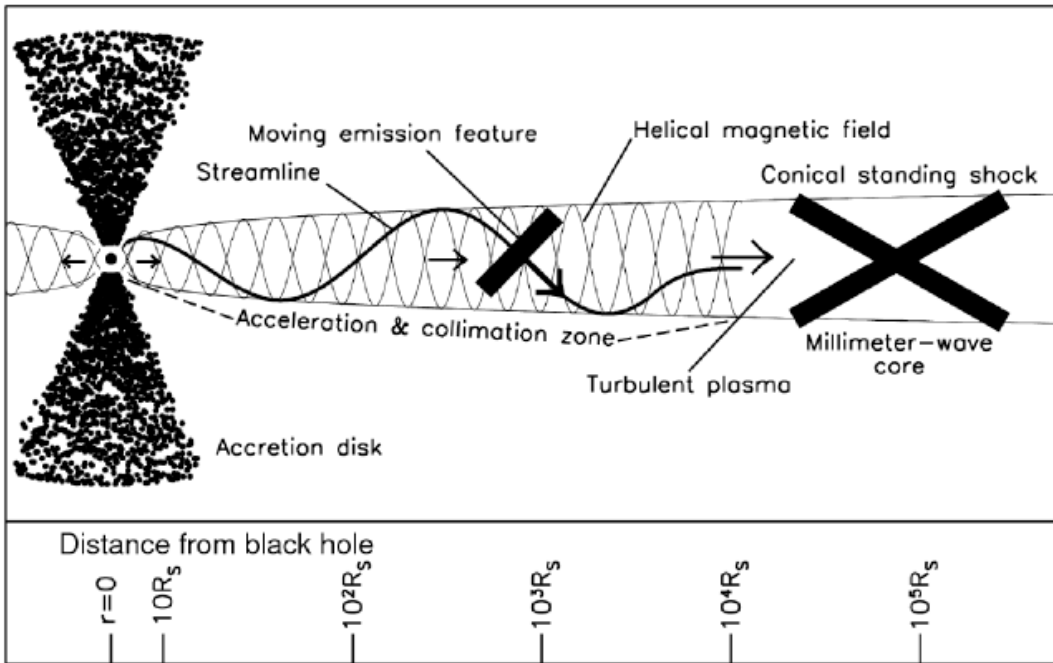


Figure 1.3: Sketch of helical jet (Marscher 2008)

1.3.4 Blazar Accretion Discs

Based upon AGN general picture, blazars should possess accretion disks. As a rule, the most direct evidence of accretion disk emission comes from the quasi-thermal big blue bumps sometimes seen in AGN spectra. While these bumps are not uncommon in quasars, their presence in blazars is rare, presumably because the disk emission is usually swamped by the boosted nearly power-law continuum (Wiita 2005). The quasi-simultaneous multiband

observations of the blazar AO 0235+164 (Raiteri et al. 2005) provided an evidence for a blue bump.

Emission lines with equivalent width in excess of 5Å have been detected several times (Vermeulen et al. 1995; Corbett et al. 1996, 2000), suggesting that blazars can possess a broad line region (BLR), but it would be usually obscured by the beamed synchrotron emission of the jet.

In both scenario of blazar jet formation (Blandford-Znajek or magneto-hydrodynamical) scenarios the magnetic field must play a major role in channelling power from the BH or from the disk into the jet; in both cases, it should be sustained by matter accreting onto the BH, leading one to expect a relation between the accretion power and the jet power.

The common view is that AGN involve two categories of accretion flows (see Wiita 2006). For accretion flows where the accretion luminosity, L, is comparable to the Eddington limit the disk becomes geometrically and optically thick (e.g. Paczynski & Wiita 1980) and the inner edge of the disk is inside the marginally stable orbit. Such a discs are quite inefficient radiators, since much of the ample quasi-thermal radiation they produce is trapped within the AD and swept through the event horizon. For flows where $L/L_E \sim 0.1$ we have geometrically thin but optically thick ADs. Here the inner edge is at the marginally stable orbit ($r_{ms} = 6GM_{BH}/c^2 \equiv 3r_s$ for a Schwarzschild BH) and the efficiency of mass to radiation conversion is high (>0.057) since most of the radiation produced in the AD can escape (Wiita 2006).

One expect the existence of instable processes of different timescales occurring in ADs. The dynamical timescale of the instability

$$t_{dyn} = 2 \times 10^3 R^{\frac{3}{2}} M_8 \text{ sec} \quad (1.9)$$

with $M_8 \equiv 10^8 M_\odot$, should be of order from minutes to hours (Wiita 2006). Another timescale, t_{sound} , associated with the time needed for a sound wave to be transmitted across a radial region of extent r , are of order of days for $10^8 M_\odot$ BHs. Nearly the same order of the duration can have the instabilities occurring on thermal timescales, t_{th} , defined as the ratio of the disk's internal energy to the heating or cooling rate.

One of the most interesting longer timescale, so-called viscous timescale, is related to the rate at which matter flows through the AD. It should be months to years order for BHs with $M \sim 10^8 M_\odot$. So, long-term flares seen in blazars can be related to viscous processes occurring in ADs.

The longest interesting timescale, t_{fuel} , is that over which the accretion rate changes through differences in the amount of gas available to the BH. While an occasional gas bolus may be come from a star disrupted in the vicinity of the BH, the fundamental availability time is comparable to the lifetime of the AGN phenomenon itself. Fueling should be driven

by processes related to galactic mergers or harassment and will typically be $t_{fuel} \sim 10^7\text{--}10^8$ yr (Wiita 2006).

According to Shakura & Sunyaev (1976), the radiation pressure instability has can afflict α -disks. Since AGN ADs should be radiation pressure dominated over substantial ranges in r and \dot{M} this instability should yield fluctuations in emission. In the case of AGN masses, the radiation pressure instability may yield big AD outbursts from the X-ray through IR over years to decades.

Because ADs are magnetized, there is a high probability that they are sheathed by coronae, which are certain to contribute substantially to the X-ray emission and should have some role to play in other bands. These coronal structures probably play a significant part in the X-ray emission and variability of Seyfert galaxies, but their importance for quasars and blazars is much less clear. The variations in energy that can be released from coronal flares are probably too small to be detected, particularly outside the X-ray band, in that individual flares are limited in their powers (e.g. Wiita 2007).

1.4 Blazar Emission Mechanisms

As mentioned above, blazer emission is of nonthermal nature. While the lower-frequency component of blazer SED is widely accepted to be of synchrotron origin, no concession has been achieved with respect to higher-frequency part of the spectrum. There are two class of models in this regard – leptonic and hadronic ones.

According to leptonic models (e. g. Ghisellini, Marashi & Dondi 1996), the synchrotron emission from relativistic electrons is responsible for the first hump. The same electron population in jet plasma up-scatters low-energy synchrotron photons (so-called Synchrotron Self-Compton (SSC) model) or “external” photons, that originate outside the jet (External Compton (EC)), to high energies, producing the second hump). Possible sources of external seed photons are accretion-disk photons entering the jet directly or after being reprocessed in the circumnuclear material (e.g. the broad line regions of quasars), jet synchrotron emission reflected off clouds in the circumnuclear material, infrared emission from a dust torus around the central engine (Kaspi et al. 2000). In addition, Ghisellini & Madau (1996) suggested that locally produced synchrotron emission may be scattered by nearby clouds surrounding the jet and enter the excited region once again where they can be scattered by relativistic electrons (mirror Compton, or MC).

The sequence FSRQ → RBL → XBL appears to be related to an decreasing external-Compton contribution to the γ -ray spectrum. While most FSRQs are successfully modelled with EC models (e.g. Dermer et al. 1997), the SEDs of XBLs are consistent with pure SSC models (e.g. Mastichiadis & Kirk 1997, Krawczynski et al. 2002). RBLs (e.g. BL Lacertae, W

Comae) often seem to require an EC component to explain their EGRET spectra (Sambruna et al. 1999, Böttcher & Bloom 2000, Böttcher et al. 2002). It is concluded that XBLs require higher average electron energies and lower magnetic fields than LBLs and FSRQs (Böttcher 2006). Cavaliere & D'Elia (2002) suggest that the decreasing importance of external radiation fields along the sequence FSRQ → RBL → XBL may be an evolutionary effect related to the gradual depletion of a limited reservoir of circumnuclear material.

Standard leptonic SSC models predict a close temporal correlation between the synchrotron and Compton components (Böttcher 2006). Here, high-energy flux variability should either be simultaneous with the lower-frequency fluctuations or slightly offset from them. Hence, there should be a correlation across wavebands with frequency-dependent time delays (Sokolov, Marscher & McHardy 2004).

However, the correlation can be only modest if there are gradients in the highest electron energies. This is possible if either electron energization is restricted to particular locations, e.g. at shock fronts (Marhsler & Gear 1985), or the efficiency of particle acceleration varies from one place to another in the jet (Marscher 2006). In the former case, rapid radiative cooling of the highest-energy electrons restricts the highest-frequency synchrotron emission to the regions very close to where the energization occurs.

If a source is uniform and the timescale of the changes in a number of radiating particles is longer than light-travel time across the emitting region, then flares should be simultaneous at all wavelengths (Marscher et al. 2004). However, the timescales are often quite short and uniform source models rarely work well. The longer-lived lower-energy electrons can spread across larger volume and low-energy flares should last longer. If the particles yield to power-law energy distribution, then in case of new shock appearance, a flare should start simultaneously at optically thin frequencies but it will peak earlier at higher frequencies. At radio frequencies an additional delay is expected since the flux density will not reach a maximum until the region starts to become optically thick as it expands down the jet. Distributed, non-uniform particle acceleration should yield a mixture of time-delayed and simultaneous flares at different frequencies (Marscher 2006).

If the jet points more closely to the line of sight than an angle Γ^{-1} , the peak of SSC light curve is subject to a geometrical time delay corresponding to the time it takes for the flare's synchrotron photons to reach the electrons that scatter them (Sokolov et al. 2004). There should be a tendency for the X-ray curves to be smoother than in optical region, since photons from millimeter to optical wavelengths will contribute roughly equally to the X-ray flux (McHardy et al. 1999). If, as discussed above, there are frequency-dependent time delays in the synchrotron light curves, these will be averaged to give X-ray light curves that have time scales characteristic of the far-infrared synchrotron emission (Marscher 2006).

Other causes of the flare are also expected to exist. For example, changes in the Doppler factor caused by acceleration or bending of the jet flow can cause nearly simultaneous variations at all wavebands, even those at somewhat optically thick frequencies

(Marscher, Gear & Travis 1992). VLBI images of jets reveal strong banding on parsec scales (e.g. Kellerman et al. 2004), so such flares are expected to appear sometimes.

For PKS 1510-89 and 3C 279, “reverse” time delays are observed, when X-ray flares lagged behind the optical/IR variations. This event is explained as a result of X-ray production in the radio jet (Marscher 2006).

The leptonic model is mainly motivated by the observed correlation between X-ray and TeV variabilities. According to Marscher (2006), most X-ray flares in PKS 1510-089 and 3C 279 were associated with ejections of superluminal radio knots with extremely high apparent speeds (21-46c).

However, the simple (thus commonly used) one-zone SSC model, where the X-rays originate as synchrotron emission of a single relativistic electron population and the TeV -rays are produced from inverse Compton scattering of the synchrotron photons by the same population of electrons, was challenged by an “orphan” flare (that is a flare in the TeV -ray band without a corresponding flare in the X-ray band) of 1ES 1959+650 on June 4, 2002.

In *hadronic* scenarios (e.g. Mannheim 1993, Beall & Bednarek 1998), protons are accelerated in blazar jet along with electrons, which again move relativistically along the jet through highly magnetized environment (Mücke et al. (2003)). The synchrotron radiation produced by means of primary and proton-induced electrons contribute to the low-energy component while the high-energy photons originate from photo-meson interactions and from proton and muon synchrotron radiation.

We have two possibilities here (Mücke et al. 2003) :

- proton-photon collisions (so-called pp-collisions or photopair production (Bethe-Heitler):

$$p + \gamma \rightarrow p + e^\pm \quad (1.10)$$

- photo-meson production:

$$p + \gamma \rightarrow p + \pi^0 (\rightarrow 2\gamma \text{ or } \pi^0 \rightarrow e^+ + e^- + \gamma) \quad (1.11)$$

$$p + \gamma \rightarrow n + \pi^+ (\rightarrow \mu^+ \rightarrow e^+) \quad (1.12)$$

The magnetic field is a key parameter in hadronic models. In order to accelerate protons to energies above the photoproduction threshold, the fields of ~10 G are necessary (Mücke et al. 2003).

Hadronic models can be distinguished from the leptonic models by the observation of high energy neutrinos generated in decay chains of mesons created in the photoproduction interactions (Mücke et al. 2003). If these models are correct, neutrino detection should be more likely during “flares”, periods of high gamma- and X-ray activity. Despite some observational hints (Halzen & Hooper 2005), neutrinos have not yet been detected at high confidence level.

The basic problem of hadronic models is linked to the low interaction rates between photons and particles which make great problems to explain of the observed fast gamma-ray

variability in terms of radiative cooling and X-ray/TeV flux correlations (Aharonian, Khangulian & Kostamante 2008).

The hadronic model is capable to explain the X-ray/TeV correlation, if an appreciable amount of X-ray emission comes from synchrotron radiation of secondary electrons. This could explain the scatters in the X-ray/TeV correlation. However, like the leptonic models, the hadronic models also face the challenge of explaining the observed TeV flares with no or offset X-ray counterparts (Blazejowski et al. 2006).

One of the ways to solve above mentioned problems consists in resorting to so-called multi-zone IC models, where the synchrotron and IC emissions are produced by different electron populations. Stratified jet and spine+sheath models, discussed above, should be considered as the varieties of multi-zone models.

Currently, the development different “hybrid” models, incorporating both leptonic and hadronic mechanisms, is under way. Hadronic processes in the context of models with leptonically dominated blazar emission have been considered by several authors, e.g.:

- hadronic synchrotron mirror model developed specially for orphan TeV flare in 1ES 1959+650 (Reimer et a. 2005). In that case, the correlated X-ray - TeV flares are explained by a standard SSC model while the “orphan” TeV-flare is explained by π^0 -decay γ -rays as a result of photomeson production from relativistic protons interacting with synchrotron photons that have been reflected off clouds located at pc-scale distances from the central engine.
- “supercritical pile” model suggested in Kazanas & Mastichiadis (1999). In this scenario, a runaway pair production avalanche is initiated by mildly relativistic protons interacting with reflected synchrotron photons via $p\gamma$ pair production, as the primary pair injection mechanism in blazar jets.
- conversion of ultrarelativistic protons into neutrons via $p\gamma$ pion production on external soft photons was suggested in Atoyan & Dermer (2002) as a way to overcome synchrotron losses of protons near the base of blazar jets and, thus, to allow blazar jets to remain collimated out to kpc scales.

The existing Multi-zone and hybrid models models need more sophistications in order to be in good agreement with different observational phenomena. As a whole, great effort is still needed in order to reconcile theoretical models with observational challenges.

1.5 Blazar Variability

1.5.1 Variability Patterns

One of the important blazar characteristics is the fact that their energy flux varies along the whole electromagnetic spectrum, spanning a wide range of time-scales. The flux variability is

an often used as a criterion for their detection. On the other hand, variability time-scales strongly constrain the sizes of the emitting regions, through light-travel arguments (the usual way to infer the size from the variability timescale is (Romero et al. 1995)

$$l \sim t_v c \Gamma^2 (1 + z), \quad (1.13)$$

where t_v is variability timescale, z – target’s redshift). Since, except for the Mpc-scale radio-jets and lobes, the other components remain spatially unresolved to astronomical observations in the vast majority of AGNs, flux variability studies are thus a powerful tool to probe those innermost regions (Cellone , Romero & Araudo 2007).

While most AGNs are variable on time-scales of a few years, blazars display both the largest amplitudes and shorter time-scales. Note, that one discriminates between microvariabilities (i.e. strictly intra-night variability with timescales from minutes to a few hours), intraday variabilities (timescales from the hours to several days), short-term outbursts (with time scales ranging from a few weeks to several months) and long-term trends lasting from several months to years (Romero, Cellone & Combi 1999, Gupta et al. 2008).

At optical wavelengths, long-term variations, with amplitudes of ~ 2 to ~ 5 mag are found through extensive monitoring in several objects, such as GC0109+224 (Ciprini et al. 2003), AO 0235+64 (Raiteri et al. 2005).

Optical fluctuations on time-scales spanning several days are also usually observed, although with smaller amplitudes (e.g. ~ 1 mag in 20 days for PKS 2005–489, Dominici et al. 2004; ~ 1.7 mag in 10 days for 3C 454.3, Fuhrmann et al. 2006).

Up to now, it is firmly established that several sources could experience remarkably large intra-night fluctuations, amounting to several tenths of a magnitude in a few hours. For example, Romero, Cellone & Combi (2000a) found changes up to 0.5 mag within one night and ~ 1.2 mag between consecutive nights for AO 0235+64. This was one of the most violent variability events ever observed at optical wavelengths in any blazar.

The investigations of Howard et al. (2004) and Stalin et al. (2004) indicated that blazar microvariability should be correlated with the presence of longer-term flux changes, rather than its apparent brightness level. Nevertheless, more observational evidences are needed to prove this suggestion.

Especial violent variability events in some blazars, with amplitudes $\Delta m \sim 1$ mag in a few tens of minutes (Bai et al. 1998; Xie et al. 1999, 2001, 2002a,b, 2004; Dai et al. 2001). For example, these authors reported a 2 mag variation in ~ 40 min for the highly polarized quasar PKS 1510–089. They also showed several sudden ($\Delta t < 15$ min) “dips” of about 0.9 mag in the light curve of OJ 248 (0827+243). If confirmed, these extremely violent phenomena would require a complete reassessment of the mechanisms which are thought to be responsible of the energy generation in AGNs. Note that optical variability time-scales of a few tens of minutes would imply emitting regions smaller than the Schwarzschild radius for certain objects. In contrast, Cellone et al. (2007) showed that the largest fast flux variations

detected them for above mentioned objects, was ~ 0.1 mag in about one hour. The results of above mentioned authors were explained as a spurious variability caused by inappropriate choice of reference stars and error estimation methods. Such a discrepancy have been found for 1ES 0323+022 during the research carried out within thesis framework (see below).

Despite the great number of observational campaigns performed in different spectral bands during past decades, we need much more experimental investigations to draw the statistical picture of blazer variability at various timescales.

1.5.2 Shock Waves in Blazar Jets

The dominant theory explaining blazar variability is based on assumption that there should be ultrarelativistic shock waves propagating through the jet (see e.g. Mücke et al. 2003). Instabilities in the inner portions of the accretion disk may lead to a deposition of large amounts of energy at the base of a relativistic jet (Marscher 1996). The speed of the deposited high energy plasma increases while its internal energy is converted into bulk kinetic energy. If the speed of the fast flow exceeds the sound speed in the quiescent plasma rest frame, the information about the incoming fast flow cannot be transmitted by sound waves in the quiescent flow (Sokolov & Marscher 2004). This leads to a pile-up of the quiescent plasma in front of the fast flow and the formation of a shock wave that separates the piled-up material from the quiescent flow. Similarly, the presence of a slow flow in front of the fast plasma will lead to the formation of a compression wave propagating into the fast plasma. This compression wave may steepen into a shock wave if the speed difference between fast and slow flow is large enough (Sokolov & Marscher 2004). A contact discontinuity separates the fast flow and the formerly quiescent material that has been piled-up in front of it. Thus, introduction of energetic plasma into the jet leads to the formation of a relativistic shell of compressed material propagating downstream.

There are two kinds of the shocks (Marscher 1996): one sort of shock can arise from the interaction of a fast medium overtaking a slower medium. In the frame of the contact discontinuity separating the two media, a forward shock propagates downstream into the slower moving medium and a reverse shock propagates upstream into the faster moving medium. A reverse shock, on other hand, slows high-velocity upstream fluid entering the shocked region from behind down to subsonic speeds, as measured in the frame of reverse shock front. The reverse shock front propagates downstream, but more slowly than does either the forward shock front or the upstream, unshocked gas. A given disturbance can have only a forward shock or both a forward and a reverse shock, with the relative strength of the shocks depending on the details of time-variable flow. The calculations of Bicknell & Wagner (2002) showed that the appearance of forward-reverse shocks depends on relative velocity of unshocked gas on both sides of the shocked region (β_{12}). If

$$\beta_{12} > \sqrt{3} \frac{\left| \frac{p_2}{p_1} - 1 \right|}{\sqrt{3 \left(\frac{p_2}{p_1} + 1 \right) \left(3 + \frac{p_2}{p_1} \right)}}, \quad (1.14)$$

we should the appearance of forward-reverse shock structure. Here, p_2 denotes the pressure in the shocked region while p_1 is the same for the material overtaking this region. The structure of knot C in the M87 jet (with a large gradient in brightness, falling rapidly moving downstream, Fig. 1.4) serves as an example of a forward shock, and the expected behaviour of a reverse shock is exemplified by knot A.

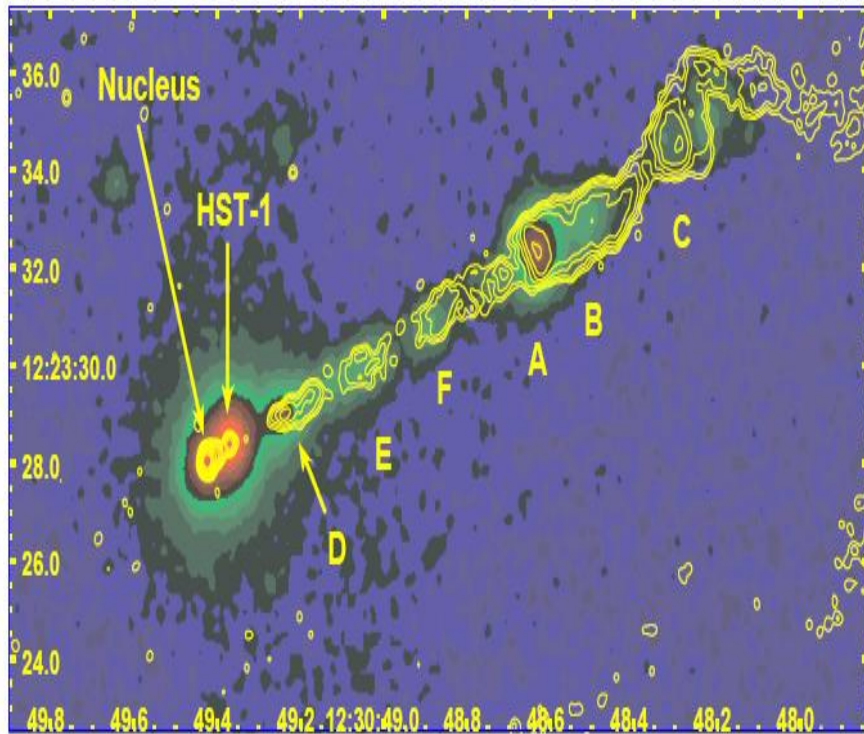


Figure 1.4: M87 CXO image with 8 GHz contours (Harris & Krawczynski 2006).

Propagating shock waves can produce long term (months to years) outbursts (Marscher & Gear 1985). A shock front compresses the plasma (causing an increase in the density as well as an adiabatic increase in internal energy and enhances the component of the magnetic field that lies parallel to the shock front. In addition, the shock can accelerate relativistic particles by means of diffusive shock acceleration mechanism which relies on particles crossing the shock front repeatedly, each time turning around through scattering off plasma waves. The acceleration is most efficient when the magnetic field is directed perpendicular to the shock front (Marscher 1996). Particle acceleration can be associated with both forward and reverse shocks.

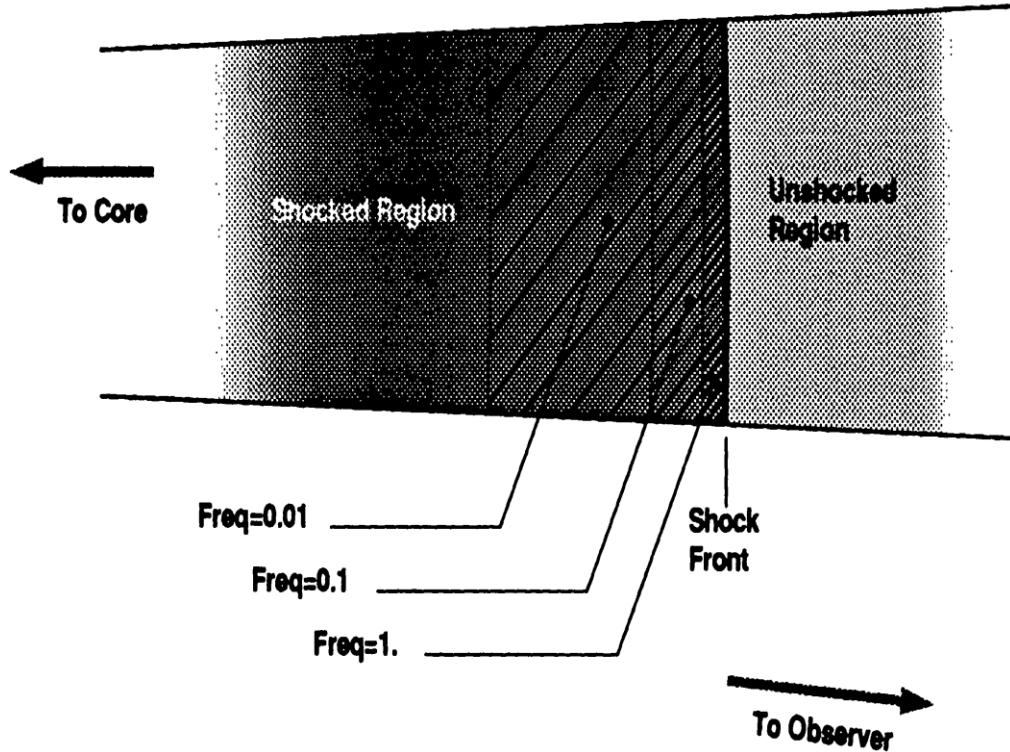


Figure 1.5: Sketch of a shock in a relativistic jet (Marscher 1996)

If the shock accelerates particles only at the shock front, then the highest energy electrons will suffer radiative losses such that they only maintain these high energies over a short distance. The highest frequency radiation can therefore be emitted only within a thin sheet behind the shock front. The thickness of this sheet increases as the frequency decreases until the frequency is so low that radiative losses are negligible across the entire shocked region (Marscher 1996).

This frequency stratification of the emission in a shock explains nicely the general characteristics of the multiwaveband blazar light curves: a flare caused by a shock is spread across many decades of the frequency, yet the time-scale of the variability should be much shorter at higher frequencies, owing to the thickness of the respective emission region behind the shock front that results from radiative energy losses of the electrons. The γ -ray and X-ray flux in a shock-induced flare should therefore peak first, followed by the optical and infrared than the radio ones.

At high frequencies, interaction with a turbulent ambient medium in the jet can generate more rapid fluctuations (Marscher & Gear 1985). The onset of short-term bursts can be triggered by the collision between a relativistic shock wave travelling down the jet and a more slowly moving (Spada et al. 2001) or stationary compressions such as the knots seen in VLBI images of blazars, Mach disc or oblique shocks.

According to Marscher (1996), frequency stratified shocks propagating through hydromagnetic turbulence (or, conversely, the turbulent jet medium passing through standing shocks) in a jet are what cause the short time-scale variability of blazars. The

Reynolds number is expected to be extremely high in relativistic jet. Consequently, jet plasma should be quite turbulent (Marsher et al. 1992). A turbulence would be responsible for inhomogeneities, the scales of which depend upon the amplitude, power spectrum and thickness of an disturbance. Consequently, when relativistic electrons cross jet regions where a magnetic field is higher, their emission brightens, while it fades when local fields is weaker.

Evidence that jets are turbulent comes from the observations on blazer linear polarization which is considerably less than that expected from standard synchrotron radiation (Marscher 1996). This fact indicates that the magnetic field contains a randomly oriented component.

According to Marscher (1996), the deviations from jet mean density and magnetic field should be smoothed out statistically at lower frequencies because the large emission regions contain very large number of turbulent cells. While emission regions are expected to be very thin at higher frequencies and therefore contain sufficiently small number of the cells, microvariabilities are much apparent.

Flux variability induced by the turbulence can arise from fluctuations not only in density of relativistic electrons and magnitude of the magnetic field, but also in the orientation of the field, since we have following expression for flux density (Marscher 1996):

$$F_\nu \sim N_0 (B \sin \theta)^{1+\alpha} \nu^{-\alpha}, \quad (1.15)$$

where N_0 is the normalization to the electron energy distribution, θ is the angle between the magnetic field and the line-of-sight, and α is the spectral index (so-called “Geometrical Model”). If the orientation of jet magnetic field changes with respect to the observer, the observed F_ν should be also variable, according to Equation (1.15)

The other prominent model for blazar variability is an emergence of the “blobs” in jet base (e.g. Marscher & Gear 1985). This formation is distinct from the ambient jet flow as opposed to a feature that is fully integrated into the flow, as is the case for a shock. This allows a blob to have its own independent magnetic field and for its destruction to require either expansion or diffusion into oblivion, or perhaps some catastrophe such as running into a cloud. The main difference for models is that the blob can expand in three dimensions, whereas steady jets only expand laterally, and the particles and magnetic field do not need to be directly related to that of the surrounding jet plasma. There are some difficulties associated with this model. For example, attempting to model an outburst of 3C 273 as an expanding blob, Marscher & Gear (1985) were led to the nonsensical requirement—despite the increased number of free parameters—that the magnetic field decreased while the particle density increased to cause the flare. The observed variability of 3C 273 could be explained in a more natural way by resorting to a shock passing through an adiabatic, conical, relativistic jet. Nevertheless, the theory of blob emergence remain still viable (see e.g. Kusunose & Takahara 2006).

Thus, despite great progress in understanding of the origin of blazar variability, this problem is not exhaustively solved, and still great observational and theoretical investigations are necessary to confirm or reject above provided considerations.

1.5.3 Quasi-periodical Flares in Blazars

Intensive observed campaigns, carried out during the decades, show quasi-periodical flux changes at different timescales. The binary BH scenario was applied by Romero, Fan & Nuza (2003) to the recurrent radio outbursts in AO 0235+16 repeating with a period of $\sim 5.7 \pm 0.5$ yr (Raiteri et al. 2001). According to this scenario, there are two black holes in a close circular orbit of radius r_m . One of the holes has an accretion disk which is non-coplanar with the orbital plane. It is usually expected that the jet is ejected perpendicularly to the disk plane, in the direction of the disk angular velocity ω_d . The gravitational torque of the companion BH onto the disk will force the innermost part of it to precess. This precession will be transmitted to the jets, which should be presented in quasi-periodical changes in the flux.

For the same object, Fan et al. (2002) discovered a quasi-periodic signal with 2.95 ± 0.15 yr period in the optical band. The similar event observed for 3C 373 was interpreted by Romero et al. (2000b) as follows: a secondary black hole in a non-coplanar circular orbit around an accreting black hole must penetrate the outer parts of the disk, producing optical flares. Since two black-hole/disk collisions are expected per orbit, the periodicity of the optical flares should be $\sim T_m/2$ where T_m is the orbital period of secondary BH.

The most remarkable event in this regard is quasi-periodical optical flares with period of about 12 yr seen in OJ 287 (observed since 1891). Lehto & Valtonen (1996) showed that the sharp outbursts fit nicely with the idea of an impact of the secondary moving on elliptical orbit on the disk of the primary. There should be two impacts per pericenter passage, hence the observed double-peak structures seen in the light curve. The model based on an “inert” accretion disk. Sundelius et al. (1997) proposed a model based on the same exact solution, but allowing for a “live” accretion disk. The “live” accretion disk bends toward the perturbing black hole before the disk impact, which causes a flare somewhat earlier than in the case of “inert” disk.

Another model for the description of the quasi-periodic optical outbursts observed in the blazar OJ 287 was proposed by Villata et al. (1998). In this scenario, the observed double-peaked structure of the cyclic outbursts are in connection with a pair of supermassive BHs in a binary system, both of them creating a jet. The two jets are bent by the interaction of their magnetized plasma with the ambient medium. The combination of this bending with a long-term precession of the jet axes gives rise to a time-dependent orientation of the emitting

outflows. The quasi-periodic optical outbursts that we observe arise from the relativistic beaming effect when part of the bent jets is directed toward us.

On basis of RXTE data analysis, Rani, Wiita & Gupta (2009) found quasi-periodical X-ray fluctuations in AO 0235+14 and 1ES 2321+419 with 17d and 420d periods, respectively. In the case of first object, the authors resort to the turbulence existing behind a shock propagating down a jet. For such turbulent flows the dominant eddies' turnover times should yield short-lived, quasi-periodic, but probably modest, fluctuations in emissivity. The effect of Doppler boosting can greatly amplify even weak intrinsic flux variations produced by small changes in the magnetic field strength or relativistic electron density, can be raised to the level at which they can be detected (Qian et al. 1991). The same Doppler boosting is able to reduce the time-scale at which these fluctuations are observed, compared to the time-scale they possess in the emission frame, as follow (Wiita 2006):

$$\Delta t_{obs} = \frac{\Delta t_{em}}{\delta} \quad (1.16)$$

The same scenario was applied to explain the optical intra-night variability with quasi-periods of tens of minutes that are only occasionally seen and that have timescales that vary from night to night in the blazar S5 0716+714 (Gupta, Srivastava & Wiita 2009). As for 1ES 2321+419, this model was found to be less possible due to great sizes of respective eddies. Instead, the model of propagation of the shock through helical jet was used. A relativistic shock propagating down such a perturbed jet will induce significantly increased emission at the locations where the shock intersects a region of enhanced magnetic field and/or electron density corresponding to such a non-axisymmetric structure. Due to the extreme sensitivity of Doppler boosting to viewing angle, significant changes in the flux should be seen by an observer at fixed angle to the jet axis if the most strongly emitting region swings with respect to him/her.

Thus, the detection of periodical flux changes at different timescales can give very valuable information about blazar central engine and structure of large-scale magnetic fields in their jets.

1.6. Motivation and Objectives

During past decades, tremendous number of the investigations are performed in order to explain the extreme nature of this kind of AGNs. The progress achieved both in observational technique and theoretical tools allowed scientists to explain many of observational puzzles. The VLA/VLBA technique is capable to resolve jet fine structures and disclose increasing number of the mysteries these super-giant cosmic laboratories. X- and γ -ray devices, mounted on the satellite boards, and ground-based Cherenkov-type telescopes, revealed unusual high-energy world sending us a number of the challenges. On other hand,

theoretical simulations have attained very high level of sophistication, which explain bulk of observed phenomena and predict the existence of many aspects for future observations.

Despite great progress in understanding of blazars nature, many problems remain to be solved both in point of their structure and emission mechanisms. Blazars are among the most intriguing astrophysical objects - even after more than three decades of observations, we know very little about the physics underlying their phenomenology and their actual origin.

Flux variability investigation is one of the main clues allowing to make further progress in these directions. Remember that the only tool to study the processes emerging in optical jet is to investigate blazar optical variabilities of different time-scales.

The essence of the thesis consists in the investigation of optical behaviour of eleven XBLs selected from the catalogue Einstein Slew Survey (Elvis et al. 1992; see Table 1.1).

XBLs are the least investigated among blazars in point of optical variability. As noted by Romero et al. (1999), on basis of the extensive study of intraday variability, this type of BL Lacs should display different duty cycles and variability amplitudes than radio-selected sources. In addition, the differences seemed to be present also at microvariability timescales: just 1 out of 3 HBLs in their sample showed microvariations, in contrast to RBLs (8 out of 12). The observed variability amplitude was also lower. These differences were attributed to the effect of stronger magnetic fields in HBLs, which might prevent the formation of features

Table 1.1: List of target objects

#	Object Name (Alternate Name)	α (2000) ¹	δ (2000) ¹	z
1	1ES 0229+200	02:32:48.60	+20:17:17.0	0.139 ²
2	1ES 0323+033 (H 0323+02.2)	03:26:13.971	+02:25:14.66	0.149 ³
3	1ES 0414+009 (H 0414+00.9)	04:16:52.462	+01:05:23.5	0.287 ²
4	1ES 0502+675	05:07:56.18	+67:37:24.3	0.314 ²
5	1ES 0647+250	06:50:46.6	+25:03:00	$\diamond 0.3^2$
6	1ES 0806+524	08:09:49.19	+52:18:58.4	0.138 ²
7	1ES 1028+511	10:31:18.52	+50:53:35.8	0.361 ²
8	1ES 1426+428 (H 1426+428)	14:28:32.6	+42:40:29	0.128 ²
9	1ES 1517+656	15:17:47.58	+65:25:23.25	>0.7 ²
10	1ES 1959+650	19:59:59.8522	+65:08:54.668	0.048 ²
11	1ES 2344+514	23:47:04.8	+51:42:18	0.044 ²

¹ <http://simbad.u-strasbg.fr/simbad/sim-fid>

² Scarpa et al. 2000

³ Feigelson et al. (1986)

like density inhomogeneities and bends in the base of the jets. Romero (1995) has shown that axial magnetic fields prevent the development of Kelvin-Helmholtz instabilities in sub-

parsec to parsec-scale jets if their values exceed the critical value B_c given as:

$$B_c = \frac{\sqrt{4\pi n m_e c^2 (\Gamma^2 - 1)}}{\Gamma} \quad (1.17)$$

where n is the local electron density. Fields with $B > B_c$ would inhibit the formation of small-scale structures reducing thus the incidence of microvariability in the optical light curves. This condition is more likely to be satisfied in XBLs, where magnetic fields are expected to be higher than in RBLs (Sambruna et al. 1996). Nevertheless, Rommero et al. (1999) noted that their conclusions had been based on very limited number of objects and, they pointed to the necessity of more observations for XBLs in order to draw any statistically significant conclusions.

Thus, optical properties of XBLs are relatively less determined and it is crucial to collect as much observational material for many objects of this type as possible. As we will see below, target objects are less (or practically not) investigated in the optical domain. Several targets are detected through TeV diapason by ground-based gamma-ray telescopes, like *HESS*, *MAGIC*, and *VERITAS*. Consequently, there is a great interest in their optical research too.

The data provided within the scopes of the thesis span a period of 10 years (1997-2007). They were obtained with a small (70 cm) telescope but with adequate instrumentation and using a correct observational methodology. Hence, this research can give a very rich information on the behavior of HBL objects. The results will help to adjust the duty cycles of HBL objects at different timescales, and, in the case of adequate interpretation, the data will help to constraint theoretical models of the innermost parts of the jets in these sources.

Based upon this motivation, the thesis purposes and expected results were as follows:

- study the manner of long-term trends; in case of proven periodicity, calculate the periods of optical variability, otherwise - find the characteristic time-scales of long-term trends; derivation of the overall flux variabilities and amplitudes; prove whether two-peak maxima exist (indicating the existence of forward and reverse shocks);
- detection of short-term bursts and study their properties; examine correlation of short-term bursts with the state of optical luminosity which would allow us to draw some conclusions about the underlying physical mechanisms;
- detection and research intra-day variabilities;
- search for intra-night variabilities (microvariabilities) and study their correlation with the brightness state of the source (in the case of their detection).

In addition, the variability duty cycles at different timescales are determined. Finally, a statistical review of obtained results is performed and the objectives for future investigations are also provided.

The investigation is based on the data obtained between 1997-2007 at Georgian National Astrophysical Observatory (Abastumani) of Ilia State University (Tbilisi, Georgia). The

author gained a rich experimental experience during his participation in different observational campaigns (see Böttcher et al. 2007; Raiteri et al. 2006; Villata et al. 2004; Kurtanidze et al. 2003a,b; 2004; 2005; 2006a,b,c; 2007a,b). Afterwards, the author continued to derive and improve the results concerning the above listed objectives. Main results of the investigation obtained within the framework of the thesis are presented in the following papers:

1. Kapanadze B. Z., *Optical R-band variability of seven X-ray-selected BL Lacertae objects*, 2009, MNRAS, 398, 832
2. Kapanadze B. Z., *Observational Evidences of Multiple Shock Waves in X-Ray Selected BL Lacertae Objects*, 2009, Astrofizika, 52, 358
3. Kapanadze B. Z., *Optical R Band Phohometry of Selected HBLs*, accepted in MmSAI

Thesis highlights were presented at the following workshops:

- May 25-30, 2009: “Multifrequency Behaviour of High-energy Cosmic Sources” (FRASCATI WORKSHOP 2009, Vulcano, Italy); given a talk: “Optical R band Photometry of Selected HBLs”;
- October 7-11, 2009: “Radiation of Cosmic Objects from Radio through Gamma-rays (devoted to 100th anniversary of prof. M. Vashakidze; Abastumani, Georgia); given a talk: “Emission Processes in Blazars”;

2 Observational Background

In this chapter, the history of the investigation of target objects is provided. It is presented separately for different spectral diapasons and the observational campaigns are described in a chronological manner.

2.1 X-ray Observations

The targets were discovered in X-rays by *HEAO 1* (1ES 0414+009 (1977, Ulmer et al. 1983), 1ES 1426+428 (1977, Remillard et al. 1989), 1ES 0323+022 (1978, Doxsey et al. 1983) in medium-hard X-rays (2-10 keV). Positions and X-ray intensities of the objects were determined. 1ES 0323+022 showed a 1 day flare with a decrease with a factor of 3 in ≤ 6 hour. About this time 1ES 1426+428 was detected by *UHURU* and *ARIEL 5*. During 1977-1979 observations, the source showed 2-10 keV flux to vary with a factor of ~ 2 .

Other objects were discovered later by *HEAO2 IPC* camera through 0.5-4 keV passband during 1980-1981 (Elvis et al. 1992; the device operated in a “slew” regime - hence the catalogue name “Einstein Slew Survey”). The same device recorded very interesting behaviour of 1ES 0323+022 which exhibited a remarkable 60 s dip at the energies greater than 0.6 keV (hard) but not at 0.25 keV (soft). During next 300 seconds, the source showed to be very rapid X-ray variations. In addition, the average rates during these variations were significantly below the values recorded at the beginning of the observations, by factors of about 2 and 3 for 0.6-1.6 keV and 1.6-4.8 keV bands, respectively (Doxsey et al. 1983). It was concluded, that X-ray source had two components: steady soft and variable ones. No rapid variations were found in the case of 1ES 0414+009.

The X-ray observations were renewed with *EXOSAT*, which investigated 1ES 0323+022, 0414+009, 1426+428 and 1959+650 using ME and LE detectors (0.07-6 KeV) during 1984-1985 intending to find variations of X-ray fluxes. Furthermore, X-ray spectral energy distributions were studied Bradt et al. (1985), Brinkmann & Siebert (1994). 1ES 0323+022 was found to be in a faint quiescent state (with no evidence for rapid variability). It was concluded that the spectrum hardened when the source brightened (Falomo et al. 1993). The same conclusion was drawn with respect to 1ES 0414+009.

1ES 0323+02.2 was investigated with *Ginga Large Area Counter* (LAC) through 1.2-10.5 KeV passband during 1987-1991 (Kohmura et al. 1994). One revealed X-ray flux variations with the timescales of several hours. During 1987 observations, X-ray counting rate varied by a factor of 3 on time scales of several hours. The light curves 1.2-4.1 keV and 4.1-10.5 keV were fairly similar, although the harder band showed a slightly larger variation in its amplitude. The variation in higher energy band preceded that in lower-energy band by

nearly 0.05d. This supported the idea that X-ray emission was of synchrotron origin. The 1988 and 1991 observations detected the source considerably fainter without significant intensity variations.

Afterwards, 1ES 0323+022, 1028+511, 1426+428, 1959+650 were observed by *ROSAT* through the energy range of 0.1-2.4 keV during 1991-1993. X-ray fluxes and SEDs were estimated (Beckmann et al. 2002, Comastri et al. 1997).

X-ray observations of 1ES 0323+022, 0414+009 and 1426+428 were performed by ASKA During 1994-1996 estimating flux levels and SEDs (Kubo et a. 1998). Afterwards, *BeppoSAX* performed spectral observations of almost all objects of our target during 1996 – 2001 through the passband of 0.1-10 KeV (Beckmann et al. 2002, Costamante et al. 2001, Tagliaferri et al. 2003, Wolter et al. 1998). The values of X-ray fluxes and SEDs were derived. No flux variations were detected. It was concluded the synchrotron peak of 1426+428 to lie near or above 100 keV.

1959+650 was observed with *USA* (*Unconventional Stellar Aspect*) about once a day between 2000 September 21 and November 11 through 1-17 keV passband estimating its X-ray flux (Giebels et al. 2002). *RXTE/PCA* (*Rossi X-Ray Timing Explorer/Proportional Counter Array*) observed 1959+650 during 2000 July –November. Both devices revealed that the source was bright and variable with the X-ray spectrum significantly harder than that observed during the periods of lower brightness. Variability with the factors of ~6 and ~3 were detected within 20 days and 7 days, respectively. The source did not appear to vary significantly shorter than a day. The variations were greater in the harder bands in the case of *PCA* observations. The X-ray spectrum followed a “loop” in the spectral index-flux plane, showing significant evolution during the flare so that there was a more rapid rise and drop in the hard X-ray band. It was concluded that the X-ray spectrum hardens as the source brightens end the Doppler factor of the jet was estimated to be greater than 1.6.

1ES 2344+514 was studied by *All-Sky Monitor (ASM)* on board of RXTE for the same time period as Whipple observations 2000 (Badran 2001). The object was investigated in three energy bands: 1.5-3.0, 3.0-5.0 and 5.0-12.0 KeV. No significant variations were detected (especially in 5.0-12.0 keV band). Later, 1ES 1426+428 was observed by the same instruments in 2002 (Falcone et al. 2004). Besides, 1ES 1959+650 was observed by *RXTE* during multiwavelength campaign 2002 in a flare state (3-25 keV passband) (Krawczynski et al. 2004). X-ray flux and spectra of 1ES 1426+428 exhibited significant variability at the timescales ranging from one day up to two weeks, implying the variability in the location of first peak of the SED.

High signal-to-noise X-ray spectrum of 1ES 0323+022, 0414+009, 0647+250, 1028+511, 1426+428, 1959+650 were obtained with *XMM-Newton* X-ray telescope during 2001-2002 (Perlman et al. 2005). In the case of 1ES 1426+428, the spectrum showed an absorption lines with equivalent width of 40 ± 10 mÅ at 10.23 Å, and could be identified as Ne Ly β .

1ES 1959+650 was investigated by *RXTE* simultaneously with *VERITAS*, Bordeaux Optical Observatory and the University of Michigan Radio Astrophysical Observatory during 2003 May 2 – 2003 June 7, when the object showed the increased level of X-ray activity (Gutierrez et al. 2006). The 10 keV X-ray flux was strongest on May 18–20. It decreased slowly by a factor of 18.7 from the maximum on May 20 to a minimum on June 17. Then X-ray flux stayed at a consistently high level: a factor of 1.7 below the maximum flux observed at the beginning of the campaign and a factor of 11.5 above the minimum flux measured on June 17. During the 2003 campaign, the highest X-ray fluxes observed were lower by a factor of five than the highest fluxes observed in 2002.

X-ray observation of 1ES 1426+428, 1959+650 and 2344+511 were performed with *Swift* in 2005 (Tramacere et al. 2007). X-ray fluxes and SEDs through 2–10 keV were investigated. 1ES 1426+428 showed larger variability in the X-ray band than at UV frequencies. Note that the flux at 0.3 keV was also rather stable in comparison with that at energies higher than 1 keV. 1ES 2344+514 was observed by *Swift* in three occasions when 2–10 keV flux was quite steady.

1ES 1959+650 was observed with *Suzaku* and *Swift-XRT* from May 19, 2006 to May 25, 2006 in the 0.2–12 keV band (Tagliaferri et al. 2008). Besides the variability of a factor of 2 in flux, the peak of the synchrotron component was moving to higher energies with the increasing flux. During the monitoring of more than two days, the source showed also some rapid variability. The data track a flare of small amplitude ($\sim 10\%$) with a rising time of $t_r \approx 20$ –30 ks. The variability was faster in the 2–10 keV band than in the 0.2–2 keV band.

1ES 2344+514 was observed by *Swift XRT* for 9 occasions and *RXTE PCA* for 52 occasions from October 2007 to January 2008. The highest known X-ray flux was recorded by SWIFT on December 8, with an X-ray power law index ranging from 2.7 ± 0.2 to 1.87 ± 0.04 .

Swift observed 1ES 1426+428 with short snapshots of 1–2 ks each from May 28 to June 10, overlapping with *MAGIC* observations when possible. The joint Japanese-US satellite *Suzaku* covered the soft and hard X-rays region (0.4–70 keV). The observations were carried out between June 5 to June 8 for a total time of 100 ks. The target was detected both by *Suzaku* and *Swift*. From the comparison with historical data it can be seen that *MAGIC* observed the source during a low VHE state, while the corresponding X-ray flux is not so low: the absolute value shows a moderate activity, but the slope is quite different from that obtained with previous observations. The historical X-ray data taken during the VHE outburst show a hardening of the spectrum with photon index < 2 with the synchrotron peak at higher energies, up to 100 keV.

Currently, all the targets have been monitored intensively by *RXTE* (see http://xte.mit.edu/ASM_lc.html).

2.2 Optical Observations

X-ray discoveries were followed by the optical identifications. Ulmer et al. (1983) performed optical identification of 1ES 0419+009 via spectral and broad-band photometrical observations carried out with the 4 m telescope of Kitt Peak observatory on November 18, 1981. It was concluded the source to be probably a BL Lacertae object. Photometrical work was done with the Mark II photometer on the Kitt Peak 1.3 m telescope. The same authors examined also 325 plates from Harvard archive, taken between 1890 and 1949, to see whether the object might have had a large optical outbursts in the past. The object was invisible on almost all these plates (their faint limits ranged from about 14 to 16 mag). It was not found in Kukarkin variable stars catalogue and in Ohio radio source catalogue, too.

The optical identification of 1ES 0323+02.2 was performed by Doxsey et al. (1983) with the 1.3 m telescope at the McGraw observatory in 1980 December which obtained $V = 16.38$, $B - V = 0.49$ and $U - B = -0.50$. It was concluded that 0323+022 could plausibly be a Bl Lacertae object. The spectral observations, carried out by same authors during 6 different night at the same telescope, did not show the absorption features. Margon & Jacoby (1984) obtained four consequent R -band images of 1ES 0323+022 and its vicinity on 1983 October 12, using 91 cm reflector of the Kitt Peak observatory and RCA CCD detector. They revealed 1ES 0323+022 to be spatially extended. This result was quickly confirmed by Feigelson et al. (1986), observing the source with the same telescope on November 28, 1983 through V filter. An elliptical galaxy of $M = -21.6 \pm 0.7$ at $z \approx 0.15$ was detected. The same authors carried out optical photometry in August, 1982 with 91 cm reflector of the Kitt Peak observatory. No intra-night variability was found. The target's brightness decreased with 0.135 ± 0.01 and with 0.062 ± 0.009 mag between two consecutive nights. Later, V band observations with Cerro Tololo 0.9- and 1.0-m telescopes showed a decrease with $\Delta V \approx 0.4$ during four days, while B and U magnitudes stayed relatively constant. $BVRI$ CCD observations, performed in 1982 December at McGraw-Hill, did not show optical flux changes within or between the consecutive nights. The average values were $V - R = 0.46 \pm 0.02$ and $V = 16.08 \pm 0.01$. The same authors performed the optical polarization measurements during 7 nights between October, 1983, and January, 1984 with the 1.5 m. telescope at the Cerro Tololo Inter-American Observatory, and the 2.2 and 1.55 m telescopes of Steward Observatory, in the spectral range of 5000-9000Å. The polarization varied between 2% and 9%. It was changing in both position angle and intensity within 24 hr.

Bradt et al. (1985) carried out UBV CCD photometry during 19-24 September, 1984 at McGraw-Hill within the frame of coordinated multiwavelength observations. They revealed the object to be faint with steady colors $V=16.56\pm0.05$, $B-V=0.47\pm0.04$, $U-B=0.62\pm0.04$.

Filippenko et al. (1986) obtained the high-quality spectra of 1ES 0323+02.2 at the Hale 5-m telescope on 1984 February 24. They revealed absorption lines (Na D, Ca II H and

K, G band) which allowed to determine the redshift. The same work was performed successfully by Halpern et al. (1991) using the Lick 3 m telescope on 1986 October 2.

The optical identification of 1ES 1426+428 was done by Remillard et al. (1989) using the data of photometrical (*KPNO* 1.0 m telescope) and spectral (1.3 m McGraw-Hill telescope) observations performed during 1983 -1989. They revealed an featureless spectra typical for BL Lacertae objects. The object was re-observed with the same telescope and spectrograph on May 19, 1985 during 2.0 hours in order to discover the absorption features. It was revealed the weak lines corresponding to the redshift of about 0.129. This result was confirmed at higher resolution, using the same telescope and Mark III CCD spectrograph on February 6 and 11, 1988. The *V* magnitude varied between 16.42 and 16.54 during six years (the source was observed four times).

Pica et al. (1988) presented the optical variability monitoring results of 1ES 0323+02.2 and 0414+00.9 performed at Rosemary Hill Observatory between 1984 - 1987 with 0.76 and 0.46m telescopes through *B* Band. The average value was 17.48+0.09 for the first object without evident variability. As for 1ES 0414+009, the overall brightness variation was $\Delta B = 0.93$ in 3 years with a minimum brightness $B=18.09$.

Jannuzi, Smith & Elston (1993) reported significant brightness variations in 1ES 0323+022 on basis of 101 sessions, performed during 1987 September–March 1990. The following values were recorded: $B = 16.90\text{--}17.34$, $V = 16.13\text{--}17.03$, $R = 15.91\text{--}16.19$, $I = 15.26\text{--}15.60$.

Intending to find the redshift of 1ES 0414+009, Halpern et al. (1991) performed spectroscopic observations with the *UV* spectrograph attached to the Lick 3-m telescope on October 2, 1986. They found $z = 0.287$, according to the weak absorption lines. McHardy et al. (1992) obtained $R = 16.64$ and $V = 17.21$ (1989 March, Kitt Peak 4-m telescope).

Based on the observations performed at European southern observatory (ESO) 1.52-m and Asiago 1.8-m telescopes, Falomo, Bouchet & Tanzi (1989) and Falomo & Tanzi (1991) found an increasing trend of $V = 17.5\text{--}16.8$ for 1ES 0414+009 during 1987–1989. Moreover, $R = 16.6$ in the case of 1989 August 12 observations. The derived contribution of stellar component, due to the host galaxy, was $\sim 8\%$, corresponding to $M_V = -22.2 \pm 0.5$.

Falomo et al. (1994) Presented the optical spectra of 1ES 0323+02.2 and 0414+00.9 obtained at ESO 1.5 m telescope with IDS and CCD detectors. The spectral energy distributions and spectral indices were obtained. Wurtz et al. (1997) observed the same objects with Canada-France-Hawaii 3.6 m Telescope on 1991 January 14 in order to reveal object's membership to any galaxy cluster. No positive results were obtained for the first object, but the second one was found to be a member of the cluster situated at $z \sim 0.3$.

The optical identifications of other our targets as BL Lacertae objects were made Shachter et al. (1993) using the spectra obtained with MARK 3 CCD spectrograph at Michigan/Dartmouth/MIT 1.3 telescope (see Fig. 2.1 as an example of typical blazer spectrum). The optical polarimetric observations of 1959+650 was performed by Marcha et al. (1996) at 90-inch and 61-inch telescopes of Steward Observatory during 1992 -1993. Its polarization was found of more than 2%. They also obtained the object spectrum at the Multiple Mirror Telescope on Mt Hopkins, on 1992 November 2-3 night, and found it featureless.

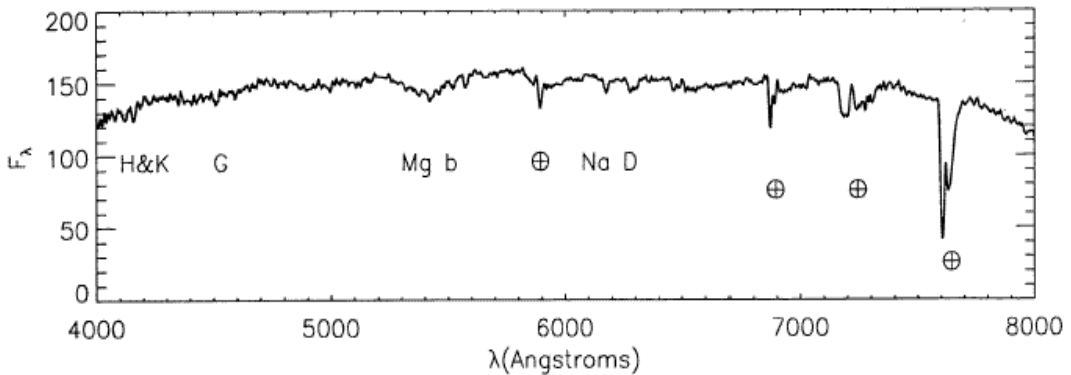


Figure 2.1: Optical spectrum of 1ES 1959+650 (Schachter et al. 1993)

Fiorucci & Tosti (1996) derived $\bar{R} = 16.28$ with $\Delta R = 0.40$ during the optical monitoring of 1ES 0323+022 (0.40m Automatic Imaging Telescope, Perugia University Observatory February, 1993 – January,1995). Xie et al. (1996) presented *BVRI* data concerning the same source taken between December 7, 1993 and December 31, 1994 (1m telescope, Yunnan Observatory). No significant variations were detected ($R = 16.15 – 16.41$) contrary to Bai et al. (1998), which observed the object with the same telescope during November 1996 to January 1997 (see below).

Perlman et al. (1996) obtained a spectrum of 1959+650 at Kitt Peak National Observatory, using 2.1 m telescope and Goldcam spectrograph. It exhibits weak absorption lines H&K, G, Mg b, Na etc. According to them, they derived $z=0.048$.

Reiteri et al. (1998) observed 1ES 0414+02.2, 0502+675, and 1517+656 during 1996–1997 with 1.05 m telescope of Torino Observatory. The first object was found in a high state with $R = 16.18–16.40$. 1ES 0502+675 showed an increasing trend with a maximum variation $\Delta R = 0.58$. The third source was also in a high state: $R = 15.95–16.10$. It exhibited very flat spectrum: $V-R \approx B-V \approx 0.35$.

The low limit on the redshift of 1ES 1ES 1517+656 was derived by Beckmann, Bade & Wucknitz (1999), based on FeII and MgII absorption lines. An optical spectrum of 1ES 0414+009 was obtained at Kitt Peak National Observatory, using 2.1 m telescope and Goldcam spectrograph, which spectrum exhibits weak absorption lines H&K, G, Mg b, Na etc. According to the identified weak absorption lines one derived $z=0.139$ (Perlman et al.

1996). Pomolsky et al. (1997) performed optical spectroscopy of 1ES 1028+511 at Kitt Peak 2.4 m Telescope on 1996 January 12. They obtained two spectra of 1800 and 3600 seconds duration, which exhibited strong, narrow forbidden lines of oxygen, neon, and sulfur, as well as the hydrogen Ballmer series allowing to determine object's redshift.

Scarpa et al. (2000) published the results of *Hubble Space Telescope (HST)* observations of almost all the targets performed during 1996–1997. Especially puzzling is the image of 1ES 1517+675. A bright, unresolved BL Lac nucleus is surrounded by three arcs describing an almost perfect ring of radius 2''.4. The ring is off-center by $\sim 0''.5$ with respect to the BL Lac object. Given the low signal-to-noise ratio in this image, it is also possible that the arclets describe two different rings centered on the BL Lac object. The two bright, resolved spots at position angles 126° and 260° have magnitudes and 23.8 mag, respectively. The authors proposed three possible explanations of this feature: (a) the arks are gravitationally lensed images of an extended background source; (b) the arks are physically associated with the object, either as nearby structure or as part of the host galaxy; (c) the arks are spiral arms of an intervening face-on spiral galaxy. In the case of 1ES1959+650, we have an elliptical galaxy plus a point source One obtained $m_R = 14.92 \pm 0.05$ and $r_e = 5''.1 \pm 0''.1$ for the galaxy and $m_R = 15.4 \pm 0.1$ for the point source. Some small deviations from Vaucouleurs law indicate a disturbed morphology. A dust lane is apparent along the major axis, $\sim 0''.2$ north to the nucleus. 1ES 2344+514 possesses the brightest host among the targets well described by Vaucouleurs law (Fig. 2.2). The same should say with respect to 1ES 0229+200, 1426+428, 0414+009 (much fainter host), 0806+524. For the last object, An unusual thing is the large arc-like structure 1''.93 south of the nucleus. The host of 1ES 0647+250 remains unresolved.

At *HST* resolution, 1ES 0502+675 was found to be clearly double, with separation of only 0.''33 and surrounded by a host galaxy. A careful comparison of the two radial profiles showed that the brighter object is more extended than the fainter one. The best fit yielded a point source of $R = 17.3 \pm 0.1$ and a surrounding galaxy of total magnitude $R = 18.9 \pm 0.1$ and half-light radius $r_e = 0''.6 \pm 0''.07$. Even at *HST* resolution the alleged companion is unresolved, and the difference in luminosity between the two objects is much less than the typical several magnitudes between BL Lac objects and companion galaxies arguing against the suggestion that they are companion objects. So, 1ES 0502+675 became one of the gravitational lens candidates. But the optical spectra, obtained with the Space Telescope Imaging Spectrograph (STIS) on 2001 March 9, indicate that the second nucleus is a galactic star.

The observations of 1ES 0414+009 were performed with *FORS1* mounted at the Cassegrain flange of *VLT - UT1* of *HST* on 1998 September 27/28 through the Bessel *B*, *R* and *I* filters (Heidt et al. 1999). The host galaxy of was well resolved in *R* and *I*, and

Table 2.2: characteristics of host galaxies of the sample

Object	Host Type	R_{host}	r_{eff} (in arcsec)	ϵ	$F_R(\text{mJy})$
1ES 0229+200	E ¹	-----	3.25 ± 0.07^1		0.98 ± 0.10^3
1ES 0323+022	E ¹	---	----	--	----
1ES 0414+009	E ¹	1749 ± 0.02^1	4.70 ± 0.50^1	--	----
1ES 0502+675	U ¹	18.90 ± 0.09^1	0.60 ± 0.07^1	--	----
1ES 0647+250	N ¹	$>19.10^1$	-----	--	----
1ES 0806+524	U ¹	16.10 ± 0.07^1	4.6 ± 0.2^3	--	0.75 ± 0.04^3
1ES 1028+511	U ¹	18.60 ± 0.22^1	2.0 ± 0.7^3	--	0.10 ± 0.02^3
1ES 1426+428	E ¹	15.93 ± 0.05^1	4.2 ± 0.2^3	--	0.96 ± 0.04^3
1ES 1517+656	E ¹	$>19.89^1$	-----	--	----
1ES 1959+650	E ¹	15.08 ± 0.03^1	6.4 ± 0.1^3	--	2.12 ± 0.05^3
1ES 2344+514	E ¹	13.90 ± 0.06^1	10.9 ± 0.6^3	0.	4.53 ± 0.05^3

^a E = elliptical , N = not resolved, U = host resolved but morphologically unclassified

¹ Scarpa et al. 2000

² Feigelson et al. (1986)

³ Nilsson et al. 2007

⁴ K. Nilsson, private communication

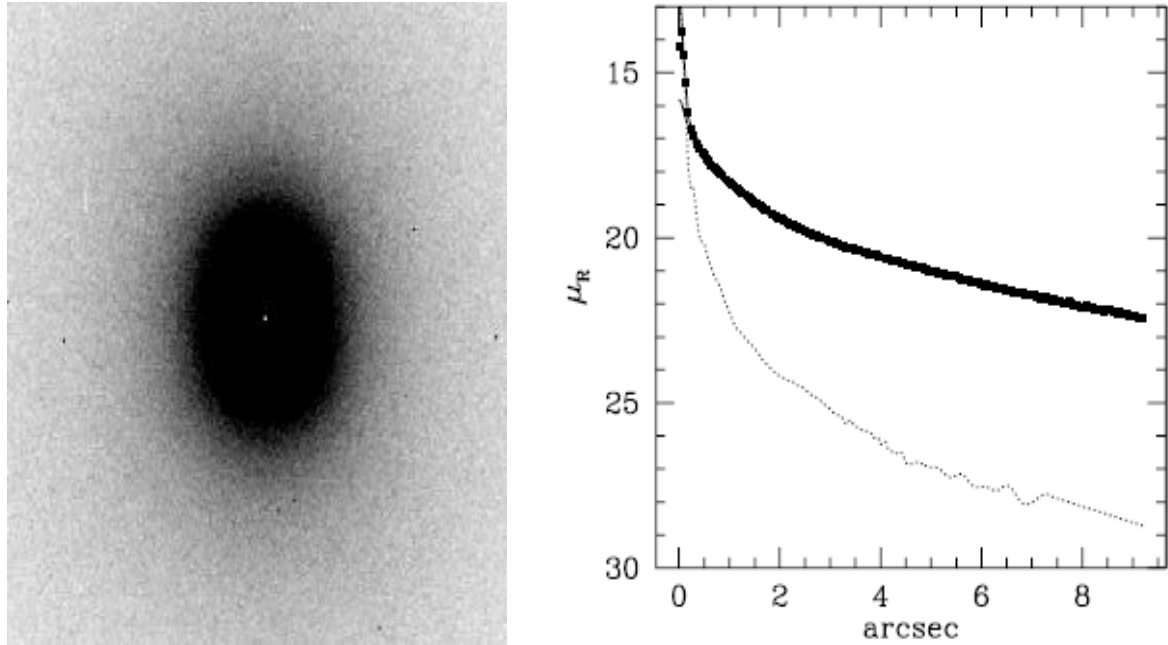


Figure 2.2: Image and de Vaucouleurs profile of the host galaxy of 1ES 2344+514 obtained by *HST* (Scarpa et al. 2000).

marginally resolved in *B*. One found a large and very luminous elliptical galaxy ($M_R = -24.6$, $r_e = 35$ kpc) with colors commonly found in elliptical galaxies ($B-R \sim 1.45$ and $R-I \sim 0.45$).

Villata et al.(2000) observed 1ES 0323+022, 1028+511, and 1959+650 with the 1.05 m telescope of Torino Astronomical Observatory revealing significant optical variations during 1996-1999. The first object showed significant variability with $\Delta R = 0.67$ and maximum brightness $R = 16.16$. The second one less variable: $\Delta R = 0.18$ with a maximum brightness $R = 16.53$. 1ES 1959+650 showed revealing rapid brightness changes. In particular, a decrease of $\Delta R=0.28$ in 4 days was recorded. The overall brightness change $\Delta R = 0.42$.

Tommasi et al. (2001) carried out polarization observations of 1ES 0414+009 at the 2.5 m NOT equipped with *Turpol* during 1999 December 10-15. One obtained $P_V(\%)=3.6 \pm 0.8$, $V=17.06 \pm 0.08$.

1ES 1028+511 and 2344+514 were observed by Xie et al. (2002) using Yunan 1.02 m telescope through V , R Bands in 2000-2001. The first source revealed a variation $\Delta R = 0.18$, with a maximum brightness $R = 16.53$. The second one underwent no significant variations in a day. The intraday maximum flickering amplitude was $\Delta V=0.18$ mag. $\Delta R=0.1$ mag. A brightness decreased of 0.35 mag (V band) between in 14 days.

1ES 1959+650 was observed by Falomo et al. (2002) in 2001 June, in order to determine BH mass by stellar dispersion, using the 2.5 m *Nordic Optical Telescope (NOT)* equipped with the *Andalucia Faint Object Spectrograph and Camera (ALFOSC)*. One obtained $\sigma = 195 \pm 15$ km s⁻¹, corresponding to $\log(M_{\text{BH}})=8.12 \pm 0.13$ (M_\odot).

Tagliaferri et all. (2003) observed 1ES 1959+650 for about nine hours in R band during the night of September 28-29 2001 with the 50 cm telescope of the Astronomical Station of Vallinfreda (Rome). The source remained constant around a mean value of $R=14^m.67$. In order to evaluate the contribution of the host galaxy within the used photometric radius, one computed its R magnitude, deriving $R=15.66$ according to Scarpa et al. (1999) method and $R=15^m.95$ following Heidt et al. (1999). Following observations were performed by Krawczynski et al. (2004) with 0.4 m Boltwood Observatory telescope during multiwavelength campaign 2002 between May 18 and August 16, using broadband B , V , and I filters. One revealed variations of about 0.1 mag on typical timescales of about 10 days. The mean optical brightness increased from during the campaign by about 0.1 mag in all the three optical bands.

Multiwavelength campaign 2006 included optical R band observations with Perugia 40 cm, *KVA* 35 cm (La Palma) and Tuorla 1.03 m telescopes (in the whole, this monitoring was stretched over the period from June 2004 to August 2006). During the more intense monitoring of May-June 2006, centred around the multiwavelength campaign, the source showed a variability of 0.1-0.2 mag around a mean value of 14.4 (including the host). In particular, in the period May 25 - June 1, the R flux increased by about 40% at odd with the 2-10 keV X-ray flux, that instead shows a decrease in the period May 25-29.

Gupta et al. (2008) observed 1ES 2344+514 on January 12, 2007 in R band at Yunnan 1.02 m telescope (1.89 hr). The source exhibited no intra-night variability ($C=1.44$) with a mean R magnitude of 14.65.

1ES1426+428 was observed with *KVA* 35 cm telescope during 3 months overlapping the multiwavelength May-June, 2008 (Leonardo et al. 2009). The light curve shows an increase the optical flux by 20 % (the contribution from the host galaxy and nearby stars ($F=0.88$ mJy) was subtracted from the overall flux).

Currently, all our targets are the subject of intensive *R*-band monitoring by means of 1m telescope of Tuorla observatory (see <http://users.utu.fi/kani/1m/>).

2.3 Radio Observations

The radio-counterpart of 1ES 0323+022 and 0414+009 was identified by Feigelson, Giommi and Maccacaro in 1982 with *NRAO VLA* observations at 5 GHz (Doxsey et al. 1983). The first object showed the flux changes of 15% in 24 hours to 50% in 5 weeks (Brandt et al. 1985). This object later observed again by *VLA* between 1982 September and 1984 March at the frequencies 1.4, 4.9 and 15 GHz by Feigelson et al. (1986). The respective fluxes were $(65\text{-}90)\pm0.5$ mJy, $(41\text{-}66)\pm0.5$ mJy and $(29\text{-}57)\pm1$ mJy. So, the object varied by $\sim40\%$ at all the three frequencies on time scales of days and longer. No correlation between intensity and spectral variations was found. Linear polarization was present at 5% (1.4GHz) and 6% (4.9 GHz) of the total intensity. No circular polarization was found.

First radio observations of 1ES 1426+428 were performed in 1983 by 27 antennas of the *NRAO VLA* at 1.4 GHz (Remillard et al. 1989). One yielded the flux of 33.7 ± 2.0 mJy (Remillard et al. 1989).

The follow-up observations of 1ES 0323+022, 0414+009, and 1426+428 with *VLA* were performed during 1986-1991 (Laurent-Muehleisen et al. 1993). Radio fluxes of compact and extended parts of the objects, as well their polarizations were measured. 1ES 0323+022 was found to be very core-dominated radio source with a faint diffuse halo at 1.5 GHz A-configuration image extending about 3" to the northeast. The 5 GHz data showed a definite extension to the South-East (the same authors). The 1.5 GHz C-configuration revealed no clear evidence of the diffuse halo on larger scales. 1ES 0414+009 exhibited a jet which broke up at about 20 kpc from the core.

The *VLBI* radio-observations of 1ES 0323+022 and 1426+428 were perormed at 5 GHz on 1991 June 7 using a nine-element array consisting of Effelsberg (100 m), Medicina (32 m), Green Bank (43 m), Haystack (36 m), Owens Valley (40 m), the Kitt peak (25 m) and Los Alamos (25 m) telescopes, the phased *Westerbork Synthesis Radio Telescope* (14×25 m), and the phased *VLA* (27×25 m). The objects fine radio structures were obtained (see Kollgaard et al. 1996). 1ES 0323+022 exhibited a faint jet extending toward the south and than banding toward the west, like the helical structure. It was suggested that the jet could be oriented at

a very small angle to the line of sight, which is consistent to rapid variability detected by Feigelson et al. (1996).

All the objects of our target, except for 1ES 0323+022 and 0414+009, were observed with the *VLA* in *CnB* array at 1.4 GHz on 1992 January 26-27 estimating their radio fluxes (Perlman et al. 1996). 1ES 1517+656 consisted of an unresolved core with no evidence of extended emission (Kollgaard et al. 1996). The objects were later studied with the *NRAO VLBA* at 5 GHz on 1997 May 17 and with *VLA* at 1.4 GHz in B array during 1997-1998 (Rector et al. 2003). 0229+200 showed a jet extending to the south, with a weak evidence for a broad opening angle of about 30°. The jet of 1ES 0414+009 was extended to the east-northeast of the core. There was also weak, extended emission to the southeast of the jet, leading to the suggestion that either the jet was collimated and bent to the south to the south about 10 pc from the core, or that the projected jet opening angle should be wide (~60°). 1ES 0806+524 exhibited a jet directed to the north. Very faint, diffuse extended emission, surrounding the jet, gave rise to the idea that it should have a broad opening angle as wide as 70°. 1ES 1959+650 showed a wide (~55°) diffuse jet directed to the north. In the case of 1ES 2344+514, the jet was extended to the southeast well-collimated for about 10 parsecs before bending 25° to the south and broadening into a cone with a ~35° opening angle. The extended structures were not expressed clearly for other sources.

Afterwards, 1ES 0502+675 was observed with the *NRAO VLA* in 1999 at 8.4, 15, and 22 GHz intending to find extended radio emission. Neither extended structure nor flux variability were found (Giovannini et al. 2004).

Intending to investigate radio jet structure and dynamics, Piner & Edwards (2004) observed 1ES 1959+650 and 2344+514 with the VLBA at 15 GHz during 1999-2000 in order. The images revealed an intriguing morphology of the first object showing a short jet extending 1 mas to the southeast of the. In addition, there was a broad, diffuse emission to the north of the core. Later (in 2002, Giroletti et al. 2004), VLBA observations confirmed a peculiar two-sided structure. It was suggested that the source should be oriented in the plane of the sky and/or that the jet is non relativistic on the arcsecond scale. As for 1ES 2344+514, VLA images showed two bright components within 200'' (180 kpc) from the position of the optical and radio-core. Furthermore, extended, low-brightness emission was presented between the core and the eastern feature indicating that this component is related to the source. On contrary, the NW component did not show any radio structure suggesting a connection.

Krawczynski et al. (2004) used the University of Michigan 26 m paraboloid to monitor 1ES 1959+650 at 4.8 and 14.5 GHz between 2002 May 5 and August 9. The 14.5 and 4.8 GHz radio data do not show any significant flux variations. Additional flux density measurements were made with *NRAO VLA* at frequencies of 43.315, 22.485, 14.965, 8.435, and 4.885 GHz on 2002 May 7 and June confirming the radio flux to be invariable.

VLBA map, obtained for 1ES 1426+428 by Piner, Pant & Edwards(2008) in 2003, shows a difference of 458 in a position angle of the jet during 12 years. The authors refrained from applying jet precession hypothesis to this fact. They noted that two position angles measured twelve years apart are not enough to place any constraints on such a motion.

1.4 Infrared Observations

Infrared observations of the sample are very few. The measurements performed with the *Infrared Telescope Facility* at Mauna-Kea for 1ES 0323+022 through *JHKL* bands showed a pronounced infrared flux ($J=14.36$, $H=13.69$, $L=12.60$, Doxsey et al. 1983).

1ES 0323+022 and 0414+009 were investigated by *IRAS* (Impey & Negebauer, 1988) at 12, 25, 60, 100 μm wavelengths. Infrared fluxes of these objects were estimated. 1ES 0323+022 was observed on 1986 January 8 with the “*Hermann*” *InSb* photometer on the Kitt Peak 1.3 m. teleskope through *K* band (Sitko & Sitko 1991). The obtained *K* magnitude was equal to 13.22 ± 0.12 .

Ballard et al. (1990) carried out Infrared polarimetric observations of 1ES 0323+022 and 0414+009 at *United Kingdom Infrared Telescope* on 1986 August and 1987 September deriving the values of 3.84% and 7.82% respectively.

During 1988-1989 *IR* observations of 1ES 0323+022 were carried out at *ESO* 3.6 and 2.2 m telescopes using standard *ESO infrared and InSb* detectors (Falomo et al. 1993). The infrared flux variations through *JHK* bands were investigated.

HST NICMOS Camera 2 obtained the *H*band images of 1ES 0229+200 and 0502+675 on January 6, 1998. The first source was found to be a bright elliptical galaxy with point-like object in the centre and the second one - with double nucleus, surrounded by a galaxy (Scarpa et al. 2000).

1ES 1426+428, 1959+650, and 2344+514 were observed with 2.5m *NOT* on 2002 using *NOTCam NIR* camera through *H* band (Kotilainen & Falomo 2004), corresponding to the minimum in the nucleus/host luminosity ratio for low redshift objects. The parameters both of nuclei and host galaxies were estimated.

1.5 Gamma-ray Observations

First gamma-ray observations of our targets were carried out during 1993 March 8 -22 for 1ES 1517+65.6 by *Compton Gamma-Ray Observatory (CGRO)* through 0.05-10 MeV range. The γ -ray SED of the object was investigated (McNaron-Browne, 1995). The object was later

investigated by *EGRET* mounted on board of *CGRO* and by *Whipple* 10 m. Cherenkov-type telescope, but the source was not detected and only upper limits were estimated (in 1995, Weekes et al. 1996)

1ES 0229+200, 0323+022, 0806+524, 1028+511, and 2344+514 were observed with *Whipple* during 1995-2002 (Catanese et al. 1998, Horan et al. 2002, Horan 2004). 1ES 2344+51.4, as a TeV object, was detected by Catanese et al. (1998) with this telescope during October, 1995 – January, 1997. There were revealed a flaring activity in both the 1995/96 and 1996/97 observing seasons. The TeV emission was detectable only in 1995/96 and only with unambiguous statistical significance on 1995 December 20 when the object was most variable and underwent a flare with the duration of about 2 hr with an average flux of F_{γ} (>350 GeV) = $(6.6 \pm 1.9) \times 10^{-11}$ photons/cm²s, which is about 0.63 of the *Crab* flux. In the case of 1996-1997 season, the observations revealed no evidence of significant variability.

HEGRA observations of 1ES 2344+514 were carried out during December 22-30, 1997. The obtained data did not indicate any TeV emission (Konopelko et al. 1999). Second observational campaign was carried out with *HEGRA* from August to November, 1998 for about 1 hour of exposure time during each moonless night detecting TeV signal several times. The highest diurnal excess rate was detected on November 11 with a 3.2σ significance. This rate corresponds to 0.63 *Crab*, which corresponds to a flaring activity (>0.5 *Crab*). In addition, 1ES 0229+200, 0323+022, 0414+009, 0647+250, 1959+650, and 2344+514 were examined with *HEGRA* during 1996-2002 (Aharonian et al., 2000, 2003; Tluczykont et al. 2003). In all the cases γ -ray fluxes and corresponding SEDs were investigated. Later, in 2000, the object was monitored again with *Whipple* detecting TeV emission at the 3σ level. There was no strong indication of flaring activity during the whole period (Badran 2001).

1ES 1426+428 was monitored by the *CAT* telescope from February 1998 to June 2000 above 250 GeV revealing TeV photons (Djannati-Ataï et al. 2003). The most energetic photons corresponded to 10 TeV. The source exhibited very steep spectrum with a differential index of $\alpha = -3.66 \pm 0.41$, which supported the suggestion about the strong absorption of VHE emission by the extragalactic infrared background. The strongest evidence of VHE emission was recorded during the 2000 and 2001 observing seasons, with the signals at the 3.1σ and 5.5σ levels, respectively, being detected. No correlation between *Whipple* gamma and *RXTE* X-ray simultaneous observations was found. The differential photon detection rate peaked about at 280 GeV.

The first detection of 1959+650, as a TeV object, was made by Nishiyama et al. (1999) using the Utah Seven Telescope Array detector. The observations were carried out during May 18 - August 30, 1998. The evidence of TeV emission were obtained with a significance of 5.3σ between May 22 and 31, and 5.0σ between July 1 and 28. The γ -ray flux variability on the timescale of a day scale was revealed.

The intensive VHE observations of TeV objects (1ES 1426+428 and 1959+650) were performed during 2002 by *VERITAS* (Falcone et al. 2004, Holder et al. 2003). The TeV emission from was detected in the case of 1ES 1959+650. The mean flux over all observations was 0.64 ± 0.03 Grab and reached its maximum of 5 Grab (May 17, June 4). During the flaring state, strong night-to-night variability was evident. The variability timescales were as short as 7 hours. On June 4, the source flared dramatically in the gamma-ray range without any coincident increase in the X-ray emission, providing the first unambiguous example of an "orphan" gamma-ray flare from a blazar. The gamma-ray spectrum of these data can also be described by a simple power law fit with $\alpha = 2.82 \pm 0.15\text{stat.} \pm 0.3\text{sys}$ (Daniel et al. 2005). The *Whipple* observations were quickly followed up and confirmed by *HEGRA* (Aharonian et al. 2002, 2003) and *CAT* (Djannati-Ataï 2003).

Taking into account its SED, Stecker, de Jager & Salamon (1996) suggested that 1ES 0229+200 is a potential source of VHE photons. After several unsuccessful attempt (*Whipple* (Horan et al. 2004), *HEGRA* (Aharonian et al. 2004), *Milagro* (Williams 2005), *HESS* detected VHE signal at the 6.6σ level during 2005–2006 observations (Aharonian et al. 2007). The observed spectrum was described by a hard power law from 500 GeV to ~ 15 TeV. This detection made 1ES 0229+200 the most distant source detected at multi-TeV energies. No evidence for significant variability on any time scale was found.

VHE gamma-ray observations of 1ES 1959+650 were performed during September–October, 2004 at a time of low activity in both optical and X-ray wavelengths, using the *MAGIC* telescope (Albert et al. 2006). The light curve, sampled over 7 days, shows no significant variations. The differential energy spectrum between 180 GeV and 2 TeV is consistent with the slightly steeper spectrum seen by *HEGRA* at higher energies, also during periods of low X-ray activity. *MAGIC* observed very high energy gamma ray emission from 2344+514 during between 2005 August 3 and 2006 January 1 (Albert et al. 2006b). No significant time variability has been observed. The corresponding SED was investigated.

VERITAS has observed the blazar 1ES 0806+524 for a total 65 hours from November 2006 to April 2008 resulting in the detection of very-high-energy gamma rays with a statistical significance of 6.3σ (Acciari et al. 2008). The differential energy spectrum between 300 GeV and 700 GeV corresponds to $(1.8 \pm 0.5)\%$ of the Crab Nebula flux. Using the *Swift UVOT* and *XRT* data, taken at March 8 and 12, 2008, target's SED was constructed.

1ES 0647+250 and 0806+524 were observed with *VERITAS* from November 2006 to March 2007. No TeV emission and any flaring activities were found (Cogan 2007).

1ES 2344+514 was observed by *VERITAS* from October 2007 to January 2008, resulting in a detection with a statistical significance of 20.5σ with 580 excess events. The TeV flux showed variability on a daily timescale, with a strong flare recorded on 6/7 December 2007 with an integral flux corresponding to 0.41 ± 0.05 of the Crab Nebula flux above 300 GeV. A linear fit with slope 0.7 ± 0.1 to the almost simultaneous X-ray and TeV

fluxes shows a correlation between X-ray and TeV emission on daily timescales (Cogan 2008).

1ES1426+428 was observed with the *MAGIC* telescope through 11 nights searching for VHE emission during the multiwavelength campaign carried out in May-June 2008 (Leonardo et al. 2009). The analysis did not reveal a significant VHE signal on the level of a few percent of Crab neither using the whole data set nor considering night by night observations. Also the search for a signal in different energy bins did not yield a significant excess.

3 Observations and Data Reduction

In this chapter, I give a detailed description of observational technique, data processing and the methods of blazar variability investigation.

3.1 Observational Conditions and Telescope

The optical CCD observations were carried out during 1997-2007 at Abastumani Astrophysical Observatory, Georgia. As a rule, the observational conditions are good here. The observatory is located at a latitude of $41^{\circ}8$ and a longitude of $42^{\circ}8$ on the top of Mt. Kanobili (1700 m from sea level). One is able to observe up to 150 full nights per year (1/3 of them with seeing <1 arcsec). The mean values of the night sky brightness are $B = 22^m.0$, $V = 21^m.2$, $R = 20^m.6$ and $I = 19^m.8$ (Kurtanidze & Kvernadze 1995).

The observations were carried out at the 70-cm meniscus-type telescope of Abastumani Astrophysical Observatory. The diameter of main mirror is 98 cm. The primary focus (focal length $f = 210$ cm) allows a wide field of view of 4.88×4.88 , and secondary one ($F=10050$ mm equivalent focus length) with $20 \text{ arcmin} \times 20 \text{ arcmin}$ field. It is also possible to perform observations by means of Newtonian focus. The mounting is fork-like.

3.2 Devices

The data were obtained by means of CCD cameras *ST-6* (1997-2006, attached to the Newtonian focus) and *APOGEE-6* (prime focus, since September 2006). Their characteristics

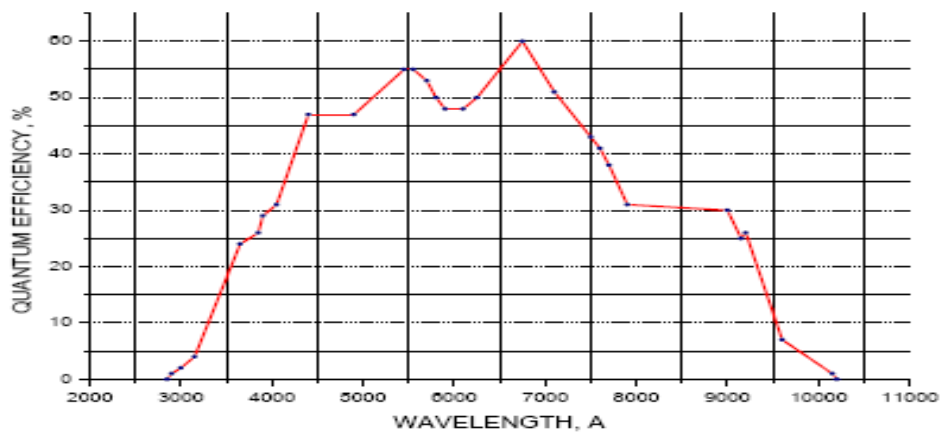


Figure 3.1: Spectral response curve of *ST-6* camera.

Table 3.1: CCD *ST-6* characteristics.

CCD Chip	TC241
Resolution	375x242 pixels
Pixel Size	23 μ x 27 μ
Total Pixels	90,750 pixels
Array Area	8.63mm x 6.53 mm (56.3 mm ²)
QE at 400 nm	30%
Peak QE (675 nm)	60%
A/D gain	6.7e ⁻ /ADU
Frame Buffer	Full Frame Buffer Present
Anti-Blooming	100 x Anti-Blooming Protection Present
Read-out Noise	30 e ⁻ RMS with Double correlated Sampling Sky Background Photon Noise Limited for Exposures Longer than 15 Seconds at F/6
Typical Dark Current	13 e ⁻ /pixel/sec at -20 °C
Field of view	14.6 x 11 Archminutes in 8" f/10 (2000mm focal length)
Pixel Size	2.3 x 2.7 Archseconds in 8" f/10 (2000 m focal length)
Limiting Magnitude	Magnitude 15 in 1 second with 20 cm Aperture Magnitude 19 in 1 minute with 20 cm Aperture Magnitude 20 in 5 minute with 20 cm Aperture
Exposure Time	10 Millisecond Minimum, 1 Hour Maximum
Mounting	1.25" OD Draw Tube
Weight	2.5 Pounds
Power Requirements	2.5A at 5V Maximum
Cooling	Peltier Cooled, -42°C from Ambient
Regulation	+/- 0.5 °C with 5° Setpoints
A/D Resolution	16 Bits
Digitation Rate	11 Seconds for Full Frame Image wothout Double Correlated Sampling, 22 Seconds with Double Correlated Sampling
PC Required	IBM PC, XT, AT, PS-2 or Compatible
Output Signals	RS422 Full Bandwith to 1000 feet RS232 Compatible e for Cable Runs <15 feet
Maximum Baud Rate	115.2K Baud on 100% Compatible PCs
Image Transmission	10 Seconds for Full Frame at 115.2K Baud
Image Sorage and Retrieval Formats	Compressed//Uncompressed//8 or 16 Bit FITS TIFF
Image Size	Full//Half//Quarter
Special Features	Automatic Vane Simplifies Taking of Dark Frames and Enhances Operation With Extremaly Bright Onjects RS422 Driver Allows PCs with RS232 to Drive Serial Cables with Lengths from 15 to 1000 Feet at Full Baud Rate of 115.2K

Table 3.2: CCD *APOGEE6* specifications.

CCD	Kodak KAF 1001E
Array Size (pixels)	1024 x 1024
Pixel Size	24 x 24 microns
Imaging Area	24.6 x 24.6 mm (604 mm ²)
Imaging Diagonal	34.8 mm
Video Imager Size	2.17"
Linear Full Well (typical)	Low noise output: 200K electrons High DR output: 500K electrons
Dynamic Range	>87 dB
QE at 400 nm	39%
Peak QE (560 nm)	>72%
A/D Gain:	2.2 e-/ADU (16 bits)
Anti-blooming	none
PC Interface	Ethernet 100 baseT
Max. Cable Length	100 meters
Digital Resolution	16 bits at 1 MHz (to camera head memory)
System Noise (typical)	8 e- RMS at 1 MHz
Pixel Binning	1x1 to 8 x 1024 on-chip
Exposure Time	30 milliseconds to 183 minutes (2.56 microsecond increments)
Image Sequencing	1 to 65535 image sequences under software control
Frame Sizes	Full frame, sub-frame, focus mode
Cooling (typical)	Thermoelectric cooler with forced air. Maximum cooling 50°C below ambient temperature
Dark Current (typical)	1 e-/pixel/sec (-25°C)
Temperature Stability	± 0.1°C
Camera Head Size	D2. Low profile: D6. Aluminium, hard blue anodized. 6" x 6" x 2.5" (15 x 15 x 6.35 cm) Weight: 3.1lb. (1.4 kg)

Table 3.2-Continued

Mounting	3.5" bolt circle. 2" 24 tpi thread. Optional Nikon F-mount or Canon FD mount
Back Focal Distance	Standard: 1.025" (2.60cm). Low profile: 0.515" (1.308 cm). [optical]
Operating Environment	-22° to 27°C. Relative humidity: 10 to 90% non-condensing.
Cable Length	Standard: 15 ft (4.5m)
Power	40W maximum power with shutter open and cooling maximum. AC/DC "brick" supply with int'l AC input plug (100-240V, 50-60 Hz)
Shutter	Standard: Melles Griot 43mm. Low profile: no shutter.
Remote Triggering	LVTTL input allows exposure to start within 25 microseconds of rising edge of trigger

are provided below in Table 3.1, and Table 3.2, respectively. Fig. 3.1 provides spectral response curve of *ST-6* camera, and Fig.3.2 – the same of *APOGEE-6*.

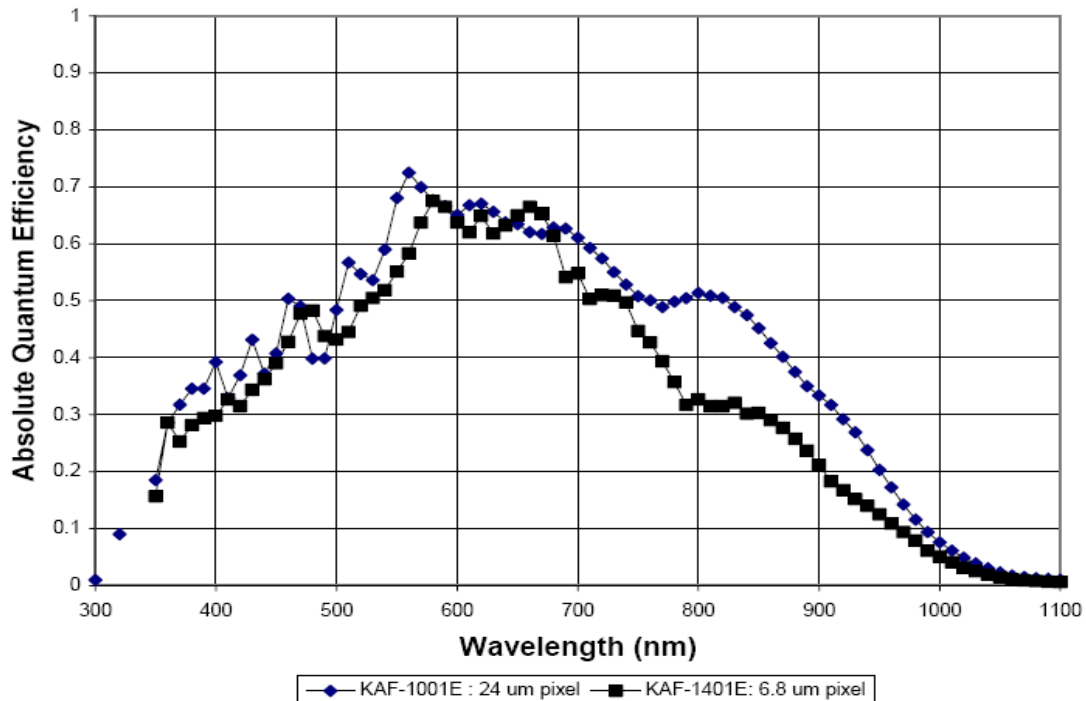


Figure 3.2: Spectral Response curve APOGEE6 camera

(<http://www.megapixelsystems.com/apogee/pdf/ccd6.pdf>)

3.3 Observations

The observations were performed mainly through *R*-band of Johnson-Cousin system due to telescope size and CCD specifications. Most of the targets were fainter than *R* = 16.00 , and

they were more fainter in V band, and especially in B band. The matters became more complicated when the observational conditions were not perfect or the target was in a state of minimal brightness. None of our objects are observed in case of full moon (in point of the accuracy). 1ES 0806+524, 1959+650 and 2344+514, as the relatively bright objects, were observed when moon phase was less than 70% and it was less than 20 per cent for other objects due to their faintness. Exceptions were made when one of the objects brightened up extremely.

The exposure time was fixed so that the counts at the central pixel of the blazar were about 25% below the saturation limit, well within the linear regime of the chip. As a rule, the frames of 3-5 min durations were obtained.

3.4 Image processing

Image processing or pre-processing (bias and dark current subtraction, flat-fielding and cosmic rays removal) are performed using standard routines of *IRAF* (Image Reduction and Analysis Facility). Besides, we use *ST6OPS* and *MaxImDL* softwares developed specially for *ST-6* and *APOGEE-6* devices (mainly during observation process). Photometric reduction or processing of the data were performed by aperture photometric technique using *IRAF/APPHOT* software.

Before an image can be used for photometry it requires a considerable amount of pre-processing in order to reduce and calibrate it. During the astronomical observations, we have to measure or estimate the uncertainties (errors) inherent to that measurement. If we measure the magnitude of a source a number of times, we will not get exactly the same number each time, due to various sources of noise. To prove, for instance, that a star is variable in brightness, we would have to find a change of magnitude several times larger than the uncertainty in our magnitude measurement.

In addition to perform a measure of the uncertainty in the data, a careful understanding of the sources of uncertainty is important, as well as a full understanding of these sources of uncertainty can suggest ways to improve our observing and reduction/analysis strategy.

A crucial concept in photometry is the signal to noise ratio (S/N or sometimes SNR). This is one way of indicating the accuracy of our measurements. Another way is a percentage error (which we can think of as the noise to signal ratio). A S/N of 50, for example, corresponds to a percentage error of about 2%.

For a CCD measurement, there are several sources of noise, as discussed in the section on CCDs. These include photon noise, readout noise, dark current noise, noise in flat-field images. We can remove or reduce their impact on obtained data by means of several pre-processing operations.

The first of the pre-processing steps is bias-subtraction. All CCD chips have what is known as a bias voltage applied to them to prevent the voltage ever dropping below zero as this would damage the chip. So, the bias is an offset of a few hundred counts added to the CCD before start of exposure and it must be subtracted from all images. The usual method of obtaining a bias image is to take a zero-duration exposures with the shutter closed so no light is falling on the chip. The resulting image will then show only the bias voltage applied to each pixel. As a rule, we obtained four or six of bias images at the beginning of the observing session. For each observing night, we generated a master bias by taking median of all bias frames in the night. The master bias frame is subtracted from all the light images.

Once the bias has been subtracted, the next step is to compensate for variations in pixel-to-pixel sensitivity, known as "flat-fielding". This step is necessary because no matter how well manufactured, CCD chips always have subtle variations in pixel sensitivity across the chip. These variations can arise from several sources. The most important of them are variations in optical transmission, quantum efficiency variations, and dust at the optical path. To overcome this problem, one observes a surface with uniform illumination to create a flat-field image which can thereafter be used to correct the images for above mentioned variations.

There are three main ways to obtain flat-field images:

- (1) observe the twilight sky at dusk and dawn through each filter. Here, it is important to ensure that there are no bright stars in the field and to select the relatively short time interval for taking flat-field images;
- (2) observe blank fields on the sky. In this method, several images of a region of the night sky, free from bright objects, are obtained. Each image is slightly offset from the previous image. These offsets enable us to detect faint stars in the field as above average pixel counts moving in tandem with the offsets. These pixels are then masked and the images rescaled to a common median pixel count value. These rescaled images are then compared pixel by pixel to derive a median ADU count for each pixel, which is then taken as the value for the sky. The image produced by these median pixel values can then be used as the flat-field (so-called "median filtering"). While this method does produce flat-fields which match exactly the colour of the sky background of the light images, it does have the major disadvantage of requiring long exposures to produce a high signal/noise ratio which can significantly reduce observing time.
- (3) "dome-flats" – we use the inside of the telescope dome or a whiteboard illuminated with filtered lamps instead of the twilight sky. This method is applied mainly for the nights with bad weather during twilight. There are two difficulties: (a) we need the uniform illumination; (b) QE variations may have a dependence on wavelength. Thus the correction is valid only if the spectral distribution of the light over the filter passband matches that of the object being observed.

Whichever method is used, a number of images should be obtained with each filter for illumination levels close to 1/2 of saturation and after bias-subtraction, are median-averaged in order to reject “spikes” and then scaled to a mean of 1. Once this is done the object image is simply divided by the flat-field image.

The dark current can cause a false signal. In order to remove it, we take a dark frames with the same exposure length as for light images, subtract the bias from the dark frames and investigate the residual signal. In case the later is high, it has to be subtracted from the light images. As a rule, we obtained three dark images for each object and then we used their median average to subtract from light images.

The background signal is made up of several contributions. We have the diffuse sources such as the terrestrial night sky emission, zodiacal light, scattered light inside the CCD camera. There are also contributions from stars and galaxies situated in the field of the target. To determine background signal, the usual procedure is took up at the signal in an annular region centered on the target object. This ensures that at least to first order any gradient presented in the background should cancel out (Da Costa 1992). Indeed, to avoid biasing the result, the inner radius of the annulus should be sufficiently far from the centre of the source in order its contribution to the signal in the background annulus is negligible. In practice, this means to select the inner radius several times greater than the FWHM of the image. As for the size of the outer annulus radius, is should be sufficiently large (in case of uncrowded fields) that it contains many hundred pixels, thereby ensuring that the uncertainty of the determined background is sufficiently small.

In the ideal case of perfect detector (in point of pixel-to-pixel sensitivity) and completely isolated star-like target, the histogram of pixel intensities for the sky annulus (i.e. a plot of a number of pixels corresponding to I intensity against I for the pixels situated within the sky annulus, would have a Gaussian shape. In such a case, it is appropriate to take a mean (being the same as *median* and *mode* – the intensity at which the histogram peaks) of the distribution as a value of sky background. In the real situations, contributions from the wings of stars and galaxies, from cosmic rays, etc. add a positive skew to the histogram which is no longer symmetrical and the *median*, *mean* and *mode* are not equal. Here, the mean is found to be most affected by the contamination and the mode – at least. So, the mode of the distribution serves a best estimate of the background signal.

As a rule, We obtain the signal-to-noice ratio by means of well-known *CCD Equation* (see e.g. Howell 1989):

$$\frac{S}{N} = \frac{N_*}{\sqrt{N_* + n_{pix} (N_{sky} + N_{dark} + N_{RON}^2)}} \quad (3.1)$$

with N_* , the total (sky subtracted) number of photons from the source; n_{pix} , the number of pixels contained within the software aperture; N_{sky} , the total number of sky photons per

pixel; N_{dark} , the dark current in photons per pixel; and N_{RON} , the read-out noise in electrons per pixel.

In the case the source is bright, the CCD equation will be reduced to

$$\frac{S}{N} = \sqrt{N_*} \quad (3.2)$$

since the extra-terms in the denominator are acceptably small compared with N_* . Thus, if we count 10000 photons from a constant source (sky subtracted), the S/N would also be 100. Note that this applies to photons actually detected. If the CCD camera has a QE of 60%, thus, it only detects 60% of the incident photons (or 6 000) and the S/N is about 77, not 100.

Another problem arises because we cannot measure just the light from the star alone - we also get photons from the sky foreground (often called the “sky background”, but most of the sky photons originate or are last scattered in the Earth atmosphere, and hence are in the foreground). So, we have to measure the star+sky, then measure the sky contribution separately, so that we can subtract the sky contribution to get the star alone. The trouble is, both these measurements carry errors which combine when we try to isolate the counts from just the star. The selection of suitable aperture radius is one of the important issues. Using a big measurement aperture also means that there is a lot of sky light contributing to the counts in the aperture containing the star. We can subtract off the average sky signal, regardless of aperture size, but we cannot subtract off the noise associated with the sky signal, and the bigger the aperture, the larger the sky noise in the aperture. Further, the bigger the measuring aperture, the more chance to have a contamination from nearby objects.

Both effects mentioned above argue for using a small measurement aperture. On its turn, a small aperture will only encompass a fraction of the total light from the source. If the seeing were constant, in case of differential photometry, the effect would cancel out. The problem, of course, is that seeing is not constant. In practice, we find that seeing (except in cases of very poor seeing) affects mostly the inner Gaussian core of the image. Using an aperture 4 to 5 times the diameter of the typical FWHM will get most of the light (Da Costa 1992). In this size aperture, reasonable variations in the seeing will not result in measurable variations in measured counts.

However, particularly for faint objects, an aperture, say, 4 times the FWHM will contain a lot of sky signal, which means a lot more noise inevitably associated with the sky signal. Since the signal of a faint object is low, this will result in a low S/N ratio. From the CCD equation, we can see that for faint sources ($N_* \ll N_{sky}$)

$$\frac{S}{N} \sim \frac{1}{N_{sky}} \quad (3.3)$$

This demonstrates quantitatively the dominant role of sky brightness in determining the S/N ratio when doing photometry of faint objects. To get a better signal-to-noise ratio, we can either increase the signal (by using a larger telescope for which

$$\frac{S}{N} \sim D_{tel}$$

or a longer integration time), or, we can try to decrease the noise. One obvious way to decrease the noise is to observe from a darker place. Getting a dark sky is to select the moonless nights for our observations. The S/N ratio is related to the integration time in following manner:

$$\frac{S}{N} \sim \sqrt{t} \quad (3.4)$$

Thus, to improve the S/N by a factor of 2, we must observe 4 times as long. The longer we observe, the greater the sky signal (and, hence, the sky noise), but the S/N increases because the signal from star-like objects increases linearly with increased exposure time, while the sky noise increases only as the square root of the exposure time. Unfortunately, we can not increase the exposure length infinitely - there would be lots of cosmic ray hits, and the telescope would not track accurately for the required time.

The most practical way to select appropriate aperture radius consists in constructing of so-called growth curves (see e.g. Da Costa 1992). In this procedure, we measure the source through the number of apertures and then we plot the measured magnitudes as a function of aperture size. As the growth curve is constructed, it is straightforward to find the aperture size for which the curve becomes asymptotic (in the case of bright source) or reaches its maximum (as it is the case for the faint sources). Consequently, we consider this aperture size as a optimal one.

What would happen to the S/N if we broke the exposure up into pieces? If the photon noise is the dominant source of the uncertainty, then in the case we combine n short images, the rms error inherent to the obtained image is related to the error of individual images as follow

$$\sigma = \frac{\sigma_{ind}}{\sqrt{n}} \quad (3.5)$$

Thus, in the case of bright source, it does not matter whether we collect the photons in one observation of exposure length t , or in a number n of observations of length t/n . Because photon noise dominates, the S/N depends only on the total number of detected photons. Unfortunately, we do not obtain the same result for the faint sources, nevertheless the combination of single images can give a positive result in point to receive better S/N ratio.

Since the blazars are extragalactic objects, we have to correct the obtained stellar magnitudes for galactic extinction. To do this, we resort to NASA/IPAC Extragalactic Database (<http://nedwww.ipac.caltech.edu>). Here, we can derive the A_λ correction using Extinction-Law Calculators based on the method developed by Schlegel et al. (1998).

3.5 Variability Investigation

Variability studies are a basic tool to understand the physical processes occurring in AGNs, especially those related to short time scales and high amplitudes observed in BL Lacs.

In order to investigate blazar variability, we construct light-curves using differential photometry, i.e., the magnitude of the target is measured against that of a reference star. Furthermore, it's necessary to choice a control star. Let's denote S1 as comparison and S2 as control star.

Simultaneous observations of the blazar, comparison stars and the sky background allow one to remove the dominant possible sources of error: fluctuations in either atmospheric seeing or transparency, since all star-like objects on the field of view are equally affected (Howell & Jacoby 1986). Carini et al. (1992) examined the plots of magnitude differences between comparison stars of different colours against air mass, and they found that over a large range of airmass, there is no evidence that colour differences in the sets of the comparison stars affect significantly the overall accuracy of blazar photometry, nor introduce systematic variations not being intrinsic to the source.

When the target – comparison star data set show a linear trend, the intra-night variability of the blazar is investigated by means of the variability confidence parameter, C , introduced by Romero et al. (1999). To do so, we determine the scatter of the differential magnitudes $T - S1$ (T denotes the target object) and $S1 - S2$, $\sigma(T-S1)$ and $\sigma(S1-S2)$, then the variability parameter C is expressed as

$$C = \frac{\sigma(T-S1)}{\sigma(S2-S1)}. \quad (3.6)$$

If $C > 2.5763$, then the target is taken to be variable at a 99% confidence level. If not, it does not mean that the object's flux was completely constant during the session. In that case, we may say that any possible variation is below our confidence threshold.

As noted by Howell et al. (1988) it is not sufficient to select simply non-variable field stars as comparison ones. They should also closely match the target's magnitude. Here, the colour matching is shown not to be so important. If not, the measured dispersion of the target-comparison light-curve (σ_T) can be different from that of the control-comparison light-curve (σ) due to photon statistics and other random-noise terms (sky, read-out noise), even in the absence of any intrinsic variations in the target.

If suitable stars are not found, we should apply to the HWM88 method developed by Howell et al. (1988) which allows us to derive a corrective factor Γ defined as follow:

$$\Gamma^2 = \left(\frac{N_{S2}}{N_T} \right)^2 \left(\frac{N_{S1}^2(N_T+P) + N_T^2(N_{S1}+P)}{N_{S2}^2(N_T+P) + N_T^2(N_{S2}+P)} \right) \quad (3.7)$$

Here N is total (sky-subtracted) counts within the selected aperture; sub-indexes T , $S1$ and $S2$ correspond to the target, comparison star, and control star, respectively, and

$$P = n_{pix} (N_{sky} + N_{RON}^2) \quad (3.8)$$

Further, using the scaled σ , we can express the confidence parameter C as the quotient between the observed target–comparison light-curve dispersion and its expected instrumental dispersion:

$$\frac{C}{\Gamma} = \frac{\sigma_T}{\Gamma\sigma} = \frac{\sigma_T}{\sigma_{inst}} \quad (3.9)$$

In the ideal case, when the target, reference and control stars are of the same magnitude, $\Gamma=1$ and we get the C parameter in its original form.

When searching for the intra-night variability, it is reasonable to observe the target during at least 3 hours. The selection of this time interval is based on the suggestion of Carini (1990) who showed that there is approximately a 50% chance of variability detection when the blazar is monitored for at least 3 hours.

When the AGN is embedded in a bright host galaxy, the matter gets much complicated. Firstly, the host adds flux to the measurement aperture. Since the amount of the additional flux depends on the aperture radius, it is difficult to compare observations made using different apertures. Sometimes, the host galaxy contribution can significantly exceed the nuclear flux. In that cases the target differential light curve will have almost the same dispersion as the comparison light curve (Cellone et al. 2000). Thus, the inclusion of a larger contribution from the host within the aperture dilutes intrinsic brightness variations of the blazar.

Using small apertures for the blazar embedded in a host which is as bright or brighter than the target itself will result in spurious variations of several hundredths of a magnitude for seeing changes of 10 or more (Cellone et al. 2000). This is due to the fact that stars and galaxies have different surface brightness profiles and thus they respond differently to changes in the FWHM. This effect is especially dangerous when investigating blazar intra-night variability. Cellone et al. (2000) showed that spurious effects are present when seeing conditions fluctuate and that they cannot be completely removed by differential photometry with stars alone. They propose to use other extended objects available within the same CCD frame in addition to several stars. If this nearby galaxy exhibits the same manner of variation with a similar light curve, there is great chance that the observed variations are spurious due to the seeing fluctuations. In such case, it is useful to investigate the differential curve BL Lac – extended object. In addition, a procedure of plotting the temporal variations in the FWHM is a powerful tool to discriminate whether the brightness variations are seeing induced or intrinsic to the sources. Thus, the case of blazars situated within the bright hosts should be

treated with extreme caution according to the magnitude of the host galaxy relative to the AGN itself, and the seeing fluctuations during the session. Jang & Miller (1997) recommended to plot the FWHM (in pixels) of target, the same for reference star and the difference between these two. If we deal with spurious variability introduced by seeing variations, there should exist a correlation of these plots with target's plot.

Jang & Miller (1997) proposed another method to check for possible contamination from the host. According to it, if the measured variation is artificial, there should be an inverse correlation between amplitude and red-shift. This relationship could be produced when the galactic contribution is diminished at higher redshift. Hence, one should plot C parameter versus z for all targets in order to examine whether such correlation exists.

In some cases the host galaxy contribution can exceed the nuclear flux by a large margin. In these cases the broadband spectra are highly distorted and relative flux variations underestimated in the optical region, unless a correction for the host galaxy contribution is determined.

Among the factors affecting the photometry of host galaxy dominated sources, the aperture radius and FWHW are the most important ones. There are other factors that may contribute noise, such as aperture centering and sky determination errors, but these factors are controlled by e.g. using an appropriate symmetry clean algorithm in the aperture centering and careful selection of the sky region.

There are two main methods capable to estimate the host galaxy contribution (see Nilsson et al. 2007). In the two-dimensional model, we represent the source as a combination of an unresolved nuclear component and a host galaxy component for each frame. The derived nuclear magnitude is considered as a true value of the AGN. But due to poor resolution and low signal-to-noise ratio for typical monitoring frames, it is impossible to characterize the host galaxy properly. Further, the uncertainties inherent to the fitting process can boost the total noise to unacceptable level, especially for sources with bright hosts.

In the second method is developed to high-resolution, high-S/N images of the sources. We use two-dimensional model here and compute aperture correction tables by means of simulated frames. This method has an advantage compared to the first one. In that case, the fitting process is much more accurate than in the case of fitting single monitoring frames.

It is impossible to use this method for Abastumani frames due to their low resolution. Thus, we have to resort to the first way. I have used the following expression which makes us possible to converted R -band magnitudes into the linear flux (in Janskies, Nillson et al. 2007):

$$F = 3080.0 \times 10^{-0.4*R} \quad (3.10)$$

In the case of mJs, we have:

$$\log F = 6.49 - 0.4 \times R \quad (3.11)$$

In this manner, I converted the set of R magnitudes into linear fluxes. Then the values of the host fluxes (Nilsson et al. 2007; K. Nilsson (private communication)) are subtracted from derived quantities. Once we have the corrected values of corrected fluxes in mJys, it is possible to convert them into R magnitudes using the following expression:

$$R = 16.22 - 2.5 * \log F \quad (3.12)$$

In order to study short-term bursts, Massaro et al. (1996) proposed to model the long term variability by means of a sequence of straight segments through the points of local minimum flux. This simple method does not introduce spurious maxima and minima, particularly in poorly sampled intervals, in opposite to continuous models, such as a cubic spline interpolation or high-degree algebraic polynomials. Then the interpolated flux values are subtracted from the observed ones and plot the flux differences against the time. The residual variations appear as a series of short-term bursts.

If the variability is proven, we determine its amplitude according to the following expression introduced by Heidt & Wagner (1996):

$$A = \sqrt{(A_{max} - A_{min})^2 - 2\sigma^2} \text{ (mag)}, \quad (3.13)$$

or,

$$A = \frac{100}{\langle A \rangle} \sqrt{(A_{max} - A_{min})^2 - 2\sigma^2} \text{ (%)} \quad (3.14)$$

where A_{max} and A_{min} are the maximum and minimum values of blazar light curve, respectively. Here σ is averaged per observation term.

One of the important variability characteristics is so-called duty cycle (DC). This characteristic is defined in different manner for the variabilities in different timescales and spectral band. Cellone et al. (2007) defined the DC for extremely violent microvariability as the fraction of the observing time for which the object displayed large amplitude ($\Delta m \gtrsim 0.5$ mag), fast ($\Delta t \lesssim 45$ min) flux changes. For 2-10 keV X-ray flux variability, Krawczynski et al. (2004) define its flare DC as the fraction of time during which the flux exceeds the time averaged flux by at least 50%. Generally, Ciprini et al. (2003) define variability DC as a fraction of time spent by the source in an active state.

Since bulk of the AGNs do not display microvariability on each night, Romero et al. (1999) propose to estimate AGN duty cycles not as a fraction of the variable objects found within a given class (see e. g. Heidt & Wagner 1996), but as the ratio of the time over which objects of the given class are seen to vary effectively to the total observing time spent on monitoring the objects in the class. In this way, we take into account the fact that there are nights in which usually variable AGNs do show microvariations. Besides, since most of the sources have not been monitored during equal spans it is better to weight the contribution to the duty cycle by the hours each source was observed during each observing session.

Consequently, one defines the following estimator for the duty cycle of objects of a given class (Romero et al. 1999):

$$DC = 100 \frac{\sum_{i=1}^n N_i \left(\frac{1}{\Delta t_i} \right)}{\sum_{i=1}^n \left(\frac{1}{\Delta t_i} \right)} (\%) \quad (3.15)$$

where

$$\Delta t_i = \Delta t_{i,obs} (1 + z)^{-1} \quad (3.16)$$

is the duration (corrected on redshift) of an i^{th} monitoring session of the source out of a total of n sessions for the selected class, and N_i equals 0 or 1, depending on whether the object was nonvariable or variable, respectively, during Δt_i .

The long-term variability time scales can tell us about how often certain objects, or certain classes of objects, are in a flaring state and how long do these flares typically last.

Many optical fluctuations are obvious from simple visual inspection. The timescales of the variations are defined as the time required for a complete cycle of brightening and fading (Smith et al. 1993). In the frequent cases when a light curve includes several cycles of clearly different lengths, these are averaged to derive a “characteristic time scale” for the source (Smith et al. 1993).

In order to quantify the slopes of the light curve, the usual technique is to apply the linear regression analysis. The results are expressed as the overall slope in magnitudes/year (Smith et al. 1993).

The ordinary Fourier transform is not optimal to use for the investigation of long-term variability in blazars because the samplings of their light curves are not exactly uniform, as a rule. Nor can simple periodograms give useful results (see e. g. Ciprini et al. 2003). In order to study the nature and the temporal structure of variability, one applies the following well-tested tools: structure function (SF), discrete Fourier transform (*DFT*) and Jurkevich method. These methods, developed for unevenly sampled datasets, give a good description of the time variability.

Structure function (*SF*) analysis is a powerful tool to determine quantitatively any time scale of variation on unevenly sampled data sets. Structure functions are not very sensitive to aliasing problems due to discrete and/or sparse time sampling (e.g. Hughes et al. 1992), which make them well suited for our purpose. Furthermore, determining the slopes of the structure function allows to characterize the underlying physical process.

Structure functions can be calculated from the light curves according to Simonetti et al. (1985). The first order structure function is defined as:

$$SF(dt) = \frac{1}{N} \sum_{i=1}^n [f(t_i + dt) - f(t_i)]^2 \quad (3.17)$$

where f is the observed flux. Alternatively, as expressed in stellar magnitudes (Smith et al. 1993)

$$SF(dt) = \frac{1}{N} \sum_{i=1}^n [mag(t_i + dt) - mag(t_i)]^2 \quad (3.18)$$

Here, $mag(t)$ and $mag(t+dt)$ are the observed magnitudes separated by the time interval dt , and the angular brackets denote an ensemble average. The slope can be written as follow (Smith et al. 1993):

$$\alpha \equiv \frac{d(\log SF(dt))}{d(\log dt)} \quad (3.19)$$

In practice, this value is determined by fitting a first order polynomial using the least-squares method (Heidt & Wagner 1998).

The structure function is equivalent to the power spectrum, with the advantage to work in the time domain, which makes it less dependent on sampling. It removes any continue component (mean value in a period, or direct current offset) from a signal. The structure function of n -th order is able remove polynomials of order $n - 1$ (Ciprini et al. 2003).

The structure function of an “ideal” measured process increases with the time lag dt in a log versus log representation (see Fig. 3.3). It shows an initial plateau for short time lags, and a second plateau for lags longer than the maximum correlation time scale. For the short

time lags, the plateau is twice the variance of the measurement noise, because this has a zero correlation time scale ($\alpha=0$). A steep curve, whose slope depends on the fluctuations nature, links these two regions. The turnover time lag between the rising part and the long-lag upper flattening of the SF identifies a characteristic variability time scale of the source (e. g. Hughes et al. 1992). For lags longer than the longest correlation time scale, there is a plateau with amplitude equal twice the variance of the fluctuation. If we have several processes mixed or the process is periodic, the situation is more complicated and it can be difficult to interpret the structure function properly.

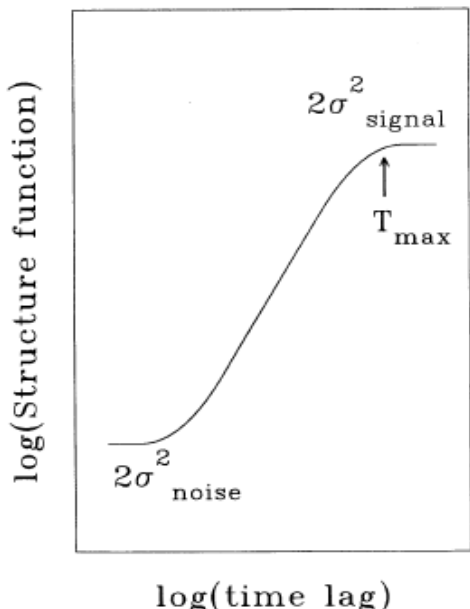


Figure 3.3: Sketch of ideal structure function (Lainela & Valtaoja 1993)

Although the SF for a real process will be a non-simple function of the lag, there are three types of ideal noise spectra that are relevant to blazar variability: white noise, flicker noise and shot noise (Lainela & Valtaoja 1993). In the case of white noise the next data point is unrelated to the preceding one (there is no “memory”). There is an

underlying normal statistical distribution. A shot or random walk or Brownian noise process would produce the following relation:

$$SF(dt) \propto dt, \quad (3.20)$$

or a slope of unity. Shot noise results from a sequence of random pulses, i.e. a superimposition of similar shaped bumps randomly distributed in time, with a long-term “memory”. It is full time integral of a normal distribution and it has an infinite memory of preceding events. Flicker or pink noise gives the following relation

$$SF(dt) \propto (dt)^0. \quad (3.21)$$

Flicker noise is halfway between the previous two ones. It has a finite memory in the sense that the next point depends on the preceding values, although with a decreasing dependence upon events further from the current time. The typical blazar variability is found to place between the shot and the flickering noise (Hufnagel & Bregmann 1992, Ciprini et al. 2003). Finally, a linear trend or strong periodic oscillation in the time series gives (Hovatta et al. 2007):

$$SF(dt) \propto (dt)^2. \quad (3.22)$$

The important parameter in the SF analysis is the T_{max} , which gives the time lag when the SF reaches the upper plateau. T_{max} is defined as a maximum timescale only in a “ideal” case (non-periodical one process case). Otherwise it can be interpreted in two ways: it is the maximum time scale of correlated behaviour or the minimum timescale in the distribution of timescales (Hughes et al. 1992). We cannot easily distinguish these two cases, but either way, the plateau of the structure function is a physically meaningful characteristic time scale for each source, which can be compared from source to source, and for different blazar subclasses.

In order to facilitate the estimate of when the long-term lag plateau occurs, Hughes et al. (1992) propose to normalize the structure function by means of σ^2 . In the ideal case, the normalized SF curve should asymptote to $\log 2 \approx 0.3$.

In order to obtain maximum amplitude of the variability, one normalize the SF by means of mean flux. In this case $SF(T_{max})$ gives a relative variability index, which can be used for comparing the relative strengths of the variable and quiescent components in the source (Lainela & Valtaoja 1993).

However, in many cases the SF deviates quite significantly from the ideal. Types of behaviour exhibited are following: a) There is no plateau. Here, we make the interpretation that the characteristic time scale is longer than the given time base of the data. In that case, the longest time lag available sets a lower limit on the characteristic timescale; b) the third plateau at intermediate time lag. We assume here that we are seeing the signature of two distinct processes. In some cases, the shorter time scale may be due to interstellar scintillation (Spangler et al. 1989), and we should use the longer time lag plateau to derive values for the intrinsic process; c) very irregular SF. Here, we presumably deal with the

variations dominated by one or a few large outburst, or variations that are more or less periodical. In that case, we derive a slope by fitting a mean slope through the rising part of the SF (Hughes et al. 1992).

If the light curve contains the cycles of period P , the plot of $SF(dt)$ will rise to a maximum at $dt = \frac{P}{2}$ and than fall to minimum at $dt = P$. When dt is extended to multiples of P , $SF(dt)$ goes itself through a series of cycles (Smith et al. 1993). Anyway, characteristic timescales show up as a maxima in the SF (Wagner et al. 1996).

A complicating factor interpreting the computed SFs is that at long time lag they undergo a rapid rise, fall, or oscillation. This is an erratic behaviour associated with the chance value of the points at the ends of data trains – we do not consider the SF to be well defined there and use only the curve at shorter time lag to derive values. In these cases we often get only a limit of the characteristic timescale. As noted above, a linear trend will contribute in structure as $(dt)^2$. The light curves show few cases where it would appear appropriate to remove such a trend (there could be exist long-term variations, but no such as extend coherently over the entire time base).

The detection of periodicities, if any exist, is extremely difficult, especially for faint objects. Unequal intervals of time between observations and annual gaps in the data extending over several months complicate any analysis, along with normal observational uncertainties and the relatively short baselines of the data sets (often only one or two “periods”).

One of the methods of investigating periodical variability is the unequal-interval Fourier transform method producing a power spectrum whose peaks imply the presence of near-sinusoidal component in at least a portion of the light curve. It also yields a spectral window that identifies aliases or spurious peaks attributable to the sampling. As a rule, well-sampled light curves generate a strong alias only at a period of one year, corresponding to the unavoidable annual observing season for each object. It is recognized that the Fourier method is most appropriate for time series containing true periodicities.

The discrete Fourier transform (DFT) over a set of N data points (Deeming 1975):

$$D(\omega, x(t)) = \frac{1}{N} \sum_{k=1}^N x(t_k) e^{i\omega t_k} \quad (3.23)$$

We define the DFT power as

$$P(\omega) = |D(\omega, x(t))|^2, \quad (3.24)$$

which is used to evaluate the ω frequency statistically. The semi-amplitude of the periodic fluctuation corresponding to a significant peak in the DFT spectrum is:

$$A = 2\sqrt{P}. \quad (3.25)$$

Fourier analysis is an ideal tool for detecting and quantifying periodic fluctuations in time series, if by periodic we mean the truly constant period, amplitude, and phase. Real

physical systems rarely exhibit such constancy of the fluctuations. Often periodic fluctuations arise intermittently, as transient phenomena (see e.g. Foster 1996). Even for a time series with consistent periodicity we usually see time evolution of fluctuation parameters. Fourier analysis can detect, and to some degree quantify such behaviour, but it is far from ideal tools for such purposes.

In the case of unevenly sampled data train, the method proposed by Jurkevich (1971) proved to be the most suitable tool to find a periodicity in blazar optical variability (see Fan 2000). Namely, it is less inclined to generate spurious periodicity than the Fourier analysis. According to Jurkevich method, we assign all the data are to m groups according to their phases around each trial period. For each group, we compute the variance:

$$V_l^2 = \sum_{i=1}^{m_l} x_i^2 - m_l \bar{x}_l^2, \quad (3.26)$$

where

$$\bar{x}_l = \frac{1}{m_l} \sum_{i=1}^{m_l} x_i \quad (3.27)$$

and m_l are mean value and number of observations in l -th group, respectively. The sum of the variances of m groups is the given by

$$V_m^2 = \sum_{l=1}^m V_l^2 \quad (3.28)$$

According to the theorem on the addition of variances $V_m^2 < V^2$ where

$$V^2 = \sum_{i=1}^{N_i} x_i^2 - N \bar{x}^2, \quad (3.29)$$

and

$$\bar{x} = \frac{1}{N} \sum_{i=1}^N x_i \quad (3.30)$$

are the overall variance and the overall mean, respectively. The parameters V_l^2 and \bar{x}_l are very sensitive functions of a trial period. If the later is incorrect, phase-reduced observations, when represented by a curve, scatter irregularly over the diagram. In this case, group means and variances are likely to be nearly the same. As one approaches the true period, the group means become quite different and if a trial period equals the true one, then V_m^2 reaches its minimum. The reduction of the later relative to V^2 can conceivably be caused by statistical fluctuations. A decision on whether this is so or not can be made either by examining the fit of the phase diagram or, since observational errors can safely be assumed to be normally distributed, by the use of the statistical F -test. However, the later should be used with caution. All the cells into which the period under investigation is divided are assumed to contain observations.

In the case of periodical behaviour and selection of true period, the quantity V_m^2 exhibits a sharp minimum with relatively broad wings in the vicinity of the true period (Jurkevich 1971). A further test is to derive the relationship between the depth of the minimum and the noise in the “flat” section of V_m^2 curve close to the adopted period. If the

absolute value of the relative change of the minimum to the “flat” section is large enough as compared with the standard error of this “flat” section (say, five times), the periodicity in the data can be considered as significant and the minimum as highly reliable.

No general formula is given with respect to a most efficient grouping of the observations for a time series with unknown periods. The author of the method suggests to use at least three groups if t_0 is fixed because with $m=2$ the centre of both intervals may occur close to the region where the data crosses the overall mean in the case the true periodicity is present. The simplest way to choose the group number consists in a visual inspection of historical light curve. As for upper limit of m , it must not be taken so large as to lead to empty groups thereby causing the difficulties in point of spurious periodicity.

4 Results

In this chapter, the detailed description of the investigation results are given. They are mainly based on the material obtained at Abastumani Astrophysical Observatory. In addition, the data of different observational campaigns are also referred. The results are given separately for each target object.

4.1 1ES 0229+200

This source was observed during 57 nights at Abastumani observatory between November 9, 1997 and November 16, 2007. Fig. 4.1a shows the historical light curve constructed on basis of R magnitudes (Appendix B1.1, column 3). Photometrical measurements are performed using the aperture radius of about 7."5 in order to make the magnitudes comparable with the preliminary values obtained during *Tuorla Blazar Monitoring Program* (see http://users.utu.fi/kani/1m/1ES_0229+200.html).

The comparison light curve (Fig. 4.1c) was generated using the instrumental magnitudes of reference stars 4 ($R=15.70$) and 6 ($R=16.00$) provided by Monet et al. (1998; see Appendix A1). Their difference showed the least scatter among the field stars during the whole observational campaign (column 2 of Appendix B1.1).

The data points are distributed along the historical light curve unevenly and we have several blank intervals here. No data are presented between JD-24450000=1141 and 2524. In the case of stellar magnitudes, not corrected on host contribution, there is no variability at 95% confidence level (as noted by Pica et al. 1998, a confidence level of 95% or more is widely accepted as a good indication that a source is actually variable).

We deal with following circumstance here: 1ES 0229+200 is hosted by very bright elliptical galaxy ($F_R=0.98(\pm 0.10)$ mJy, K. Nillson, private communication). Its contribution varies from 80% to 91% in total R band flux. Thus, the host could dilute of intrinsic variability (if any exists).

In order to correct the stellar magnitudes on host contribution, they were converted into linear fluxes (Appendix B1.1, column 4). The host level was subtracted from these values and the obtained linear fluxes (column 5) were converted back into stellar magnitudes (column 6). Finally, these data were corrected on galactic absorption (column 7, $A_R=0.36$). Fig. 4.1b presents the historical light curve constructed on basis of corrected R magnitudes (averaged per a session).

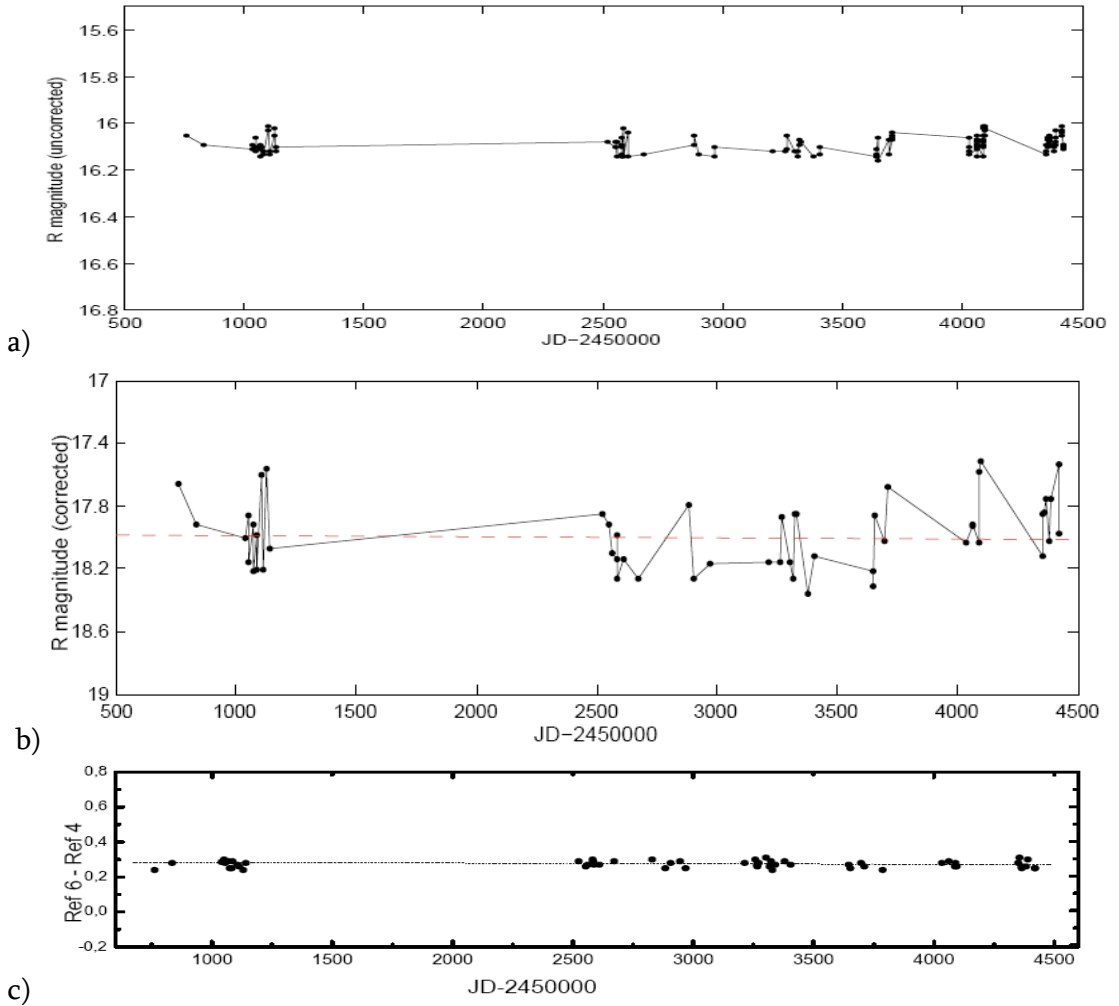


Figure 4.1: Historical R band light curves of 1ES 0229+200 with a) magnitudes including host contribution and not corrected on galactic absorption; b) magnitudes corrected on host contribution and galactic absorption; c) comparison light curve.

Despite this operation, no clear long-term variability has been found but some short-term bursts. The base level does not show a variability at 95% confidence level. This feature is very unusual for blazars. Note that the uncertainty becomes of 0.2 mag order after the correction of host contribution (rms error is about 0.08 otherwise) and the amplitudes long-term changes should be below this value (if any exists). Nevertheless, *RXTE* X-ray observations show clearly expressed long-term variability (see Wagner 2008).

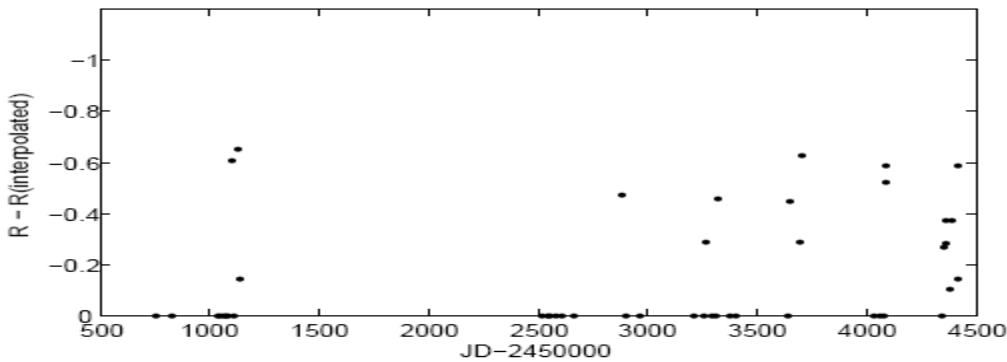


Figure 4.2: Short-term busts in 1ES 0229+200.

In order to detect optical short-term bursts, the method proposed by Massaro et al. (1996) has been used. Fig. 4.2 presents the obtained results. Totally 7 bursts at 95% confidence level and more are found (see Table 4.1). Their amplitudes are confined between 0.30 to 0.58 mag (corresponding to the increases with 33-36% in R band flux compared to

Table 4.1: Short-term busts in 1ES 0229+200.

Moment of Maximum Brightness (JD-2450000) (1)	Number of “Active” Nights (2)	Amplitude (mag) (3)	Amplitude (%) (4)
1106.3888	2	0.55	60
2884.5278	1	0.41	44
3272.5518	1	0.34	36
3323.3335	2	0.41	43
3329.5261	2	0.58	63
4095.2339	2	0.55	60
4366.3765	1	0.30	32

the local base level. Because we deal with great uncertainties, these values may be significantly exaggerated). Due to no perfect coverage with data points, the investigation of burst durations has not been performed. The duty cycle of short-term burst was determined as a ratio of “active” sessions (i.e. when the source was active at 95% confidence level or more) with total number of sessions. Here, $DC \approx 19\%$ was obtained (11 “active” sessions vs. total 57 ones).

Table 4.2: Intraday changes in 1ES 0229+200.

Time Interval (JD-2451000)	Δt (days, redshift corrected)	ΔR (mag)	$\frac{\Delta F}{F}$ (%/d)	Comment
4088.19-4090.20	1.77	-0.45	25	host subtracted

One occasion of intraday changes was detected (Table 4.2). The source underwent a brightening with 0.45 mag during 1.77 day (this interval is corrected on source’s redshift). Thus, we have an increase with 25% a day (Note that due to great uncertainties this value is less credible).

4.2 1ES 0323+022

Fig. 4.3a presents the results of optical *R* band monitoring performed during October 8, 1997 and February 14, 2007 (51 sessions, see column 3 in Appendix B2.1). The comparison light curve (Fig. 4.3c) was constructed using the instrumental magnitudes of reference stars 4 ($R=14.01$) and 7 ($R=15.36$) provided by Fiorucci et al. (1998, Appendix A2). The scatter in their difference was the least as during the whole campaign (see column 2 of Appendix B2.1). In addition, the data points obtained at Perugia 40 cm (February 2, 1993 – January 9, 1995; Fiorucci & Tosti 1996) and Torino 1.05 m (December 17, 1996 - 23 January 23, 1999; Villata et al. 2000) telescopes are plotted too.

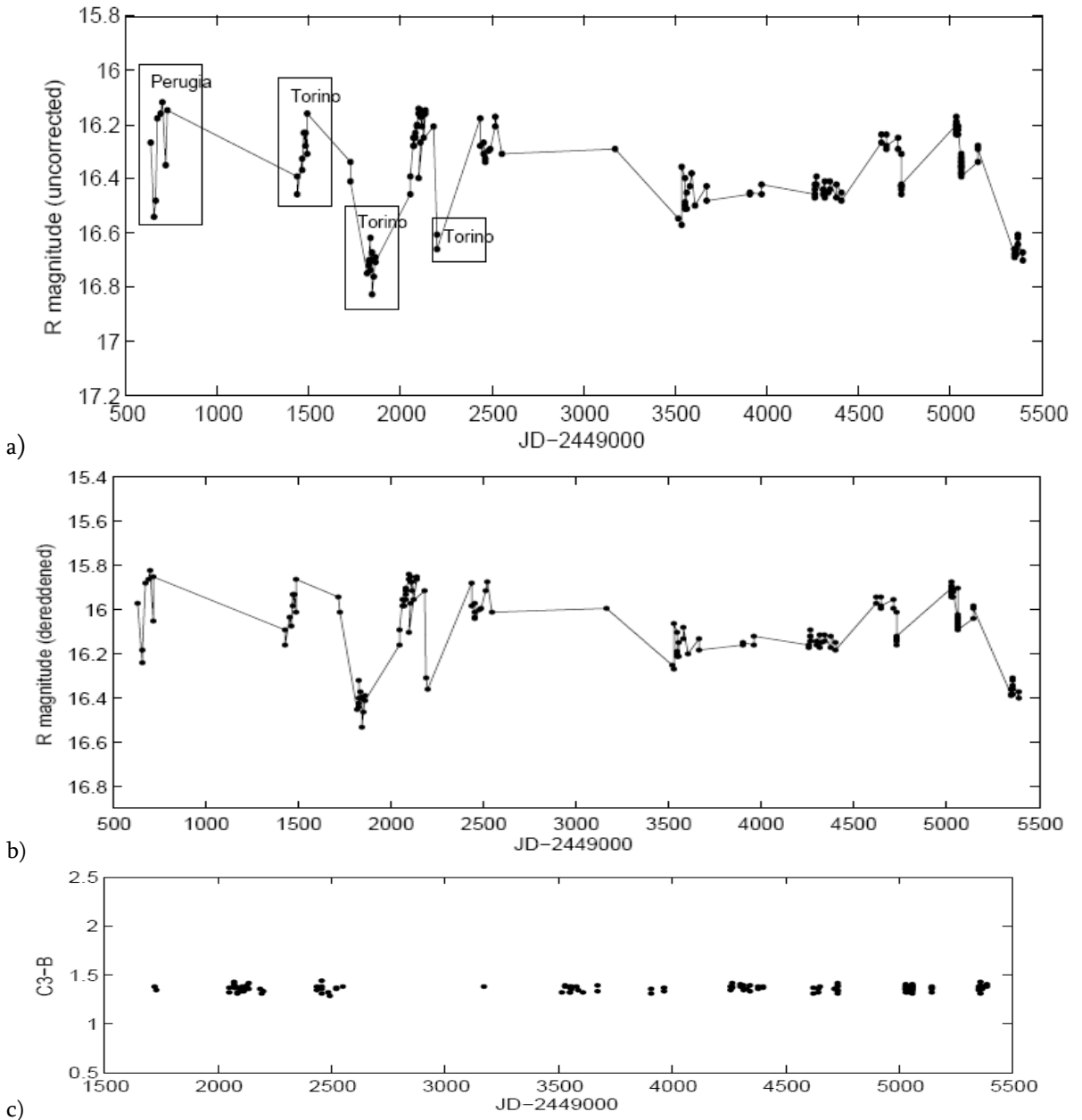


Figure 4.3: Historical *R* band light-curves of 1ES 0323+022 with a) magnitudes not corrected on galactic absorption; b) magnitudes corrected on galactic absorption; c) comparison light curve.

The data are corrected on galactic absorption ($A_R = 0.30$) and the derived results (Appendix B2.1, column 4) are plotted in Fig. 4.3b .

The data points are distributed along historical light curve sparsely. We have no data between $JD-2449000=727$ and 1435 and there is only one data point in (2551, 3520) interval. None of the optical maxima are observed perfectly and it is impossible to determine their locations accurately. Relatively well observed is the minimum situated around $JD-2449000=1850$ by Villata et al. (2000). Hence, it is very hard to make conclusions about the timescales of long-term variability.

The structure function constructed on the basis binned within 1-year intervals is presented at Fig. 4.4. In the case of shorter intervals, we have number of blank intervals due to sparsely distributed data points which existence caused spurious maxima and minima in structure function, which locations varied greatly with slight change in bin size. The constructed curve has a minimum at 5 yr indicating that there should be the long-term flares with characteristic timescales of 5 yr order (4.3 yr, corrected on target redshift). If this conclusion is true, we should have three optical maxima situated about at $JD-2449000=1100$, 3000 and 5000, respectively. In that case, the data $JD-2449000=1425$ and 1497 can be considered as a part of powerful short-term burst at decreasing phase of long-term trend. Anyway, the object should undergo long-term flares with duration greater than two year.

Fig. 4.5 provides the V band light curve of 1ES 0323+022 constructed on basis of the data provided by Jannuzi et al. (1993; Appendix B2.3, column 2). It is clear that the observations are confined between two consequent optical maxima separated by the interval of about three years. The respective R magnitudes should be ≤ 15.91 and ≤ 15.67 (they are calculated on basis of $\langle V - R \rangle = 0.45$ derived during the campaign). The amplitude exceeds 0.9 mag in that case.

During 25-year term (1982-2007), the source displayed overall brightness change $\Delta R \approx 1.20$ mag with maximum prightness correponding to $R=15.62$ (obtained by Feigelson et al. 1986).

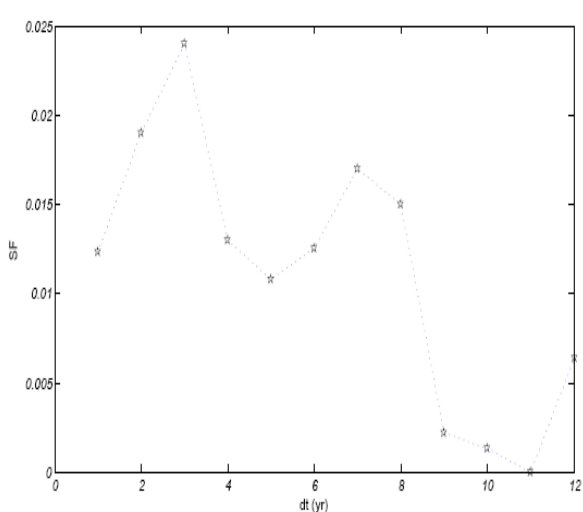


Figure 4.4: Structure function of 1ES 0323+022.

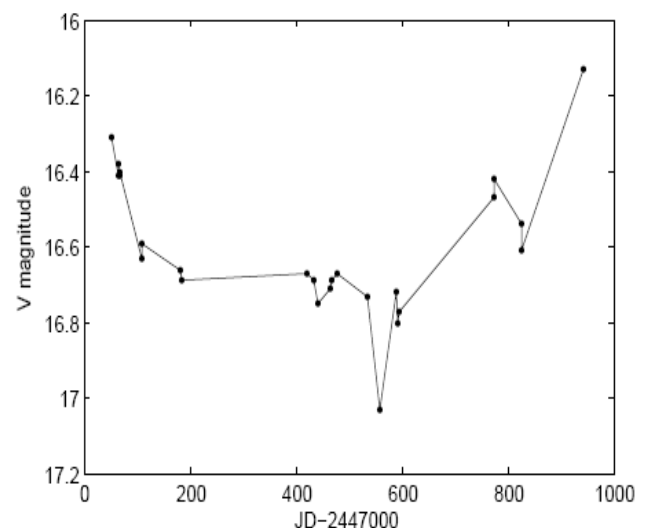


Figure 4.5: V band light curve constructed on basis of Jannuzi et al. (1993) data.

Intending to investigate the behaviour of the colour index $V-R$, V band observations were performed during 21 nights (see Appendix B.2.2). $B-R$ index was not investigated due to great error (sometimes exceeding 0.20 mag). Fig. 4.6 presents the results of the monitoring, including the data of 10 sessions performed at Torino Observatory (Villata et al. 2000). In the case Abastumani observations, no changes in $V-R$ values are detected at 95% confidence level. We have only the fluctuations around the average value $\langle V - R \rangle = 0.49$ between 0.41 and 0.55 while the uncertainties are of 0.09-0.11 mag. As for Torino data, three point are beyond of error range ($V-R=0.55$ at JD-2450000=84.34, $V-R=0.38$ at JD-2450000=837.29, $V-R=0.55$ at JD-2450000=837.29, $V-R=0.43$ at JD-2450000=857.30, $\langle V - R \rangle = 0.49$, uncertainties are of 0.05 mag). But at in that cases, only one V data point is presented. Hence, it is hard to say whether we have intrinsic $V-R$ variability or these values are due to fluctuations of statistical origin.

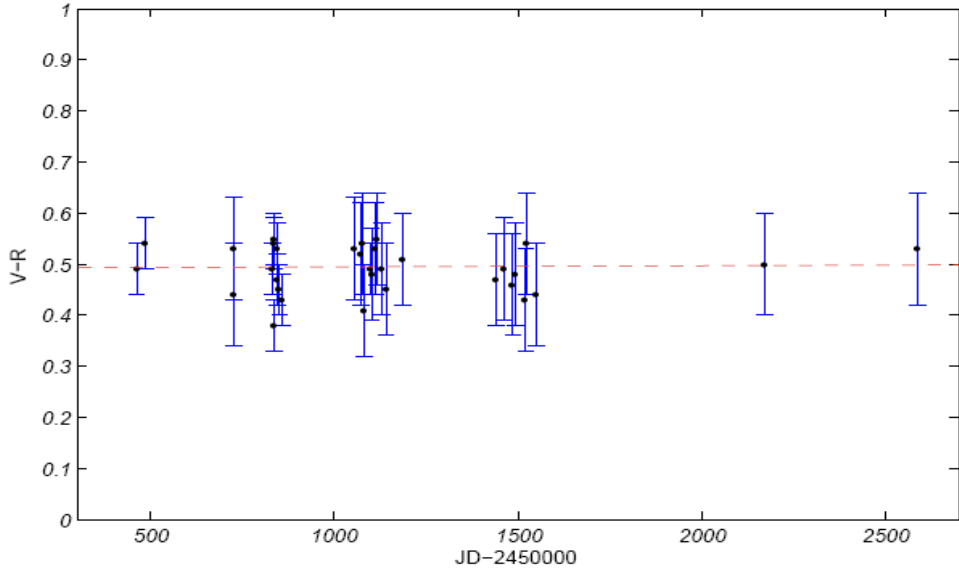


Figure 4.6: $V-R$ values for 1ES 0323+022.

The results of Jannuzzi et al. (1993) do not show also the variability of $V-R$ values (upper panel in Fig. 4.7; column 4 in Appendix B2.3). But $B-R$ colour index varies with 0.23 during 57 days (second panel; column 5 in Appendix B2.3). The same situation is in the case of Torino observation. Here, $B-R$ index varied with 0.27 during JD-2449000=462 and 831 (Fig. 4.8; see column 5 in Appendix B2.2) Thus, the variability of colour index should be inherent to this source.

Fig. 4.9 presents the short-term bursts revealed by means of Massaro et al. (1996) method. Totally 9 bursts at 95% confidence level and more are found (see Table 4.3). Seven of them occurred during long-term flaring activity, one – in minimum epoch (around JD-2449000=1851), and it is hard to say whether the flare with maximum at JD-2449000=3532

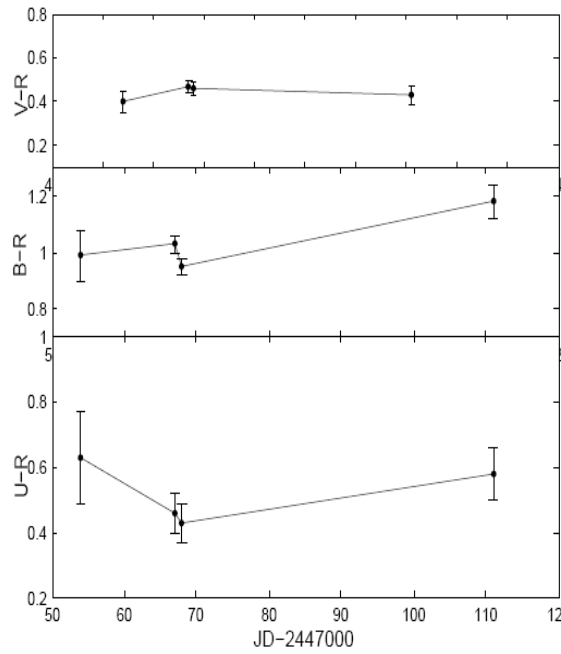


Figure 4.7: Colour indices derived from Jannuzzi et al. (1993)

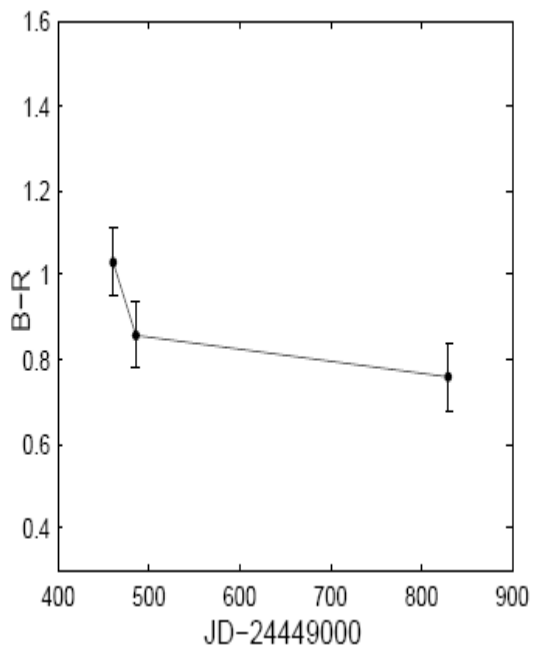


Figure 4.8: $B-R$ values of 1ES 0323+022 derived from Villata et al. (2000).

belongs to “active” or quiet epoch. This statistics shows that the shock-jet inhomogeneity interactions should be considered as a major mechanism responsible for short-term bursts in this object.

The amplitudes of short-term bursts ranged between 0.11 to 0.45 mag. Especially powerful burst is revealed by Abastumani observations at an ascending stage of blazar optical brightness peaking at $JD-2449000=2101$. Its amplitude was 0.45 mag (increase with 51% in R band flux compared to local base level). The slopes of ascending and descending parts of the bursts, indicating the rates source brightening or decay, were calculated if they were covered by the observations relatively well (in the units of magnitude per month, column 4 of Table 4.3; time intervals are corrected on target redshift; sign “–“ indicates a

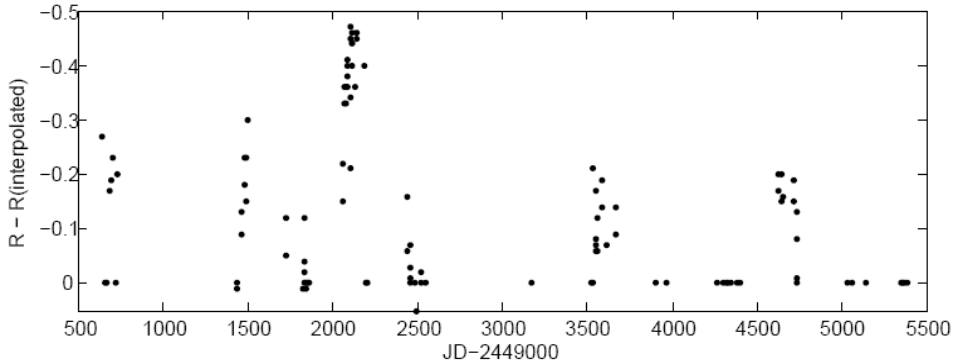


Figure 4.9: Short-term bursts in 1ES 0323+022.

brightening). In average, the decays were faster (0.27 mag/month) than brightenings (-0.18 mag/month). Due to no perfect coverage with data points, the investigation of burst durations was not carried out.

Table 4.3: Short-term busts in 1ES 0323+022.

Moment of Maximum Brightness (JD-2449000) (1)	Number of “Active” Nights (2)	Amplitude (mag) (3)	Amplitude (%) (4)	Slope (mag/month) (5)	Comment
640	1	0.25	29	0.37	Perugia
705	3	0.20	23	-0.30 0.40	Perugia
1497.2699	7	0.29	33	-	Torino
1834.3483	1	0.11	14	-	Torino
2101.513	11	0.45	51	-0.16 0.18	-
2439.449	1	0.15	17	0.08	-
2523.435	1	0.15		-0.08	-
3531.523	2	0.16	18	-	-
3587.493	1	0.17	19	-	-
4628.558	4	0.18	21	0.34	-
4649.5100					

The duty cycle of short-term bursts $DC \approx 40\%$ is derived (32 “active” nights among 80 (includiing Perugia and Torino observations)).

The source showed intraday variations twice (in the case of Torino observations, see Table 4.4). The fastest one is a decrease with 0.13 mag in 4.36 days (i.e. 3.2% a day). Thus, the source did not show dramatic changes in this regard.

As for other bands, the data provided by Jannuzzi et al. (1993) show intraday changes only once in B band between JD-2447000=67 and 68, when the source increased its brightness with 0.08 mag. The Most dramatic intraday variability is that in V band when a

Table 4.4: Intraday changes in 1ES 0323+022.

Time interval (JD-2449000) (1)	Δt (days, redshift corrected) (2)	ΔR (mag) (3)	$\frac{\Delta F}{F}$ (%/d) (4)	Comment
1490.2764-1497.2699	6.10	-0.15	2.8	Torino
1846.3073-1851.3007	4.36	0.13	3.2	Torino

source underwent a decrease with about 0.40 mag in four day reported by Feigelson et al. (1986). Thus, the fastest optical change ever observed is a decrease with 0.10 mag a day. This corresponds to less than 0.04 mag per a single session with optimal duration. Consequently, it is quite insensible to search for intranight variabilities in 1ES 0323+022 by means of such telescopes as 70 cm meniscus telescopes of Abastumani Observatory. In such situation, the

results of intranight observations obtained by Bai et al. (1998) seem to be incredible. Fig. 4.10 presents their results obtained during the night January 5, 1997.

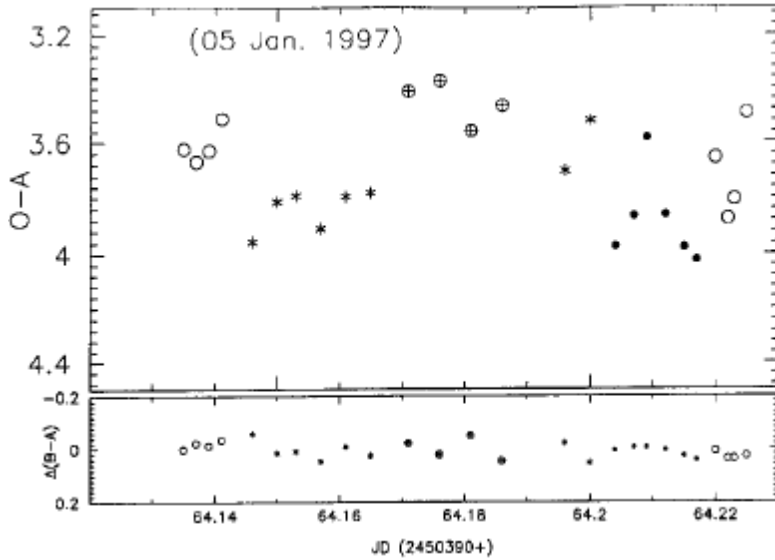


Figure 4.10: Example of intarnight optical observations carried out by Bai et al. (1998). Open circles – I band data, filled circles – R , asterisks – V and \oplus symbol – B magnitudes (adopted from the same paper).

Let us cite the part of the paper describing this session: “From JD = 2450450.137 to 2450450.141 the source brightened by $\Delta I = 0.15$ mag in about five minutes. In the subsequent V , B band observation it continued this rise till JD = 2450454.176, then faded by $\Delta B = 0.22$ mag. On JD = 2450451.181 the source brightened again by $\Delta V = 0.18$ mag in five minutes then $\Delta R = 0.38$ mag in 8 minutes, then quickly faded by $\Delta R = 0.42$ mag in 12 minutes, $\Delta I = 0.21$ mag in about 2 minutes, and again began to brighten. The amplitude of this flicker is about $\Delta R = 0.63$ mag (take $R - I = 16.33 - 15.47$)”. It is conspicuous that that the comparison light curves in each band have practically the same shapes as the respective target light curves. Thus, above cited ultra-fast microvariabilities , in fact, are of statistical origin and they should not be intrinsic to the source. Further, the authors do not write about the criterion used for variability confirmation. The star A, used as a comparison one, is with 4 magnitude brighter than the target and, one must to calculate corrective factor Γ in that case according to HWM88 method which is not done here. Thus, the violent microvariabilities, reported by Bai et al. (1998), should be considered as spurious.

4.3 1ES 0414+009

Fig. 4.11a presents the results of optical R band monitoring performed during October 4, 1997 and February 14, 2007 (56 sessions, column 3 of Appendix B3.1). The comparison light curve (Fig 4.11c) is constructed using the instrumental magnitudes of reference stars C1 ($R=13.56$) and C2 ($R=14.63$) provided by Fiorucci et al. et al. (1998, Appendix A.3). In

addition, the data points obtained at Torino 1.05m telescope (November 21, 1996 and February 10, 1997; Raiteri et al. 1998; values between JD-2450000=408 and 492 in Appendix B.3) are also plotted.

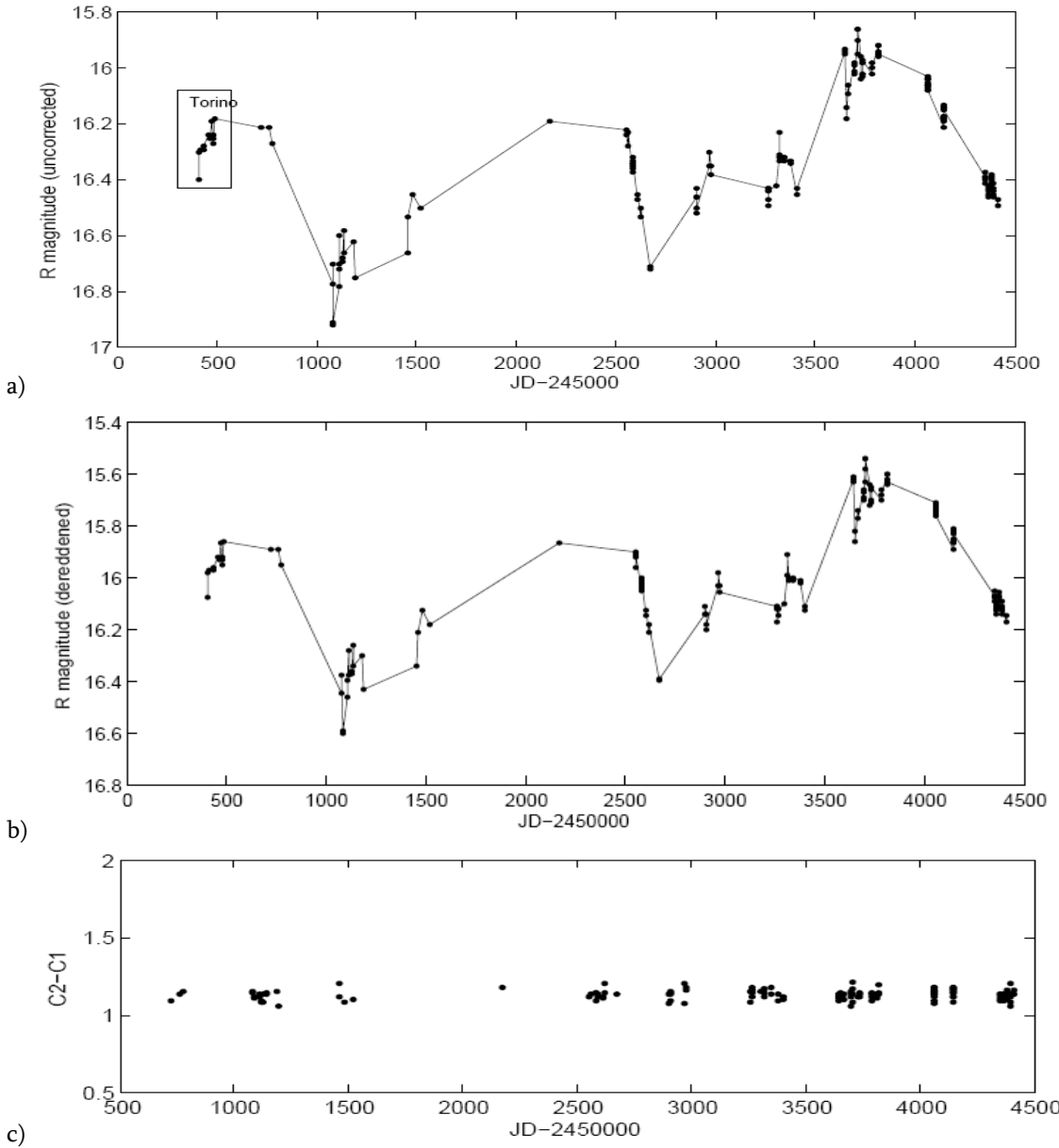


Figure 4.11: Historical R band light-curves of 1ES 0414+009 with a) magnitudes not corrected on galactic absorption; b) magnitudes corrected on galactic absorption; c) comparison light curve.

The data are corrected on galactic absorption (column 4, $A_R = 0.32$) and the derived results are plotted at Fig. 4.11b.

As in the case of 1ES 0323+022, the data points are distributed along historical light curve sparsely. There are especially long blank intervals between JD-2449000=490 and 1725, 778-1083 and we have only one data point in (1523, 2553) interval. Only one optical maximum (JD-2449000=3648) is observed perfectly. Due to this reason, the optical minima are used to derive the timescales of long-term variability (see Table 4.5). Here, the location

of the second minimum is determined roughly. The third one is observed during Tuorla Blazar Monitoring Program (<http://users.utu.fi/kani/1m/>).

Table 4.5: Long-term variability in 1ES 0414+009.

Minimum Location (JD-2449000) (1)	Δt_{obs} (yr) (2)	Δt_{corr} (yr) (3)	Comment
1086	-	-	-
2720	4.47	3.45	rough
4775	5.67	4.37	Tuorla

On basis of corrected time intervals between the optical minima, I derived the characteristic timescale of long-term variability of about 4 yr (corrected on redshift; otherwise the characteristic timescale is nearly 5 yr).

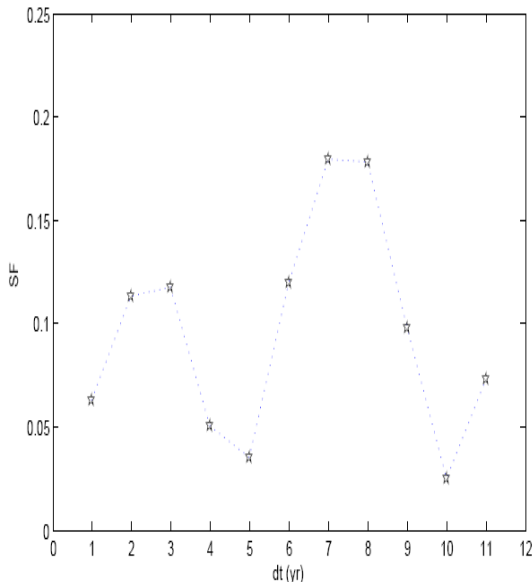


Figure 4.12: Structure function of 1ES 0414+009.

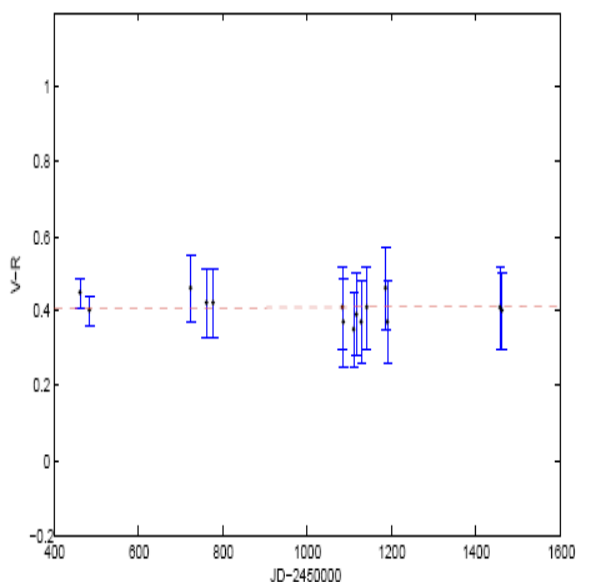


Figure 4.13: $V-R$ values for 1ES 0414+009.

Fig. 4.12 presents the plot of structure function constructed on basis of the data binned within one-year intervals. We see that there is a hint about quasi-periodical behaviour with a period of about 5 year (this value is in agreement with uncorrected characteristic timescale). Nevertheless, because we very few data points around the maximum to be presumably situated around $JD-2450000=200$, the existence of some more points could change the situation dramatically.

Intending to investigate the behaviour of the colour index $V-R$, V band observations were performed during 13 sessions (see Appendix B.3.2). Fig. 4.13 presents the results of the

monitoring, including the data of two sessions performed at Torino Observatory (Raiteri et al. 2000). No variability of $V-R$ values is found at 95% confidence level. We see only the fluctuations around the average value $\langle V - R \rangle = 0.41$ between 0.35 and 0.46 while the uncertainties are of 0.10-0.11 mag in the case of Abastumani observations.

Fig. 4.15 presents the short-term bursts revealed by means of Massaro et al. (1996) method. Totally 6 bursts at 95% confidence level and more are found (Table 4.6). Four of them occurred during long-term flaring activity, two – in minimum epochs. Thus, besides the shock-jet inhomogeneity interactions, another mechanisms causing short-term bursts should be important in this object.

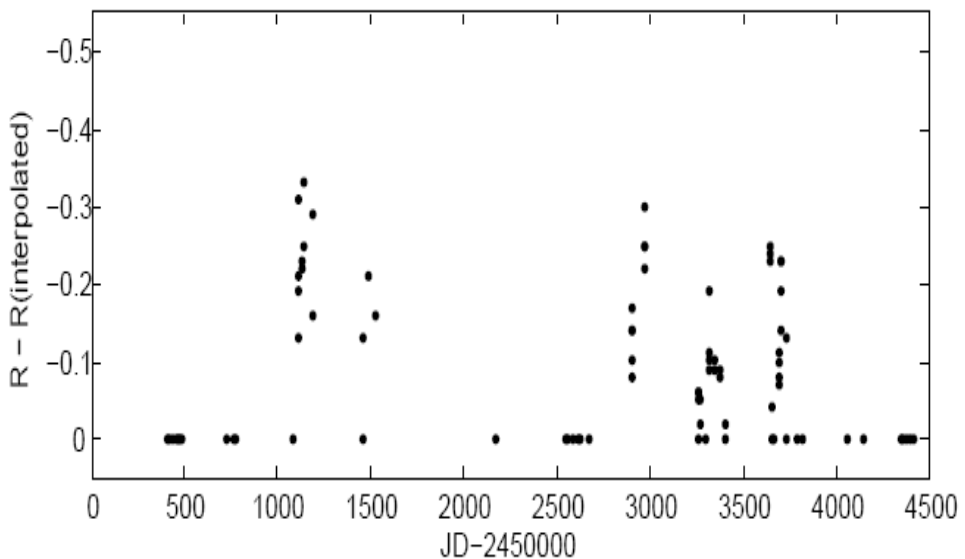


Figure 4.14: Short-term bursts in 1ES 0414+009.

The amplitudes of short-term bursts varied between 0.18 to 0.32 mag. Especially powerful burst is revealed in first minimum epoch peaking at $JD-2449000=1141$. Its amplitude was 0.32 mag (increase with 36% in R band flux compared to local base level). The slopes of ascending and descending parts of the busts are provided in the last column of Table 4.6. In average, the brightenings were a bit faster (-0.19 mag/month) than decays (0.16 mag/month). As in the previous case, no investigation of burst durations was carried out.

The duty cycle of short-term bursts was about 22% (16 “active nights versus total 68 nights (including Torino observations).

The source showed intraday variations in three occasions (Table 4.7; time intervals are corrected on redshift). The fastest change was an increase with 0.10 mag in 1.52 days (i.e. 6.2% a day). In the case of time interval not corrected on redshift, the fastest change is in increase 0.05 mag and the maximum expected change per session is 0.02 mag. Thus, it is not sensible to search for intranight changes in this object with small telescopes.

Table 4.6: Short-term busts in 1ES 414+009.

Moment of maximum brightness (JD-2450000) (1)	Number of “Active” Nights (2)	Amplitude (mag) (3)	Amplitude (%) (4)	Slope (mag/month, redshift corrected) (5)
1141.385	6	0.32	36	-0.20
1486.463	2	0.18	19	-0.25
2968.191	2	0.20	27	-0.13
3317.496	1	0.25	30	-0.18 0.09
3648.318	2	0.23	26	0.85
3709.314	2	0.21	23	-0.20 0.22

Table 4.7: Intraday changes in 1ES 0414+009.

Time interval (JD-2450000) (1)	Δt (days, redshift corrected) (2)	ΔR (mag) (3)	$\frac{\Delta F}{F}$ (%/d) (4)	Comment
408.5177-410.4695	1.52	-0.10	7.2	Torino
1111.488-1117.465	4.65	-0.18	4.3	-
3648.321-3653.527	4.04	0.23	6.2	-

4.4 1ES 0502+675

The source was monitored during 105 nights at Abastumani observatory between November 9,1997 and March 10, 2007. The historical light curve constructed on basis of R magnitudes (Appendix B4.1, column 3) is presented in Fig. 4.16a. The comparison light curve (Fig. 4.16c is constructed using the instrumental magnitudes of reference stars 5 ($R=14.31$) and 6 ($R=14.49$) provided by Villata et al. (1998; Appendix A4). In addition, the data points obtained at Torino 1.05 m telescope (October 31, 1996 and February 22, 1997; 17 sessions; values between JD-2450000=387 and 502 in Appendix B4.1, column 3; Raiteri et al. 1998) are also plotted. The data are corrected on galactic absorption ($A_R = 0.41$) and the derived results (column 4 in Appendix B4.1) are plotted at Fig. 4.16b.

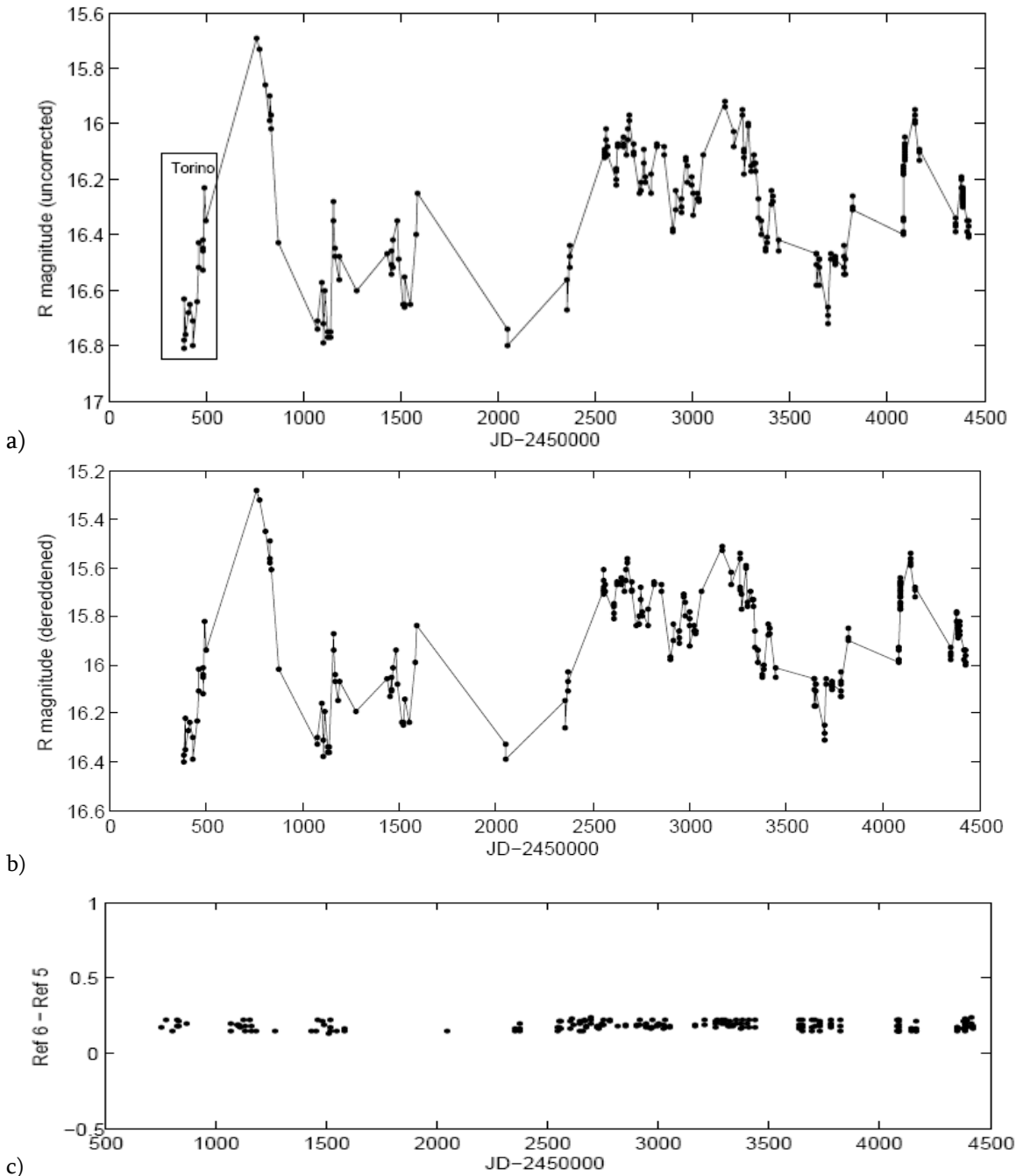


Figure 4.15: Historical R band light-curves of 1ES 0502+675 with a) magnitudes not corrected on galactic absorption; b) magnitudes corrected on galactic absorption; c) comparison light curve.

The data points are distributed along historical light curve relatively better compared to previous three objects. But large observational gaps are presents also here. There are especially long blank intervals between Abastumani and Torino observations (260 days); between JD-2449000=1587 and 2051. Due to the later gap, the optical maximum situated presumably around JD-2449000=1750 is omitted. Here, the optical minima are used to derive the timescales of long-term variability (see Table 4.8). The location of the third minimum is determined roughly. The last minimum is observed during Tuorla Blazar Monitoring Program (<http://users.utu.fi/kani/1m/>).

Table 4.8: Long-term variability in 1ES 0502+675.

Maximum Location (JD-2450000) (1)	Δt_{obs} (yr) (2)	Δt_{corr} (yr) (3)	Slope (mag/yr, per corrected term) (4)	Comment (5)
762			-1.38	Torino
1750	2.70	1.53	1.20	estimated roughly
2678	2.54	2.21	-	-
3171	1.35	1.47	0.85	-
4146	2.67	1.65	0.78	-
4800	1.80	1.91	-	Tuorla

According to the time intervals between the optical maxima, the characteristic timescale of long-term variability of about 2.2 yr is calculated (1.7 yr after correction on target redshift).

Fig. 4.17 presents the plot of structure function constructed on basis of the data binned within 250d intervals. Its first minimum at $dt = 750$ d is in agreement with the characteristic timescale derived above. The second minimum at $dt = 1750$ d almost agree with the interval between the minima JD-2450000≈ 2050 and 3700. Within this term, we have an increase in base level with about 0.5 mag. Because such changes do not carry a regular character for this object, we can suggest that the optical maxima at JD-2450000=2678 and 3171 are the example of two-peak maxima reflecting the propagation of forward and reverse shocks in blazar jet due to single disturbance at its base, as proposed by Marscher (1996).

In order to study the behaviour of the colour index $V-R$, V band observations were performed during 23 sessions (see Appendix B.5.2). Fig. presents the results of the monitoring, including the data of two sessions performed at Torino Observatory (Raiteri et al. 2000). No variability of $V-R$ values was found at 95% confidence level. They fluctuate around the average value $\langle V - R \rangle = 0.21$ between 0.20 and 0.34 while the uncertainties are of 0.09-0.10 mag for Abastumani observations.

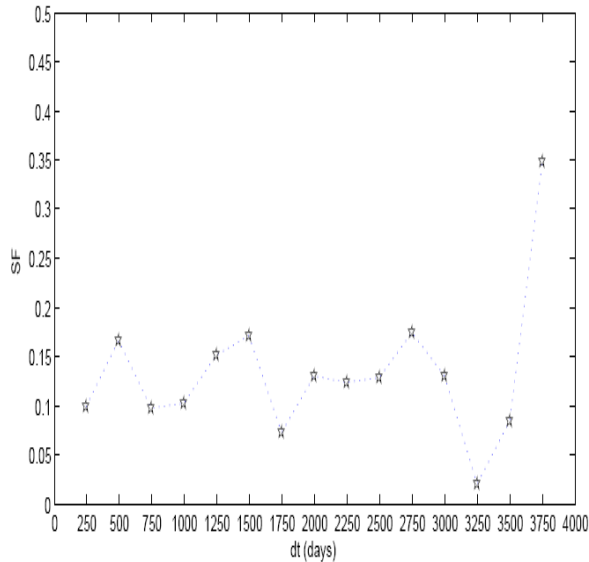


Figure 4.16: Structure function of 1ES 0502+675.

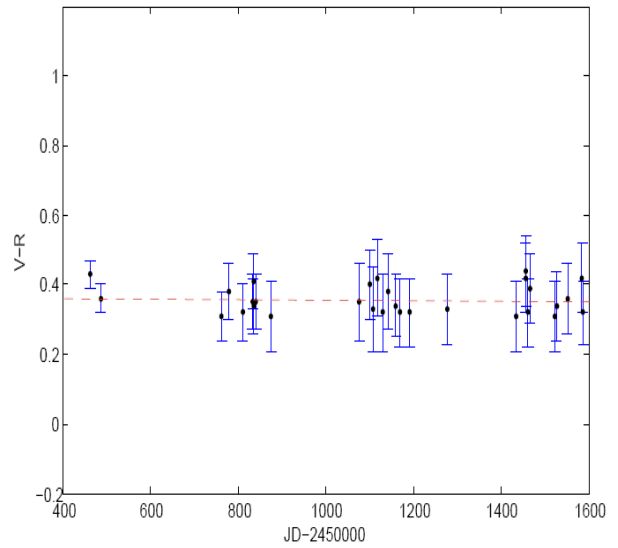
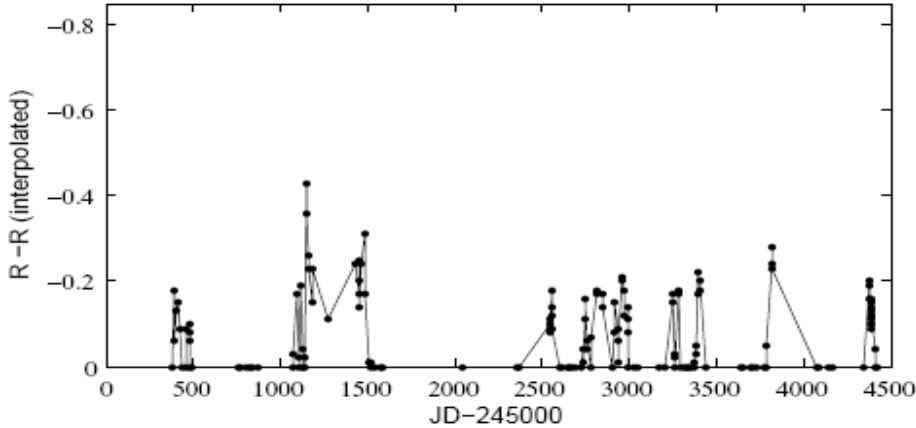
Figure 4.17: $V-R$ values for 1ES 0502+675.

Figure 4.18: Short-term bursts in 1ES 0502+675.

1ES 0502+675 is notable with its numerous and powerful short-term bursts (see Fig. 4.19). Thus, the jet of 1ES 0502+675 should be very inhomogenous (if the shock-in-jet scenario is true). Totally 15 bursts were observed (Table 4.9). Ten of them occurred during long-term flaring activity, five – in minimum epochs. The amplitudes of short-term bursts varied between 0.18 to 0.32 mag. Especially dramatic was a flare during the “quiet” stage of source optical brightness peaking at $JD-245000=1160$. Its amplitude is 0.45 mag. There was an increase with 52% in R band flux in 20 days.

The slopes of ascending and descending parts of the busts are provided in the column 5. In average, the brightenings and decays have nearly the same rates (-0.33mag/month vs. 0.35 mag/month). The duty cycle of short-term bursts was about 31% (38 “active nights” among total 122 sessions (including Torino observations).

Table 4.9: Short-term bursts in 1ES 0502+675.

Moment of maximum brightness (JD-2450000) (1)	Number of “Active” Nights (2)	Amplitude (mag) (3)	Amplitude (%) (4)	Slope (mag/month, redshift corrected) (5)	Comment (6)
391.6188	4	0.17	19	-0.30 0.34	Torino
1101.582	1	0.17	19	-0.24 1.00	-
1117.54	1	0.17	19	-0.67 0.26	-
1160.358	3	0.45	52	-0.73	-
1486.478	7	0.29	34	0.30	-
2559.457	1	0.18	22	0.13	-
2678.389	8	0.23	26	-0.13 0.20	-
2751.2900	1	0.15	16	-0.26 0.16	-
2817.494	2	0.15	16	-0.19 0.14	-
2968.521	2	0.18	20	-0.30 0.22	-
3259.475	1	0.15	16	-0.13 0.98	-
3290.525	1	0.19	22	-0.33 0.50	-
3405.311	2	0.20	23	-0.30 0.20	-
3823.253	1	0.26	28	-0.24	-
4383.380	3	0.17	19	-0.22 0.19	-

1ES 0502+675 is much active in point of intraday changes than the previous three sources. During 11-year term, 11 occasions of such changes are detected at 95% confidence level (Table 4.10). Especially fast changes are recorded during Torino observations. For example, we have a decrease with 15.5% in *R* band flux a day (0.11 mag in 0.78 days (1.02 days without correction on source’s redshift)) or an increase with 12.6% a day (corresponding to 0.18 mag in 1.58 days).

In average, the brightness increased faster ($9\text{ \%}/\text{d}$, $\frac{\Delta F}{F} = (5.0\text{--}12)\text{ \%}/\text{d}$, 5 occasions) than decayed ($5.5\text{ \%}/\text{d}$, $\frac{\Delta F}{F} = (3.7\text{--}5.4)\text{ \%}/\text{d}$, 6 occasions). Fig. 4.20 shows intraday changes occurring in 1ES 0502+675 between JD-2450000=1100 and 1170. As a rule, intraday changes are associated with short-term bursts.

Table 4.10: Intraday changes in 1ES 0502+675.

Time interval (JD-2450000)	Δt (days, redshift corrected)	ΔR	$\frac{\Delta F}{F}$ (%/d)	Comment
389.5394-391.6188	1.58	-0.18	12.6	Torino
391.6188-396.5763	3.77	0.13	3.7	Torino
435.4473-436.4143	0.74	0.09	13.7	Torino
459.4171-465.4248	4.57	-0.21	5.0	Torino
489.3146-490.3372	0.78	0.11	15.4	Torino
490.3372-494.2837	3.00	-0.30	11.0	Torino
494.2837-502.3079	5.26	0.12	2.5	Torino
1101.582-1107.576	4.57	0.25	5.9	-
1584.39-1587.426	2.31	-0.15	7.0	-
3259.475-3264.574	3.88	0.15	4.1	-
4083.379-4087.460	3.11	-0.25	8.7	-

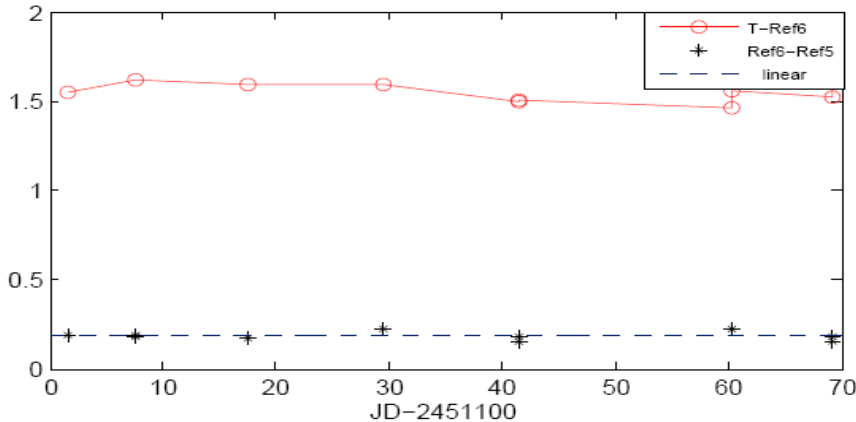


Figure 4.19: Example of intraday changes in 1ES 0502+675.

As mentioned above, the fastest optical change is a decrease with 0.11 mag a day which corresponds to maximum expected variation of 0.05 mag per session. This value is below the accuracy achieved for this source in the case of 70 cm meniscus telescope.

4.5 1ES 0647+250

The source was monitored during 53 nights at Abastumani observatory between November 25, 1997 and March 28, 2007. The historical light curve constructed on basis of R magnitudes (Appendix B5.1, column 3) is presented in Fig. 4.21a. The comparison light curve (4.21c) is constructed using the instrumental magnitudes of reference stars C6 and C7 (corresponding to the star F($R=14.89$) in Nilsson et al. 2007) provided at <http://astro.fisica.unipg.it/PGblazar/0647.html> (see Appendix A5). I have corrected the data

on galactic absorption ($A_R = 0.26$) and the light curve corrected on basis of de-reddened values (column 4) are provided in Fig. 4.21b.

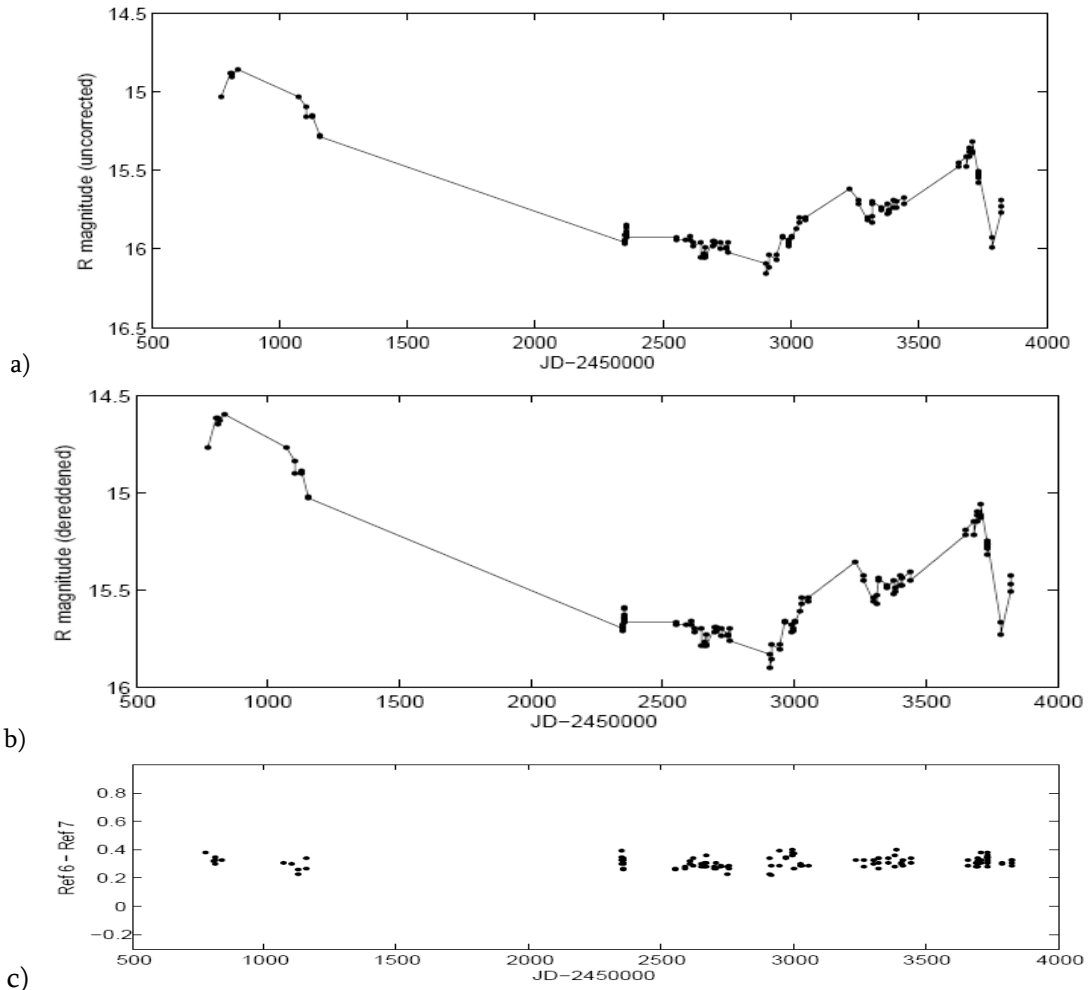


Figure 4.20: Historical R band light-curves of 1ES 0647+250 with a) magnitudes not corrected on galactic absorption; b) magnitudes corrected on galactic absorption; c) comparison light curve.

Here, we have especially great observational gap between $JD=1160$ and 2354 . On basis of characteristic timescale of long-term variability (see table 4.11) we can suggest that a couple of optical maximum and minimum is omitted.

On basis of the time intervals between the optical minima (the third one is observed during Tuorla Blazar Monitoring Program), the characteristic timescale of long-term variability of about 2 yr is calculated (1.5 yr after the correction on target redshift).

Note that the observed peaks are of very different heights (their difference equals 0.5 mag). It is quite possible that this difference is caused by the change in the base level with timescales of decade order. The overall variation is $\Delta R = 1.29$ per 10 yr term with maximum brightness corresponding to $R=14.86$.

Table 4.11: Long-term variability in 1ES 0647+250.

Minimum location (JD-2450000) (1)	Δt_{obs} (yr) (2)	Δt_{corr} (yr) (3)	Slope (mag/yr, per corrected term) (4)	Comment (5)
2907			-0.62	
3787	2.40	1.85		
4406	1.70	1.3	3.80	Tuorla

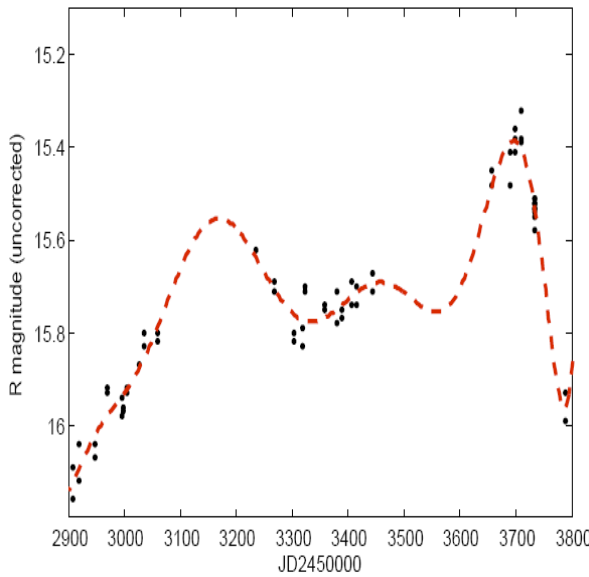
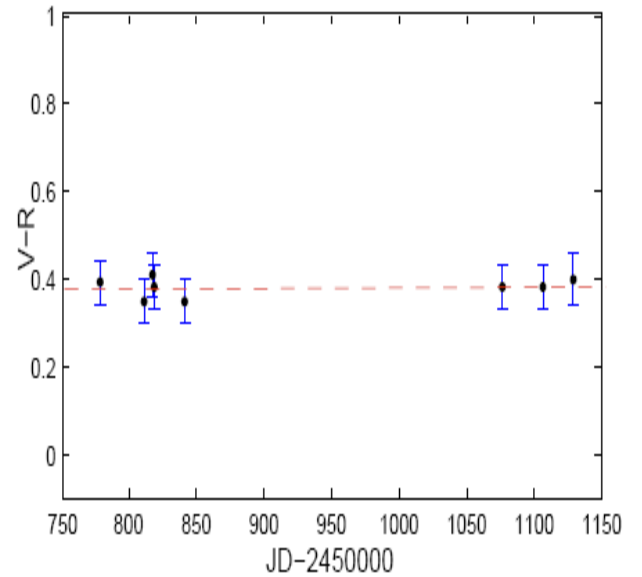


Figure 4.21: Two-peak maximum in the historical light curve of 1ES 0647+250.

Figure 4.22: $V-R$ values for 1ES 0647+250.

During long-term flare between $JD - 452000 = 907$ and 1782 , we presumably deal with a double-peak maximum. The first peak is not expressed perfectly due to some gap and it is recovered by the interpolation (Fig. 4.22).

In order to study the behaviour of the colour index $V-R$, V band observations were performed during 8 sessions (see Appendix B.5.2). No variability of $V-R$ values was found (Fig 4.23). They fluctuate around the average value $\langle V - R \rangle = 0.38$ between 0.35 and 0.41 while the uncertainties are of 0.05–0.06 mag.

Neither fast brightness changes nor short-term bursts are detected. Consequently, the jet of 1ES 0647+250 may be considered as homogenous compared to the jets of previous objects.

4.6 1ES 0806+524

The source was monitored during 111 nights at Abastumani observatory between December 29, 1997 and May 30, 2007. Fig. 4.24a shows its historical light curve constructed on basis of R magnitudes (Appendix B6.1, column 3). The comparison light curve (Fig. 4.24c) was generated using the instrumental magnitudes of reference stars C2 ($R=14.22$) and C5 ($R=15.32$) provided by Fiorucci et al. (1998; see Appendix A6). They match the target closely in colour ($V-R=0.36$ and 0.30 ; see the target colour indices below) and their difference gave the least scatter during the whole observational campaign (see column 2 of Appendix B6.1).

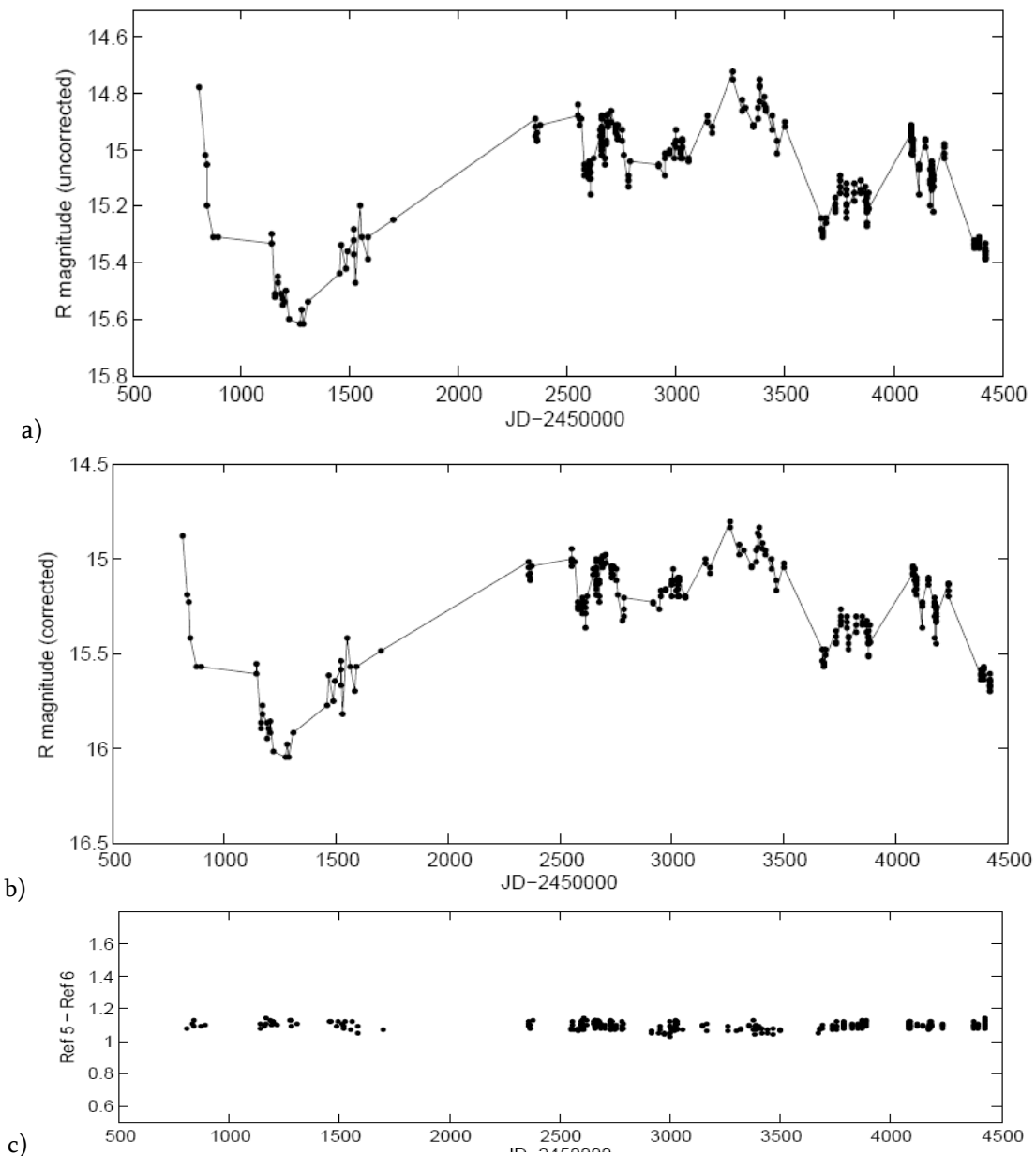


Figure 4.23: Historical R band light-curves of 1ES 0806+524 with a) magnitudes including host contribution and not corrected on galactic absorption; b) magnitudes corrected on host contribution and galactic absorption; c) comparison light curve.

1ES 0806+524 is hosted by the luminous galaxy which contribution varies from 18% to 40% (in the case of aperture radius of 7."5) depending on the state blazar flux level. Thus, it can dilute the intrinsic optical variability significantly. Here the aperture radius of about 7."5 was used in order to make R magnitudes comparable with the preliminary values obtained at Tuorla Observatory, see <http://users.utu.fi/kani/1m/>). In order to correct R magnitudes on host contribution, they were converted into linear fluxes (Appendix B6.1, column 5) and the obtained values were corrected according to Nilsson et al. (2007). The derived linear fluxes (column 6) were converted back into stellar magnitudes (column 7) and corrected on galactic absorption ($A_R=0.12$). In this case, rms errors is about 0.06. The data were corrected on galactic absorption ($A_R =0.41$) and the derived results (column 8 in Appendix B6.1) are plotted at Fig. 4.24b. Fig. presents the historical light curve constructed on basis of corrected R magnitudes.

Historical light curve of 1ES 0806+524 contains especially great observational gap between JD=1702 and 2358. On basis of characteristic timescale of long-term variability (see below) we can suggest that there should be a couple of optical maximum and minimum during this term.

Table 4.12: Long-term variability in 1ES 0806+524.

Minimum Location (JD-2450000) (1)	Δt_{obs} (yr) (2)	Δt_{corr} (yr) (3)	Slope (per corrected term, mag/yr) (4)	Comment (5)
460	-	-	-	Perugia
1 286	2.26	1.98	0.70	-
2 050	2.09	1.84	-	probable
2 800	2.05	1.80	-0.50	-
3 600	2.19	1.92	0.50	-
4 500	2.46	2.17	0.60	-

According to the time intervals between the optical minima (Table 4.12), the characteristic timescale of long-term variability of about 2.2 yr is calculated (nearly 2yr after the correction on target redshift). The first minimum was observed at Perugia Observatory (see <http://astro.fisica.unipg.it/PGblazar/0806lc.gif>), and the last one during Tuorla Blazar Monitoring Program. It is clear that the source does not show periodical flares of the years order.

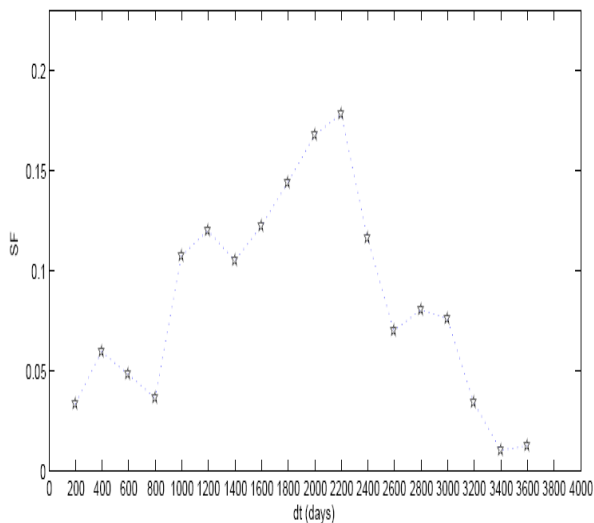


Figure 4.24: Structure function of 1ES 0806+524.

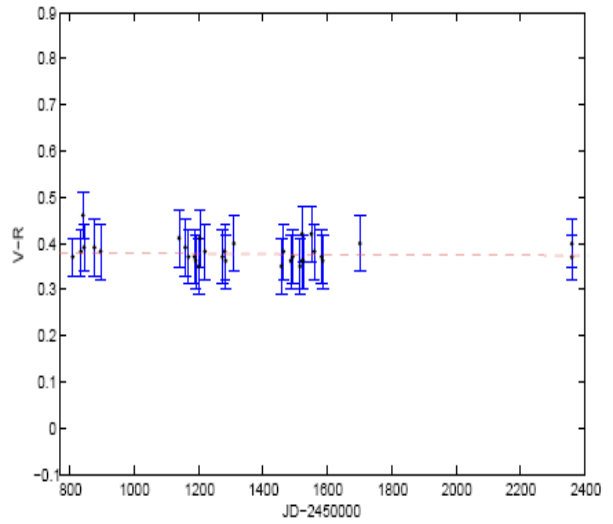
Figure 4.25: $V-R$ values for 1ES 0806+524.

Fig. 4.25 presents the plot of structure function constructed on basis of the data binned within 200d intervals. Its first minimum at $dt = 750$ d is in agreement with the characteristic timescale derived above. Both visual inspection of the historical light curve and the shape of structure function allow us to suggest that the source possesses a variable base level of the optical flux. Hence, the source shows presumably another long-term trend with timescales of decade order.

Fig. 4.27 presents the results of the study of the $V-R$ colour index behaviour performed during 33 sessions (see Appendix B.6.2). The average value $\langle V - R \rangle = 0.38$. Data points range between 0.35 and 0.43 with the uncertainties of 0.05–0.06 mag. Thus, there is no variability of $V-R$ values at 95% confidence level.

The historical light curve exhibits powerful short-term bursts (see Fig. 4.27). Totally 10 bursts were observed (Table 4.13). Seven of them occurred during long-term flaring activity, two – in minimum epochs and it is hard to say whether the flare with maximum at around $JD-2449000=4081$ belongs to “active” or “quiet” epoch.

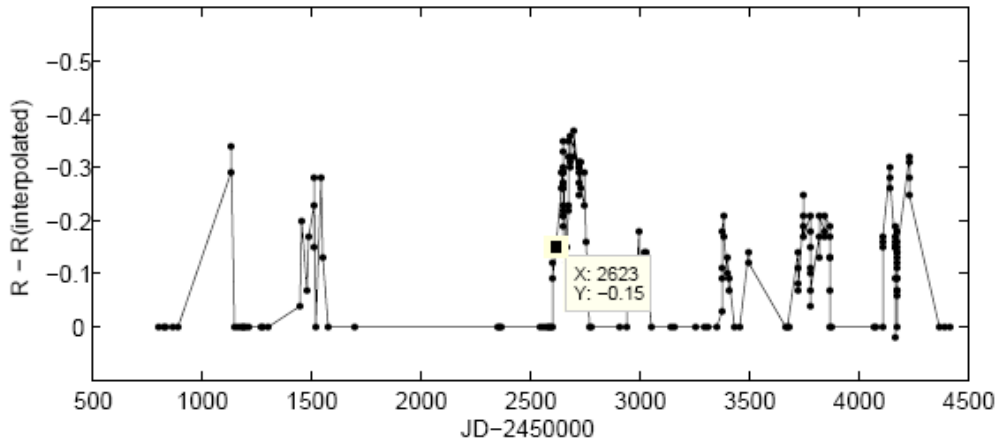


Figure 4.26: Short-term bursts in 1ES 0806+524.

Table 4.13: Short-term bursts in 1ES 0806+524.

Moment of maximum brightness (JD-2450000) (1)	Number of “Active” Nights (2)	Amplitude (mag) (3)	Amlitude (%) (4)	Slope (mag/month, redshift corrected) (5)
1141.4988	1	0.45	52	0.54
1517.5061	1	0.18	21	-0.10 0.55
1551.4333	1	0.38	42	-0.53 0.28
2704.4494	14	0.42	49	-0.21 0.21
3 003.5287	3	0.19	21	-0.11 0.09
3 388.5742	2	0.19	22	-0.21 0.16
3 501.2854	1	0.16	18	-0.14
3 752.3914	6	0.27	30	-0.10 0.50
4 145.4025	4	0.31	34	-0.33 0.32
4 235.2719	2	0.30	33	-0.19

The amplitudes of shot-term bursts varied between 0.18 to 0.32 mag. The slopes of ascending and descending parts of the busts are provided in the last column. In average, the source decayed much faster (-0.32 mag/month) than brightened (-0.21 mag/month). The duty cycle of short-term bursts was about 22% (32 “active” nights versus total 111 nights).

Table 4.14: Intraday changes in 1ES 0806+524.

Time interval (JD-2450000) (1)	Δt (days, redshift corrected) (2)	ΔR (mag) (3)	$\frac{\Delta F}{F}$ (%/d) (4)	Comment (5)
1523.5395-1526.4218	2.56	0.28	11.1	host subtracted
2678.4444-2682.5331	3.63	-0.13	3.9	host subtracted
3385.3435-3388.5742	2.86	-0.13	4.9	host subtracted
3784.3331-3786.3186	2.65	0.16	6.4	host subtracted
3878.2560-3881.2701	2.68	-0.14	5.6	host subtracted

5 occasions of intraday changes are detected at 95% confidence level (Table 4.14) which are associated with short-term bursts. The fastest change was recorded between JD-2450000=1523 and 1526. In that case, we have a decrease with 0.28 mag in 2.56 days (11.1% a day).

In average, the brightness decayed faster ($8\%/\text{d}$, $\frac{\Delta F}{F} = (5.0\text{-}12)\%/\text{d}$, 2 occasions) than increased ($4.8\%/\text{d}$, $\frac{\Delta F}{F} = (3.7\text{-}5.4)\%/\text{d}$, 6 occasions). This result is in agreement to that obtained for short-term bursts.

The fastest optical change, detected for this source, corresponds to a decrease with about 0.10 mag a day. So, the expected maximum intranight change is about 0.04 mag and it can be detected in rare occasions by means of very precise observations. Fig. 4.28 presents the results of intranight observations which show no variability at 99 confidence level ($C=1.21$).

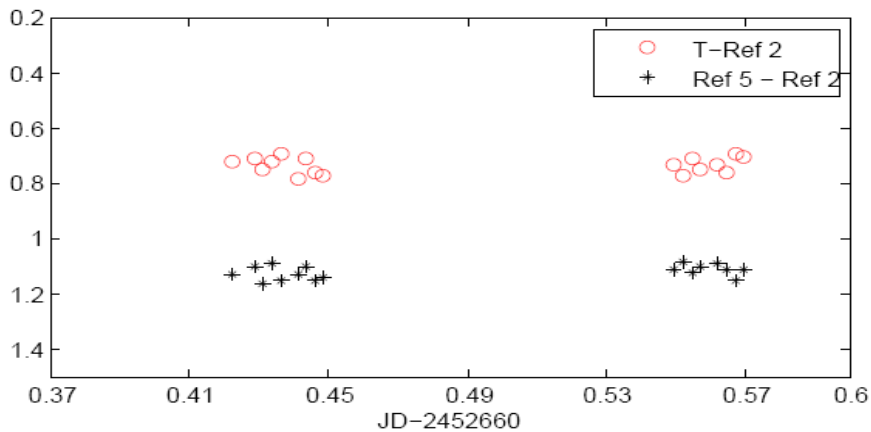


Figure 4.27: Example of intranight R band light curve of 1ES 0806+524.

4.7 1ES 1028+511

The source was monitored during 78 nights at Abastumani observatory between January 28, 1998 and November 18, 2007. Fig. 4.29 exhibits its historical light curve constructed on basis of R magnitudes (Appendix B7.1, column 3). Furthermore, the data points obtained at Torino 1.05 m telescope (December 3, 1996 and May 8, 1997; Villata et al. 1998; values between $\text{JD-2450000}=420$ and 577 in Appendix B7.1) are also plotted. The comparison light curve (Fig. 4.29b) was derived on basis of the instrumental magnitudes of reference stars 5 ($R=14.75$) and C5 ($R=14.87$) provided by Villata et al. (1998; see Appendix A7).

R band flux level is low for this source: $F_R=0.1$ mJy (Nilsson et al. 2007). Galactic reddening is very small too: $A_R = 0.03$ mag. Hence, no historical light curve, constructed on basis of host-subtracted and de-reddened values has been constructed.

Historical light curve of 1ES 1028+511 shows that the optical minima are sparcely observed. In order to derive the characteristic timescale of long-term variability, the moments of optical maxima were used (Table 4.15). According to the time intervals between the optical maxima, the characteristic timescale of long-term variability of about 4.3 yr is obtained (nearly 3.1 yr after the correction on target's redshift).

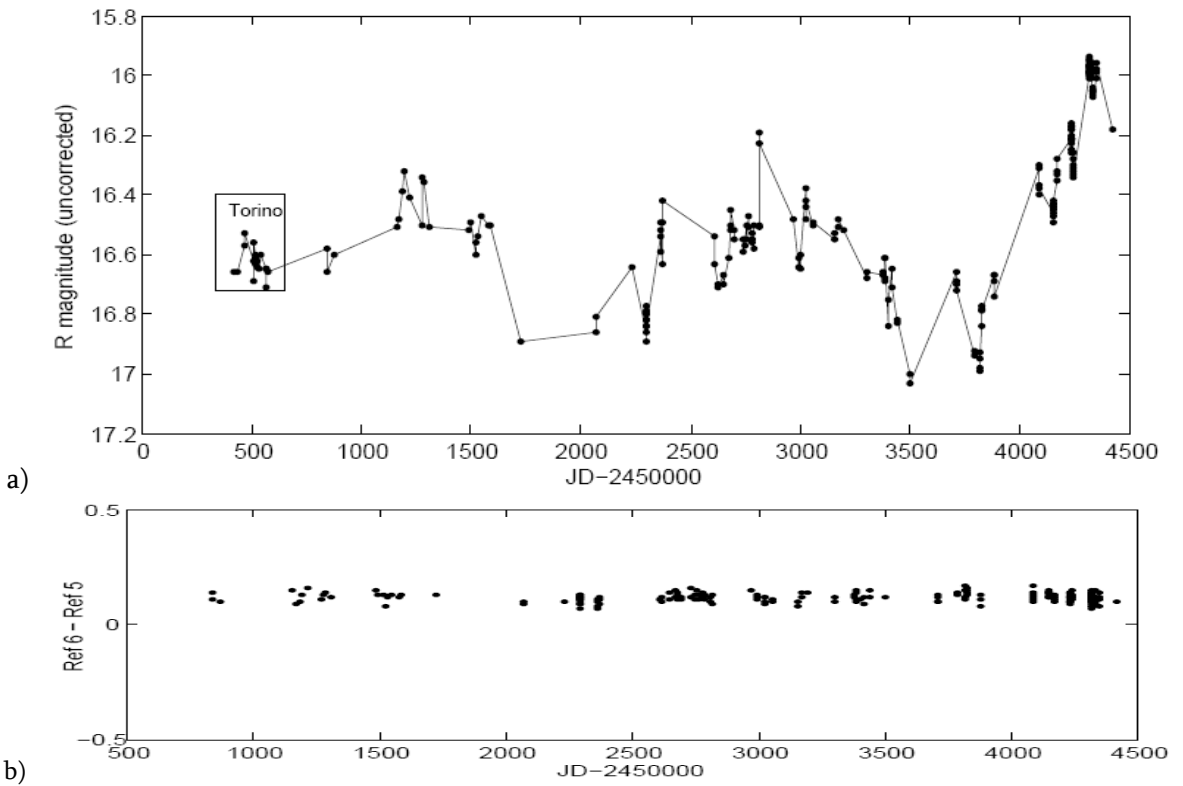


Figure 4.28: a) Historical R band light curve of 1ES 1028+511; b) comparison light curve.

It is interesting that the intervals between the consequent maxima are nearly the same (4.4 yr and 4.1 yr). This fact gives rise to the suggestion that the source undergo quasi-periodical flares. The same result can be obtained from the structure function constructed on basis of the data binned within 250 d intervals (Fig. 4.30).

Table 4.15: Long-term variability in 1ES 1028+511.

Maximum location (JD-2450000) (1)	Δt_{obs} (yr) (2)	Δt_{corr} (yr) (3)	Slope (mag/yr) (4)
1194	-	-	-
2817	4.44	3.26	0.57
4 320	4.11	3.02	-0.76

Note that this result should be regarded as very preliminary due to sparse distribution of the data points and relatively low number of flaring cycles. Among three flaring cycles, only the second one is included completely within the monitoring term. The later is too short to confirm periodical variability of 1ES 1028+511 – it includes only two “periods” which is very few in statistical point of view. Thus, future monitoring is needful for periodicity confirmation.

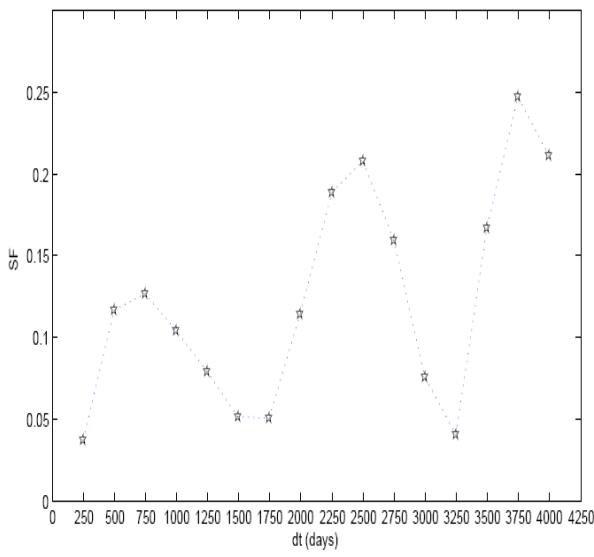
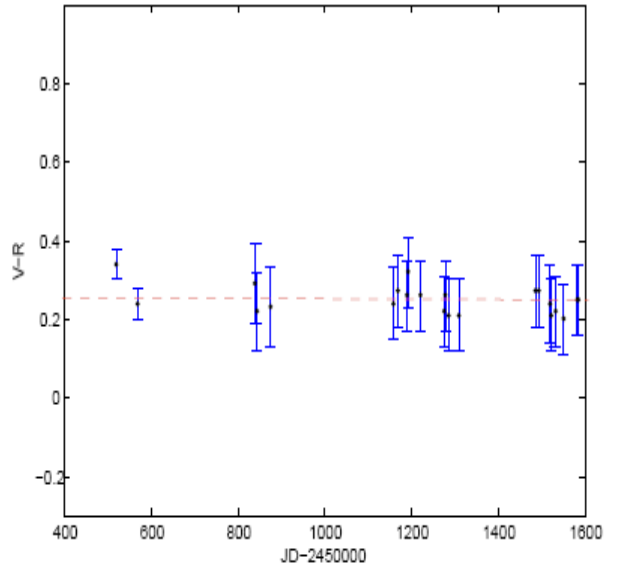


Figure 4.29: Structure function of 1ES 1028+511.

Figure 4.30: $V-R$ values for 1ES 1028+511.

It is conspicuous that the heights of the optical maxima has been increasing with time: $R=16.32$ at $JD-2450000=1193$, $R=16.19$ at $JD-2450000=2817$, and $R=15.94$ at $JD-2450000=430$. It is possible that this linear trend is caused by the change in optical base level at decade-order timescales. Unfortunately, the lack of observational data around the minima does not allow to confirm this suggestion.

In order to study the behaviour of the colour index $V-R$, V band observations were performed during 20 sessions (see Appendix B.7.2). Fig. 4.31 presents the results of this investigation, including the data of two sessions performed at Torino Observatory (Villata et al. 2000). I have not found any variability of $V-R$ values at 95% confidence level. They fluctuate around the average value $\langle V-R \rangle = 0.21$ between 0.20 and 0.34 while the uncertainties are of 0.09-0.10 mag for Abastumani observations.

Fig. 4.32 presents the short-term bursts revealed during 11 yr term. Totally 9 bursts at 95% confidence level and more are found (Table 4.16). Eight of them occurred during long-term flaring activity, only one burst – in minimum epoch (peaking at $JD-2450000=3710$). Thus, the shock-jet inhomogeneity interactions should be considered as a basic mechanism responsible for short-term bursts in this object.

The amplitudes of short-term bursts ranged between 0.16 to 0.36 mag. Especially dramatic is the burst at the second maximum epoch peaking at $JD-2449000=2817$. Its amplitude is 0.30 mag (an increase with 33% in R band flux compared to local base level in 5 days). The slopes of ascending and descending parts of the busts are given in the last column. In average, the brightenings were much faster (-0.49 mag/month) than decays (0.15

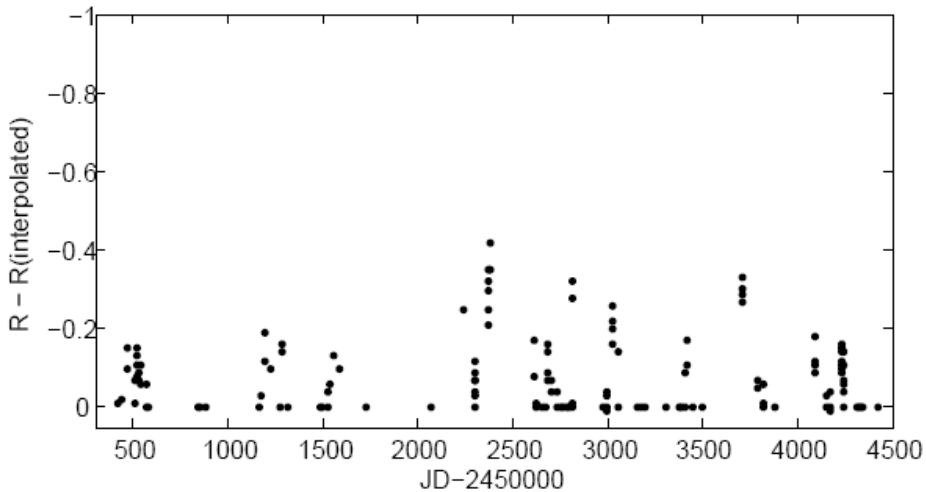


Figure 4.31: Short-term bursts in 1ES 1028+511.

mag/month).

As in the previous cases, no statistical investigation of burst durations was carried out. The duty cycle of short-term bursts was about 20% (19 “active” nights versus total 86 sessions (including Torino observations).

Table 4.16: Short-term busts in 1ES 1028+511.

Moment of maximum brightness (JD-2450000) (1)	Number of “Active” Nights (2)	Amplitude (mag) (3)	Amplitude (%) (4)	Slope (mag/month, redshift corrected) (5)	Comment (6)
466.5331	7	0.14	16	-0.20 0.10	Torino
1193.522	1	0.17	19	-0.21 0.08	
2237.555	1	0.22	25	0.15	
2375.270	3	0.33	36	-0.25	
2682.552	1	0.17	19	-0.30	
2817.299	1	0.30	33	-1.50 0.10	
3023.588	2	0.24	26	-0.39	
3417.458	1	0.17	19	-0.58	
3709.528	1	0.31	32	0.12	
4088.506	1	0.17	19	0.20	

4 occasions of intraday changes are detected at 95% confidence level (Table 4.17) which are associated with short-term bursts, as a rule. The fastest change was recorded between JD-2450000=4236 and 4239. Here, there is a decrease with 0.18 mag in 2.15 days (8.8 % a day; the interval is corrected on redshift). In three cases, the source underwent fast flares with 0.13-0.21 mag during 2.92-4.36 days (an increase with (4.8-8.0)% a day in *R* band flux).

Table 4.17: Intraday changes in 1ES 1028+511

Time interval (JD-2450000) (1)	Δt (days, redshift corrected) (2)	ΔR (mag) (3)	$\frac{\Delta F}{F}$ (%/d) (4)	Comment (5)
509.4744-513.448	2.92	-0.13	4.8	Torino
1276.344-1279.418	2.26	-0.17	8.0	
2369.348-2375.27	4.36	-0.21	5.3	
4236.378-4239.308	2.15	0.18	8.8	

The fastest optical change, detected for this source, corresponds to a decrease with about 0.06 mag a day. So, the expected maximum intranight change is about 0.02 mag and it can be detected in rare occasions by means of great telescopes. Fig. 4.33 presents the results of intranight observations which show no variability at 99% confidence level ($C=1.18$).

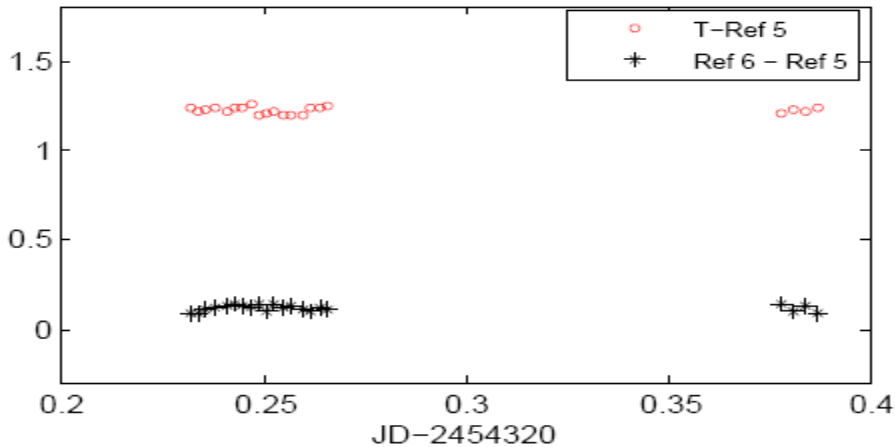


Figure 4.32: Intranight R band light curve of 1ES 0806+524.

4.8 1ES 1426+428

The source was monitored during 87 nights at Abastumani observatory between March 31, 2003 and October 9, 2007. Fig. 4.35a shows its historical light curve constructed on basis of R magnitudes (Appendix B8.1, column 3). The comparison light curve (Fig. 4.35c) was generated using the instrumental magnitudes of reference stars 4 ($R=15.20$, Smith et al. 1991) and 5, selected among field stars (see Fig. 4.34). Their difference gave the least scatter during the whole observational campaign.



Figure 4.33: Reference stars in the field of 1ES 1426+428.

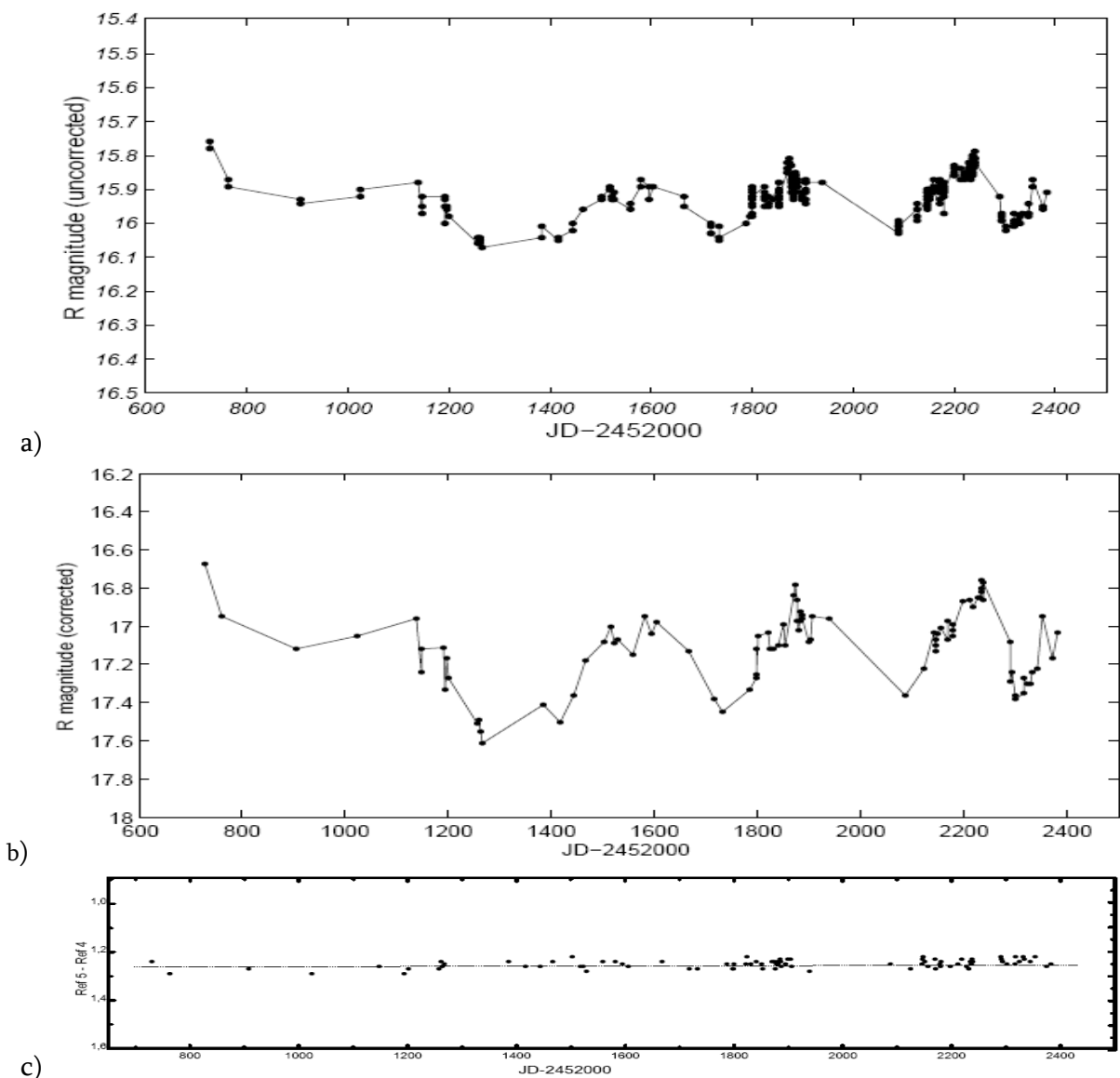


Figure 4.34: Historical R band light-curves of 1ES 1426+428 with a) magnitudes including host contribution and not corrected on galactic absorption; b) magnitudes corrected on host contribution and galactic absorption; c) comparison light curve.

1ES 1426+428 is hosted by the luminous galaxy which contribution varies from 59% to 76% (in the case of aperture radius of 7."5). depending on the state of source brightness. Consequently, it can dilute the intrinsic optical variability greatly. In order to correct R magnitudes on host contribution, they were converted into linear fluxes (Appendix B9.1, column 5) and the obtained values were corrected according to Nilsson et al. (2007). The derived linear fluxes (column 6) were converted back into stellar magnitudes (column 7) and corrected on galactic absorption (column 8; $A_R=0.03$). In this case, the uncertainties become about 0.15 mag. Fig. 4.35b presents the historical light curve constructed on basis of corrected R magnitudes (averaged per session).

None optical minima in the historical light curve is covered well by the observations, except for the last one. The same should say about first two maxima. Using the time intervals between the optical maxima (Table 4.17; the last minimum is observed during Tuorla Blazar

Table 4.17: Long-term variability in 1ES 1426+428.

Maximum location (JD-2452000) (1)	Δt_{obs} (yr) (2)	Δt_{corr} (yr) (3)	Slope (mag/yr, per corrected term) (4)	Comment (5)
730	-	-	-	-
1141	1.13	1	1.35	rough
1582	1.21	1.07	-1.15	-
1885	0.83	0.73	-1.5	-
2237	0.96	0.85	-1.5	-
2633	1.08	0.96	-	Tuorla

Monitoring Program, see <http://users.utu.fi/kani/1m/>), the characteristic timescale of long-term variability of about one yr was obtained (≈ 0.9 yr after the correction on target redshift; see also the location of first peak of the structure function at Fig. 4.36). Thus, 1ES 1426+428 is the fastest object among the targets in point of long-term variability. It is clear that the source does not show periodical flares of years order. In average, decays were faster (1.7 mag/yr, see 4th column of Table 4.17) than brightenings (-1.4 mag/yr).

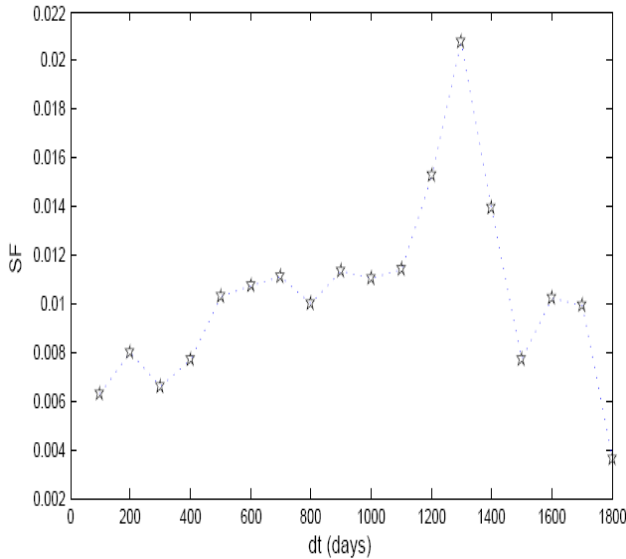


Figure 4.35: Structure function of 1ES 1426+428.

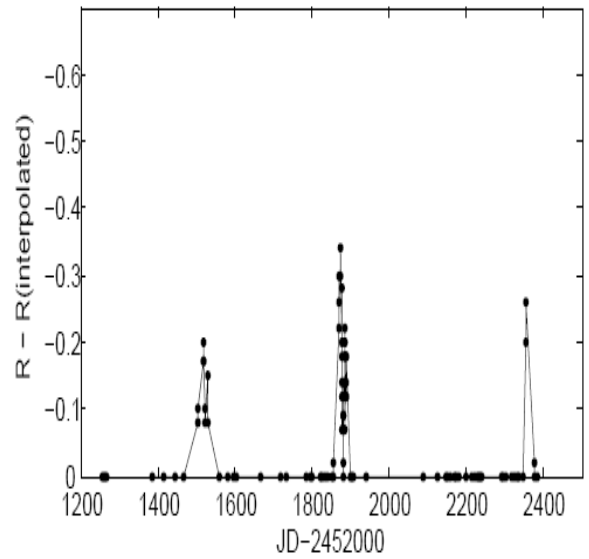


Figure 4.36: Short-term bursts in 1ES 1426+428.

Only 2 short-term bursts are detected at 95% confidence level and more (Fig. 4.37, Table 4.19) and both belong to flaring epochs. Thus no other mechanism bur shock-in-jet scenario should be important for this source.

Table 4.19: Short-term busts in 1ES 1426+428

Moment of maximum brightness (JD-2 450000) (1)	Number of “Active” Nights (2)	Amplitude (mag) (3)	Amplitude (%) (4)	Slope (mag/month, redshift corrected) (5)
3871.4300	3	0.33	38	-0.51 0.40
4354.519	1	0.24	27	-0.55 0.23

The amplitudes of short-term bursts were between 0.24 to 0.33 mag (corresponding to the increases with 38% and 27% in R band flux compared to local base level). In average, the brightenings were much faster (-0.53 mag/month) than decays (0.31 mag/month). The duty cycle of short-term bursts was about 5% (4 “active” nights versus total 87 nights).

No intraday variabilities were seen for the source. The fastest change was an increase with 32 mag in 9 d ($JD-2452000=2345-2354$) associated with the second short-term burst.

The source was examined for microvariabilities during three sessions. No positive results were obtained in this respect. Fig. 4.38 presents the results of intranight observations which show no variability at 99% confidence level ($C=1.21$).

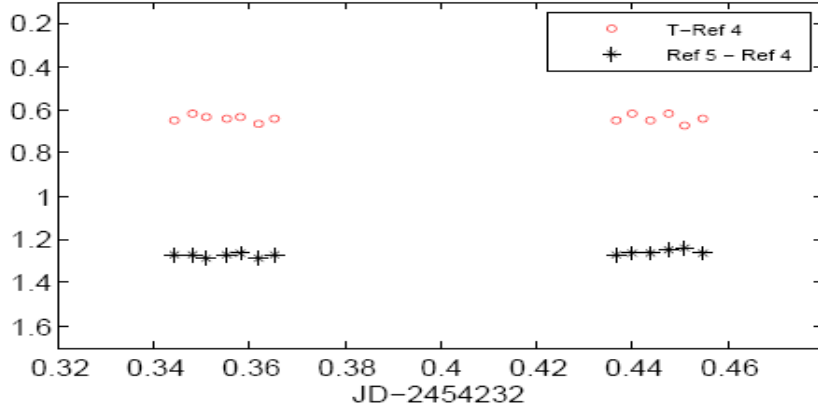


Figure 4.37: Intranight R band light curve of 1ES 1426+428.

4.9 1ES 1517+656

The source was observed during 56 nights at Abastumani observatory between January 28, 1998 and May 15, 2007. Its historical light curve is plotted at Fig. 4.39a (see respective R magnitudes in third column of Appendix B9.1). The comparison light curve (Fig. 4.39b) is constructed by means of the instrumental magnitudes of reference stars 6 ($R=14.07$) and 7 ($R=14.26$) provided by Villata et al. (1998; see Appendix A9). In addition, the data points obtained at Torino 1.05 m telescope (February 18, 1996 and May 29, 1997; 17 sessions; Raiteri et al. 1998; values between JD-2450000=497 and 598 in Appendix B9.1) are also plotted.

This source does not possess bright host galaxy. Nor galactic absorption is high ($A_R=0.07$, see corrected R magnitudes in the column 5 of Appendix B9.1). Hence, no historical light curve, constructed on basis of corrected R magnitudes, is provided here.

Historical light curve of 1ES 1517+656 shows that the distribution of data point with time is very uneven. We have only two points in the interval between JD-2450000=598-2660. It is evident that a couple of optical minima should be take place within this interval. The maximum (nearly JD-2450000=2200) was recovered by polynomial fitting.

In order to derive the characteristic timescale of long-term variability, the moments of optical maxima were used (Table 4.20). According to the time intervals between the optical maxima, the characteristic timescale of long-term variability of about 4.5 yr is obtained (nearly 2.7 yr after the correction on target redshift).

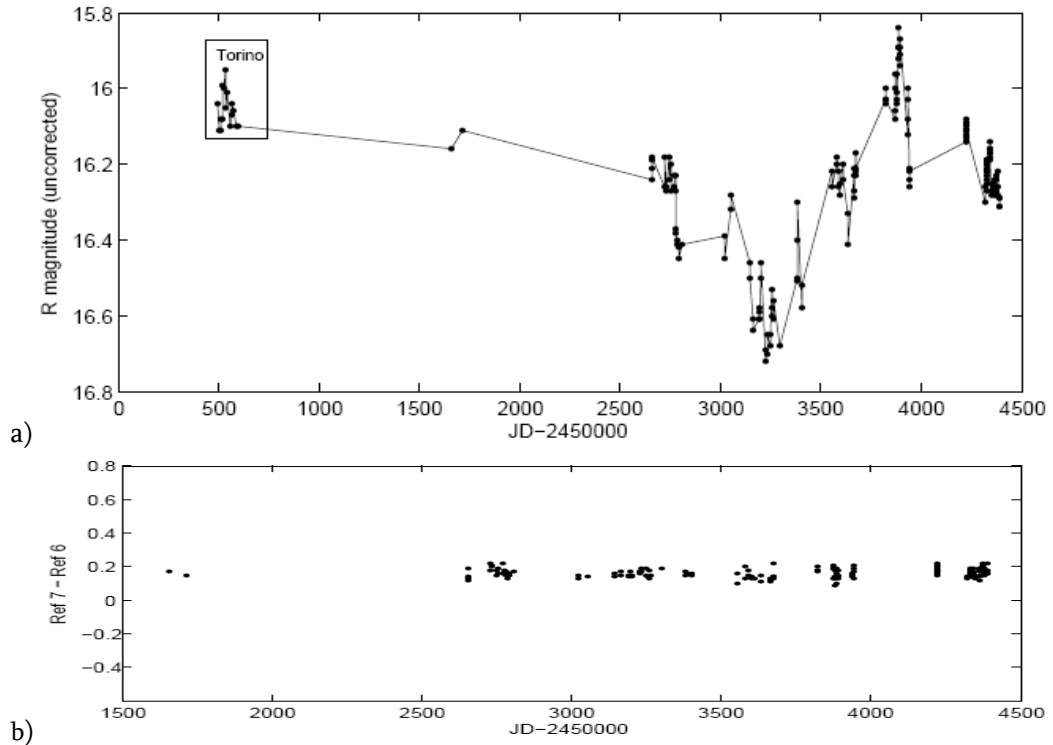


Figure 4.38: a) Historical R band light curve of 1ES 1517+656; b) comparison light curve.

Table 4.20: Long-term variability in 1ES 1517+656

Maximum Location (JD-2450000) (1)	Δt_{obs} (yr) (2)	Δt_{corr} (yr) (3)	slope (mag/yr) (4)	Comment (5)
536	-	-	-	-
2250	4.70	2.76	-	recovered by means of polynomial fitting
3890	4.50	2.65	-0.80	-

Due very great gap in the observations, no structure function is calculated for this source. R magnitude ranged between 15.84 and 16.72. The maximum observed amplitude is $\Delta R = 0.87$.

It seems reasonable to suggest that there is a two-peak maximum around $JD-450000 \approx 4000$. The second peak is not expressed perfectly due to some observational gap.

Fig. 4.40 shows the behaviour of the colour index $V-R$ during three sessions (including two data points obtained at Torino Observatory, see Raiteri et al. 1998). The

respective numerical values are provided in Appendix B9.2. We have no variability here but a fluctuation of statistical origin with a average value of $\langle V - R \rangle = 0.35$.

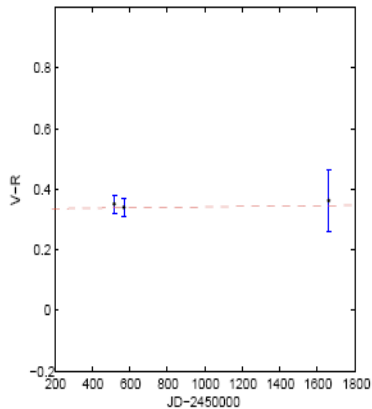


Figure 4.39: $V - R$ values for 1ES 1517+656.

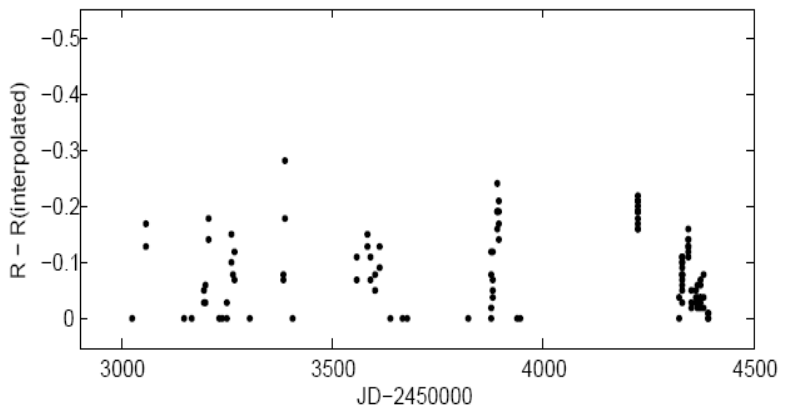


Figure 4.40: Short-term bursts in 1ES 1517+656.

We see that powerful short-term bursts are familiar for this source. Fig. 4.41 presents these bursts revealed during 11 yr term. Totally 9 bursts at 95% confidence level and more are found (Table 4.21). Seven of them occurred during long-term flaring activity, two bursts – in minimum epoch (peaking at $JD-2450000=3710$). Thus, the shock-jet inhomogeneity interactions should be considered as a basic mechanism responsible for short-term bursts in this source.

Table 4.21: Short-term bursts in 1ES 1517+656.

Moment of maximum brightness (JD-2450000) (1)	Number of "Actine" nights (2)	Amplitude (mag) (3)	Amplitude (%) (4)	Slope (mag/month, redshift corrected) (5)	Comment (6)
536.5002	4	0.15	17	-0.28 0.27	Torino
3059.578	1	0.16	18	-0.24 0.10	-
3206.306	1	0.16	18	-0.24 0.50	-
3259.235	1	0.13	14	-0.50 0.41	-
3387.396	1	0.30	33	0.71	-
3582.377	1	0.13	14	0.40	-
3890.486	4	0.23	25	-0.98 0.38	-
4226.464	1	0.20	22	-	-
4345.614	1	0.15	17	-0.36 0.18	-

The amplitudes of short-term bursts varied between 0.13 to 0.32 mag. Especially fast is that one peaking at JD-2449000=3387. Its amplitude was 0.3 mag (increase with 33% in *R* band flux compared to local base level in several days). The slopes of ascending and descending parts of the busts are provided in the last column. In average, the brightenings were slower (-0.45 mag/month) than decays (0.55 mag/month). The duty cycle of short-term bursts was about 21% (16 “active” nights versus total 73 nights, including the Torino observations).

The source is active in point of intraday changes too. During 11-year term, 7 occasions of such changes are detected at 95% confidence level (including Torino data, Table 4.22). Especially dramatic change is detected during Abastumani observations between JD-2450000=3384-3387. In that case, the brightness increased with 0.21 mag in 1.84 days (2.8 d without correction on redshift) which corresponds to the rate 14.0 %/d.

Table 4.22: Intraday changes in 1ES 1517+656.

Time Interval (JD-2450000) (1)	Δt (days, redshift corrected) (2)	ΔR (mag) (3)	$\frac{\Delta F}{F}$ (%/d) (4)	Comment (5)
520.6658-525.5604	2.88	-0.09	3.5	Torino
536.5002-541.5087	2.94	0.10	3.7	Torino
2780.363-2788.427	5.00	0.18	3.8	-
3384.617-3387.400	1.64	-0.21	14.0	-
3881.448-3890.486	5.58	-0.20	3.9	-
3939.308-3945.286	3.52	0.26	8.0	-
4345.614-4352.601	4.11	0.15	4.1	-

In average, the brightness increased faster (7.1 %/d , $\frac{\Delta F}{F} = (3.5-14.0)\text{ %/d}$, 3 occasions) than decayed (4.9 %/d , $\frac{\Delta F}{F} = (3.7-8.0)\text{ %/d}$, 4 occasions). Fig. 4.42 shows intraday changes occurred in 1ES 1517+656 between JD-2450000=497 and 562.

The fastest optical change, detected for this source, corresponds to a increase with about 0.08 mag a day. So, the expected maximum intranight change is about 0.03 mag and it can be detected in rare occasions by means of great telescopes. Fig. 4.43 presents the results of intranight observations which show no variability at 99% confidence level ($C=1.04$).

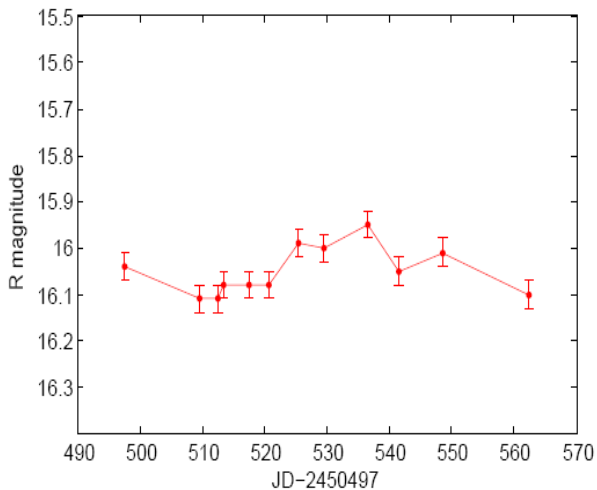


Figure 4.41: Example of intraday changes in 1ES 1517+656.

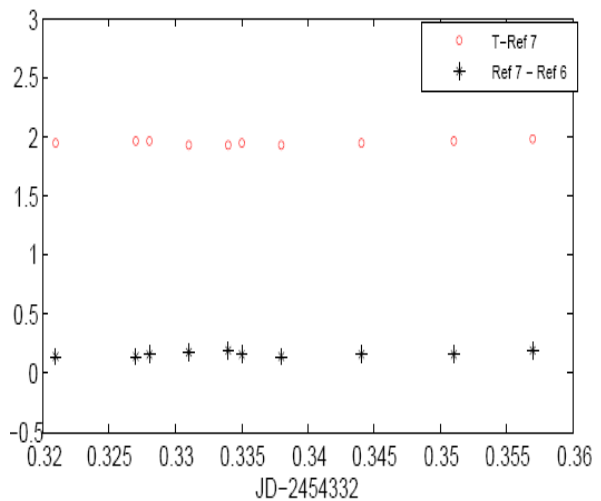


Figure 4.42: Intranight R band light curve of 1517+656.

4.10. 1ES 1959+650

This object is the most luminous among the targets with $\langle R \rangle = 14.46$ (not corrected on galactic reddening and host galaxy contribution). Its declination is high ($+65^{\circ}09'$), and, due to these two reasons, 1ES 1959+650 is the most frequently monitored source in the sample. Fig. 4.44a shows the results of long-term optical R band monitoring performed at Abastumani observatory, comprising up to 340 sessions (Mai 16, 1997 – November 10, 2007). R magnitudes are provided in column 3 of Appendix B10.1. As a rule, uncertainties are of about 0.03 mag (observations with greater uncertainties have not been included). Here, the aperture radius of about $7.^{\circ}5$ was used in order to make R magnitudes comparable with the preliminary values of obtained at Tuorla Observatory (see <http://users.utu.fi/kani/1m/>). The results obtained at Torino (Villata et al. 20000), Perugia and Rome (Tagliaferri et al. 2003, Fiorucci & Tosti 1996) observatories are not plotted due the significant difference in aperture radius (4–5 arcseconds). But these data have been used to establish the characteristic timescale of long-term variability and for the study of short-term bursts and intraday optical changes. The comparison light curve (Fig. 4.44c) is constructed using the instrumental magnitudes of reference stars 4 ($R=14.08$) and 7 ($R=14.79$) provided by Villata et al. (1998; see Appendix A10). These stars match the target closely both in magnitude and in colour ($V-R=0.45$ for these stars and $\langle V-R \rangle=0.48$ for the blazar). The scatter in their differences was the least as during the single nights as almost during the whole observing campaign (see the second column of Appendix B.10).

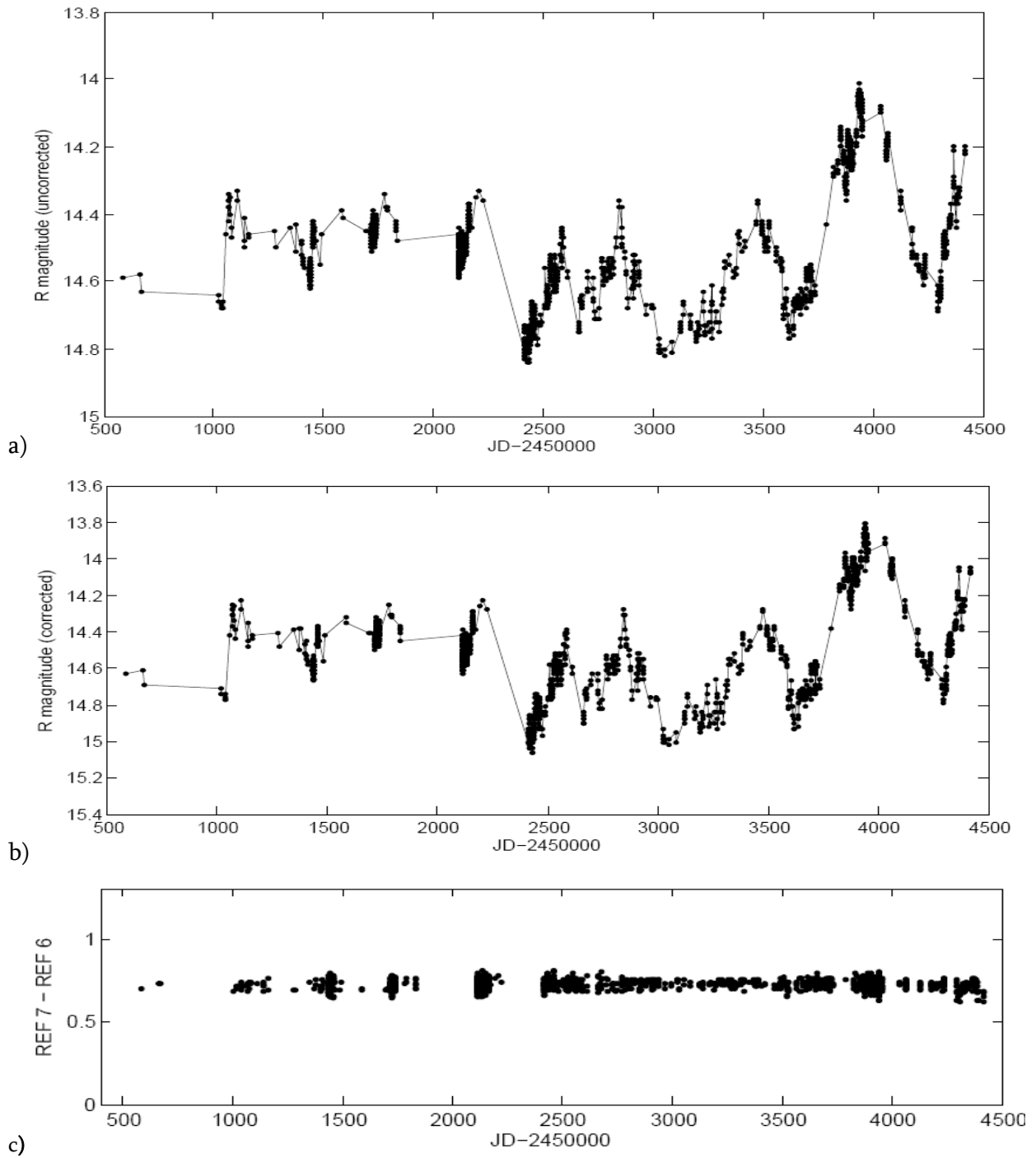


Figure 4.43: Historical R band light-curves of 1ES 1959+650 with a) magnitudes including host contribution and not corrected on galactic absorption; b) magnitudes corrected on host contribution and galactic absorption; c) comparison light curve.

1ES 1959+650 is hosted by the elliptical galaxy which contribution varies from 22% to 47% (in the case of aperture radius of $7.^{\circ}5$). Thus, it can dilute the intrinsic optical variability significantly. In order to correct R magnitudes (see column 4 of Appendix B10.1) on host contribution, they are converted into linear fluxes (column 4) and the obtained values were corrected according to Nilsson et al. (2007). The derived linear fluxes (column 5) were converted back into stellar magnitudes (column 6) and corrected on galactic absorption

(column 7; $A_R=0.473$). Fig. 4.44b presents the historical light curve constructed on basis of corrected R magnitudes (here, *rms* errors are of about 0.06).

After the correction, I obtained the overall brightness variation $\Delta R=1.26$ mag instead $\Delta R=0.83$ which we have in the case of non-corrected values. The maximum brightness, corrected on galactic absorption and host contribution, corresponds to $R=13.80$ while $R=14.01$ otherwise. The maximum amplitude has also increased (1.12 mag versus 0.77, for the flare reaching its maximum at JD-2450000=3939.45). The R band flux varied from 3.54 mJy to 7.68 mJy (including host contribution).

Historical light curve does not show periodical flares on timescales of years. The long-term variability patterns are provided in Table 4.23. The time intervals between consequent minima (including the minimum epochs in the case of Torino and Perugia (<http://astro.fisica.unipg.it/PGblazar/1959lc.gif>) observations) are uneven and they range from 0.85 yr to 1.62 yr (corrected on redshift). The minimum epochs are chosen for timescale derivation that there are clearly expresses two-peak maxima. For example, The maxima at JD-2450000=2584.20 and 2847.30 should be considered as a results of forward and reverse shocks arisen from a single disturbance at jet base (Fig. 4.45).

According to the minima of historical light curves, we obtain characteristic timescale of long-term variability which is equal to 1.35 yr (uncorrected on target's redshift; otherwise we have 1.29 yr).

Fig. 4.46 presents the structure function of 1ES 1959+650 constructed on basis of data binned within 150d intervals. Its first maximum situated at $dt \approx 500d$ is in accordance with characteristic timescale of long-term variability derived above. The second minimum at $dt \approx 1350d$ is presumably due to the fact that the bulk of data points situated between JD-2450000=1000 and 2350 (i.e. within 1350 d interval) are close each to other in magnitude. As for the deep minimum at $dt = 3150 d$, it probably expresses the existence of another longer trend with duration of decade order. Even the visual inspection of historical light curve gives an indication about such a trend. Namely, for well-sampled observations since JD-2450000=2430, we observe a permanent increase in base level.

Column 4 of Table 4.23 provides the slopes of ascending (sign “-“) and descending parts of historical light curve for each long-term flare. The values of ascending parts (indicating the rates of brightness increase) vary within very large diapason from -4.1 mag/yr to -0.41 mag/yr (note that this values are derived on basis of corrected R magnitudes and time intervals). This fact gives rise to the suggestion that the parameters of respective shock waves (if long-term blazar variability is the result of shock evolution) vary from flare to flare. Very different heights of flare peaks indicate that the strengths of respective shocks should be different.

Table 4.23: Long-term variability in 1ES 1959+650.

Minimum Location (JD-2450000) (1)	Δt_{obs} (yr) (2)	Δt_{corr} (yr) (3)	Slope (mag/yr)	Comment
246	-	-	-1.70 1.74	Torino
570	0.89	0.85	-4.1 1.45	Torino
1 005	1.20	1.14	-3.1 0.4	Perugia
1439	1.19	1.13	-0.41	-
1950	1.40	1.34	-2.3 1.59	rough
2417	1.28	1.22	-1.75 2.15	-
3026	1.70	1.62	-0.97 2.25	-
3621	1.63	1.55	-1.6 0.95	-
4295	1.85	1.76	-1.55	-
4658	1.00	0.95	-	Tuorla

The slopes of decaying parts vary also within broad diapason of 2.25-0.40 mag/yr. In average, increases in optical brightness occurred much faster (2.03 mag/yr) then decays (1.35 mag/yr).

In order to study the behaviour of colour index $V-R$, V band observations were performed during 73 night (see Appendix B10.2). Fig. 4.47 presents the results of this monitoring, including the data of 5 nights obtained at Torino observatory (Villata et al. 2000). The plot does not show any variability of $V-R$ values at 95% confidence level. They fluctuate around the average value $\langle V - R \rangle = 0.48$ between 0.43 and 0.52 while the uncertainties are of 0.05 mag in the case of Abastumani observations. $B-R$ data, constructed on basis of Torino observations, do not show variability too (Fig. 4.48).

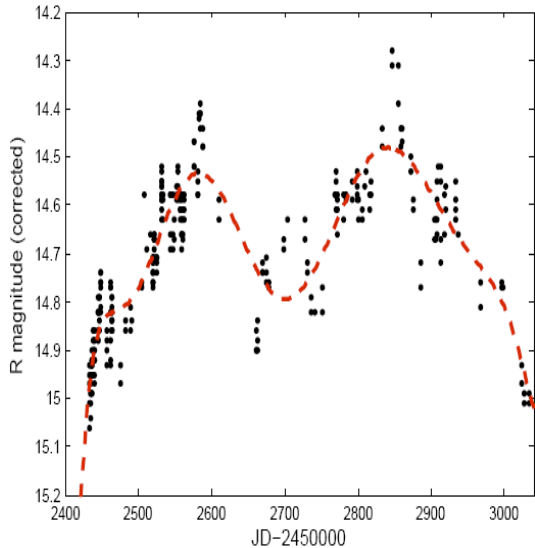


Figure 4.44: Two-peak maximum in the historical light curve of 1ES 1959+650.

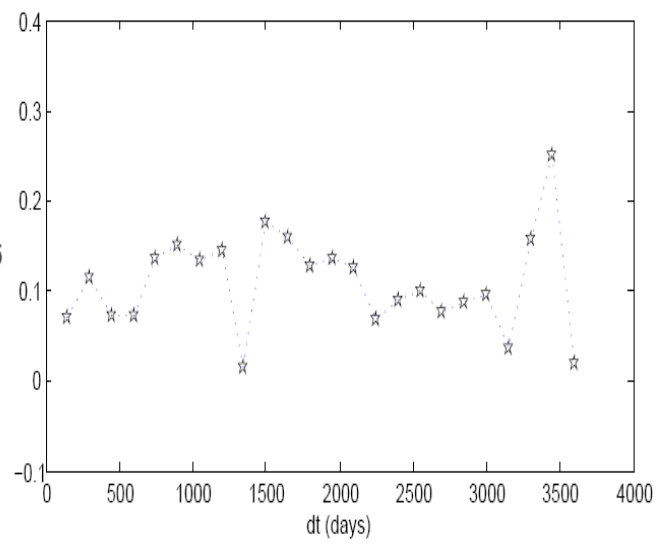


Figure 4.45: Structure function of 1ES 1959+650.

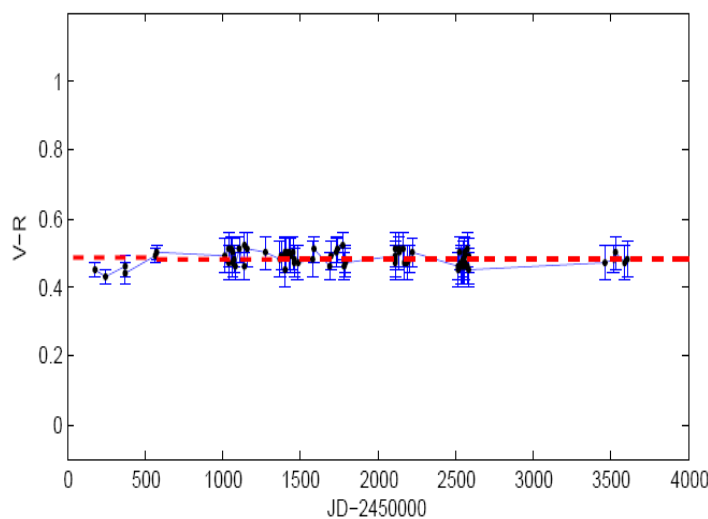


Figure 4.46: $V-R$ values for 1ES 1959+650.

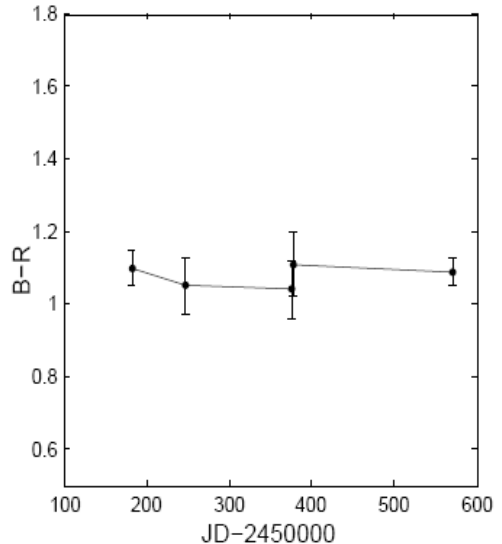


Figure 4.47: $B-R$ values for 1ES 1959+650.

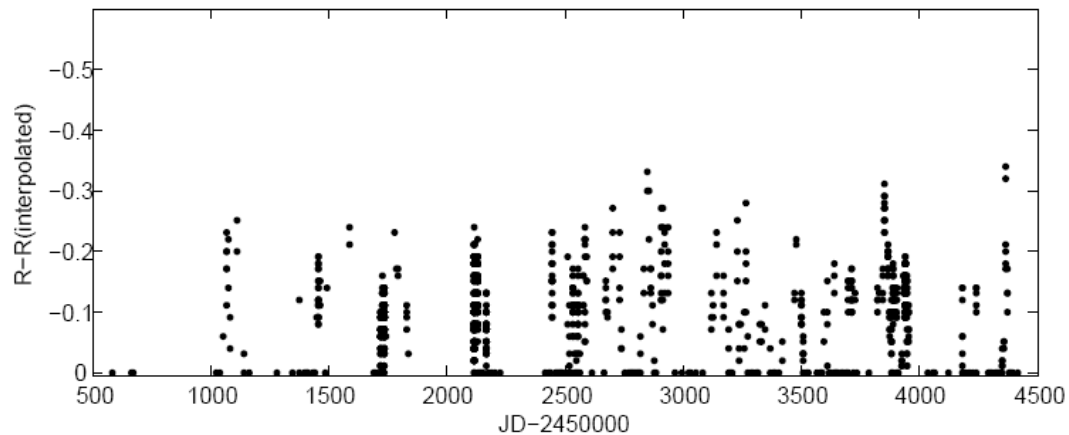


Figure 4.48: Short-term bursts in 1ES 1959+650.

Table 4.24: Short-term bursts in 1ES 1959+650.

Moment of Maximum Brightness (JD-2450000) (1)	Number of "Active" Nights (2)	Amplitude (mag) (3)	Amplitude (%) (4)	Slope (mag/month) (5)	Comment (6)
142.7238	1	0.14	14	0.11	Torino
242.5526	1	0.31	33	-0.16 2.02	Torino
376.2877	3	0.32	34	-0.11 0.21	Torino
529.6526	1	0.12	12	-0.04 0.32	Torino
1071.3497	3	0.15	15	-0.29 0.45	Abastumani
1110.2639	4	0.20	21	-0.23 0.24	Abastumani
1455.2935	3	0.17	18	-0.35 0.18	Abastumani
1585.6141	3	0.23	24	-0.07	Abastumani
1779.4183	9	0.23	24	-0.13 0.11	Abastumani
2127.3051	7	0.20	21	-0.34 0.25	Abastumani
2448.3071	3	0.23	24	-0.38 0.23	Abastumani
2507.5288	1	0.17	18	-1.50 0.75	Abastumani
2532.4809	5	0.15	16	-0.50 0.38	Abastumani
2584.1988	4	0.23	25	-0.33 0.25	Abastumani
2704.5770	6	0.26	28	-0.19 0.17	Abastumani
2769.4819	5	0.18	19	-0.31 0.15	Abastumani
2847.2964	5	0.32	33	-0.25 0.23	Abastumani
2913.3820	10	0.26	27	-0.17 0.20	Abastumani
3137.4949	4	0.20	21	-0.12 0.12	Abastumani
3265.2855	5	0.27	29	-0.25 0.28	Abastumani
3475.5536	3	0.19	20	-0.10 0.19	Abastumani
3529.3446	1	0.11	11	-0.20 0.16	Abastumani
3709.1584	7	0.13	13	-0.23 0.40	Abastumani
3852.5252	6	0.28	29	-0.30 0.35	Abastumani
3888.4979	5	0.15	15	-0.75 0.32	Abastumani
3939.3547	7	0.16	18	-0.27 0.45	Abastumani
4237.5034	2	0.12	12	-0.40	Abastumani
4366.2202	3	0.30	32	-0.47 0.82	Abastumani

Table 4.25: Intraday changes in 1ES 1959+650.

Time Interval (JD-2450000) (1)	Δt (days, redshift corrected) (2)	ΔR (mag) (3)	$\frac{\Delta F}{F}$ (%/d) (4)	Comment (5)
242.5526-246.5493	3.80	0.28	7.6	Torino
577.5435-584.6119	6.74	-0.21	3.3	Torino
584.6119-590.5588	5.67	0.21	3.9	Torino
1068.4036-1071.3497	2.80	-0.08	2.9	Abastumani
1141.2202-1142.1468	0.88	-0.13	14.8	Abastumani
1373.4292-1375.4848	1.97	-0.12	6.1	Abastumani
1719.3297-1725.3412	5.74	-0.18	3.3	Abastumani
2113.3654-2115.4504	1.99	0.21	11.0	Abastumani
2461.4466-2462.3201	0.85	-0.17	20.0	Abastumani
2505.4636-2507.5288	1.97	-0.19	10.1	Abastumani
2581.3206-2584.1988	2.74	-0.19	7.3	Abastumani
2854.6087-2859.4926	4.77	0.17	3.8	Abastumani
3262.3125-3265.2855	2.84	-0.18	6.6	Abastumani
3265.2855-3270.4102	4.89	0.27	5.7	Abastumani
3318.3810-3324.4906	5.84	-0.17	3.1	Abastumani
3380.1533-3384.6263	4.27	-0.19	4.7	Abastumani
3588.3067-3591.3713	2.93	-0.27	9.6	Abastumani
3637.2004-3641.2485	3.86	0.16	4.3	Abastumani
3641.2485-3645.4506	4.01	-0.20	5.2	Abastumani
3698.2240-3699.2288	0.96	-0.19	20	Abastumani
3714.3205-3718.1501	3.66	0.18	5.2	Abastumani
3867.4927-3870.5165	2.88	0.17	5.9	Abastumani
3880.4595-3886.4680	5.73	-0.29	5.4	Abastumani
3947.4403-3950.2528	3.64	0.14	3.8	Abastumani
4292.4363-4295.3525	2.79	0.13	4.7	Abastumani
4364.4889-4366.2202	2.61	-0.17	6.6	Abastumani
4375.4158-4377.4912	1.98	-0.17	8.6	Abastumani
4377.4912-4383.256	5.50	-0.17	3.1	Abastumani

1ES 1959+650 underwent 27 short-term bursts during 1996-2007 (including Fiorucci & Tosti (1996) and Villata et al. (2000) observations; see Fig. 4.49). 24 of them belong to the epochs of long-term flaring activities (Table 4.24; provided results correspond to host-subtracted magnitudes). Thus, shock-jet inhomogeneity interactions should be very important for this object.

The burst amplitudes cover wide range of 0.11-0.34 mag. Especially powerful bursts were revealed by Villata et al. (2000) peaking at JD-2450000=242 and 376. Their amplitude are equal to 0.31 mag and 0.32 mag, respectively (increase with 33-34% in *R* band flux

compared to local base levels). The first one was followed with very fast decay (0.28 mag in four days). The slopes of ascending and descending parts of the busts are provided in the column 5 of Table 4.24. In average, the brightenings were slower (-0.32 mag/month) than decays (0.38 mag/month). The duty cycle of short-term bursts was about 32% (114 “active” nights versus total 353 nights).

1ES 1959+650 is the most active in point of intraday changes among the targets. During 11-year term, 28 occasions of such changes are detected at 95% confidence level (including Villata et al. (2000) data, see Table 4.25; the results are obtained on basis of host subtracted and de-reddened magnitudes). Especially fast change occurred between JD-2450000=2461.4466 and 2462.3201 when the target underwent an increase with 0.17 mag in 0.85 days (in that case, the magnitudes are corrected on host contribution. Otherwise we have an increase with 0.10 mag). This corresponds to flux increase rate of 20.0% a day. The same rate was recorded during JD-2450000=3698.224-3699.229 when an increase with 0.19 mag occurred (0.11 mag including host contribution).

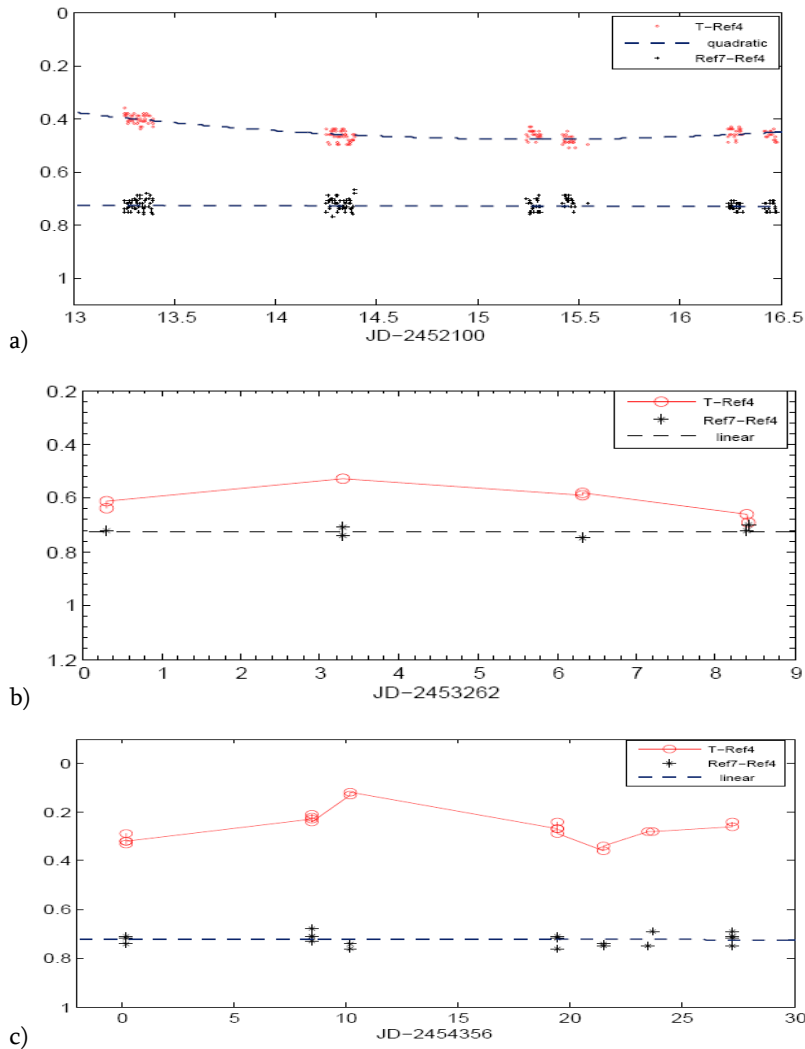


Figure 4.49: Examples of intraday changes in 1ES 1959+650.

Table 4.26. Results of intranight optical observations for 1ES 1959+650.

Session Beginning (JD-2450000) (1)	Duration (hr) (2)	Number of Frames (3)	C(7."5) (4)	C(6."0) (5)	C(4."0) (6)
1439.3427	1.49	18	1.11	1.15	1.20
1440.2709	3.96	60	1.18	1.20	1.25
1455.2869	2.72	23	1.12	1.29	1.37
1719.3047	4.39	24	1.11	1.22	1.29
1722.3540	3.85	58	1.17	1.41	1.53
1725.3311	2.17	33	1.05	1.25	1.17
1733.3498	2.23	34	0.94	1.00	1.13
1734.3224	2.05	30	1.07	1.20	1.31
1735.3245	1.33	21	1.53	1.67	1.75
1736.3278	2.05	32	1.00	1.05	1.11
2113.2505	3.49	48	0.87	1.10	1.07
2114.2524	3.36	46	0.88	0.92	1.03
2115.2421	5.73	45	0.97	1.21	1.22
2116.2372	5.78	42	1.24	1.57	1.65
2124.2708	0.79	12	1.33	1.37	1.45
2126.2599	0.79	12	1.43	1.40	1.51
2127.2376	5.81	44	0.87	0.96	1.06
2131.2368	1.26	16	1.06	1.12	1.21
2132.2439	6.16	53	1.04	1.21	1.19
2133.2391	5.51	45	1.09	1.14	1.22
2142.2241	1.08	17	1.12	1.24	1.20
2150.3502	1.86	26	1.30	1.50	1.43
2164.2650	3.50	44	0.95	1.17	1.22
2416.3857	1.52	14	1.36	1.45	1.47
2417.3202	4.00	23	1.15	1.60	1.54
2439.3080	2.44	11	1.24	1.35	1.38
2463.3876	3.25	13	1.27	1.63	1.78
3496.4396	1.35	12	1.33	1.38	1.47
3508.3729	1.23	12	1.08	1.14	1.18
3867.4789	0.90	16	1.27	1.54	1.43
3889.3961	2.69	11	1.36	1.50	1.55
3921.4497	1.52	14	1.80	2.04	1.97
3939.3497	3.15	42	1.13	1.20	1.26
3940.3240	3.00	35	1.37	1.46	1.43
3942.2451	5.13	56	1.31	1.37	1.42

In average, the brightness increased faster ($7.7\%/\text{d}$, $\frac{\Delta F}{F} = (2.9\text{-}20)\%/\text{d}$) than decayed ($4.8\%/\text{d}$, $\frac{\Delta F}{F} = (3.8\text{-}11)\%/\text{d}$). In addition, fast brightenings occurred almost twice more often than decays (18 vs 10 occasions).

Fig. 4.50 shows three occasion of intraday changes occurring between JD-25000=2113-2116 (panel A, a decay), 3262-3268 (panel B, consequent brightening and fade), 4356-4384 (panel C, a sequence of brightenings and decays).

The source was examined on intranight optical variability during 35 sessions. Table 4.26 provides the results of this monitoring. Because 1ES 1959+650 is hosted by bright galaxy, the measurements are performed using the apertures of three different sizes (with radii about $7.^{\circ}5$, $6.^{\circ}0$, and $4.^{\circ}0$, respectively). As a rule, star 4 (Villata et al. 1998) was used as a comparison star, and star 7 – as a control one.

None of the sessions showed a microvariability at 99% confidence level. The greatest value $C=2.04$ was derived for the session performed during JD-2450000=3921. The decrease in aperture size was accompanied by increasing $\sigma(T - S1)$ values but, at the same time, the value of $\sigma(S2 - S1)$ values were also increasing. Thus, no especial gain by decreasing in aperture radius was achieved in point of intranight variability detection.

Fig. 4.51 presents the data obtained during the sessions JD-2450000=1725 ($C=1.05$, panel a)) and JD-2450000=2416 ($C=1.36$, panel b)).

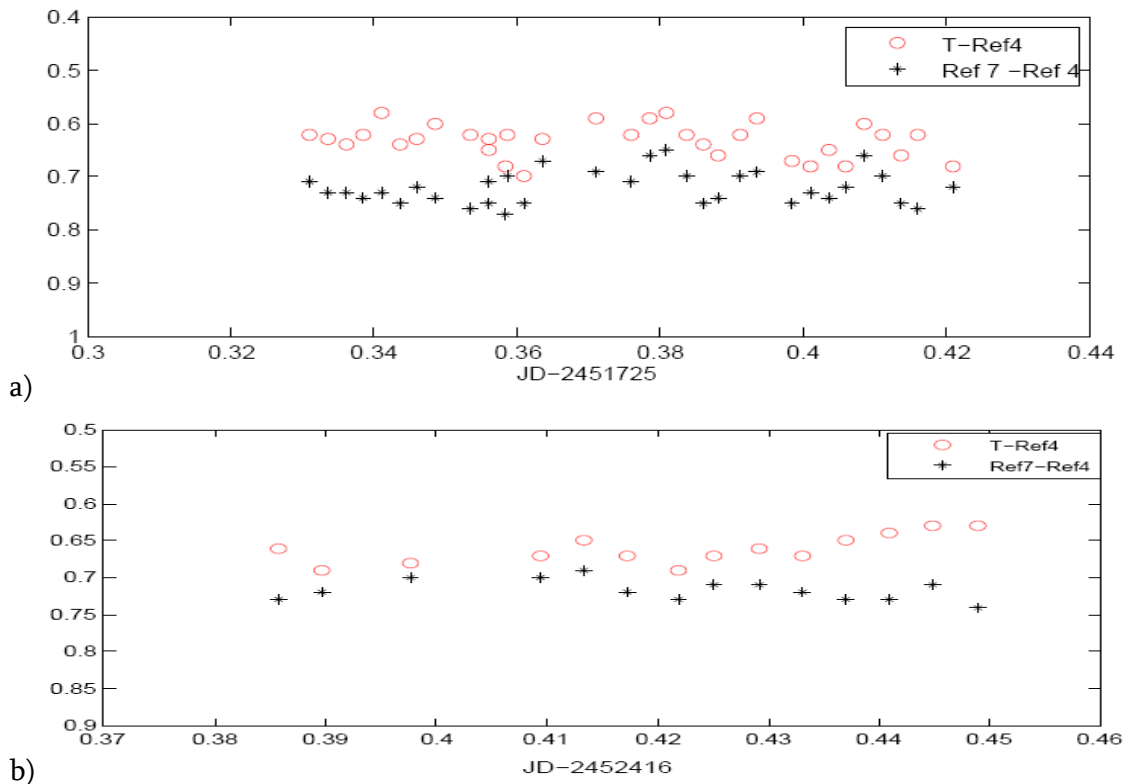


Figure 4.50. Intranight observations of 1ES 1959+650 during two different nights.

The fastest intraday change of 0.11 mag a day detected for 1ES 1959+650 (in the case of uncorrected R magnitudes and time interval), the maximum expected intranight change should be about 0.05 mag. In principle, such changes can be detected by means of 70 cm meniscus telescope in the case very good observational conditions.

4.11 1ES 2344+514

This source is the second in point of optical brightness with average R magnitude of 14.62. It was monitored during 149 nights at Abastumani observatory between July 26, 1998 and November 13, 2007. Fig. 4.52a shows its historical light curve constructed on basis of R magnitudes (Appendix B11.1, column 3).

It is especially difficult to perform photometrical measurements for this blazar. The AGN is hosted by very bright elliptical galaxy as we have seen above. Its contribution in total R band flux varies from 76% to 91% for the aperture radius of 7."5 (as in the previous cases, such a aperture size was selected in order to make R magnitudes comparable with the results of obtained at Tuorla Observatory). The comparison light curve (Fig. 4.52c) was generated using the instrumental magnitudes of reference stars C1 ($R=12.20$) and C2 ($R=14.16$), provided at <http://astro.fisica.unipg.it/PGblazar/2344.htm>. Their difference showed mainly the least scatter during the whole observational campaign. But, in some occasions, the star C1 underwent some very fast flares with up to 0.2 mag which duration was of ten minutes order. Since JD-2451000=303, the star showed the dips in its brightness (column 2 of Appendix B11.1). Star C2 also underwent sudden dips (eight occasions during the whole campaign) with 0.15-0.30 mag on the timescales of one day order. Thus, one should be especially careful when performing the photometrical measurements for 1ES 2344+514.

In order to correct R magnitudes on host contribution, they were averaged per session (Appendix B11.1, column 4) and converted into linear fluxes (column 5). These values were corrected according to Nilsson et al. (2007). The obtained linear fluxes (column 6) were converted back into stellar magnitudes (column 7) and then they were corrected on galactic absorption (column 8; $A_R=0.57$; uncertainties became ~ 0.15 mag vs 0.04 mag in the case of non-corrected values). Fig. 4.52b presents the historical light curve constructed on basis of corrected R magnitudes.

After the correction, I obtained the overall brightness variation $\Delta R=1.33$ mag instead $\Delta R=21$ which we have in the case of non-corrected values. The maximum brightness, corrected on galactic absorption and host contribution, corresponds to $R=15.45$ while $R=14.50$ for non-corrected values. The maximum amplitude also has increased greatly (1.20 mag versus 0.18, for the flare reaching its maximum about at JD-2451000=350).

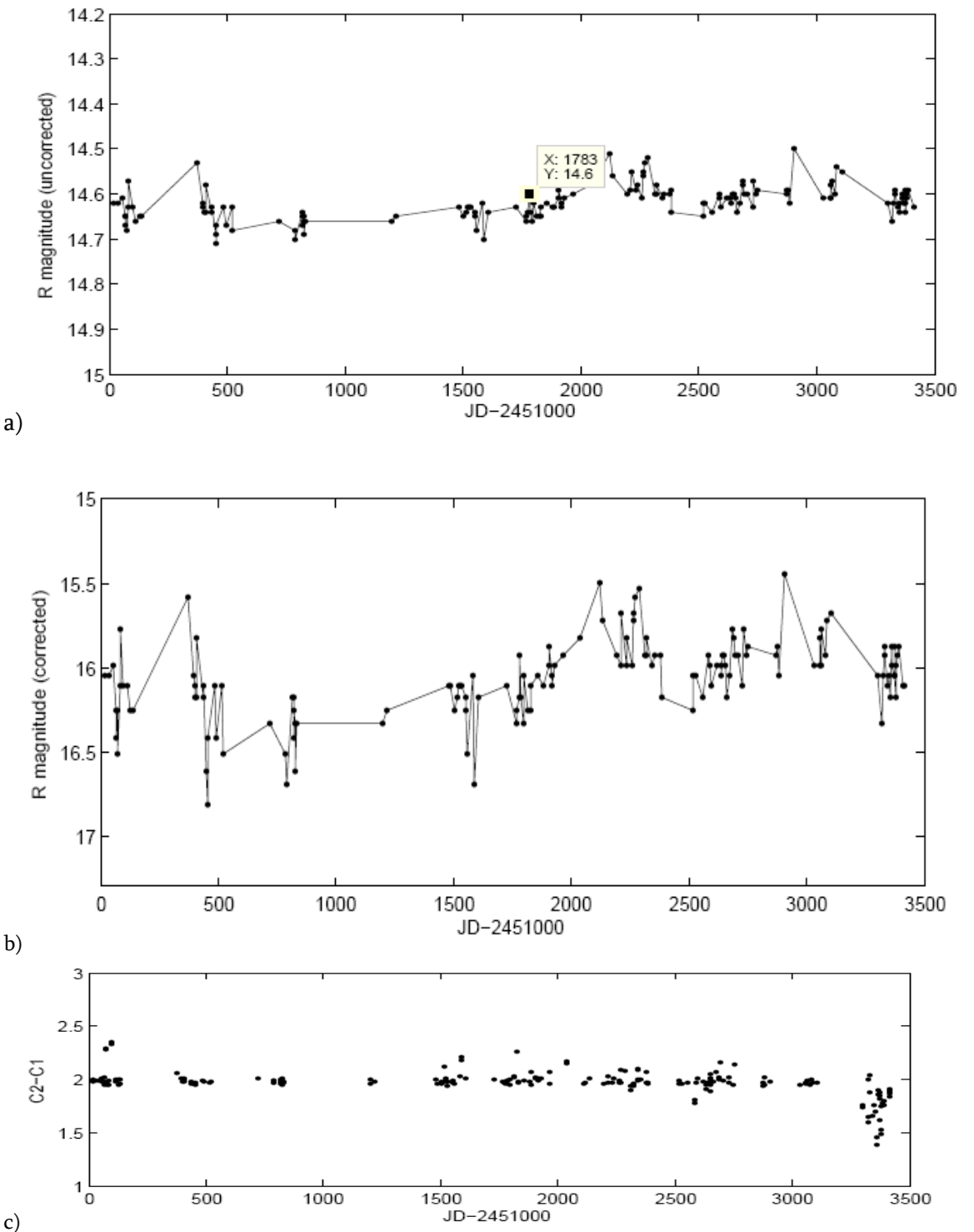


Figure 4.51: Historical R band light-curves of 1ES 2344+514 with a) magnitudes including host contribution and not corrected on galactic absorption; b) magnitudes corrected on host contribution and galactic absorption; c) comparison light curve.

The data points are distributed along the historical light curve unevenly and we have several blank intervals here. Between $JD-2449000=820$ and 1484, there are only two data points and one flaring cycle is practically omitted here. Due to this fact, the second minimum in structure function at $dt=5.5$ yr (nearly equal to the time interval between optical maxima $JD-2451000=350$ ad 2100) is probable spurious (Fig. 4.53).

According to the first minimum of structure function, the source show optical flares of 2-3 yr duration.

In order to study the behaviour of colour index $V-R$, V band observations were performed during 27 nights (see Appendix B.11.2). Fig. 4.54 presents the results of the investigation. The source did not show any variability of $V-R$ values at 95% confidence level. They fluctuate around the average value $\langle V - R \rangle = 0.61$ between 0.58 and 0.67 while the uncertainties are of 0.05 mag.

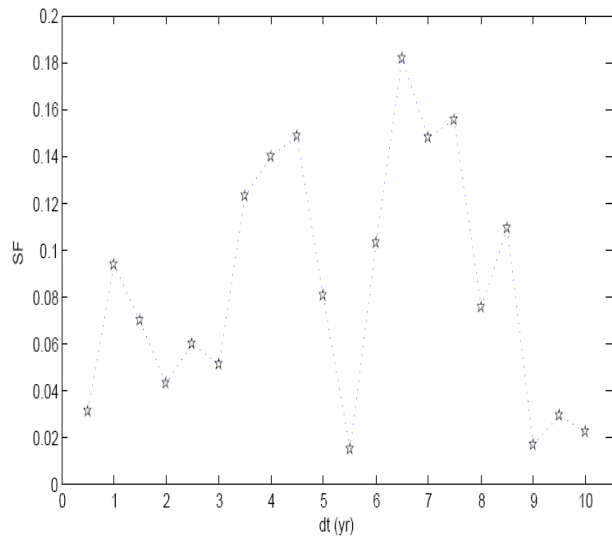


Figure 4.52: Structure function of 1ES 2344+514.

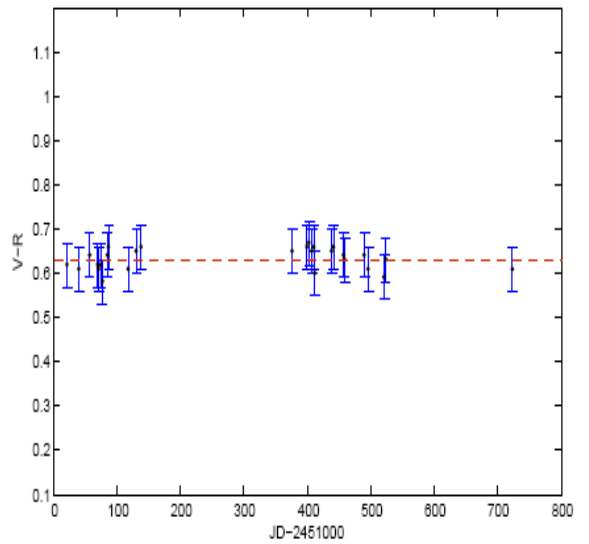


Figure 4.53: $V-R$ values for 1ES 2344+514.

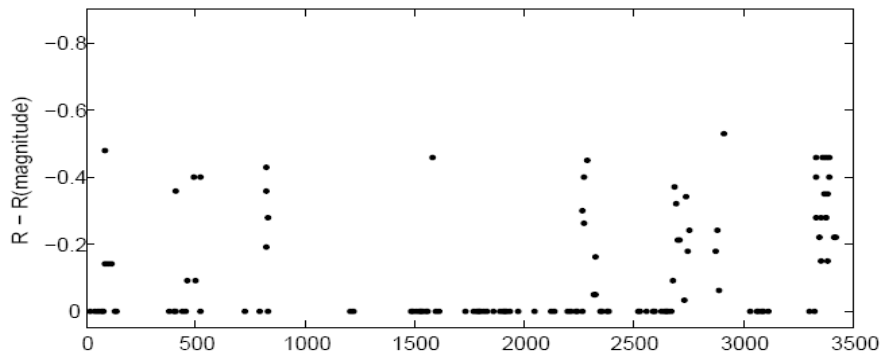


Figure 4.54: Short-term bursts in 1ES 2344+514.

Only 8 short-term bursts are revealed at 95% confidence level and more are found (Fig. 4.55). Such a low number is caused mainly by dilution of blazar variability by powerful host (in the case of uncorrected R magnitudes) or by great uncertainties after the removal of host contribution.

The amplitudes of short-term bursts varied between 0.23 to 0.43 mag (corresponding to the increases with 25-49% in R band flux compared to local base levels; see Table 4.27). Due to great uncertainties, no investigation flare slopes have been carried out. The duty cycle of short-term bursts was about 15% (22 “active nights versus total 149 nights).

Table 4.27: Short-term bursts in 1ES 2344+514.

Moment of Maximum Brightness (JD-2451000) (1)	Number of “Active” nights (2)	Amplitude (mag) (3)	Amplitude (%) (4)
86.40443	1	0.43	49
521.39215	1	0.23	25
820.22785	4	0.38	41
1584.27932	1	0.41	45
2289.57118	3	0.40	43
2688.20458	3	0.31	33
2909.46630	1	0.43	47
3332.55706	8	0.41	45

The source showed intraday variations twice at 95% confidence level (see Table 4.28). As a rule, they are associated with short-term flares. The fastest one is an increase with 0.36 mag in 1.91 days (i.e. 20.4 % a day). This result is obtained for the data corrected on host contribution. Otherwise we have an increase only with 0.07 mag.

Table 4.28: Intraday changes in 1ES 2344+514.

Time interval (JD-2451000) (1)	Δt (days) (2)	ΔR (mag) (3)	$\frac{\Delta F}{F}$ (%/d) (4)	Comment (5)
84.41-86.41	1.92	-0.34	18.8	host subtracted
438.50-440.49	1.91	-0.36	20.4	host subtracted

The source was examined on intranight optical variability during 9 sessions. Table 4.29 provides the results of the monitoring. Because 1ES 2344+514 is hosted by a luminous galaxy, the measurements are performed using the apertures of different sizes (with radii about 7."5, and 4."0, respectively). In the first case, the stars C2 (comparison) and C1(control), were used. For the aperture radius of 4."0, stars C3 (comparison) and C4 (control) were applied (in the case of 7."5, star C3 undergo the contamination from 1ES 2344+514).

Like the previous source, none of the sessions showed a microvariability at 99% confidence level. The greatest value $C=1.31$ was derived for the session performed during JD-2450000=824. Decrease in aperture size caused an increase in $\sigma(T - S1)$ values but, at the same time, the value of $\sigma(S2 - S1)$ was also increasing. Thus, no gain was achieved by decreasing in aperture radius in point of intranight variability detection.

Fig. 4.56 presents the data obtained during the sessions JD-2451=1203 for aperture radii of 7."5 (upper panel) and 4."0 (second panel), respectively.

Table 4.29. Results of intranight optical observations for 1ES 2344+514.

Session Beginning (JD-2451000) (1)	Duration (hr) (2)	Number of Frames (3)	C/ Γ (7."5) (4)	C (4."0) (5)
458.3880-5584	4.33	37	1.04	1.14
789.5012-5365	0.85	15	0.97	1.12
820.2279-3980	4.26	46	1.09	1.17
821.4007-4808	1.94	24	0.98	1.05
822.3965-4767	1.95	27	1.01	1.06
824.2976-3452	1.15	12	1.17	1.31
825.3931-5038	2.67	25	0.93	1.07
1203.3531-4107	1.39	17	0.78	0.88
1221.3255-3831	1.39	18	1.03	1.11

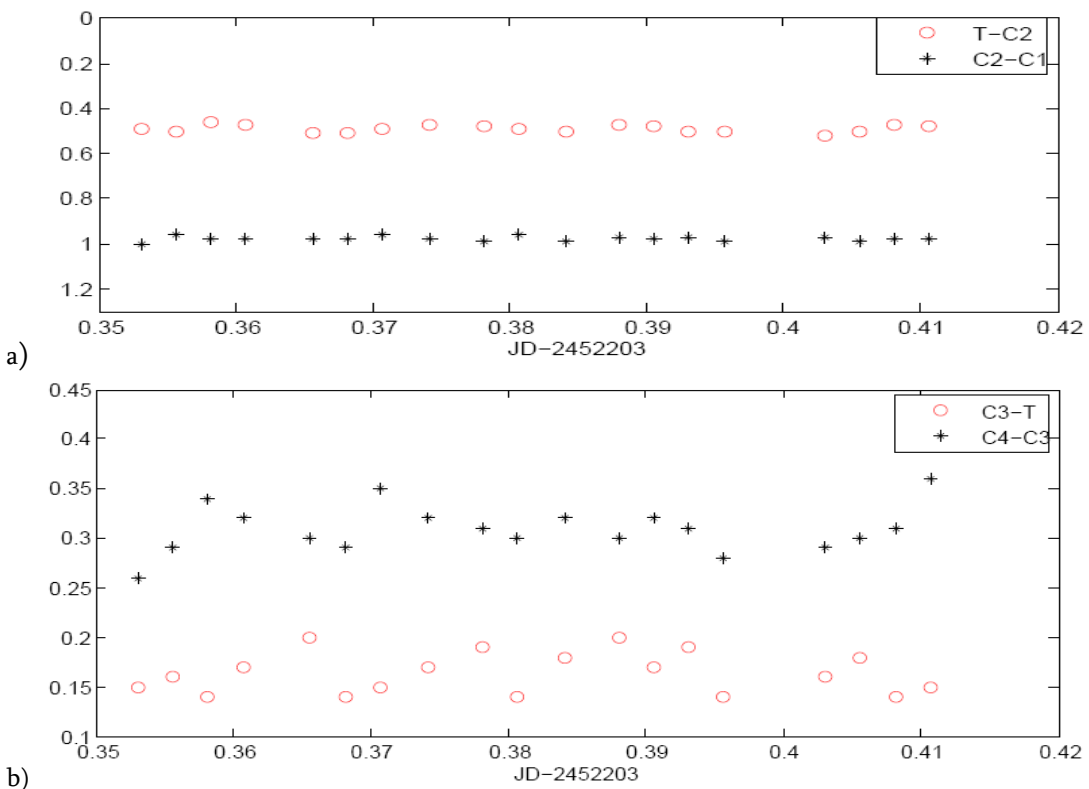


Figure 4.55. Intranight behaviour of 1ES 2344+514: a) aperture radius of 7."5 is used. C2-C1 values are shifted with -1.00; b) the same observation in the case of 4."0. C4-C3 values are shifted with 0.1.

6 Summary and Future Investigations

In previous chapter, the detailed information about optical R band behaviour of each XBL was provided. Now, we are able to summarize the obtained results and make up some conclusions about the physical mechanisms responsible for observed phenomena. In addition, the objectives of future investigations are also presented.

5.1 Long-term Variability

In this thesis, the characteristics of long-term optical behaviour of selected XBLs have been studied using the data obtained with 70 cm meniscus telescope of Georgian National Astrophysical Observatory. For completeness, the optical data about the targets, included in different publications and databases, are also referred. Historical light curves are constructed and variability characteristics are derived. Despite some gaps in the observations (which are sometimes very great), we can make some conclusion about the highlights of long-term variability.

Table 5.1 provides the summary of the results of long-term behaviour of the targets. Column (2) gives the term of the monitoring performed at Abastumani observatory and column (3) – number of the sessions performed for each target during this terms; column (4) lists the years of optical identifications.

Table 5.1: Summary of long-term variations.

Object (1)	ΔT_{Abast} (2)	N_{tot} (3)	t_{id} (4)	Variability Detection (5)	Maximum Brightness (mag, uncorrected) (6)
1ES 0229+200	11/09/97-11/16/2007	57	1993	No	16.01
1ES 0323+022	10/08/1997-2/14/2007	51	1980	Yes	15.62
1ES 0414+009	10/04/1997-02/14/2007	56	1981	Yes	15.86
1ES 0502+675	11/09/1997-03/10/2007	105	1993	Yes	15.69
1ES 0647+250	11/25/1997-03/28/2006	53	1993	Yes	14.86
1ES 0806+524	12/29/1997-05/30/2007	111	1993	Yes	14.72
1ES 1028+511	01/28/1998-11/18/2007	78	1993	Yes	15.94
1ES 1426+428	03/31/2003-10/09/2007	87	1989	Yes	15.76
1ES 1517+656	01/28/1998-05/15/2007	56	1993	Yes	15.84
1ES 1959+650	05/16/1997-11/10/2007	348	1993	Yes	14.01
1ES 2344+514	07/26/1998-11/13/2007	186	1996	Yes	14.50

Table 5.1-Continued

Object	Maximum Maximum Brightness (corrected)	ΔR (mag, uncor- rected)	ΔR (mag, corrected)	Maximum Observed Amplitude (mag, uncorrected)	Maximum Observed Amplitude (mag, corrected)	Characteristic Timescale (redshift corrected)
	(7)	(8)	(9)	(10)	(11)	(12)
1ES 0229+200	17.51	-	0.85	-	-	-
1ES 0323+022	15.32	1.21	1.21	0.90	-	4.35
1ES 0414+009	15.54	1.06	1.06	0.84	0.84	3.90
1ES 0502+675	15.28	1.12	1.12	1.10	1.10	1.75
1ES 0647+250	14.60	1.29	1.29	0.82	0.82	1.58
1ES 0806+524	14.81	0.90	1.24	0.83	1.16	1.96
1ES 1028+511	15.91	1.09	1.09	1.08	-	3.14
1ES 1426+428	16.67	0.31	0.91	0.23	0.65	0.91
1ES 1517+656	15.77	0.88	0.88	0.87	0.87	~ 2.80
1ES 1959+650	13.80	0.83	1.26	0.77	1.12	1.30
1ES 2344+514	15.45	0.21	1.33	0.18	1.20	~ 2.00

Table 5.1-Continued

Object	Minimum Observed Timescale (yr, redshift corrected)	Maximum Observed Timescale (yr, redshift corrected)	$V-R$ Variability	$\langle V - R \rangle$
	(13)	(14)	(15)	(16)
1ES 0229+200	-	-	-	-
1ES 0323+022	4.06	5.25	Yes	0.49
1ES 0414+009	3.45	4.37	No	0.46
1ES 0502+675	1.47	2.21	No	0.36
1ES 0647+250	1.30	1.85	No	0.38
1ES 0806+524	1.80	2.17	No	0.38
1ES 1028+511	4.11	4.14	No	0.25
1ES 1426+428	0.73	1.07	-	-
1ES 1517+656	-	-	No	0.35
1ES 1959+650	0.85	1.76	No	0.48
1ES 2344+514	-	-	No	0.63

10 out of 11 sources exhibit clearly expressed long-term variability (column (5)). 1ES 0229+200 did not revealed long-term trend at 95% confidence level but some short-term bursts. While *RXTE* X-ray observations show clear long-term changes, optical “passivity” can be explained by possible great misalignment of jet part where predominantly optical

photons originate with respect line of sight or shock waves are very attenuated when reaching this jet place (this issue can serve as a subject for future investigations). Instensive short-term bursts can be originated by the mechanism different from shock-jet inhomogeneity interacions, such as powerful hot spots on blazar accretion disc (an objective for future investigations!).

The duty cycle of long-term variability for the sample can be determined as the ratio of the number of variable sources to total numbers of the objects in the sample. Thus, $DC=10/11$, i.e. $DC \approx 91\%$.

The variability carry mainly clear non-periodical character (in the cases of 1ES 0502+675, 0806+524, 1426+428, 1959+650, 2344+514). 1ES 1028+511 varies quasiperiodically but we have observed yet only three cycles and this is not sufficient to draw firm conclusion about variability character. In addition, there are sparcely distributed data points during two flaring cycles and some additional data points could change the results basically. So, future optical monitoring is necessary for periodicity confirmation/denial and period derivation. As for 1ES 0647+250 and 1517+650, it is impossible to make up any conclusion about variability character due to great gaps in their observations. Up to now, no claim about the detection of long-term (quasi)periodical flares in any HBL has been made.

Column (12) summarizes characteristic timescales (corrected on redshifts) of long-term changes. Here, we have wide range of 0.91-4.35 yr. The fastest object is 1ES 1426+429 and the slowest one -1ES 0323+022. But the result is less credible in later case due to sparcely distributed observations. Otherwise, the slowest object is 1ES 0414+009 with characteristic timescale of 3.9 yr.

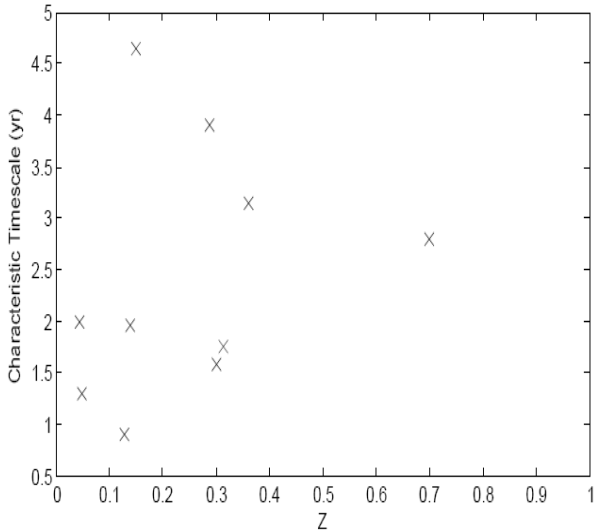


Figure 5.1: Correlation of characteristic timescales with redshifts.

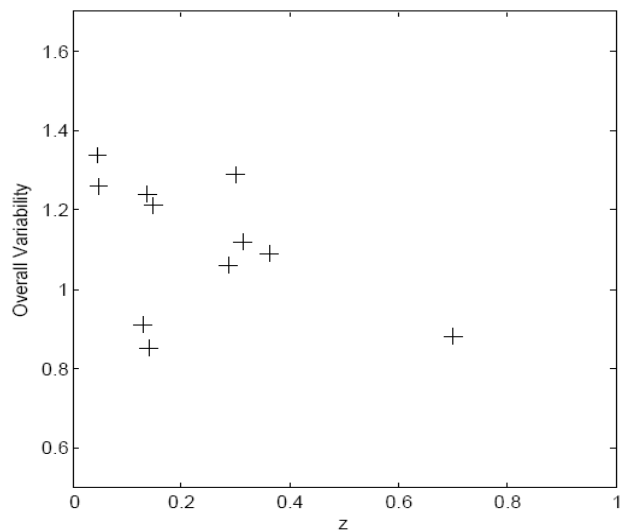


Figure 5.2: Correlation of overall variabilities with redshifts.

In Fig. 5.1, the characteistic timescales are plotted vs. target redshifts which could give an indication about the evolution of the processes responsible for long-term flares. No

correlation between this two parameters was revealed. Thus, flare durations show no dependence to target distance.

In the case of 1ES 0806+524 and 1959+650, we see clear change in base level of R band flux (i. e. flux level corresponding to optical minimum). The duration of such changes should be of decade order. This phenomenon gives rise to an idea that there is another longer variations in XBLs which are superimposed with the flares of years order. As for other targets, unfortunately, we have no well-sampled observations to see whether they display such a feature. It seems important to investigate all well-observed sources on the existence of such trend not only among XBLs but for RRBLs and FSRQs, too. This research will allow us to find another kind of the variability in blazars (if any exists).

Overall changes in R magnitudes range from 0.85 to 1.34 mag. The greatest diapason is observed for 1ES 2344+514 revealed by means of the data corrected on host contribution (otherwise ΔR equals only to 0.21 mag.). Thus, the overall variability in XBLs are small compared to these observed in RBLs (for example, $\Delta R \approx 3$ mag for PKS 0735+138, Ciprini et al. 2007)). ΔR values show no correction with z redshift (Fig. 5.2)

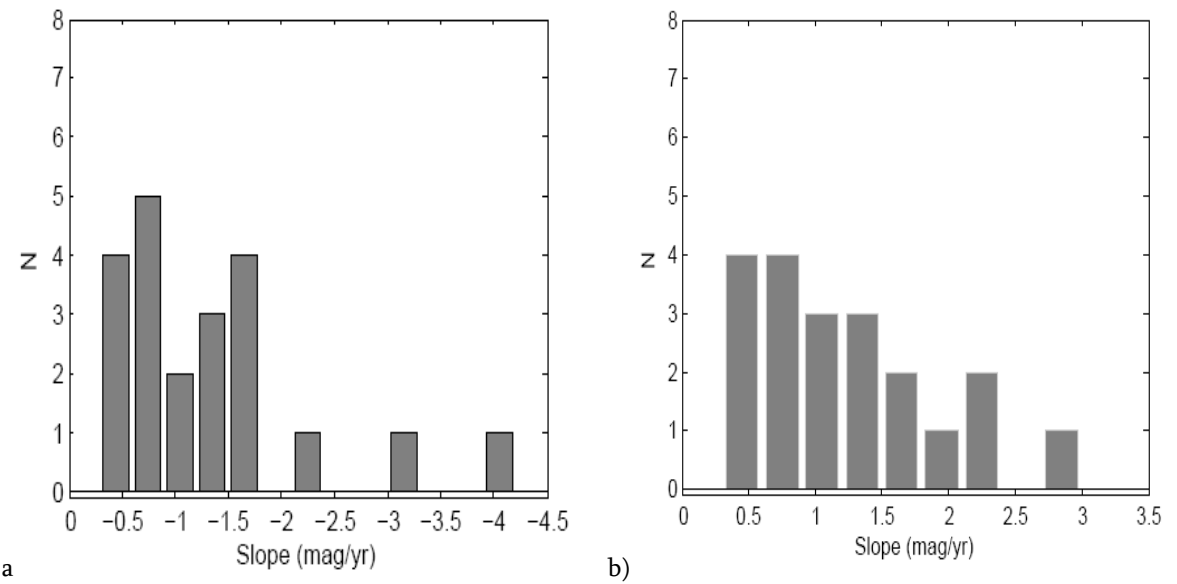


Figure 5.3: Distributions of the slopes of historical light curves during flares (a) and decays (b).

Fig. 5.3 provides the statistics of the slopes derived for long-term flares. We see that the slopes of ascending parts have two maxima at -0.7 mag/yr and -1.60 mag/yr values (5.3a), while the targets decay preferentially with the rates of 0.4–0.8 mag/yr (Fig. 5.3b).

Column (7) provides R magnitudes corresponding to maximum brightness in this band (for the values corrected on galactic absorption and host contribution (if any exists)). 1ES 1959+650 is the most luminous among the targets ($R=13.80$) while 1ES 0229+200 is the faintest AGN in the sample ($R=17.51$).

Two-peak maxima whose existence was predicted theoretically by Marscher (1996) as a result of propagation both forward and reverse shocks, are found for 1ES 0502+675,

0647+250, 1517+656 and 1959+650. In the case of 1ES 0806+524, we may assume that there is a two-peak maximum between JD-2450000 \approx 2300 and 3500 if the suggestion about possible decade-order variabilities is not true. The minima between these peaks are much less deeper compared to other minima in the historical lightcurve of a given source. In the case of well expressed structures, the second peak is mainly higher than the first one. The fact that two-peaks maxima are not revealed for every long-term flare gives rise to the suggestion that bulk flow velocities and shock characteristics are variable in different flaring epochs, and the criterion of appearance of both forward and reverse shocks (Equation 1.14) has not been always satisfied.

The targets do not show the variability in colour indices but 1ES 0323+022. This source shows $\Delta(V - R) = 0.17$ and $\Delta(B - R) = 0.27$ during Torino observations. In addition, the change $\Delta(B - R) = 0.23$ is derived from the data Jannuzi et al. (1993). Note, that there are very few data points indicating colour variability and further monitoring is necessary to confirm this result. The diapason of average $V-R$ indexes is broad – they vary from 0.25 (1ES 0502+675) to 0.63 (1ES 2344+514) (column 16 of Table 5.1) i.e. the targets show different spectral energy distributions. Hence, there should be a broad variety of physical conditions in their jets (search for the respective reasons can serve as another objective for future research).

5.2 Short-term Bursts

The sample show short term bursts except for 1ES 0647+250 which displayed the smoothest historical light curve among the targets. Table 5.2 provides the summary of

Table 5.2: Summary of short-term bursts.

Object (1)	N_r (2)	N_f (3)	N_q (4)	N_u (5)	N_{act} (6)	DC (7)	Slope (ascending) (8)	Slope (desc.) (9)	Amp (mag) (10)	Amp (%) (11)
1ES 0229+200	7	-	-	-	-	-	-	-	0.30-0.58	33-66
1ES 0323+022	9	7	1	1	32	40	-0.08—0.30	0.08-0.40	0.11-0.45	14-51
1ES 0414+009	6	4	2	0	15	22	-0.13—0.25	0.09-0.85	0.18-0.32	19-36
1ES 0502+675	15	10	5	0	38	31	-0.13—0.73	0.13-1.00	0.15-0.45	16-52
1ES 0647+250	0	-	-	-	-	-	-	-	-	-
1ES 0806+524	10	7	2	1	35	32	-0.10—0.53	0.09-0.54	0.16-0.45	18-52
1ES 1028+511	9	8	1	0	19	20	-0.20—1.50	0.08-0.20	0.14-0.33	16-36
1ES 1426+428	2	2	0	0	4	5	-0.51—0.55	0.23-0.40	0.24-0.33	27-38
1ES 1517+656	9	7	2	0	15	21	-0.24—0.98	0.10-0.71	0.13-0.30	14-33
1ES 1959+650	27	24	2	1	114	32	-0.04—1.50	0.11-2.02	0.11-0.32	11-34
1ES 2344+514	8	4	2	2	22	14	-	-	0.23-0.43	25-49

short-term characteristics with N_t =total number of bursts, N_f =number of busts detected during long-term flares, N_q =the same during target's "quiescence", N_u – number of events when its unknown whether the bust occurred during flaring or quiescent states; N_{act} = number of "active" sessions; DC = duty cycles of short-term bursts in percents. Note that this quantity is sensitive with respect to rms errors and it could be much higher in the case of the telescopes greater than the 70cm meniscus telescope of Abastumani Observatory. Thus, the data provided in column (7) should be considered as low limits of actual duty cycles. Otherwise, if we determine DC characteristic as a ratio of sources showing short-term bursts with the total number of sampled objects, we get $DC \approx 91\%$.

The fact that 73 out of 102 bursts are belong to epochs of long-term flares gives rise to the suggestion that interaction between jet inhomogeneities and shock waves, propagating through blazar jets, can serve as a primary mechanism responsible for short-term bursts. In that case, the homogeneity of jets should vary from object to object, according to different duty cycles. For example, the jets of 1ES 0647+250 and 1426+428 seem to be fairly homogenous while the jet of 1ES 0323+022 should be the most turbulent among the targets ($DC=40\%$). Thus, we probably deal with the variety of physical conditions within the jets of sampled objects. It seems very important spread this task over the whole XBL subclass and investigate the reasons of above mentioned difference.

Nevertheless, other hypothetic mechanism can be at work while about 24% of the bursts belong to quiescence epochs. For example, hot spots emerging on blazar accretion discs should be more conspicuous when the source is quiet. The investigation of the importance of different possible mechanisms in development of blazar short-term bursts can serve as an objective of future investigations.

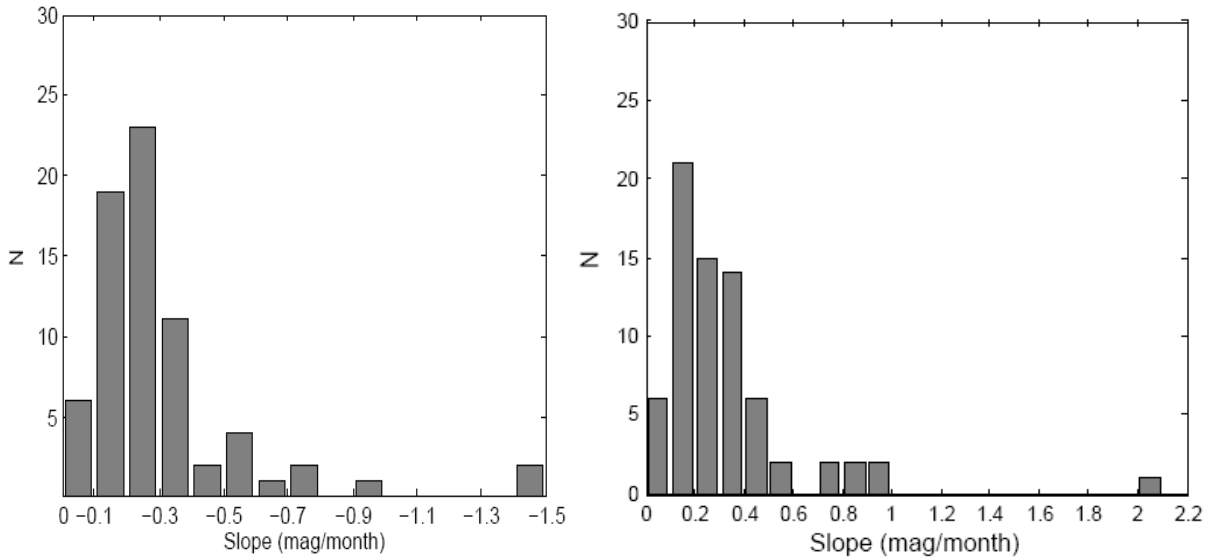
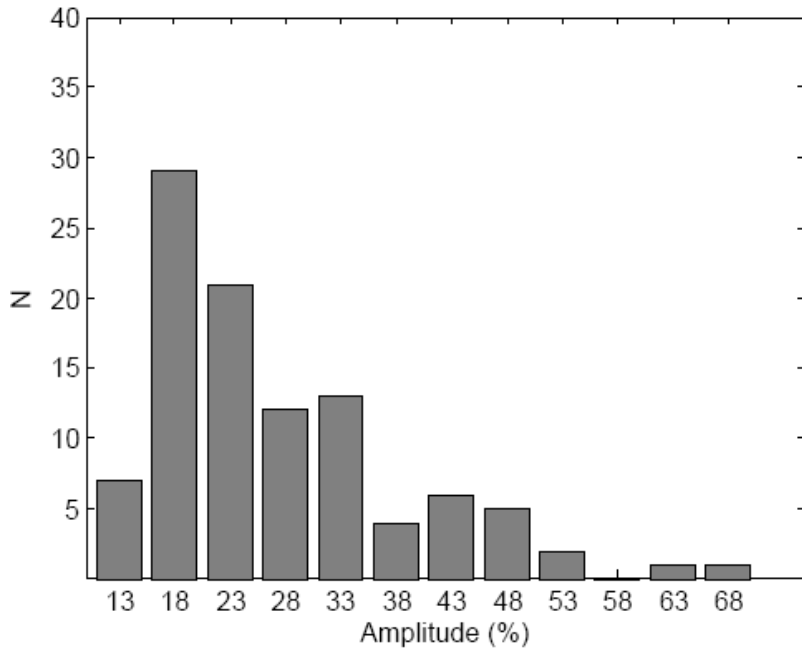


Figure 5.4: Distributions of burst slopes during brightenings (a) and decays (b).

Fig. 5.4 provides the statistics of brightness increase (a) and decay (b) during short-term bursts (see columns (9) and (10) in Table 5.2). We see that the targets flare preferentially with the rates 0.20-0.25 mag/month, while decay predominantly with 0.15

mag/month. Thus, brightening are faster than decays, in average. It is interesting to prove which of hypothetic mechanisms fitting better with this statistics.



Columns (10) and (11) summarize the amplitudes of the bursts in stellar magnitudes and in percents, respectively. So, the targets “preferred” to increase in R band flux with 15-20% (Fig. 5.5). It is important to investigate which of hypothetic mechanisms can produce such a distribution in amplitudes expressed in Fig. 5.5.

Figure 5.5: Statistics of burst amplitudes (amplitude vs. respective number).

5.3. Intra-day Variability

The targets are active at intraday timescales, too. Below, Table 5.3 provides the summary of intraday changes with N_t =total number of detected events, N_{inc} =number of events corresponding to brightness increase, N_{dec} - the same for brightness decay; Δt - change duration (corrected on target’s redshift).

Intraday changes are associated mainly with short-term bursts. Greatest number of the events is found for 1ES 1959+650 (28 occasions) mainly due to low rms errors. The number of intraday brightnings are almost twice greater than decays in this object. Fig. 5.6 shows the distribution of the flux change rates during intraday brightenings (a) and decays (b). We see that these distributions are mainly similar. In both case, distribution maxima are situated at 4% a day.

Column (12) provides the average amplitudes of short-term bursts in percents. In average, this characteristic is equal to 17% for sampled XBL group (no data of 1ES 0229 and 2344+514 are included here due to great uncertainties). This result is fairly below the characteristic obtained by Heidt et la. (1996) for RBLs. This fact is in agreement with Jannuzzi et al. (1994) suggestion that XBLs are less variable compared with RBLs.

Table 5.3: Summary of intraday changes.

Object (1)	N_t (2)	N_{inc} (3)	N_{dec} (4)	Δt (d) (5)	ΔR_{inc} (mag) (6)	ΔR_{dec} (mag) (7)	$\frac{\Delta F}{F}$ (%/d) (inc.) (8)
1ES 0229+200	1	1	0	1.77	-0.45	-	25
1ES 0323+022	2	1	1	4.36-6.10	-0.15	0.13	2.8
1ES 0414+009	2	1	1	4.04-4.65	-0.18	0.26	4.3
1ES 0502+675	11	5	6	0.74-5.26	-0.15-0.30	0.09-0.25	5.0-12.6
1ES 0647+250	0	-	-	-	-	-	-
1ES 0806+524	5	3	2	2.56-3.63	-0.13-0.14	0.16-0.28	3.9-5.6
1ES 1028+511	4	3	1	2.26-4.36	-0.13-0.21	0.18	4.8-8.0
1ES 1426+428	0	-	-	-	-	-	-
1ES 1517+656	7	3	4	1.64-5.58	-0.09-0.20	0.10-0.26	3.5-14.0
1ES 1959+650	28	18	10	0.85-6.74	-0.08-0.29	0.13-0.27	2.9-20.0
1ES 2344+514	2	2	0	1.91-1.92	-0.34--0.36	-	18.8-20.4

Table 5.3-Continued

Object	$\frac{\Delta F}{F}$ (%/d)(dec) (9)	$\overline{\Delta F/F_{inc}}$ (10)	$\overline{\Delta F/F_{dec}}$ (11)	\bar{A} (%) (12)
1ES 0229+200	-	25	-	-
1ES 0323+022	3.2	2.8	3.2	14
1ES 0414+009	6.2	4.3	6.2	17
1ES 0502+675	2.5-15.4	8.9	7.5	18
1ES 0647+250	-	-	-	-
1ES 0806+524	6.4-11.1	4.8	8.8	17
1ES 1028+511	8.8	6.0	8.8	18
1ES 1426+428	-	-	-	-
1ES 1517+656	3.7-8.0	7.1	4.9	17
1ES 1959+650	3.8-11.0	7.7	4.8	18
1ES 2344+514	-	19.6	-	-

5.4 Microvariability

Search for intranight optical variability (i.e. microvariability) was performed mainly for brightest objects of the sample - for 1ES 1959+650 (35 sessions) and 1ES 2344+514 (9 sessions). The measurements were performed with the apertures of different radii (4."0-7."5) due the fact that these objects are hosted by powerful elliptical galaxies.

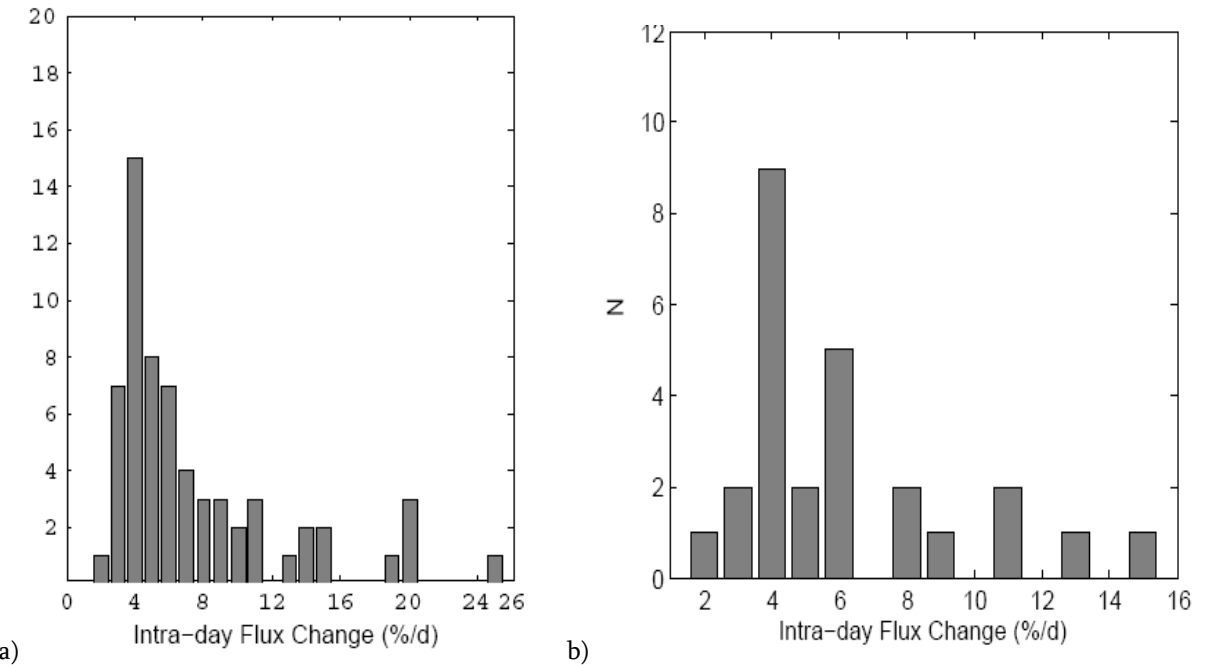


Figure 5.6: Statistics of intraday flux changes during increases (a) and decays (b).

Despite these attempts, no intranight variability was found at 99 % confidence level. The maximum value of C parameter was 2.04 while the value $C=2.5763$ is accepted as a threshold for microvariability confirmation (Romero et al. 1999). In that case, we may say that any possible variation is below our confidence threshold. Extremely violent microvariations, reported by Bai et al. (1998) are found to be the artefacts of misappropriate use of variability investigation methods.

The statistics of intraday variabilities has shown that the detection of intranight changes with 70 cm meniscus telescope of Abastumani observatory is possible only for 1ES 0806+524 and 1959+650 in rare occasions by means of very good observational conditions.

Duty cycle of intranight variability is equal to zero for selected XBL group in the case of Abastumani Observations. Note that this parameter is very sensitive to the characteristics of the telescope used for investigation. Nevertheless, the observations performed with the same telescope showed intranight variabilities for the objects from other blazer subclasses. For example, S5 0716+714 showed changes with 0.20 and 0.20 mag in 2.5 hr and 1.5 hr, respectively (Ostorero & Wagner 2004). This fact is in agreement with Romero et al. (1999) results showing that XBLs are less variable objects at intranight timescales.

As a final remark, I would like to point out that the optical behaviour of selected blazars is found to be very complex. Therefore, the underlying physical processes should also carry very complicated character. In addition to the objectives for future research, provided above, the investigation of cross-correlation between the data obtained in different spectral diapason, and constructing theoretical models, fitting well with observed features, will be a good job in the study of different phenomena inherent to XBLs.

Bibliography

- Acciari, V., et al. 2009, ApJ, 690, 126
- Aharonian, F.A., et al. 2000, A&A, 353, 847
- Aharonian, F., et al. 2002, A&A, 384, L23
- Aharonian, F., et al. 2003, 460L, L9
- Aharonian, F., et al. 2003, A&A, 403, 523
- Aharonian, F., et al. 2005, A&A, 441, 465
- Aharonian, F., et al. 2005, A&A, 442, 895.
- Aharonian, F., et al. 2007, A&A, 475, L9
- Albert, J., et al. 2006, ApJ, 639, 761
- Atoyan, A., & Dermer, C. D. 2003, ApJ 586, 79
- Badran, H., et al. 2001, ICPC, 7, 2653
- Bai, J. M., Xie, G. Z., & Li, K. H. 1998, A&AS, 132, 83
- Ballard, K. R., Mead, A. R. G., Brand, P. W. J., & Hough, J. H. 1990, MNRAS, 243, 640
- Beall, J. H., & Bednarek, W., 1998, ApJ, 510, 188
- Beckmann, V., Bade, N., & Wucknitz, O. 1999, A&A, 352, 395
- Beckmann, V., et al. 2002, A&A, 383, 410
- Begelman, M. C., Blandford, R. D., & Rees, M. J. 1984, RvMP, 56
- Bicknell, G. V., & Wagner, S. J. 2002, PASA, 19, 129
- Blandford, R. D. 1976, MNRAS, 176, 465
- Blandford, R. D., & Znajek, R. L. 1977, MNRAS, 179, 433
- Blandford, R. D., & Königl, A. 1979, ApJ, 232, 34
- Böttcher, M., & Bloom, S. D. 2000, AJ 119, 469
- Böttcher, M., Mukherjee, R., & Reimer, A. 2002, ApJ 581, 143
- Böttcher, M. 2007, Ap&SS, 309, 95
- Böttcher, M., et al. 2007, ApJ, 670, 968
- Bradt, H., et al. 1985, SSRv, 40, 613
- Brinkmann, W., & Siebert, J. 1994, ApJ, 285, 812
- Brinkmann, W., Siebert, J., Kollgaard, R.I., & Thomas, H.-C. 1996, A&A 313, 356
- Carini, M. T., Ph.D. thesis, Georgia State University press, 1990
- Carini, M. T., Nonle, J. C., & Goodrich, B. D. 1992, AJ, 104, 15
- Cavaliere, A., & D'Elia, V. 2002, ApJ 571, 226
- Catanese, M., Akerlof, C. W., & Badran, H. M. 1998, ApJ, 501, 616
- Cellone, S. A., Romero, G. E., & Combi, J. A. 2000, AJ, 119, 1534
- Cellone, S. A., Romero, G., & Araudo, A. 2007, MNRAS, 374, 357
- Ciprini, S., Tosti, G., & Raiteri, C. 2003, A&A, 400, 487
- Ciprini, S., Takalo, L. O., Tosti, G. et al. 2007, A&A, 467, 465

- Cogan, P. for the VERITAS collaboration 2008a, ICPC, 3,921
- Cogan, P. for the VERITAS collaboration 2008b, 2008, AIPC, 1085, 403
- Comastri, A., Fossati, G., Ghisellini, G., & Molendi, S. 1997, ApJ, 480, 534
- Coppi, P. S., & Aharonian, F. 1999, ApJ, 521, L33
- Corbett, E. A., et al. 1996, MNRAS, 281, 737
- Curtis, H. D. 1918, Pub. Lick. Obs., 13, 31
- Corbett, E. A., Robinson, A., Axon, D. J., & Hough, J. H. 2000, MNRAS, 311, 485
- Da Costa, G. S. 1992, in Astronomical CCD Observing and Reduction Techniques, ASPC, 23, 90.
- Deeming, T. J. 1975, Astrophys. Space Sci., 36, 137
- Dermer, C., Sturner, S., & Schlickeiser, R. 1997, ApJSS, 109, 103
- Djannati-Ataiï, A., et al. 2003, A&A, 391, L25
- Doxsey, R., et al. 1983, ApJ, 264, L43
- Edelson, R. A., & Krolik, J. H. 1988, ApJ, 333, 646
- Edwards, P., & Piner, B. 2002, ApJ, 579, iss.2, L67
- Elvis, M., Plummer, D., Schachter, J., & Fabbiano, G. 1992, ApJS, 80, 257.
- Falcone, A.D., Cui, W., & Finley, J. P. 2004, ApJ, 601, 165.
- Falomo, R., Bouchet, P., & Tanzi, E. G. 1989, IAUC, 4759
- Falomo, R., & Tanzi, E. 1991, AJ, 102, 1294
- Falomo, R., Bersanelli, M., Bouchet, P., & Tanzi, E.G. 1993, AJ, 106, 11
- Falomo, R., Scarpa, R., & Bersanelli, M. 1994, ApJS, 93, 125
- Falomo, R., et al. 1997, A&A, 321, 374
- Falomo, R., Kotilainen, J. K., & Treves, A. 2002, ApJ, 569, L35
- Fan, J. H., et al. 1998b, A&AS, 136, 217
- Fan, J. H. 1999, ASP Conference Series, 159, 57
- Fan, J. H., & Lin, R. 2000. ApJ, 537, 101
- Fan, J.H., Lin, R.G., Xie, G.Z. et al. 2002, A&A, 381, 1
- Fan, J. H. 2005, C JAA, Vol. 5 Suppl., 213
- Fath, E. A. 1908, Lick Obs. Bull., 5, 71
- Feigelson, E. D., et al. 1986, ApJ, 302, 337
- Filipenko, A.V., Djorgovski, S., Spinrad, H., & Sargent, W. L. W. 1986, AJ, 91, 49
- Fiorucci, M., & Tosti, G. 1996, A&AS, 117, 475
- Fiorucci, M., Tosti, G., & Rizzi, N. 1998, PASP, 110, 105
- Foster, G., 1996, AJ, 112, 4
- Gabuzda, D. C. 1999, New Astron. Rev., 43, 691
- Gabuzda, D. C., Pushkarev, A. B., & Cawthorne, T. V. 2000, MNRAS, 319, 1109
- Gabuzda, D. C., Murray, E., & Cronin, P. 2004, MNRAS, 351, L89
- Georganopoulos, M., & Marscher, A. 1996a, AAS, 188.2302 G.

- Georganopoulos, M., & Marscher, A. 1996b, ASP Conference Series, 110, 262
- Georganopoulos, M., & Kazanas, D. 2003, ApJ, 594, L27
- Ghisellini, G., Padovani, P., Celotti, A., & Maraschi, L. 1993, ApJ, 407, 65
- Ghisellini, G., & Madau, P. 1996, MNRAS, 280, 67
- Ghisellini, G., Marashi, L., Dondi, L. 1996, A&AS, 120, 503
- Ghisellini, G., et al. 1998, MNRAS, 301, 451
- Ghisellini, G., Celotti, A., & Costamante, L., 2002, A&A, 386, 833
- Ghisellini, G. 2004, NewAR, 48, 375
- Ghisellini, G., Tavecchio, F., & Chiaberge, M. 2005, A&A, 432, 401
- Ghisellini, G., & Tavecchio, F. 2008, MNRAS, 386, 628
- Giebels, B., et al. 2002, ApJ, 763
- Giommi, P., & Padovani, P. 1994, MNRAS, 268, L51
- Giommi, P., Ansari, S. G., & Micol, A. 1995, A&AS, 109, 267
- Giovannini, G., et al., 2004, ApJ, 613, 747.
- Giroletti, M., Giovannini, G., Taylor, G.B., & Falomo R. 2004, ApJ, 613, 752
- Gomez , J., et al. 1997, ApJ, 482, L33
- Gopal-Krishna, & Wiita P. 1992, A&A, 259, No.1, 109
- Gopal-Krishna, Stalin, C. S., Sagar, R., & Wiita P. J. 2003, ApJ, 586, L25
- Gopal-Krishna, Dhurde, S. & Wiita, P. J. 2004, ApJ, 615, L81
- Gupta, A., Fan , J., Bai, J., Wagner, S. 2008, AJ, 135, 1384
- Gupta, A. C., Srivastava, A. K., & Wiita, P. J. 2009, ApJ, 690, 216
- Gutierrez K., Badran H. M., & Bradbury S. M. 2006, ApJ, 644, 742
- Halpern, J. P., Chen, V. S., Madejski, G. M., & Chanan ,G.A. 1991, AJ, 101, 818
- Hanski, M. T., Takalo, L. O., & Valtaoja E. 2002, A&A 394, 17
- Harris, D. E., & Krawczynski, H. 2006, ARA&A, 44,463
- Heidt, J. &Wagner, S. J. 1996, A&A, 305, 42
- Heidt J., & Wagner, S. J. 1998, A&A, 329, 853
- Heidt, J., et al. 1999, A&A, 341, 683
- Heidt, J., et al. 1999, A&A, 352, L11
- Heidt, J., Jäger, K., Nilsson, K. et al. 2003, A&A, 406, 565
- Holder, J., et al. 2003, ApJ, 583, L9
- Hovatta, T., et al. 2007, 469, 899
- Howard, E. S., Webb, J. R., Pollock, J. T., & Stencel, R. E. 2004, AJ, 127, 17
- Howell, S. B., & Jacoby, G. H. 1986, PASP, 98, 802
- Howell, S. B., Warnoc, A. I., & Mitchell, K. J. 1988, AJ, 95, 247
- Howell, S. B. 1989, PASP, 101, 616
- Hufnagel, B.R., & Bregman, J. N. 1992, ApJ, 386,473
- Hughes, P. A., Aller, H. D., & Aller, M. F. 1992, ApJ, 396, 469
- Humason, M. L. 1932, PASP, 44, 267

- Impey, C.D. & Neugebauer, G. 1988, AJ, 95, 307
- Jang M., & Miller, H. R. 1997, AJ, 114, 565
- Januzzi, B., Smith, P., & Elston, R. 1993, ApJS, 85, 265
- Jannuzi, B. T., Smith, P. S., & Elston, R. 1994, ApJ, 428, 130
- Jurkevich. I. 1971, Ap&SS, 13, 154
- Jones, T. W., et al. 1985, ApJ, 290, 627
- Kaspi, S., et al. 2000, ApJ, 533, 631
- Kazanas, D., & Mastichiadis, A. 1999, APh, 11, 41
- Kellermann, K. I., et al. 2004, ApJ, 609, 539
- Kohmura, Y., et al. 1994, PASJ, 46, 113
- Kollgaard, R. I., Gabuzda, D.C., & Feigelson, E. D. 1996, ApJ, 460, 174
- Kollgaard, R., Palma C., Laurent-Muehleisen S., & Feigelson E. 1996, ApJ, 465, 115
- Kotilainen, J.K. & Falomo, R. 2004, A&A, 424, 107
- Krawczynski, H., Coppi, P. S., & Aharonian, F. 2002, MNRAS, 336, 721
- Krawczynski, H. 2004, NewAR, 48, 367
- Krawczynski, H., et al. 2004, ApJ, 601, 151
- Kurtanidze, O. M., & Kvernadze T. M. 1995, ASP Conf. Ser., 84, 56
- Kurtanidze, O. M., et al. 2003a, A&AT, 22, 699
- Kurtanidze, O. M., et al. 2003b, A&AT, 22, 703
- Kurtanidze, O. M., et al. 2004a, NuPhS, 132, 197
- Kurtanidze, O. M., et al. 2004b, NuPhS, 132, 193
- Kurtanidze, O. M., et al. 2005, MmSAI, 76, 53
- Kurtanidze, O. M., et al. 2006a, Proceedings of the The X-ray Universe 2005 (ESA SP-604). 26-30 September 2005, El Escorial, Madrid, Spain. Editor: A. Wilson, p. 639
- Kurtanidze, O. M., et al. 2006b, Proceedings of the The X-ray Universe 2005 (ESA SP-604), p. 637
- Kurtanidze, O. M., et al. 2006c, Proceedings of the The X-ray Universe 2005 (ESA SP-604), p.635
- Kurtanidze, O. M., et al. 2007a, Black Holes from Stars to Galaxies -- Across the Range of Masses. Edited by V. Karas and G. Matt. Proceedings of IAU Symposium #238, held August 21-25, 2006 in Prague, Czech Republic. Cambridge University Press, p. 397
- Kurtanidze, O. M., et al. 2007b, Black Holes from Stars to Galaxies -- Across the Range of Masses. Edited by V. Karas and G. Matt. Proceedings of IAU Symposium #238, held August 21-25, 2006 in Prague, Czech Republic. Cambridge University Press, p. 399
- Kusunose, M., & Takahara, F. 2006, ApJ, 651, 113
- Lainela, M., & Valtaoja, E. 1993, ApJ, 416, 485
- Laurent-Muehleisen, S., Kollgaard, R., Moellenbrock, G., & Feigelson, E. 1993, ApJ, 106, 875

- Lehto, H. J., & Valtonen, M. J. 1996, ApJ, 460, 207
- LeVeque, R. J., Mihalas, D., Dorfi, D. A., & Müller, E. 1997, in Computational Methods for Astrophysical Fluid Flow, SAAS-Fee advanced Course 27, Springer, p. 445
- Leonardo, E., et al. 2009, astro-ph/0907.0959
- Levinson, A., & Van Putten, M. V. P. 1997, ApJ, 488, 69
- Levinson, A. 2008, astro-ph/08080310
- Lewis, G. & Ibata, R. 2000, ApJ, 528, 650
- Lynden-Bell, D. 1969, Nature, 223, 690
- Lister, M. L., & Homan, D. C. 2005, AJ, 130, 1389
- Mangalam, A., & Wiita, P. 1993, ApJ, 406, Part 1, No. 2, 420
- Mannheim, K. & Biermann, P. L. 1992, A&A ,253, L21
- Mannheim, K. 1993, A&A, 269, 67
- Marcha, M. J. M., Browne, I. W. A., Impey, C. D., & Smith, P. S. 1996, MNRAS, 281, 425
- Margon, B., & Jacoby, G. H. 1983, ApJ, 286, L31
- Marscher, A. P., & Gear, W. K. 1985, ApJ, 298, part 1, 114
- Marscher, A. P., Gear, W. K., & Travis, J. P. 1992, in Variability of Blazars, ed. E. Valtaoja & M. Valtonen, Cambridge U. Press, 85
- Marscher, A. P. 1996, ASPC, 100, 248
- Marscher, A. P. 2006, AIP Conf. Proc., 856, Iss. 1, 1
- Marscher, A. P., Workshop on Blazar Variability across the Electromagnetic Spectrum, Palaiseau, France April 22nd-25th 2008
- Marscher, A., et al. 1999, PTEP Proc., 327
- Massaro, E., et al. 1996, A&A, 87, 1996
- Mastichiadis, A., & Kirk, J. G. 1997, A&A 320, 19
- McHardy, I. M., et al. 1992, MNRAS, 256, 655
- McHardy, I. M., et al. 1999, MNRAS, 310, 571
- McKinney J. A. 2006, MNRAS, 367, 1797
- Meier, D., Koide S., & Uchida Y. 2001, Science, Vol. 291, Iss. 5501, 84
- Mayall N. U. 1934, PASP, 46, 134
- Miller, H. R., Carini, M. T., & Goodrich, B. D. 1989, Nature, 337, 627
- Mizuta, A., Yamada, S. & Takabe, H. 2004, ApJ, 606, 804
- Morris, S. L., et al. 1991, ApJ 380, 49
- Mücke , A., et al., 2003, ApH, 18, 593
- Nilsson, K., et al. 2007, A&A, 475,199
- Nilsson, K., et al. 1999, PASP, 111, 1223
- Nishiyama, T. & Utah Seven Telescope Array detector collaboration, Proceedings of the 26th International Cosmic Ray Conference, p. 370
- Ostorero, L., & Wagner, S., Proceedings of Third ENIGMA Meeting, Jerisjärvi, Finland - April 25-28, 2004

- Ostriker, J., & Vietri, M., Nature, vol. 344, 1990, p. 45
- Padovani, P., & Giommi, P. 1995, ApJ, 444, 567
- Perlman, E. S., et al. 1996, ApJS, 104, 251
- Perlman, E. S., et al. 2005, ApJ, 625, 727
- Pica, A. J., et al. 1988, AJ, 96, 1215
- Piner, B. G. & Edwards, P. G. 2004, ApJ, 600, 115
- Piner, B. G., Pant, N., & Edwards P.G., 2008, ApJ, 678, 64
- Qian, S. J., et al. 1991, A&A, 241, 15
- Raiteri, C. M., et al., 1998, A&AS, 132, 361
- Raiteri, C.M., et al. 2001, A&A, 377, 396
- Raiteri, C. M., et al. 2005, A&A, 438, 39
- Rani, B., Wiita, P., & Gupta, A. C., 2009, ApJ, 696, 2170
- Rector, T.A., Gabusda, D.C., & Stocke, J. T., 2003, AJ, 125, 1060
- Reimer, A., Böttcher, M., & Postnikov, S., 2005, ApJ 630, 186
- Raiteri, C. M., et al. 2006, A&A, 459, 731
- Remillard, R., et al. 1989, ApJ, 345, 140
- Rieger, F., & Duffy M. 2004, ApJ, 617, 155
- Romero, G.E. 1995, Ap&SS, 234, 49
- Romero, G.E., Surpi, G., & Vucetich, H., 1995a, A&A 301, 641
- Romero, G. E.; Cellone, S. A., & Combi, J. 1999, ApJSS, 135, 477
- Romero, G. E., Cellone, S. A., & Combi, J. A. 2000a, A&A, 360, L47
- Romero, G.E., et al. 2000b, A&A, 360, 57
- Romero, G. E., Cellone, S. A., Combi, J. A., & Andruchow, I., 2002, A&A, 390, 431
- Romero, G.E., Fan, J.H., & Nuza S.E. 2003, ChJAA, 3, 513
- Sagar, R., Stalin, C. S., Gopal-Krishna, & Wiita P. J., 2004, MNRAS, 348, 176
- Salpeter, E. E. 1964, ApJ, 140, 796
- Sambruna, R., Maraschi, L., & Urry C.M., 1996, ApJ 463, 444
- Sbarufatti, B., Proceedings of the first ENIGMA meeting, Mayschoss, May 11-14, 2003
- Scarpa ,R. et al. 1999, A&A, 521, 134
- Scarpa, R., et al. 2000, ApJ, 532, 740
- Schachter, J.F., et al. 1993, ApJ, 412, 541
- Schlegel, D. J., Finkbeiner, D. P., & Davis, M. 1998, ApJ, 500, 525
- Seyfert, C. K. 1943, ApJ, 97, 28
- Shakura, N. I., & Sunyaev, R. A. 1976, MNRAS, 175, 613
- Sikora, M., Sol, H., Begelman, M. C., & Madejski, G. M. 1996, MNRAS, 280, 781
- Sikora, M., Begelman, M., Madejski, G., & Lasota J., 2005, ApJ, 625, 72
- Simonetti, J. h., Cordes, J. M. & Heeschen, D. S., 1985, ApJ, 296, 46
- Sitko, M.L., & Sitko A.K. 1991, PASP, 103, 160
- Slipher, V. M. 1917, Lowell Obs. Bull., 3, 59

- Smith, P.S., Jannuzzi, B.T., & Elston, R. 1991, ApJS, 77, 67
- Smith, A.G., Nair, A.D., Leacock, R.J., & Clements, S.D. 1993, AJ 105, 437
- Sokolov, A., & Marsher, A. 2004, AIP Conf. Proc., 714, 198
- Sokolov, A. & McHardy I. 2004, ApJ, 613, 725
- Spada, M., Lazzati, D., Ghisellini, G., & Celotti, A. 2001, MmSAI, 72, 157
- Spangler, S., Fanti, R., Gregorini, L. & Padrieli L. 1989, A&A, 209, 315
- Stalin, C. S., Gopal-Krishna, Sagar, R., & Wiita, P. J. 2004b, JA&A, 25, 1
- Stawarz, L., & Ostrowski, M. 2002, ApJ, 578, 763
- Stecker, F.W., de Jager, O.C., & Salamon, M.H. 1996, ApJ, 473, L75
- Sundelius, B., Wahde, H., Lehto, H. J., & Valtonen, M. J. 1997, ApJ, 484, 180
- Swain, M. R., Bridle, A. H., & Baum, S. A. 1998, ApJ, 507, L33
- Tagliaferri, G., et al. 2003, A&A, 412, 711
- Tagliaferri, G., et al. 2008, ApJ, 679, 1029
- Tavecchio, G., & Ghisellini, G., 2008, MNRAS, 395, L98
- Tluczykont M., et al. 2003, 28th International Cosmic Ray Conference, 2547
- Tommasi, L., et al. 2001, MmSAI, 72, 123.
- Torres, D.F., et al. 2003, MNRAS, 339, 335
- Tramacere, A. et al., 2007, A&A, 467, 501
- Valtonen, M. J., Nilsson, K., & Sillanpää ,A., 2006, ApJ, 643, L9
- Ulmer, M.P., et al. 1983, ApJ, L1
- Vermeulen, R. C., et al. 1995, ApJ, 52, L5
- Villata, M., Raiteri, C.M., & Lanteri, L. 1998a, A&AS, 130, 305
- Villata, M., et al. 1998b, MNRAS, 293, L13
- Villata, M., et al. 2000, ApJS, 144, 481
- Villata, M., et al., 2004, A&A, 421, 103
- Vlahakis, N., & Königl, A. 2004, ApJ, 605, 656
- Wagner, S.J., et al., 1996, AJ 111, 2187
- Wagner, R. M., 2008, MNRAS, 35, 185
- Weekes, T.C., Akerlof C.W., Biller S. et al., 1996, A&A, 120C, 603
- Wiita, P. 2005, ACPC, 350, 183
- Wiita, P. 2006, astro-ph/0603728
- Wurtz, R., Ph.D. thesis, Univ. Colorado press, 1994
- Wurtz, R., Stocke, J.T., & Yee, H.K.C. 1996, ApJS 103, 109
- Wurtz, R., Stocke, J.T., Ellingson, E., & Yee ,H.K.C., 1997, ApJ, 480, 547
- Xie, G.Z., et al. 1996, AJ, 111, 1065
- Xie ,G.Z., Zhou, S.B., & Dai, B.Z., 2002, MNRAS, 329, 689
- Zeldovich, Y. B. 1964, Doklady Akademii Nauk SSSR, 155, 67

Acknowledgements

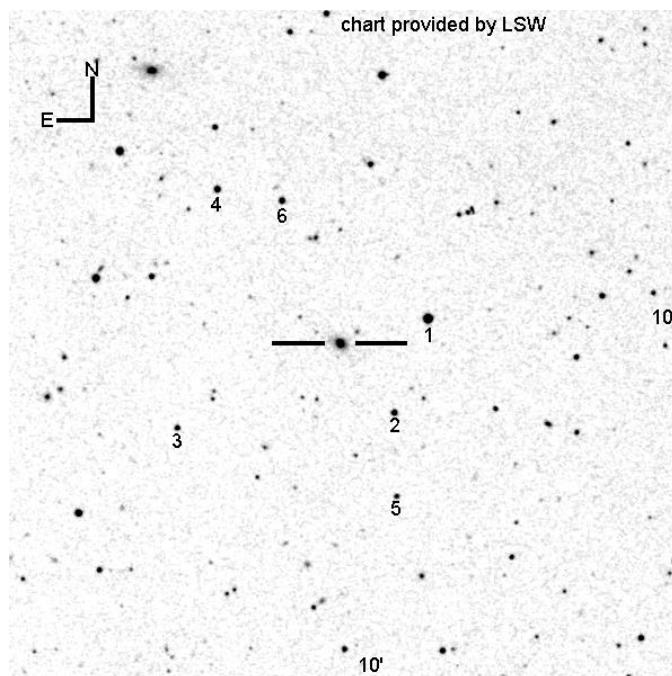
I would like to express my acknowledgements with respect to prof. Ivane Murusidze, and prof. George Javakhishvili (thesis supervisor) for their invaluable support in my scientific activities.

I thank Mr. Omar Kurtanidze and Mrs. Maria Nikolashvili for their support in mastering of observational skills and for kind provision of observational material obtained during 1997-2000. I owe great respect to prof. George Malasidze, Revaz Chigladze, Givi Kimeridze, Shalva Sabashvili, Rolan Kiladze etc. who made me familiar with different astronomical fields during my student years.

I would like to thank Edward Janiashvili, Gustavo E. Romero, Sergio Cellone, Gabriele Ghisellini, Kari Nilsson, Alok C. Gupta, Massimo Fiorucci for their useful suggestions. In addition, I am very respectful to Gustavo E. Romero, Sergio Cellone, and Gabriele Ghiselini for the reviews concerning my thesis prospectus.

I thank Dr. Kari Nilsson for provision numerical values of host galaxy fluxes for some targets, and Dr. Franco Giovannelli, for my invitation at FRASCATI WORKSHOP 2009 where the highlights of the investigation were presented.

A1 1ES 0229+200



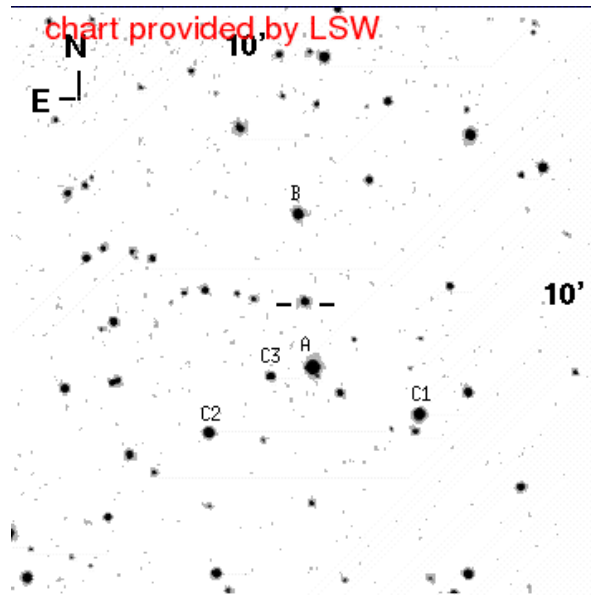
(<http://www.lsw.uni-heidelberg.de/projects/extragalactic/charts>)

Comparison stars

star	B	R
1	14.7	13.7
2	16.9	16.3
3	17.4	16.6
4	16.7	15.7
5	19.4	17.4
6	17.7	16.0

(Monet et.al., 1998, USNO 2.0 Catalogue)

A2 1ES 0323+022

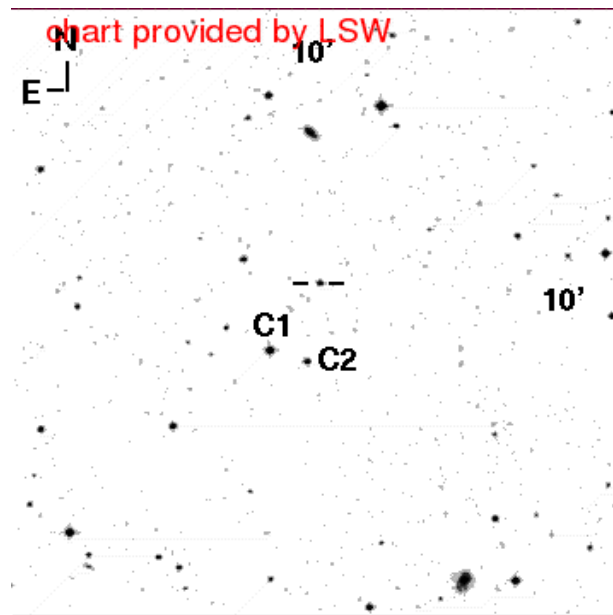


(<http://www.lsw.uni-heidelberg.de/projects/extragalactic/charts>)

Comparison stars

Star	<i>V</i>	<i>R</i>	<i>I</i>
A	12.85 (0.03)	12.33 (0.03)	11.82 (0.03)
B	14.38 (0.04)	14.01 (0.04)	13.64 (0.04)
C1	14.00 (0.04)	13.34 (0.04)	12.81 (0.04)
C2	14.44 (0.04)	13.84 (0.04)	13.32 (0.04)
C3	15.75 (0.05)	15.36 (0.05)	14.93 (0.05)

(Fiorucci, Tosti, Rizzi, 1998)

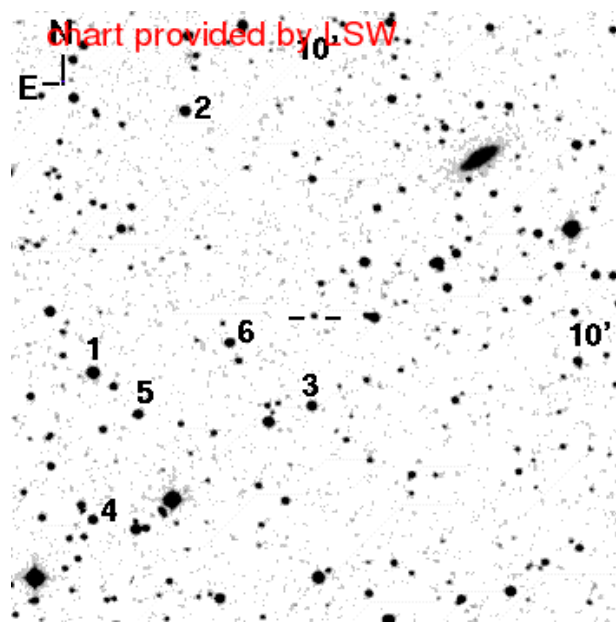


(<http://www.lsw.uni-heidelberg.de/projects/extragalactic/charts/>)

Comparison stars

Star	<i>V</i>	<i>R</i>	<i>I</i>
C1	13.95 (0.05)	13.56 (0.05)	13.15 (0.05)
C2	15.17 (0.07)	14.63 (0.07)	14.06 (0.07)

(Fiorucci, Tosti, Tanzi, 1998)



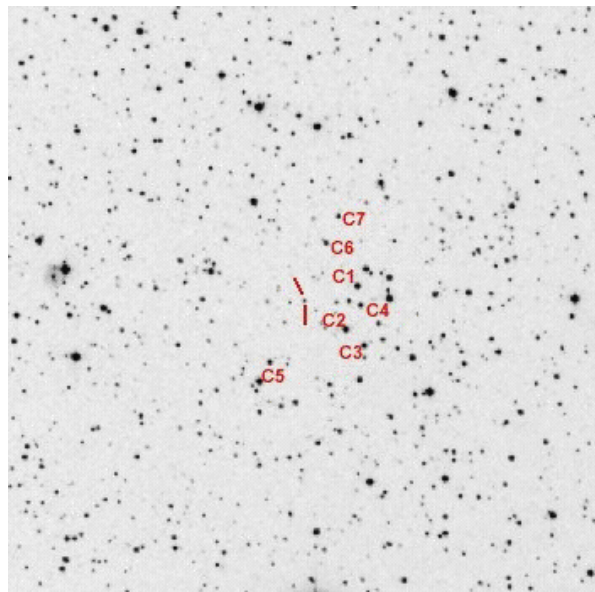
(<http://www.lsw.uni-heidelberg.de/projects/extragalactic/charts/>)

Comparison stars

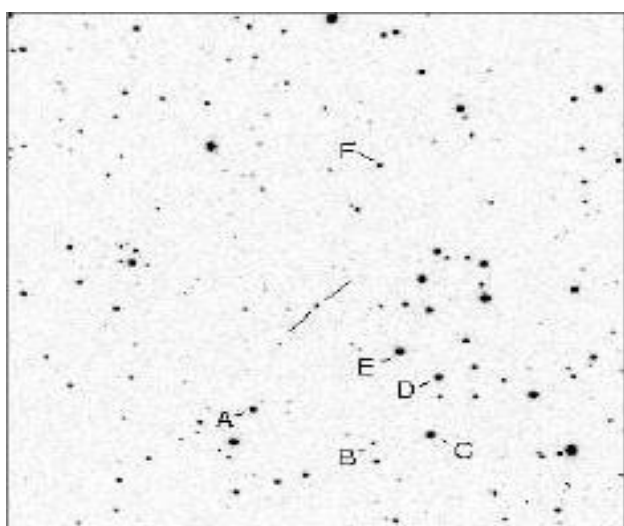
Star	<i>B</i>	<i>V</i>	<i>R</i>
1	14.12 (0.03)	13.08 (0.03)	12.60 (0.04)
2	15.19(0.04)	14.18 (0.03)	13.69 (0.05)
3	15.07 (0.04)	14.28 (0.03)	13.89 (0.04)
4	15.24 (0.04)	14.51 (0.03)	14.16 (0.04)
5	15.95 (0.04)	14.82 (0.03)	14.31 (0.03)
6	16.94 (0.04)	15.19 (0.03)	14.49) (0.03)

(Villata et al. 1998)

A5 1ES 0647+250



(<http://astro.fisica.unipg.it/PGblazar/0647.html>)

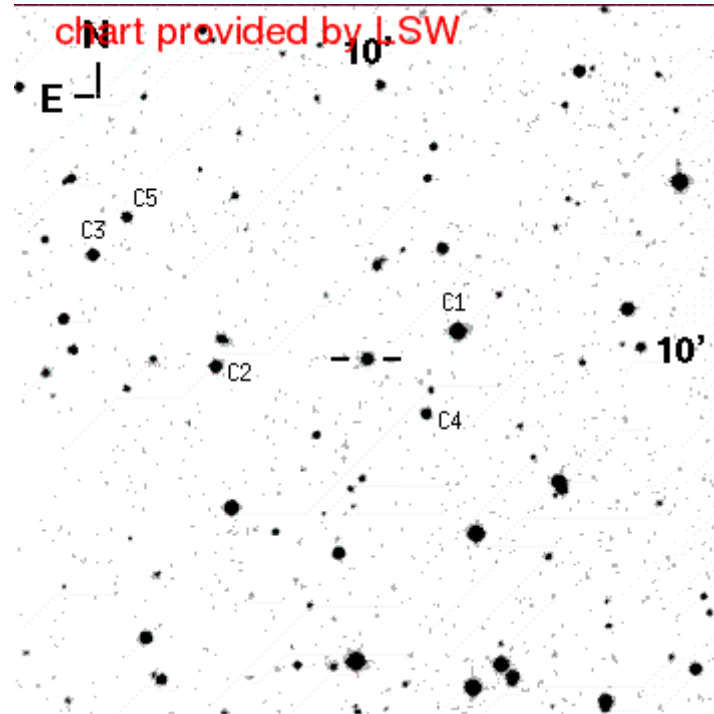


Comparison stars:

Star	<i>R</i>	<i>V-R</i>
A	13.83±0.04	0.33±0.05
B	15.22±0.04	0.38±0.06
C	13.40±0.04	0.40±0.05
D	13.44±0.04	0.34±0.05
E	13.03±0.04	0.59±0.05
F	14.89±0.04	0.38±0.05

(Nilsson et al. 2007)

A6 1ES 0806+524



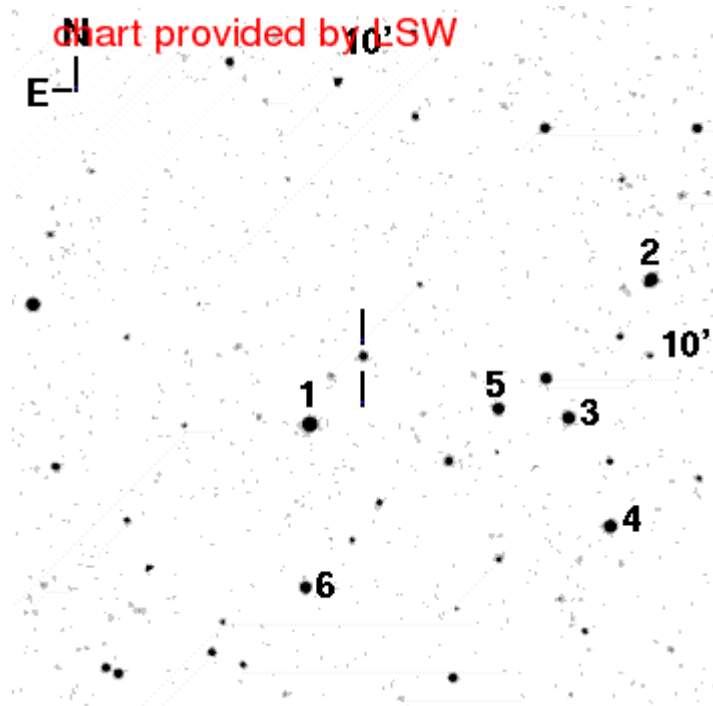
(<http://www.lsw.uni-heidelberg.de/projects/extragalactic/charts/>)

Comparison stars

Star	<i>V</i>	<i>R</i>	<i>I</i>
C1	13.04 (0.05)	12.56 (0.05)	12.14 (0.05)
C2	14.61 (0.05)	14.22 (0.04)	13.86 (0.04)
C3	14.77 (0.05)	14.39 (0.05)	14.04 (0.05)
C4	15.49 (0.06)	15.14 (0.06)	14.81 (0.06)
C5	15.62 (0.06)	15.32 (0.05)	14.99 (0.06)

(Fiorucci, Tosti, Rizzi, 1998)

A7 1ES 1028+511



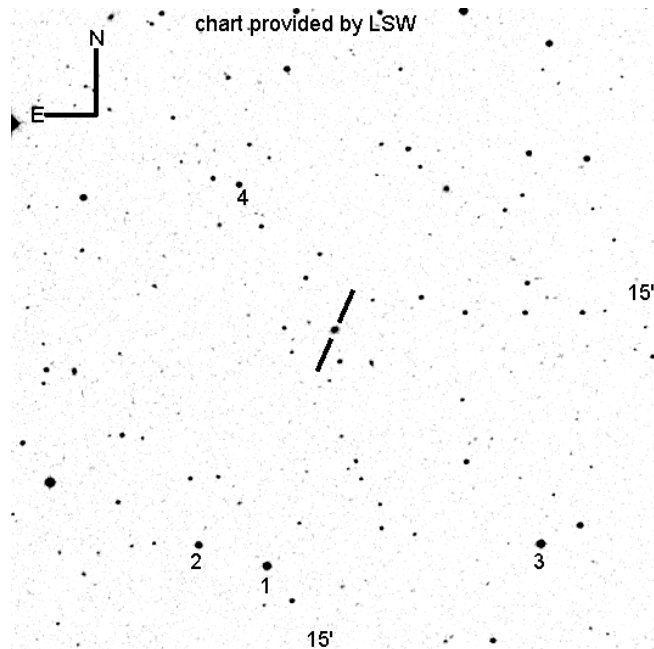
(<http://www.lsw.uni-heidelberg.de/projects/extragalactic/charts/>)

Comparison stars

Star	<i>B</i>	<i>V</i>	<i>R</i>
1	13.91 (0.03)	13.20 (0.02)	12.93 (0.03)
2	14.93 (0.03)	14.29 (0.03)	14.04 (0.03)
3	15.02 (0.03)	14.40 (0.03)	14.18 (0.03)
4	15.05 (0.05)	14.40 (0.03)	14.17 (0.03)
5	15.17 (0.04)	15.03 (0.03)	14.75 (0.03)
6	15.66 (0.03)	15.06 (0.03)	14.87 (0.04)

(Villata et al.1998)

A8 1ES 1426+428



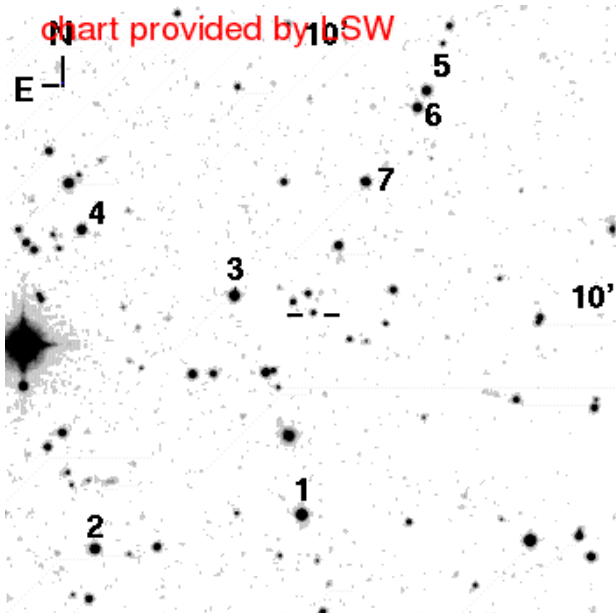
(<http://www.lsw.uni-heidelberg.de/projects/extragalactic/charts/>)

Comparison Stars

star	<i>U</i>	<i>B</i>	<i>V</i>	<i>R</i>	<i>I</i>
1	16.72 (0.07)	15.63 (0.03)	14.13 (0.02)	13.23 (0.02)	12.43 (0.02)
2	15.80 (0.04)	15.47 (0.02)	14.61 (0.02)	14.17 (0.02)	13.79 (0.02)
3	14.55 (0.04)	14.22 (0.02)	13.00 (0.02)	13.00 (0.02)	12.62 (0.03)
4	16.26 (0.09)	16.14 (0.06)	15.20 (0.02)	15.20 (0.04)	14.82 (0.02)

(Smith, Jannuzzi & Elston, 1991)

A9 1ES 1517+656



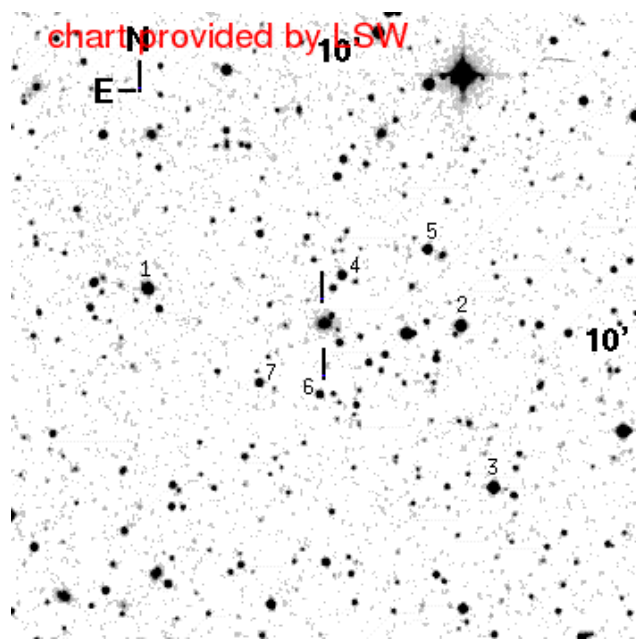
(<http://www.lsw.uni-heidelberg.de/projects/extragalactic/charts/>)

Comparison stars

Star	<i>B</i>	<i>V</i>	<i>R</i>
1	13.45(0.05)	12.88(0.03)	12.54(0.02)
2	14.29(0.02)	13.70(0.02)	13.42(0.02)
3	14.40(0.05)	13.73(0.02)	13.35(0.02)
4	14.94(0.04)	14.27(0.02)	13.85(0.03)
5	14.89(0.07)	14.31(0.03)	13.90(0.02)
6	15.33(0.07)	14.56(0.02)	14.07(0.03)
7	15.34(0.07)	14.70(0.02)	14.26(0.03)

(Villata et al. 1998)

A10 1ES 1959+650



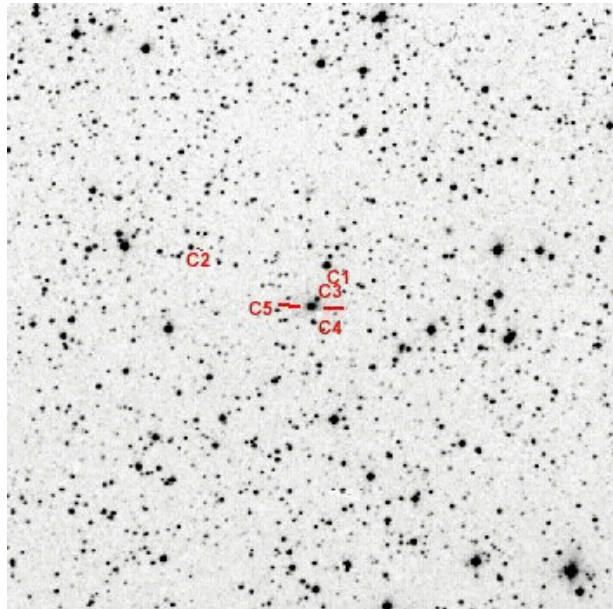
(<http://www.lsw.uni-heidelberg.de/projects/extragalactic/charts/>)

Comparison stars

Star	<i>V</i>	<i>R</i>
1	12.67(0.04)	12.29(0.02)
2	12.86(0.02)	12.53(0.02)
3	13.18(0.02)	12.27(0.02)
4	14.53(0.03)	14.08(0.03)
5	14.54(0.03)	14.00(0.02)
6	15.20(0.03)	14.78(0.03)
7	15.24(0.03)	14.79(0.03)

(Villata et al. 1998)

A11 1ES 2344+514



Comparison stars

Star	<i>V</i>	<i>R</i>	<i>I</i>
C1	12.59 (0.06)	12.20 (0.06)	11.89 (0.06)
C2		14.16 (0.05)	
C3	15.34 (0.08)	15.05 (0.08)	14.58 (0.07)
C4	15.89 (0.12)	15.35 (0.08)	14.72 (0.08)
C5	16.00 (0.08)	15.51 (0.08)	14.95 (0.08)

(<http://astro.fisica.unipg.it/PGblazar/2344.htm>)

Appendix B. Observational Data

B.1 R Band Data of 1ES 0229+200

JD-2450000 (1)	Ref6-Ref4 (2)	R (3)	F (4)	F_{corr} (5)	R_{hs} (6)	R_{hsd} (7)
762.4844	0.27	16.05	1.17	0.19	18.02	17.66
835.2488	0.24	16.09	1.13	0.15	18.28	17.92
1041.4897	0.28	16.11	1.11	0.13	18.44	18.08
1041.4981	0.29	16.09	1.13	0.15	18.28	17.92
1051.5119	0.30	16.10	1.12	0.14	18.35	17.99
1051.5225	0.28	16.06	1.16	0.18	18.08	17.72
1055.5093	0.29	16.12	1.10	0.12	18.52	18.16
1055.5179	0.25	16.12	1.10	0.12	18.52	18.16
1070.5182	0.25	16.09	1.13	0.15	18.28	17.92
1074.4933	0.29	16.14	1.08	0.10	18.72	18.36
1074.5035	0.27	16.11	1.11	0.13	18.44	18.08
1083.4215	0.26	16.10	1.12	0.14	18.35	17.99
1083.4315	0.24	16.10	1.12	0.14	18.35	17.99
1086.4947	0.28	16.12	1.10	0.12	18.52	18.16
1086.5032	0.29	16.13	1.09	0.11	18.62	18.26
1106.3808	0.26	16.05	1.17	0.19	18.02	17.66
1106.3888	0.27	16.04	1.16	0.21	17.91	17.55
1114.3921	0.30	16.12	1.10	0.12	18.52	18.16
1114.3996	0.29	16.13	1.09	0.11	18.62	18.26
1130.4215	0.27	16.05	1.17	0.19	18.02	17.66
1130.4292	0.27	16.02	1.21	0.23	17.82	17.46
1141.2904	0.29	16.12	1.10	0.12	18.52	18.16
1141.2984	0.30	16.10	1.12	0.14	18.35	17.99
2524.4262	0.25	16.08	1.14	0.16	18.21	17.85
2553.4090	0.28	16.10	1.12	0.14	18.35	17.99
2553.4129	0.29	16.08	1.14	0.16	18.21	17.85
2561.5225	0.25	16.14	1.08	0.10	18.72	18.36
2561.5265	0.28	16.08	1.14	0.16	18.21	17.85
2582.4554	0.3	16.09	1.13	0.15	18.28	17.92
2582.4594	0.27	16.14	1.08	0.10	18.72	18.36
2584.4637	0.26	16.13	1.09	0.11	18.62	18.26
2584.4684	0.28	16.06	1.16	0.18	18.08	17.72
2584.4750	0.31	16.10	1.12	0.14	18.35	17.99
2587.4180	0.26	16.12	1.10	0.12	18.52	18.16
2587.4684	0.29	16.14	1.08	0.1	18.72	18.36

Appendix B1-Continued

1	2	3	4	5	6	7
2610.4585	0.24	16.09	1.13	0.15	18.28	17.92
2610.4643	0.27	16.13	1.08	0.10	18.72	18.36
2672.2863	0.29	16.13	1.08	0.10	18.72	18.36
2884.5278	0.27	16.09	1.13	0.15	18.28	17.92
2884.5318	0.27	16.05	1.17	0.19	18.02	17.66
2906.4915	0.25	16.13	1.09	0.11	18.62	18.26
2906.4952	0.28	16.13	1.09	0.11	18.62	18.26
2968.4109	0.26	16.14	1.08	0.10	18.72	18.36
2968.4153	0.24	16.10	1.12	0.14	18.35	17.99
3214.5190	0.28	16.12	1.10	0.12	18.52	18.16
3264.5607	0.29	16.12	1.10	0.12	18.52	18.16
3272.5477	0.26	16.11	1.11	0.13	18.44	18.08
3272.5518	0.28	16.05	1.17	0.19	18.02	17.66
3302.5325	0.26	16.12	1.10	0.12	18.52	18.16
3302.5372	0.28	16.12	1.10	0.12	18.52	18.16
3317.4331	0.31	16.14	1.08	0.10	18.72	18.36
3317.4373	0.26	16.12	1.10	0.12	18.52	18.16
3323.3335	0.25	16.07	1.15	0.17	18.14	17.78
3323.3377	0.26	16.09	1.13	0.15	18.28	17.92
3329.5217	0.30	16.08	1.14	0.16	18.21	17.85
3329.5261	0.25	16.08	1.14	0.16	18.21	17.85
3380.2072	0.26	16.14	1.08	0.10	18.72	18.36
3405.2430	0.28	16.13	1.09	0.11	18.62	18.26
3405.2475	0.29	16.10	1.12	0.14	18.35	17.99
3646.4555	0.25	16.14	1.08	0.10	18.72	18.36
3646.4595	0.28	16.11	1.11	0.13	18.44	18.08
3646.4674	0.27	16.13	1.09	0.11	18.62	18.26
3653.4488	0.26	16.06	1.16	0.18	18.08	17.72
3653.4530	0.27	16.10	1.12	0.14	18.35	17.99
3698.2352	0.31	16.07	1.15	0.17	18.14	17.78
3698.2392	0.26	16.13	1.09	0.11	18.62	18.26
3711.3837	0.29	16.07	1.15	0.17	18.14	17.78
3711.3876	0.24	16.06	1.16	0.18	18.08	17.72
3711.3915	0.27	16.05	1.17	0.19	18.02	17.66
3711.3954	0.29	16.04	1.19	0.21	17.91	17.55
4034.3501	0.27	16.06	1.16	0.18	18.08	17.72
4034.3522	0.27	16.10	1.12	0.14	18.35	17.99
4034.3543	0.25	16.12	1.10	0.12	18.52	18.16
4034.3564	0.28	16.13	1.09	0.11	18.62	18.26
4062.3920	0.26	16.11	1.11	0.13	18.44	18.08
4062.4003	0.24	16.07	1.15	0.17	18.14	17.78

Appendix B1-Continued

1	2	3	4	5	6	7
4062.4024	0.28	16.09	1.13	0.15	18.28	17.92
4062.4045	0.29	16.05	1.17	0.19	18.02	17.66
4062.4066	0.28	16.08	1.14	0.16	18.21	17.85
4062.4087	0.26	16.10	1.12	0.14	18.35	17.99
4062.4108	0.24	16.10	1.12	0.14	18.35	17.99
4062.4129	0.28	16.09	1.13	0.15	18.28	17.92
4062.4150	0.29	16.07	1.15	0.17	18.14	17.78
4062.4172	0.26	16.14	1.08	0.10	18.72	18.36
4062.4793	0.28	16.09	1.13	0.15	18.28	17.92
4088.1901	0.26	16.14	1.08	0.10	18.72	18.36
4088.1922	0.29	16.10	1.12	0.14	18.35	17.99
4088.1943	0.31	16.08	1.14	0.16	18.21	17.85
4088.1964	0.24	16.09	1.13	0.15	18.28	17.92
4090.2015	0.25	16.02	1.21	0.23	17.82	17.46
4090.2050	0.26	16.01	1.22	0.24	17.77	17.41
4090.2085	0.27	16.05	1.17	0.19	18.02	17.66
4090.2120	0.27	16.07	1.15	0.17	18.14	17.78
4095.2339	0.25	16.05	1.17	0.19	18.02	17.66
4095.2360	0.28	16.03	1.20	0.22	17.86	17.50
4095.2381	0.26	16.01	1.22	0.24	17.77	17.41
4095.2401	0.24	16.02	1.21	0.23	17.82	17.46
4351.3348	0.28	16.13	1.09	0.11	18.62	18.26
4351.3382	0.29	16.09	1.13	0.15	18.28	17.92
4351.3417	0.24	16.12	1.10	0.12	18.52	18.16
4351.3452	0.28	16.12	1.10	0.12	18.52	18.16
4356.3711	0.26	16.07	1.15	0.17	18.14	17.78
4356.3745	0.28	16.10	1.12	0.14	18.35	17.99
4356.3790	0.31	16.06	1.16	0.18	18.08	17.72
4356.3825	0.26	16.09	1.13	0.15	18.28	17.92
4364.3798	0.25	16.09	1.13	0.15	18.28	17.92
4364.8260	0.26	16.09	1.13	0.15	18.28	17.92
4364.3854	0.30	16.07	1.15	0.17	18.14	17.78
4364.3882	0.23	16.06	1.16	0.18	18.08	17.72
4366.3765	0.25	16.05	1.17	0.19	18.02	17.66
4366.3800	0.28	16.07	1.15	0.17	18.14	17.78
4366.3834	0.29	16.06	1.16	0.18	18.08	17.72
4366.3869	0.26	16.08	1.14	0.16	18.21	17.85
4383.3197	0.28	16.10	1.12	0.14	18.35	17.99
4383.3267	0.28	16.09	1.13	0.15	18.28	17.92
4391.3342	0.31	16.09	1.13	0.15	18.28	17.92
4391.3376	0.26	16.08	1.14	0.16	18.21	17.85

Appendix B1-Continued

1	2	3	4	5	6	7
4391.3411	0.25	16.03	1.20	0.22	17.86	17.50
4391.3446	0.26	16.06	1.16	0.18	18.08	17.72
4420.4628	0.30	16.05	1.17	0.19	18.02	17.66
4420.4663	0.25	16.01	1.22	0.24	17.77	17.41
4420.4698	0.26	16.04	1.19	0.21	17.91	17.55
4420.4633	0.28	16.03	1.20	0.22	17.86	17.50
4431.3777	0.29	16.09	1.13	0.15	18.28	17.92
4431.3812	0.23	16.11	1.11	0.13	18.44	18.08
4431.3847	0.28	16.09	1.13	0.15	18.28	17.92
4431.4782	0.25	16.10	1.12	0.14	18.35	17.99

B2.1 *R* Band Data of 1ES 0323+022

JD-2449000 (1)	<i>C3-B</i> (2)	<i>R</i> (3)	<i>R_d</i> (4)	Error (5)	Observatory (6)
640		16.27	15.97	0.10	Perugia
662		16.54	16.24	0.10	Perugia
669		16.48	16.18	0.10	Perugia
681		16.18	15.88	0.10	Perugia
698		16.16	15.86	0.10	Perugia
705		16.12	15.82	0.10	Perugia
723		16.35	16.05	0.10	Perugia
727		16.16	15.86	0.10	Perugia
1435.3461		16.39	16.09	0.05	Torino
1436.3567		16.46	16.16	0.05	Torino
1462.3221		16.33	16.03	0.05	Torino
1465.3073		16.37	16.07	0.05	Torino
1478.3112		16.23	15.93	0.05	Torino
1481.2783		16.28	15.98	0.05	Torino
1486.2778		16.23	15.93	0.05	Torino
1490.2764		16.31	16.01	0.05	Torino
1497.2699		16.16	15.86	0.05	Torino
1725.5950	1.38	16.34	15.94	0.08	Abastumani
1729.6070	1.34	16.41	16.01	0.08	Abastumani
1824.3358		16.75	16.45	0.05	Torino
1831.3934		16.72	16.42	0.05	Torino
1831.4109		16.70	16.40	0.05	Torino
1834.3483		16.62	16.32	0.05	Torino

Appendix B2.1-Continued

1	2	3	4	5	6
1836.3091	-	16.74	16.44	0.05	Torino
1837.2983	-	16.70	16.40	0.05	Torino
1844.2999	-	16.67	16.37	0.05	Torino
1846.3073	-	16.70	16.40	0.05	Torino
1851.3007	-	16.83	16.53	0.05	Torino
1857.2992	-	16.76	16.46	0.05	Torino
1863.3018	-	16.69	16.39	0.05	Torino
1863.3109	-	16.71	16.41	0.05	Torino
2056.5152	1.36	16.46	16.16	0.08	Abastumani
2056.5238	1.31	16.39	16.09	0.08	Abastumani
2071.4975	1.36	16.25	15.95	0.07	Abastumani
2071.5059	1.39	16.28	15.98	0.07	Abastumani
2075.5077	1.42	16.25	15.95	0.07	Abastumani
2075.5143	1.41	16.28	15.98	0.07	Abastumani
2082.4767	1.38	16.25	15.95	0.07	Abastumani
2082.4852	1.36	16.23	15.93	0.07	Abastumani
2089.4963	1.30	16.20	15.90	0.07	Abastumani
2089.5023	1.31	16.21	15.91	0.07	Abastumani
2101.5047	1.33	16.16	15.86	0.08	Abastumani
2101.5126	1.35	16.14	15.84	0.08	Abastumani
2111.4748	1.37	16.15	15.85	0.07	Abastumani
2111.4826	1.33	16.17	15.87	0.07	Abastumani
2117.3669	1.35	16.21	15.91	0.07	Abastumani
2117.3764	1.33	16.17	15.87	0.07	Abastumani
2130.4432	1.39	16.25	15.95	0.07	Abastumani
2141.3698	1.41	16.16	15.86	0.07	Abastumani
2141.3780	1.35	16.15	15.85	0.07	Abastumani
2187.4229	1.35	16.21	15.91	0.08	Abastumani
2199.3064	1.30	16.61	16.31	0.05	Torino
2202.3271	1.33	16.66	16.36	0.05	Torino
2439.4494	1.38	16.18	15.88	0.07	Abastumani
2439.4543	1.34	16.28	15.98	0.07	Abastumani
2457.4834	1.44	16.31	16.01	0.07	Abastumani
2457.48989	1.38	16.27	15.97	0.07	Abastumani
2461.4201	1.35	16.33	16.03	0.07	Abastumani
2486.4295	1.31	16.30	16.00	0.07	Abastumani
2494.4345	1.28	16.29	15.99	0.07	Abastumani
2521.4356	1.36	16.21	15.91	0.07	Abastumani
2523.4349	1.35	16.17	15.87	0.07	Abastumani
2551.3860	1.37	16.31	16.01	0.07	Abastumani
3172.5534	1.37	16.29	15.99	0.07	Abastumani

Appendix B2.1-Continued

1	2	3	4	5	6
3520.4505	1.31	16.55	16.25	0.08	Abastumani
3531.5183	1.39	16.37	16.07	0.08	Abastumani
3531.5225	1.37	16.36	16.06	0.07	Abastumani
3552.4137	1.32	16.40	16.10	0.07	Abastumani
3552.4207	1.36	16.49	16.19	0.07	Abastumani
3553.4262	1.31	16.51	16.21	0.07	Abastumani
3553.4313	1.37	16.50	16.20	0.07	Abastumani
3558.5670	1.35	16.51	16.21	0.07	Abastumani
3558.5709	1.37	16.45	16.15	0.07	Abastumani
3584.3797	1.38	16.43	16.13	0.07	Abastumani
3587.4929	1.34	16.38	16.08	0.07	Abastumani
3611.4009	1.32	16.50	16.20	0.07	Abastumani
3672.3096	1.39	16.43	16.13	0.07	Abastumani
3672.3143	1.33	16.48	16.18	0.07	Abastumani
3907.5286	1.30	16.46	16.16	0.07	Abastumani
3907.5330	1.35	16.45	16.15	0.07	Abastumani
3968.4464	1.33	16.46	16.16	0.07	Abastumani
3968.4510	1.36	16.42	16.12	0.07	Abastumani
4262.4481	1.37	16.46	16.16	0.07	Abastumani
4262.4545	1.34	16.47	16.17	0.07	Abastumani
4265.4784	1.41	16.44	16.14	0.07	Abastumani
4265.4830	1.36	16.42	16.12	0.07	Abastumani
4268.4442	1.38	16.39	16.09	0.07	Abastumani
4268.4483	1.37	16.42	16.12	0.07	Abastumani
4302.5450	1.38	16.46	16.16	0.07	Abastumani
4302.5494	1.40	16.44	16.14	0.07	Abastumani
4317.4500	1.39	16.41	16.11	0.07	Abastumani
4317.4538	1.34	16.47	16.17	0.07	Abastumani
4329.5460	1.35	16.45	16.15	0.07	Abastumani
4347.3012	1.39	16.44	16.14	0.07	Abastumani
4347.3057	1.33	16.41	16.11	0.07	Abastumani
4380.2377	1.38	16.47	16.17	0.07	Abastumani
4380.2422	1.35	16.42	16.12	0.07	Abastumani
4405.3007	1.36	16.45	16.15	0.07	Abastumani
4405.3052	1.38	16.48	16.18	0.07	Abastumani
4628.5512	1.30	16.27	15.97	0.07	Abastumani
4628.5576	1.36	16.24	15.94	0.07	Abastumani
4649.5100	1.32	16.24	15.94	0.07	Abastumani
4653.5094	1.37	16.28	15.98	0.07	Abastumani
4717.2715	1.35	16.25	15.95	0.07	Abastumani
4717.2756	1.35	16.29	15.99	0.07	Abastumani

Appendix B2.1-Continued

1	2	3	4	5	6
4732.2613	1.37	16.31	16.01	0.07	Abastumani
4732.2656	1.34	16.46	16.16	0.07	Abastumani
4734.2819	1.41	16.43	16.13	0.07	Abastumani
4734.2859	1.39	16.44	16.14	0.07	Abastumani
4734.298	1.33	16.43	16.13	0.07	Abastumani
4734.2937	1.30	16.42	16.12	0.07	Abastumani
5034.2983	1.31	16.20	15.90	0.07	Abastumani
5034.3001	1.35	16.23	15.93	0.07	Abastumani
5034.3033	1.37	16.20	15.90	0.07	Abastumani
5034.3944	1.35	16.23	15.93	0.07	Abastumani
5034.3960	1.40	16.22	15.92	0.07	Abastumani
5034.3985	1.37	16.17	15.87	0.07	Abastumani
5038.4581	1.32	16.21	15.91	0.07	Abastumani
5038.4603	1.36	16.24	15.94	0.07	Abastumani
5038.4620	1.34	16.21	15.91	0.07	Abastumani
5038.4643	1.37	16.22	15.92	0.07	Abastumani
5062.4466	1.38	16.34	16.04	0.07	Abastumani
5062.4487	1.40	16.32	16.02	0.07	Abastumani
5062.4508	1.39	16.36	16.06	0.07	Abastumani
5062.4529	1.34	16.35	16.05	0.07	Abastumani
5062.4553	1.35	16.31	15.90	0.07	Abastumani
5062.4634	1.39	16.38	16.08	0.07	Abastumani
5146.2305	1.36	16.34	16.04	0.07	Abastumani
5146.2340	1.32	16.28	15.98	0.07	Abastumani
5146.2375	1.35	16.28	15.98	0.07	Abastumani
5146.2409	1.37	16.29	15.99	0.07	Abastumani
5352.4391	1.35	16.68	16.38	0.08	Abastumani
5352.4426	1.38	16.66	16.36	0.08	Abastumani
5352.4460	1.37	16.69	16.39	0.08	Abastumani
5352.4495	1.34	16.66	16.36	0.08	Abastumani
5358.3873	1.42	16.66	16.36	0.08	Abastumani
5358.3908	1.39	16.68	16.38	0.08	Abastumani
5358.3943	1.35	16.66	16.36	0.08	Abastumani
5358.3977	1.3	16.68	16.38	0.08	Abastumani
5364.4004	1.36	16.61	16.31	0.08	Abastumani
5364.4039	1.35	16.64	16.34	0.07	Abastumani
5364.4074	1.37	16.62	16.32	0.07	Abastumani
5364.4109	1.35	16.62	16.32	0.07	Abastumani
5391.3522	1.40	16.70	16.40	0.07	Abastumani
5391.3557	1.37	16.67	16.37	0.07	Abastumani

B2.2 Color Indices of 1ES 0323+022 derived from Abastumani and Torino observations

JD-2450000 (1)	<i>V</i> (2)	<i>V-R</i> (3)	<i>ERROR</i> (4)	<i>B-R</i> (Error) (5)	Observatory (6)
462.33	16.82	0.49	0.05	1.03(0.08)	Torino
486.28	16.77	0.54	0.05	0.82(0.08)	Torino
725.60	16.78	0.44	0.10	-	Abastumani
726.61	16.84	0.53	0.10	-	Abastumani
831.40	17.21	0.49	0.05	0.76(0.08)	Torino
834.34	17.17	0.55	0.05	-	Torino
836.31	17.28	0.54	0.05	-	Torino
837.29	17.08	0.38	0.05	-	Torino
844.30	17.20	0.53	0.05	-	Torino
846.31	17.17	0.47	0.05	-	Torino
851.30	17.28	0.45	0.05	-	Torino
857.30	17.19	0.43	0.05	-	Torino
1056.52	16.84	0.53	0.10	-	Abastumani
1071.51	16.80	0.52	0.10	-	Abastumani
1075.52	16.82	0.54	0.10	-	Abastumani
1082.48	16.64	0.41	0.09	-	Abastumani
1101.51	16.62	0.48	0.09	-	Abastumani
1111.48	16.70	0.53	0.09	-	Abastumani
1117.38	16.72	0.55	0.09	-	Abastumani
1129.45	16.74	0.49	0.09	-	Abastumani
1141.38	16.61	0.45	0.09	-	Abastumani
1187.43	16.72	0.51	0.09	-	Abastumani
1439.45	16.65	0.47	0.09	-	Abastumani
1461.42	16.82	0.49	0.10	-	Abastumani
1486.43	16.76	0.46	0.10	-	Abastumani
1494.44	16.77	0.48	0.10	-	Abastumani
1521.44	16.64	0.43	0.10	-	Abastumani
1523.44	16.71	0.54	0.10	-	Abastumani
1551.39	16.75	0.44	0.10	-	Abastumani
2172.56	16.79	0.50	0.10	-	Abastumani
2587.50	16.91	0.53	0.11	-	Abastumani

B2.3 Color Indices of 1ES 0323+022 derived from Jannuzi et al. (1993) observations

JD-2447000 (1)	<i>V</i> (2)	<i>R</i> (3)	<i>V-R</i> (4)	<i>B-R</i> (5)	<i>U-R</i> (6)
54	16.31	15.91	0.40(0.05)	0.99(0.09)	0.63(0.14)
67	16.41	15.93	0.48(0.03)	1.04(0.03)	0.46 (0.06)
67	16.38	15.93	0.45(0.03)	1.02(0.03)	0.49(0.06)
68	16.41	15.93	0.48(0.03)	1.01(0.03)	0.46(0.06)
68	16.40	15.94	0.46(0.03)	0.95(0.03)	0.43(0.06)
111	16.63	16.19	0.42(0.04)	1.15(0.06)	0.58(0.08)
111	16.59	16.16	0.43(0.04)	1.18(0.06)	0.58(0.08)
184	16.66	-	-	-	-
185	16.69		-	-	-
423	16.67	-	-	-	-
436	16.69	-	-	-	-
443	16.75	-	-	-	-
466	16.71	-	-	-	-
470	16.69	-	-	-	-
479	16.67	-		-	-
536	16.73	-	-	-	-
561	17.03		-	-	-
592	16.72	-	-	-	-
594	16.80	-		-	-
596	16.77	-	-	-	-
775	16.47	-	-	-	-
775	16.42		-	-	-
827	16.54	-	-	-	-
827	16.61	-	-	-	-
944	16.13	-	-	-	-

B3.1 *R* Band Data of 1ES 0414+009

JD-2449000 (1)	C2-C1 (2)	<i>R</i> (3)	<i>R_d</i> (4)	Error (5)
408.5177	-	16.40	16.08	0.04
410.4695	-	16.30	15.98	0.04
420.4634	-	16.29	15.97	0.04
435.4032	-	16.29	15.97	0.04
436.3687	-	16.28	15.96	0.04
462.4088	-	16.24	15.92	0.04
465.3400	-	16.25	15.93	0.04
478.3322	-	16.19	15.87	0.04
481.2985	-	16.27	15.95	0.04
485.3102	-	16.24	15.92	0.04
486.3542	-	16.25	15.93	0.04
490.2966	-	16.18	15.86	0.04
725.6069	1.09	16.21	15.89	0.08
762.5522	1.13	16.21	15.89	0.08
778.4456	1.15	16.27	15.95	0.08
1083.4900	1.15	16.77	16.45	0.09
1083.4979	1.14	16.70	16.38	0.08
1086.548	1.11	16.92	16.60	0.08
1086.556	1.12	16.91	16.59	0.08
1111.4880	1.12	16.78	16.46	0.08
1111.4958	1.13	16.72	16.40	0.08
1117.4651	1.09	16.60	16.28	0.08
1117.4728	1.08	16.70	16.38	0.08
1129.4465	1.08	16.68	16.36	0.08
1129.4543	1.13	16.69	16.37	0.08
1141.3850	1.14	16.58	16.26	0.08
1141.3927	1.13	16.66	16.34	0.08
1187.4291	1.15	16.62	16.30	0.08
1191.4103	1.06	16.75	16.43	0.08
1457.5527	1.12	16.66	16.34	0.08
1461.4567	1.20	16.53	16.21	0.07
1486.4632	1.08	16.45	16.13	0.08
1523.4653	1.10	16.50	16.18	0.08
2172.5771	1.18	16.19	15.87	0.07
2553.4444	1.12	16.22	15.9	0.07
2553.4484	1.13	16.28	15.96	0.07
2558.5834	1.13	16.23	15.91	0.07
2558.5892	1.14	16.37	16.05	0.08

Appendix B3.1-Continued

1	2	3	4	5
2582.4900	1.09	16.34	16.02	0.08
2584.3456	1.09	16.32	16.00	0.08
2584.3494	1.14	16.36	16.04	0.08
2588.4283	1.13	16.35	16.03	0.08
2588.4351	1.12	16.33	16.01	0.08
2611.4234	1.12	16.47	16.15	0.08
2611.4281	1.11	16.45	16.13	0.08
2622.4025	1.20	16.53	16.21	0.08
2622.4076	1.14	16.5	16.18	0.08
2677.3269	1.13	16.72	16.40	0.08
2677.3316	1.13	16.71	16.39	0.08
2904.4106	1.13	16.46	16.14	0.07
2904.4152	1.07	16.43	16.11	0.07
2907.5446	1.14	16.46	16.14	0.07
2907.5487	1.13	16.52	16.20	0.07
2908.4769	1.15	16.50	16.18	0.07
2908.4811	1.09	16.50	16.18	0.07
2968.4864	1.20	16.35	16.03	0.07
2968.1910	1.07	16.30	15.98	0.07
2975.4311	1.18	16.35	16.03	0.07
2975.4357	1.16	16.38	16.06	0.07
3262.4985	1.15	16.43	16.11	0.08
3262.5029	1.08	16.49	16.17	0.08
3265.5546	1.18	16.43	16.11	0.08
3265.5730	1.16	16.44	16.12	0.08
3268.5276	1.12	16.47	16.15	0.08
3268.5321	1.14	16.44	16.12	0.08
3302.5674	1.15	16.42	16.10	0.08
3317.4922	1.12	16.31	15.99	0.07
3317.4963	1.17	16.23	15.91	0.07
3322.3403	1.14	16.32	16.00	0.07
3322.3454	1.17	16.33	16.01	0.07
3346.5455	1.18	16.33	16.01	0.07
3346.5590	1.13	16.32	16.00	0.07
3380.2566	1.13	16.34	16.02	0.07
3380.2609	1.12	16.45	16.13	0.07
3405.2765	1.10	16.43	16.11	0.07
3405.2810	1.11	15.94	15.62	0.06
3648.3111	1.09	15.93	15.61	0.06
3648.3143	1.12	15.95	15.63	0.06

Appendix B3.1-Continued

1	2	3	4	5
3653.5226	1.13	16.14	15.82	0.07
3653.5268	1.14	16.18	15.86	0.07
3668.4413	1.10	16.06	15.74	0.07
3668.4481	1.10	16.09	15.77	0.07
3668.4528	1.13	16.09	15.77	0.07
3698.3877	1.14	15.98	15.66	0.07
3698.3913	1.15	16.02	15.7	0.07
3698.3956	1.06	15.99	15.67	0.07
3698.3995	1.12	16.01	15.69	0.07
3709.3111	1.21	15.9	15.58	0.06
3709.3143	1.08	15.86	15.54	0.06
3709.3175	1.13	15.95	15.63	0.06
3709.3207	1.17	15.86	15.54	0.06
3732.2730	1.12	15.96	15.64	0.07
3732.2771	1.12	16.04	15.72	0.07
3734.3098	1.13	16.02	15.7	0.07
3734.3200	1.13	16.03	15.71	0.07
3734.3176	1.14	15.98	15.66	0.07
3734.3215	1.12	15.97	15.65	0.07
3787.2332	1.09	16.02	15.7	0.07
3787.2371	1.14	15.98	15.66	0.07
3787.2410	1.13	15.98	15.66	0.07
3787.1439	1.12	16.00	15.68	0.07
3816.2159	1.13	15.92	15.6	0.07
3816.2198	1.11	15.96	15.64	0.07
3819.2380	1.19	15.94	15.62	0.07
3819.2414	1.14	15.92	15.6	0.07
3819.2458	1.13	15.95	15.63	0.07
4062.4634	1.13	16.03	15.71	0.07
4062.4655	1.13	16.06	15.74	0.07
4062.4676	1.07	16.06	15.74	0.07
4062.4013	1.14	16.04	15.72	0.07
4146.2503	1.08	16.21	15.89	0.07
4146.2537	1.18	16.18	15.86	0.07
4146.2572	1.12	16.18	15.86	0.07
4352.4813	1.13	16.39	16.07	0.07
4352.4847	1.09	16.37	16.05	0.07
4352.4882	1.13	16.39	16.07	0.07
4352.4917	1.12	16.41	16.09	0.07
4352.4952	1.10	16.4	16.08	0.07
4364.4180	1.11	16.46	16.14	0.07

Appendix B3.1-Continued

1	2	3	4	5
4364.4241	1.11	16.43	16.11	0.07
4364.4275	1.09	16.44	16.12	0.07
4364.4300	1.12	16.45	16.13	0.07
4364.4343	1.13	16.42	16.1	0.07
4381.3965	1.14	16.39	16.07	0.07
4381.4001	1.10	16.41	16.09	0.07
4381.4034	1.10	16.43	16.11	0.07
4381.4068	1.13	16.4	16.08	0.07
4381.4100	1.16	16.38	16.06	0.07
4395.5001	1.13	16.46	16.14	0.07
4395.5034	1.06	16.44	16.12	0.07
4395.5071	1.12	16.43	16.11	0.07
4395.4499	1.20	16.45	16.13	0.07
4395.5140	1.08	16.41	16.09	0.07
4415.4862	1.13	16.49	16.17	0.07
4415.4893	1.16	16.47	16.15	0.07

B3.2 Color Indices of 1ES 0414+009

JD-2450000 (1)	<i>V</i> (2)	<i>V-R</i> (3)	Error (4)	Observatory (5)
462.41	16.69	0.45	0.04	Torino
486.36	16.65	0.4	0.04	Torino
725.61	16.67	0.46	0.09	Abastumani
762.55	16.63	0.42	0.09	Abastumani
778.45	16.69	0.42	0.09	Abastumani
1083.55	17.11	0.41	0.11	Abastumani
1086.56	17.28	0.37	0.12	Abastumani
1111.50	16.97	0.35	0.10	Abastumani
1117.47	17.04	0.39	0.11	Abastumani
1129.45	17.06	0.37	0.11	Abastumani
1141.39	17.07	0.41	0.11	Abastumani
1187.43	17.08	0.46	0.11	Abastumani
1191.41	17.12	0.37	0.11	Abastumani
1457.56	17.07	0.41	0.11	Abastumani
1461.46	16.93	0.4	0.10	Abastumani

B4.1 *R* Band Data of 1ES 0502+675

JD-2450000 (1)	Ref 6 -Ref 5 (2)	<i>R</i> (3)	<i>R_d</i> (4)	Error (5)
387.5853	-	16.78	16.37	0.04
389.5394	-	16.81	16.40	0.04
391.6188	-	16.63	16.22	0.04
396.5763	-	16.76	16.35	0.04
410.5154	-	16.68	16.27	0.04
420.5123	-	16.65	16.24	0.04
435.4473	-	16.71	16.3	0.04
436.4143	-	16.80	16.39	0.04
459.4171	-	16.64	16.23	0.04
462.4799	-	16.52	16.11	0.04
465.4248	-	16.43	16.02	0.04
485.3745	-	16.45	16.04	0.04
486.3817	-	16.46	16.05	0.04
489.3146	-	16.42	16.01	0.04
490.3372	-	16.53	16.12	0.04
494.2837	-	16.23	15.82	0.04
502.3079	-	16.35	15.94	0.04
762.3787	0.17	15.69	15.28	0.05
778.4728	0.22	15.73	15.32	0.05
810.5319	0.15	15.86	15.45	0.05
833.2872	0.18	15.99	15.58	0.06
834.3654	0.22	15.90	15.49	0.06
835.2827	0.18	15.97	15.56	0.06
841.3801	0.21	16.02	15.61	0.06
875.2312	0.20	16.43	16.02	0.07
1076.4632	0.15	16.74	16.33	0.08
1076.4715	0.20	16.71	16.30	0.08
1101.5820	0.19	16.54	16.13	0.08
1107.5683	0.18	16.72	16.31	0.08
1107.5760	0.19	16.79	16.38	0.08
1117.5400	0.17	16.6	16.19	0.08
1129.5067	0.22	16.75	16.34	0.08
1129.5144	0.22	16.77	16.36	0.08
1141.4555	0.18	16.77	16.36	0.08
1141.4633	0.15	16.75	16.34	0.08
1160.3486	0.22	16.28	15.87	0.07
1160.3575	0.22	16.35	15.94	0.07
1169.2741	0.18	16.45	16.04	0.07
1169.2866	0.15	16.48	16.07	0.07

Appendix B4.1-Continued

1	2	3	4	5
1187.4416	0.15	16.56	16.15	0.07
1191.4313	0.15	16.48	16.07	0.07
1276.2209	0.15	16.60	16.19	0.07
1434.4691	0.15	16.47	16.06	0.07
1455.5693	0.15	16.54	16.13	0.07
1457.5174	0.15	16.46	16.05	0.07
1457.5206	0.15	16.51	16.10	0.07
1461.3930	0.15	16.51	16.10	0.07
1465.4630	0.22	16.42	16.01	0.07
1486.4781	0.21	16.35	15.94	0.07
1493.5527	0.19	16.49	16.08	0.07
1517.4838	0.13	16.65	16.24	0.08
1521.4868	0.22	16.65	16.24	0.08
1523.4819	0.15	16.66	16.25	0.08
1526.4026	0.17	16.55	16.14	0.07
1551.4250	0.15	16.65	16.24	0.07
1584.3896	0.15	16.40	15.99	0.07
1587.4261	0.16	16.25	15.84	0.07
2051.1410	0.15	16.74	16.33	0.07
2051.1435	0.15	16.80	16.39	0.07
2358.2817	0.16	16.56	16.15	0.08
2358.2908	0.15	16.67	16.26	0.08
2376.2438	0.20	16.44	16.03	0.07
2376.2501	0.16	16.52	16.11	0.07
2376.2555	0.15	16.48	16.07	0.07
2553.4652	0.15	16.10	15.69	0.07
2553.4691	0.17	16.12	15.71	0.07
2554.5434	0.16	16.09	15.68	0.07
2554.5475	0.17	16.11	15.70	0.07
2559.4567	0.16	16.00	15.59	0.07
2559.4606	0.21	16.06	15.65	0.07
2566.5631	0.21	16.08	15.67	0.07
2566.5682	0.16	16.11	15.70	0.07
2607.6328	0.16	16.20	15.79	0.07
2610.4864	0.16	16.16	15.75	0.07
2610.4913	0.21	16.22	15.81	0.07
2612.5367	0.23	16.17	15.76	0.07
2622.4694	0.19	16.07	15.66	0.06
2648.3848	0.20	16.05	15.64	0.06
2650.4180	0.21	16.08	15.67	0.06
2650.4226	0.15	16.07	15.66	0.06

Appendix B4.1-Continued

1	2	3	4	5
2661.4577	0.15	16.11	15.70	0.06
2672.3740	0.22	16.06	15.65	0.06
2672.3779	0.21	16.02	15.61	0.06
2678.3889	0.18	15.97	15.56	0.06
2678.3931	0.17	15.99	15.58	0.06
2699.3843	0.22	16.10	15.69	0.07
2699.3888	0.24	16.07	15.66	0.07
2700.3517	0.20	16.11	15.70	0.07
2728.4190	0.17	16.25	15.84	0.07
2728.4236	0.18	16.25	15.84	0.07
2737.4549	0.18	16.21	15.80	0.07
2737.4595	0.16	16.24	15.83	0.07
2751.2848	0.20	16.12	15.71	0.07
2751.2899	0.19	16.07	15.66	0.07
2758.3339	0.22	16.21	15.80	0.07
2758.3381	0.19	16.19	15.78	0.07
2788.2665	0.21	16.25	15.84	0.07
2788.2723	0.22	16.18	15.77	0.07
2817.4904	0.18	16.08	15.67	0.07
2817.4942	0.18	16.07	15.66	0.07
2854.5142	0.19	16.08	15.67	0.07
2854.5186	0.18	16.11	15.70	0.07
2904.3907	0.18	16.38	15.97	0.07
2904.3954	0.19	16.39	15.98	0.07
2918.5592	0.22	16.29	15.88	0.07
2918.5632	0.19	16.21	15.80	0.07
2946.5840	0.18	16.30	15.89	0.07
2946.5880	0.20	16.32	15.91	0.07
2946.5919	0.17	16.27	15.86	0.07
2968.5214	0.17	16.12	15.71	0.07
2968.5258	0.16	16.13	15.72	0.07
2975.4664	0.17	16.15	15.74	0.07
2975.4709	0.22	16.21	15.80	0.07
2998.4760	0.19	16.22	15.81	0.07
3003.4747	0.20	16.33	15.92	0.07
3026.4554	0.19	16.25	15.84	0.07
3026.4599	0.16	16.27	15.86	0.07
3034.3887	0.17	16.28	15.87	0.07
3034.3930	0.22	16.27	15.86	0.07
3059.4132	0.18	16.11	15.70	0.07

Appendix B4.1-Continued

1	2	3	4	5
3059.4169	0.17	16.11	15.70	0.07
3171.4945	0.18	15.92	15.51	0.07
3171.4980	0.19	15.94	15.53	0.07
3214.4755	0.22	16.03	15.62	0.07
3214.4822	0.19	16.08	15.67	0.07
3259.4702	0.20	15.97	15.56	0.06
3259.4747	0.20	15.95	15.54	0.06
3264.5740	0.21	16.10	15.69	0.07
3264.5782	0.17	16.09	15.68	0.07
3267.5473	0.21	16.12	15.71	0.07
3267.5515	0.22	16.18	15.77	0.07
3290.5209	0.22	16.01	15.60	0.07
3290.5249	0.20	16.00	15.59	0.07
3303.5147	0.22	16.17	15.76	0.07
3303.5200	0.20	16.15	15.74	0.07
3317.5891	0.19	16.11	15.70	0.07
3321.6143	0.18	16.14	15.73	0.07
3329.5778	0.18	16.17	15.76	0.07
3329.5822	0.21	16.14	15.73	0.07
3342.3751	0.19	16.27	15.86	0.07
3342.3795	0.18	16.34	15.93	0.07
3357.3588	0.20	16.4	15.99	0.07
3357.3629	0.22	16.35	15.94	0.07
3380.3179	0.20	16.46	16.05	0.07
3380.3232	0.16	16.45	16.04	0.07
3387.4503	0.17	16.41	16.00	0.07
3387.4543	0.22	16.43	16.02	0.07
3405.3105	0.20	16.24	15.83	0.07
3405.3150	0.20	16.29	15.88	0.07
3415.3464	0.22	16.28	15.87	0.07
3415.3507	0.17	16.26	15.85	0.07
3443.2210	0.17	16.46	16.05	0.07
3443.2250	0.22	16.42	16.01	0.07
3641.4153	0.16	16.47	16.06	0.07
3641.4231	0.22	16.47	16.06	0.07
3641.4271	0.19	16.58	16.17	0.07
3654.5232	0.17	16.49	16.08	0.07
3654.5272	0.15	16.58	16.17	0.07
3656.5306	0.22	16.49	16.08	0.07
3656.53506	0.19	16.52	16.11	0.07
3698.4285	0.17	16.69	16.28	0.07

Appendix B4.1-Continued

1	2	3	4	5
3698.4363	0.22	16.72	16.31	0.07
3698.4403	0.15	16.66	16.25	0.07
3710.3395	0.18	16.47	16.06	0.07
3710.3435	0.22	16.49	16.08	0.07
3734.4088	0.18	16.50	16.09	0.07
3734.4127	0.21	16.51	16.10	0.07
3734.4166	0.20	16.48	16.07	0.07
3734.4205	0.15	16.49	16.08	0.07
3784.2460	0.20	16.52	16.11	0.07
3784.24990	0.19	16.48	16.07	0.07
3784.2538	0.18	16.54	16.13	0.07
3784.2577	0.19	16.44	16.03	0.07
3786.2972	0.17	16.54	16.13	0.07
3786.3013	0.22	16.49	16.08	0.07
3823.2489	0.22	16.30	15.89	0.07
3823.2528	0.18	16.26	15.85	0.07
3823.2567	0.15	16.31	15.90	0.07
4083.3788	0.22	16.40	15.99	0.07
4083.3808	0.22	16.39	15.98	0.07
4083.3830	0.18	16.35	15.94	0.07
4083.3851	0.15	16.34	15.93	0.07
4087.45134	0.15	16.18	15.77	0.07
4087.4530	0.15	16.16	15.75	0.07
4087.4550	0.15	16.17	15.76	0.07
4087.4576	0.15	16.17	15.76	0.07
4087.4600	0.15	16.15	15.74	0.07
4087.4618	0.15	16.18	15.77	0.07
4093.3923	0.15	16.08	15.67	0.07
4093.3957	0.15	16.12	15.71	0.07
4093.4026	0.21	16.07	15.66	0.07
4093.4061	0.19	16.13	15.72	0.07
4093.4096	0.15	16.07	15.66	0.07
4146.4145	0.16	15.95	15.54	0.07
4146.4179	0.15	15.97	15.56	0.07
4146.4215	0.15	15.99	15.58	0.07
4146.4250	0.16	16.00	15.59	0.07
4170.3501	0.15	16.13	15.72	0.07
4170.3522	0.21	16.10	15.69	0.07
4170.3544	0.16	16.10	15.69	0.07
4170.3565	0.15	16.09	15.68	0.07
4352.4609	0.15	16.34	15.93	0.07

Appendix B4.1-Continued

1	2	3	4	5
4352.4643	0.17	16.37	15.96	0.07
4352.4676	0.16	16.36	15.95	0.07
4352.4710	0.17	16.39	15.98	0.07
4383.3803	0.16	16.19	15.78	0.07
4383.3843	0.21	16.20	15.79	0.07
4383.3871	0.21	16.20	15.79	0.07
4383.3808	0.16	16.23	15.82	0.07
4391.3722	0.16	16.30	15.89	0.07
4391.3761	0.16	16.28	15.87	0.07
4391.3788	0.21	16.24	15.83	0.07
4391.3834	0.23	16.27	15.86	0.07
4391.3861	0.20	16.26	15.85	0.07
4391.3899	0.19	16.29	15.88	0.07
4391.3940	0.22	16.27	15.86	0.07
4391.3973	0.21	16.24	15.83	0.07
4395.5257	0.21	16.23	15.82	0.07
4395.5290	0.18	16.25	15.84	0.07
4395.5332	0.17	16.29	15.88	0.07
4395.5361	0.22	16.27	15.86	0.07
4416.5044	0.24	16.35	15.94	0.07
4416.5068	0.20	16.39	15.98	0.07
4423.4835	0.17	16.40	15.99	0.07
4423.4871	0.18	16.37	15.96	0.07
4423.4902	0.18	16.41	16.00	0.07
4423.4943	0.16	16.35	15.94	0.07

B4.2 Color Indices of 1ES 0502+675

JD-2450000 (1)	<i>V</i> (2)	<i>V-R</i> (3)	Error (4)	Comment (5)
462.48	16.95	0.43	0.04	Torino
486.38	16.82	0.36	0.04	Torino
762.38	16.00	0.31	0.07	Abastumani
778.47	16.11	0.38	0.08	Abastumani
810.53	16.18	0.32	0.08	Abastumani
833.29	16.34	0.35	0.08	Abastumani
834.37	16.31	0.41	0.08	Abastumani
835.28	16.31	0.34	0.08	Abastumani
841.38	16.37	0.35	0.08	Abastumani
875.23	16.76	0.31	0.10	Abastumani
1076.46	17.06	0.35	0.11	Abastumani
1101.58	16.94	0.40	0.10	Abastumani
1107.58	17.12	0.33	0.12	Abastumani
1117.54	17.02	0.42	0.11	Abastumani
1129.51	16.99	0.32	0.11	Abastumani
1141.46	17.03	0.38	0.11	Abastumani
1160.35	16.69	0.34	0.09	Abastumani
1169.27	16.80	0.32	0.10	Abastumani
1191.43	16.80	0.32	0.10	Abastumani
1276.22	16.93	0.33	0.10	Abastumani
1434.47	16.78	0.31	0.10	Abastumani
1455.57	16.96	0.42	0.10	Abastumani
1457.52	16.90	0.44	0.10	Abastumani
1461.40	16.83	0.32	0.10	Abastumani
1465.46	16.81	0.39	0.10	Abastumani
1521.49	16.96	0.31	0.10	Abastumani
1523.48	16.97	0.31	0.10	Abastumani
1526.41	16.89	0.34	0.10	Abastumani
1551.43	17.01	0.36	0.10	Abastumani
1584.39	16.82	0.42	0.10	Abastumani
1587.426	16.57	0.32	0.09	Abastumani

B5.1 *R* Band Data of 1ES 0647+250

JD-250000 (1)	Ref6-Ref7 (2)	<i>R</i> (3)	<i>R_d</i> (4)	Error (5)
778.4902	0.38	15.03	14.77	0.04
810.4531	0.32	14.88	14.62	0.03
817.4503	0.30	14.88	14.62	0.03
817.4556	0.33	14.91	14.65	0.03
818.4149	0.35	14.89	14.63	0.03
841.3603	0.33	14.86	14.60	0.03
1076.4873	0.31	15.03	14.77	0.04
1106.5461	0.30	15.10	14.84	0.04
1106.5541	0.30	15.16	14.90	0.04
1129.4744	0.26	15.16	14.90	0.04
1129.4823	0.23	15.15	14.89	0.04
1160.5119	0.34	15.28	15.02	0.04
1160.5201	0.27	15.29	15.03	0.04
2354.1963	0.33	15.96	15.70	0.06
2354.1927	0.35	15.97	15.71	0.06
2354.1998	0.39	15.95	15.69	0.06
2354.2023	0.30	15.94	15.68	0.06
2355.2588	0.30	15.91	15.65	0.06
2358.2635	0.33	15.86	15.60	0.06
2358.2684	0.31	15.85	15.59	0.06
2358.2719	0.30	15.91	15.65	0.06
2358.2754	0.30	15.89	15.63	0.06
2358.2783	0.26	15.92	15.66	0.06
2358.2818	0.27	15.90	15.64	0.06
2358.2855	0.34	15.93	15.67	0.06
2553.4844	0.27	15.93	15.67	0.06
2555.4883	0.26	15.94	15.68	0.06
2592.5708	0.27	15.94	15.68	0.06
2592.5749	0.28	15.94	15.68	0.06
2610.5404	0.30	15.94	15.68	0.06
2610.5453	0.32	15.92	15.66	0.06
2622.5071	0.34	15.96	15.70	0.06
2622.5145	0.29	15.98	15.72	0.06
2650.4755	0.28	15.96	15.70	0.06
2650.4808	0.30	16.05	15.79	0.06
2661.4712	0.28	16.03	15.77	0.06
2661.4741	0.31	16.05	15.79	0.06
2669.4733	0.31	15.99	15.73	0.06
2669.4772	0.36	16.04	15.78	0.06

Appendix B5.1-Continued

1	2	3	4	5
2669.4812	0.28	16.05	15.79	0.06
2700.4022	0.27	15.95	15.69	0.06
2700.4061	0.28	15.98	15.72	0.06
2706.4061	0.27	15.95	15.69	0.06
2706.4103	0.31	15.97	15.71	0.06
2727.3708	0.28	16.00	15.74	0.06
2727.3755	0.29	15.96	15.70	0.06
2751.2674	0.28	15.99	15.73	0.06
2751.2720	0.23	16.00	15.74	0.06
2758.2668	0.27	15.96	15.70	0.06
2758.2708	0.29	16.02	15.76	0.06
2907.5589	0.34	16.09	15.83	0.07
2907.5630	0.23	16.16	15.90	0.07
2918.5299	0.22	16.12	15.86	0.06
2918.5346	0.29	16.04	15.78	0.06
2946.5628	0.29	16.07	15.81	0.06
2946.5670	0.39	16.04	15.78	0.06
2968.5440	0.35	15.92	15.66	0.06
2968.5483	0.34	15.93	15.67	0.06
2995.4593	0.36	15.94	15.68	0.06
2995.4637	0.40	15.98	15.72	0.06
2997.4353	0.36	15.96	15.70	0.06
2997.4399	0.38	15.97	15.71	0.06
3003.4558	0.37	15.92	15.66	0.06
3003.4603	0.27	15.93	15.67	0.06
3026.4387	0.29	15.87	15.61	0.06
3026.4434	0.30	15.87	15.61	0.06
3034.4063	0.29	15.83	15.57	0.05
3034.4108	0.29	15.80	15.54	0.05
3059.3985	0.29	15.82	15.56	0.05
3059.4033	0.29	15.80	15.54	0.05
3234.0000	0.33	15.62	15.36	0.05
3268.5694	0.28	15.69	15.43	0.05
3268.5733	0.33	15.71	15.45	0.05
3303.5288	0.30	15.82	15.56	0.05
3303.5332	0.33	15.80	15.54	0.05
3318.4532	0.34	15.83	15.57	0.05
3318.4571	0.31	15.79	15.53	0.05
3321.5815	0.34	15.71	15.45	0.05
3321.5856	0.27	15.70	15.44	0.05
3357.3727	0.34	15.74	15.48	0.05

Appendix B5.1-Continued

1	2	3	4	5
3380.3339	0.28	15.71	15.45	0.05
3380.3380	0.36	15.78	15.52	0.05
3387.4728	0.40	15.77	15.51	0.05
3387.4768	0.40	15.75	15.49	0.05
3405.3240	0.31	15.69	15.43	0.05
3405.3287	0.30	15.74	15.48	0.05
3415.3771	0.33	15.74	15.48	0.05
3415.3814	0.29	15.70	15.44	0.05
3443.2761	0.34	15.67	15.41	0.05
3443.2802	0.31	15.71	15.45	0.05
3656.5566	0.33	15.48	15.22	0.05
3656.5611	0.29	15.45	15.19	0.05
3688.5839	0.28	15.41	15.15	0.05
3688.5878	0.31	15.48	15.22	0.05
3698.5279	0.28	15.38	15.12	0.05
3698.5318	0.32	15.38	15.12	0.05
3698.5357	0.34	15.36	15.10	0.05
3698.5396	0.30	15.41	15.15	0.05
3709.3627	0.38	15.39	15.13	0.05
3709.3654	0.33	15.38	15.12	0.05
3709.3691	0.31	15.32	15.06	0.05
3733.3785	0.28	15.52	15.26	0.05
3733.3824	0.36	15.58	15.32	0.05
3733.3863	0.38	15.55	15.29	0.05
3733.3902	0.38	15.55	15.29	0.05
3733.4612	0.35	15.53	15.27	0.05
3733.4651	0.33	15.52	15.26	0.05
3733.4690	0.31	15.51	15.25	0.05
3733.4729	0.35	15.54	15.28	0.05
3787.3334	0.31	15.93	15.67	0.05
3787.3373	0.30	15.99	15.73	0.05
3823.2241	0.33	15.77	15.51	0.05
3823.2280	0.29	15.77	15.51	0.05
3823.2319	0.33	15.69	15.43	0.05
3823.2358	0.31	15.73	15.47	0.05

B5.2 Color Indices of 1ES 0647+250

JD-2450000 (1)	<i>V</i> (2)	<i>V-R</i> (3)	Error (4)
778.4902	15.42	0.39	0.05
810.4531	15.23	0.35	0.05
817.4503	15.29	0.41	0.05
818.4149	15.27	0.38	0.05
841.3603	15.21	0.35	0.05
1076.4873	15.41	0.38	0.05
1106.5461	15.48	0.38	0.05
1129.4744	15.56	0.40	0.06

B6.1 *R* Band Data of 1ES 0806+524

JD-2450000 (1)	Ref 5-Ref 2 (2)	<i>R</i> (3)	Error (4)	<i>F</i> (mJy) (5)	<i>F</i> _{corr} (6)	<i>R</i> _{hs} (7)	<i>R</i> _{hsd} (8)
810.5082	1.08	14.78	0.03	3.78	3.08	15.00	14.88
834.4140	1.11	15.02	0.03	3.02	2.32	15.31	15.19
841.4318	1.13	15.05	0.03	2.93	2.23	15.35	15.23
845.5055	1.09	15.20	0.03	2.57	1.87	15.54	15.42
876.4644	1.09	15.31	0.04	2.33	1.63	15.69	15.57
895.3949	1.10	15.31	0.04	2.33	1.63	15.69	15.57
1141.4873	1.08	15.33	0.04	2.28	1.58	15.72	15.61
1141.4988	1.11	15.30	0.04	2.34	1.64	15.68	15.56
1160.5642	1.09	15.52	0.05	1.91	1.21	16.01	15.90
1160.5721	1.10	15.51	0.05	1.94	1.24	15.99	15.87
1170.4212	1.14	15.45	0.05	2.04	1.34	15.90	15.78
1170.4292	1.11	15.47	0.05	2.00	1.30	15.94	15.82
1187.4902	1.13	15.51	0.05	1.94	1.24	15.99	15.87
1191.4906	1.10	15.55	0.05	1.85	1.15	16.07	15.95
1194.3918	1.12	15.53	0.05	1.90	1.20	16.02	15.90
1201.5404	1.12	15.54	0.05	1.88	1.18	16.04	15.92
1205.5882	1.11	15.50	0.05	1.95	1.25	15.98	15.86
1221.4477	1.10	15.60	0.05	1.78	1.08	16.14	16.02
1276.2663	1.13	15.62	0.05	1.75	1.05	16.17	16.05
1283.3362	1.09	15.57	0.05	1.82	1.12	16.10	15.98
1286.3678	1.13	15.62	0.05	1.75	1.05	16.17	16.05
1310.3054	1.11	15.54	0.05	1.88	1.18	16.04	15.92
1457.5383	1.12	15.44	0.05	2.05	1.35	15.89	15.78
1465.5134	1.12	15.34	0.05	2.26	1.56	15.74	15.62
1486.4994	1.09	15.42	0.05	2.08	1.38	15.87	15.75
1493.5730	1.12	15.36	0.05	2.22	1.52	15.77	15.65
1517.5061	1.11	15.32	0.05	2.30	1.6	15.71	15.59
1521.5034	1.08	15.37	0.05	2.19	1.49	15.79	15.67
1523.5395	1.09	15.28	0.05	2.38	1.68	15.66	15.54
1526.4218	1.12	15.47	0.05	2.00	1.3	15.94	15.82
1551.4333	1.07	15.20	0.05	2.57	1.87	15.54	15.42
1559.5117	1.12	15.31	0.05	2.33	1.63	15.69	15.57
1584.4237	1.09	15.39	0.05	2.15	1.45	15.82	15.70
1587.4695	1.05	15.31	0.05	2.33	1.63	15.69	15.57
1702.2607	1.07	15.25	0.05	2.45	1.75	15.61	15.49
2358.3051	1.09	14.89	0.03	3.42	2.72	15.13	15.02
2358.3097	1.12	14.92	0.03	3.33	2.63	15.17	15.05
2358.3144	1.11	14.95	0.03	3.24	2.54	15.21	15.09

Appendix B6.1-Continued

1	2	3	4	5	6	7	8
2364.2943	1.08	14.94	0.03	3.27	2.57	15.20	15.08
2364.2968	1.10	14.96	0.03	3.21	2.51	15.22	15.10
2364.2993	1.08	14.97	0.03	3.18	2.48	15.23	15.12
2375.2157	1.13	14.91	0.03	3.36	2.66	15.16	15.04
2553.5440	1.08	14.88	0.03	3.45	2.75	15.12	15.00
2553.5479	1.07	14.85	0.03	3.58	2.88	15.07	14.95
2554.5642	1.12	14.91	0.03	3.36	2.66	15.16	15.04
2554.5669	1.10	14.89	0.03	3.42	2.72	15.13	15.02
2565.5642	1.07	14.89	0.03	3.42	2.72	15.13	15.02
2581.5771	1.06	15.05	0.03	2.93	2.23	15.35	15.23
2581.5624	1.08	15.09	0.03	2.85	2.15	15.39	15.27
2581.5669	1.07	15.07	0.03	2.89	2.19	15.37	15.25
2594.5209	1.10	15.09	0.03	2.85	2.15	15.39	15.27
2594.5248	1.12	15.09	0.03	2.85	2.15	15.39	15.27
2594.5287	1.11	15.09	0.03	2.85	2.15	15.39	15.27
2594.5326	1.11	15.08	0.03	2.87	2.17	15.38	15.26
2601.6788	1.09	15.05	0.03	2.93	2.23	15.35	15.23
2601.6814	1.13	15.07	0.03	2.89	2.19	15.37	15.25
2601.6839	1.11	15.06	0.03	2.91	2.21	15.36	15.24
2601.6864	1.10	15.10	0.03	2.82	2.12	15.40	15.29
2601.6890	1.11	15.05	0.03	2.93	2.23	15.35	15.23
2601.6915	1.08	15.05	0.03	2.93	2.23	15.35	15.23
2601.6940	1.09	15.07	0.03	2.89	2.19	15.37	15.25
2601.6966	1.07	15.04	0.03	2.98	2.28	15.33	15.21
2610.5931	1.14	15.10	0.03	2.82	2.12	15.40	15.29
2610.5994	1.07	15.16	0.03	2.67	1.97	15.48	15.37
2610.5532	1.10	15.05	0.03	2.93	2.23	15.35	15.23
2610.5578	1.09	15.08	0.03	2.87	2.17	15.38	15.26
2622.5532	1.13	15.03	0.03	3.00	2.30	15.32	15.20
2622.5578	1.10	15.03	0.03	3.00	2.30	15.32	15.20
2650.4949	1.12	14.95	0.03	3.24	2.54	15.21	15.09
2650.4997	1.11	14.93	0.03	3.30	2.60	15.18	15.06
2660.4224	1.13	14.94	0.03	3.27	2.57	15.20	15.08
2660.4287	1.10	14.93	0.03	3.30	2.60	15.18	15.06
2660.4312	1.16	14.97	0.03	3.18	2.48	15.23	15.12
2660.4338	1.09	14.94	0.03	3.27	2.57	15.20	15.08
2660.4363	1.15	14.91	0.03	3.36	2.66	15.16	15.04
2660.4412	1.13	15.00	0.03	3.09	2.39	15.27	15.16
2660.4437	1.10	14.93	0.03	3.30	2.60	15.18	15.06
2660.4463	1.15	14.98	0.03	3.15	2.45	15.25	15.13
2660.4486	1.14	14.99	0.03	3.12	2.42	15.26	15.14

Appendix B6.1-Continued

1	2	3	4	5	6	7	8
2660.5519	1.08	14.99	0.03	3.12	2.42	15.26	15.14
2660.5545	1.12	14.93	0.03	3.30	2.60	15.18	15.06
2660.5570	1.10	14.97	0.03	3.18	2.48	15.23	15.12
2660.5619	1.09	14.95	0.03	3.24	2.54	15.21	15.09
2660.5644	1.11	14.98	0.03	3.15	2.45	15.25	15.13
2660.5670	1.15	14.91	0.03	3.36	2.66	15.16	15.04
2660.5695	1.11	14.92	0.03	3.33	2.63	15.17	15.05
2672.4324	1.13	15.05	0.03	2.93	2.23	15.35	15.23
2672.4370	1.11	15.03	0.03	3.00	2.30	15.32	15.20
2678.4444	1.12	14.98	0.03	3.15	2.45	15.25	15.13
2678.4483	1.09	14.97	0.03	3.18	2.48	15.23	15.12
2682.5331	1.10	14.88	0.03	3.45	2.75	15.12	15.00
2682.5377	1.10	14.90	0.03	3.39	2.69	15.15	15.03
2688.5011	1.09	14.91	0.03	3.36	2.66	15.16	15.04
2688.5039	1.08	14.92	0.03	3.33	2.63	15.17	15.05
2688.5065	1.11	14.90	0.03	3.39	2.69	15.15	15.03
2688.5091	1.10	14.87	0.03	3.48	2.78	15.11	14.99
2727.3275	1.12	14.92	0.03	3.33	2.63	15.17	15.05
2727.3300	1.13	14.93	0.03	3.30	2.60	15.18	15.06
2727.3326	1.09	14.92	0.03	3.33	2.63	15.17	15.05
2727.3351	1.07	14.91	0.03	3.36	2.66	15.16	15.04
2704.4444	1.08	14.90	0.03	3.39	2.69	15.15	15.03
2704.4494	1.10	14.86	0.03	3.51	2.81	15.10	14.98
2728.4325	1.07	14.94	0.03	3.27	2.57	15.20	15.08
2728.4398	1.11	14.94	0.03	3.27	2.57	15.20	15.08
2730.3788	1.12	14.91	0.03	3.36	2.66	15.16	15.04
2730.3843	1.10	14.96	0.03	3.21	2.51	15.22	15.10
2734.4141	1.10	14.91	0.03	3.36	2.66	15.16	15.04
2734.4201	1.12	14.95	0.03	3.24	2.54	15.21	15.09
2751.3015	1.09	14.97	0.03	3.18	2.48	15.23	15.12
2751.3061	1.07	14.93	0.03	3.30	2.60	15.18	15.06
2758.3525	1.08	15.02	0.03	3.02	2.32	15.31	15.19
2758.3602	1.10	15.02	0.03	3.02	2.32	15.31	15.19
2780.2796	1.07	15.13	0.03	2.74	2.04	15.45	15.33
2780.2832	1.09	15.13	0.03	2.74	2.04	15.45	15.33
2783.3089	1.12	15.09	0.03	2.85	2.15	15.39	15.27
2783.3134	1.08	15.11	0.03	2.78	2.08	15.42	15.31
2788.2894	1.08	15.04	0.03	2.98	2.28	15.33	15.21
2788.2936	1.11	15.04	0.03	2.98	2.28	15.33	15.21
2918.5465	1.05	15.06	0.03	2.91	2.21	15.36	15.24
2946.6070	1.05	15.09	0.03	2.85	2.15	15.39	15.27

Appendix B6.1-Continued

1	2	3	4	5	6	7	8
2946.6110	1.05	15.09	0.03	2.85	2.15	15.39	15.27
2951.4247	1.07	15.02	0.03	3.06	2.36	15.29	15.17
2951.4291	1.09	15.03	0.03	3.00	2.30	15.32	15.20
2973.4388	1.05	15.00	0.03	3.09	2.39	15.27	15.16
2973.4430	1.04	15.01	0.03	3.06	2.36	15.29	15.17
2996.4630	1.05	14.98	0.03	3.15	2.45	15.25	15.13
2996.4675	1.03	15.03	0.03	3.00	2.30	15.32	15.20
2998.4951	1.12	14.99	0.03	3.12	2.42	15.26	15.14
2998.4992	1.09	14.97	0.03	3.18	2.48	15.23	15.12
3003.5287	1.08	14.93	0.03	3.30	2.60	15.18	15.06
3003.5310	1.07	14.97	0.03	3.18	2.48	15.23	15.12
3019.4600	1.06	14.97	0.03	3.18	2.48	15.23	15.12
3019.4641	1.07	15.01	0.03	3.06	2.36	15.29	15.17
3024.5696	1.11	15.00	0.03	3.09	2.39	15.27	15.16
3024.5739	1.10	15.03	0.03	3.00	2.30	15.32	15.20
3026.5158	1.13	14.99	0.03	3.12	2.42	15.26	15.14
3026.5198	1.09	15.03	0.03	3.00	2.30	15.32	15.20
3026.5237	1.12	14.99	0.03	3.12	2.42	15.26	15.14
3026.5276	1.10	14.96	0.03	3.21	2.51	15.22	15.10
3031.4510	1.08	15.03	0.03	3.00	2.30	15.32	15.20
3031.4558	1.07	14.97	0.03	3.18	2.48	15.23	15.12
3033.5128	1.12	14.96	0.03	3.21	2.51	15.22	15.10
3033.5173	1.11	14.97	0.03	3.18	2.48	15.23	15.12
3059.4382	1.07	15.04	0.03	2.98	2.28	15.33	15.21
3059.4428	1.07	15.03	0.03	3.00	2.30	15.32	15.20
3149.3097	1.10	14.88	0.03	3.45	2.75	15.12	15.00
3149.3140	1.09	14.90	0.03	3.39	2.69	15.15	15.03
3168.3576	1.11	14.94	0.03	3.27	2.57	15.20	15.08
3168.3615	1.06	14.92	0.03	3.33	2.63	15.17	15.05
3262.5257	1.06	14.72	0.03	4.00	3.30	14.92	14.81
3262.5298	1.09	14.75	0.03	3.89	3.19	14.96	14.84
3302.4413	1.06	14.86	0.03	3.51	2.81	15.10	14.98
3302.4439	1.06	14.82	0.03	3.65	2.95	15.05	14.93
3321.5316	1.08	14.85	0.03	3.55	2.85	15.08	14.96
3358.3591	1.10	14.91	0.03	3.36	2.66	15.16	15.04
3358.3617	1.09	14.92	0.03	3.33	2.63	15.17	15.05
3379.5304	1.13	14.89	0.03	3.42	2.72	15.13	15.02
3379.5330	1.07	14.85	0.03	3.55	2.85	15.08	14.96
3385.3435	1.09	14.83	0.03	3.61	2.91	15.06	14.94
3385.3528	1.04	14.77	0.03	3.82	3.12	14.98	14.87
3388.5742	1.10	14.75	0.03	3.89	3.19	14.95	14.84

Appendix B6.1-Continued

1	2	3	4	5	6	7	8
3388.5788	1.07	14.78	0.03	3.78	3.08	15.00	14.88
3405.3411	1.08	14.84	0.03	3.58	2.88	15.07	14.95
3405.3471	1.09	14.81	0.03	3.68	2.98	15.03	14.92
3416.3873	1.08	14.86	0.03	3.51	2.81	15.10	14.98
3416.3919	1.05	14.85	0.03	3.55	2.85	15.08	14.96
3443.3483	1.05	14.93	0.03	3.30	2.6	15.18	15.06
3443.3509	1.07	14.88	0.03	3.45	2.75	15.12	15.00
3466.4383	1.08	14.97	0.03	3.18	2.48	15.23	15.12
3466.4689	1.04	15.01	0.03	3.06	2.36	15.29	15.17
3501.2854	1.07	14.90	0.03	3.39	2.69	15.15	15.03
3501.2880	1.06	14.92	0.03	3.33	2.63	15.17	15.05
3670.5689	1.05	15.24	0.04	2.48	1.78	15.59	15.48
3670.3730	1.05	15.28	0.04	2.38	1.68	15.66	15.54
3688.6058	1.10	15.24	0.04	2.48	1.78	15.59	15.48
3688.6104	1.08	15.26	0.04	2.43	1.73	15.62	15.51
3679.4951	1.08	15.31	0.04	2.33	1.63	15.69	15.57
3679.4990	1.07	15.30	0.04	2.34	1.64	15.68	15.56
3679.5030	1.07	15.29	0.04	2.37	1.67	15.66	15.55
3679.5069	1.07	15.29	0.04	2.37	1.67	15.66	15.55
3733.5461	1.07	15.17	0.04	2.64	1.94	15.50	15.38
3733.5500	1.09	15.19	0.04	2.59	1.89	15.53	15.41
3733.5539	1.10	15.21	0.04	2.54	1.84	15.56	15.44
3733.5579	1.08	15.22	0.04	2.52	1.82	15.57	15.45
3752.3889	1.12	15.11	0.03	2.78	2.08	15.42	15.31
3752.3914	1.09	15.09	0.03	2.85	2.15	15.39	15.27
3752.3939	1.07	15.13	0.03	2.74	2.04	15.45	15.33
3752.3964	1.09	15.15	0.03	2.69	1.99	15.47	15.35
3784.3331	1.09	15.12	0.03	2.77	2.07	15.43	15.31
3784.3370	1.11	15.14	0.03	2.72	2.02	15.46	15.34
3784.3409	1.12	15.16	0.03	2.67	1.97	15.48	15.37
3786.3186	1.08	15.24	0.04	2.48	1.78	15.59	15.48
3786.3218	1.10	15.20	0.04	2.57	1.87	15.54	15.42
3786.3251	1.11	15.19	0.04	2.59	1.89	15.53	15.41
3786.3283	1.08	15.22	0.04	2.52	1.82	15.57	15.45
3823.3057	1.09	15.15	0.04	2.69	1.99	15.47	15.35
3823.3096	1.10	15.15	0.04	2.69	1.99	15.47	15.35
3823.3135	1.08	15.18	0.04	2.62	1.92	15.51	15.39
3823.3174	1.11	15.12	0.03	2.77	2.07	15.43	15.31
3852.2881	1.10	15.15	0.03	2.69	1.99	15.47	15.35
3852.2920	1.11	15.15	0.03	2.69	1.99	15.47	15.35
3852.2959	1.09	15.11	0.03	2.78	2.08	15.42	15.31

Appendix B6.1-Continued

1	2	3	4	5	6	7	8
3871.2789	1.08	15.13	0.03	2.74	2.04	15.45	15.33
3871.2828	1.10	15.18	0.03	2.62	1.92	15.51	15.39
3871.2867	1.12	15.15	0.03	2.69	1.99	15.47	15.35
3871.2906	1.13	15.18	0.03	2.62	1.92	15.51	15.39
3878.2521	1.10	15.22	0.04	2.52	1.82	15.57	15.45
3878.2560	1.11	15.27	0.04	2.41	1.71	15.64	15.52
3878.2600	1.12	15.26	0.04	2.43	1.73	15.62	15.51
3878.2640	1.12	15.20	0.04	2.57	1.87	15.54	15.42
3881.2622	1.11	15.22	0.04	2.52	1.82	15.57	15.45
3881.2662	1.12	15.21	0.04	2.54	1.84	15.56	15.44
3881.2701	1.11	15.17	0.04	2.64	1.94	15.50	15.38
3881.2741	1.10	15.19	0.04	2.59	1.89	15.53	15.41
3886.2726	1.11	15.21	0.04	2.54	1.84	15.56	15.44
3886.2765	1.09	15.21	0.04	2.54	1.84	15.56	15.44
3886.2804	1.12	15.15	0.04	2.69	1.99	15.47	15.35
3886.2843	1.13	15.21	0.04	2.54	1.84	15.56	15.44
4080.6397	1.11	14.94	0.03	3.27	2.57	15.20	15.08
4080.6418	1.11	14.93	0.03	3.30	2.60	15.18	15.06
4080.6439	1.09	14.94	0.03	3.27	2.57	15.20	15.08
4080.6460	1.11	14.91	0.03	3.36	2.66	15.16	15.04
4080.6481	1.11	14.92	0.03	3.33	2.63	15.17	15.05
4080.6503	1.12	14.95	0.03	3.24	2.54	15.21	15.09
4082.5049	1.08	14.93	0.03	3.30	2.60	15.18	15.06
4082.5070	1.09	14.93	0.03	3.30	2.60	15.18	15.06
4082.5091	1.08	14.93	0.03	3.30	2.60	15.18	15.06
4082.5112	1.11	14.95	0.03	3.24	2.54	15.21	15.09
4082.5133	1.10	14.93	0.03	3.30	2.60	15.18	15.06
4082.5154	1.11	14.97	0.03	3.18	2.48	15.23	15.12
4088.3715	1.08	14.99	0.03	3.12	2.42	15.26	15.14
4088.3740	1.12	14.97	0.03	3.18	2.48	15.23	15.12
4088.3775	1.11	15.00	0.03	3.09	2.39	15.27	15.16
4088.3810	1.12	14.96	0.03	3.21	2.51	15.22	15.10
4088.4730	1.09	15.00	0.03	3.09	2.39	15.27	15.16
4088.4800	1.09	14.96	0.03	3.21	2.51	15.22	15.10
4088.4835	1.12	14.97	0.03	3.18	2.48	15.23	15.12
4088.4870	1.09	14.98	0.03	3.15	2.45	15.25	15.13
4088.4904	1.10	14.96	0.03	3.21	2.51	15.22	15.10
4088.4939	1.10	14.96	0.03	3.21	2.51	15.22	15.10
4118.3902	1.09	15.16	0.03	2.67	1.97	15.48	15.37
4118.3943	1.09	15.07	0.03	2.89	2.19	15.37	15.25
4118.3964	1.09	15.06	0.03	2.91	2.21	15.36	15.24

Appendix B6.1-Continued

1	2	3	4	5	6	7	8
4118.3985	1.11	15.05	0.03	2.93	2.23	15.35	15.23
4145.4025	1.09	14.96	0.03	3.21	2.51	15.22	15.10
4145.4059	1.10	14.96	0.03	3.21	2.51	15.22	15.10
4145.4094	1.10	14.99	0.03	3.12	2.42	15.26	15.14
4145.4129	1.09	14.97	0.03	3.18	2.48	15.23	15.12
4171.3190	1.07	15.07	0.03	2.89	2.19	15.37	15.25
4171.3211	1.08	15.11	0.03	2.78	2.08	15.42	15.31
4171.3133	1.09	15.12	0.04	2.77	2.07	15.43	15.31
4171.3154	1.08	15.12	0.04	2.77	2.07	15.43	15.31
4174.3564	1.09	15.04	0.03	2.98	2.28	15.33	15.21
4174.3599	1.08	15.07	0.03	2.89	2.19	15.37	15.25
4174.3633	1.11	15.06	0.03	2.91	2.21	15.36	15.24
4174.3668	1.10	15.05	0.03	2.93	2.23	15.35	15.23
4174.3703	1.11	15.07	0.03	2.89	2.19	15.37	15.25
4179.2506	1.09	15.10	0.03	2.82	2.12	15.40	15.29
4179.2527	1.10	15.09	0.03	2.85	2.15	15.39	15.27
4179.2548	1.09	15.08	0.03	2.89	2.19	15.37	15.25
4179.2569	1.12	15.08	0.03	2.87	2.17	15.38	15.26
4180.2489	1.09	15.13	0.03	2.74	2.04	15.45	15.33
4180.2510	1.10	15.12	0.03	2.77	2.07	15.43	15.31
4180.2531	1.10	15.14	0.03	2.72	2.02	15.46	15.34
4180.2552	1.09	15.11	0.03	2.78	2.08	15.42	15.31
4181.3500	1.12	15.13	0.03	2.74	2.04	15.45	15.33
4181.3521	1.09	15.12	0.03	2.77	2.07	15.43	15.31
4181.3542	1.11	15.13	0.03	2.74	2.04	15.45	15.33
4181.3563	1.09	15.10	0.03	2.82	2.12	15.40	15.29
4181.3584	1.10	15.09	0.03	2.85	2.15	15.39	15.27
4181.3604	1.10	15.11	0.03	2.78	2.08	15.42	15.31
4235.2719	1.09	14.98	0.03	3.15	2.45	15.25	15.13
4235.2754	1.11	14.99	0.03	3.12	2.42	15.26	15.14
4235.2790	1.10	15.01	0.03	3.06	2.36	15.29	15.17
4235.2825	1.08	15.03	0.03	3.00	2.30	15.32	15.20
4376.5783	1.12	15.34	0.05	2.26	1.56	15.74	15.62
4376.5838	1.08	15.32	0.05	2.30	1.60	15.71	15.59
4376.5870	1.10	15.33	0.05	2.28	1.58	15.72	15.61
4395.5586	1.11	15.35	0.05	2.23	1.53	15.76	15.64
4395.5621	1.09	15.32	0.05	2.30	1.60	15.71	15.59
4395.5655	1.08	15.34	0.05	2.26	1.56	15.74	15.62
4395.5690	1.10	15.31	0.05	2.33	1.63	15.69	15.57
4423.4500	1.11	15.38	0.05	2.18	1.48	15.79	15.68
4423.4535	1.14	15.33	0.05	2.28	1.58	15.72	15.61

Appendix B6.1-Continued

1	2	3	4	5	6	7	8
4423.4570	1.13	15.36	0.05	2.22	1.52	15.77	15.65
4423.4604	1.10	15.37	0.05	2.19	1.49	15.79	15.67
4423.5468	1.12	15.35	0.05	2.23	1.53	15.76	15.64
4423.5503	1.13	15.37	0.05	2.19	1.49	15.79	15.67
4423.5538	1.08	15.36	0.05	2.22	1.52	15.77	15.65
4423.5573	1.09	15.39	0.05	2.15	1.45	15.82	15.70
4423.5608	1.10	15.38	0.05	2.18	1.48	15.79	15.68
4423.5643	1.08	15.36	0.05	2.22	1.52	15.77	15.65
4423.5678	1.11	15.39	0.05	2.15	1.45	15.82	15.70

B6.2 Color Indices of 1ES 0806+524

JD-2450000 (1)	<i>V</i> (2)	<i>V-R</i> (3)	Error (4)
810.5082	15.15	0.37	0.05
834.4140	15.40	0.38	0.05
841.4318	15.49	0.43	0.05
845.5055	15.59	0.39	0.05
876.4644	15.70	0.39	0.06
895.3949	15.69	0.38	0.06
1141.4873	15.74	0.41	0.06
1160.5642	15.91	0.39	0.06
1170.4212	15.84	0.37	0.06
1187.4902	15.88	0.37	0.06
1191.4906	15.91	0.36	0.06
1201.5404	15.89	0.35	0.06
1205.5882	15.91	0.41	0.06
1221.4477	15.98	0.38	0.06
1276.2663	15.99	0.37	0.06
1283.3362	15.95	0.38	0.06
1286.3678	15.98	0.36	0.06
1310.3054	15.94	0.40	0.06
1457.5383	15.89	0.35	0.06
1465.5134	15.72	0.38	0.06
1486.4994	15.78	0.36	0.06
1493.5730	15.73	0.37	0.06
1517.5061	15.67	0.35	0.06
1521.5034	15.73	0.36	0.06
1523.5395	15.70	0.42	0.06
1526.4218	15.83	0.36	0.06
1551.4333	15.62	0.42	0.06
1559.5117	15.69	0.38	0.06
1584.4237	15.76	0.37	0.06
1587.4695	15.67	0.36	0.06
1702.2607	15.65	0.40	0.06
2358.3051	15.26	0.37	0.06
2358.3097	15.32	0.40	0.06

B7.1 *R* Band Data of 1ES 1028+511

JD-245000 (1)	Ref 6-Ref 5 (2)	<i>R</i> (3)	<i>R_d</i> (4)	Error (5)
420.6785	-	16.66	16.63	0.04
435.6741	-	16.66	16.63	0.04
465.6199	-	16.57	16.54	0.04
466.5331	-	16.53	16.52	0.04
506.4996	-	16.62	16.59	0.04
509.4744	-	16.69	16.66	0.04
513.448	-	16.56	16.53	0.04
516.4458	-	16.60	16.57	0.04
517.5128	-	16.61	16.58	0.04
521.4354	-	16.63	16.6	0.04
525.3586	-	16.64	16.61	0.04
529.4164	-	16.62	16.59	0.04
536.3867	-	16.65	16.62	0.04
541.4016	-	16.60	16.57	0.04
568.4146	-	16.65	16.62	0.04
569.3990	-	16.71	16.68	0.04
570.3638	-	16.65	16.62	0.04
577.3303	-	16.66	16.63	0.04
841.5094	0.14	16.58	16.55	0.08
845.538	0.11	16.66	16.63	0.08
876.4879	0.10	16.60	16.57	0.08
1160.5983	0.15	16.51	16.48	0.08
1170.4575	0.09	16.48	16.45	0.08
1191.5470	0.10	16.39	16.36	0.08
1193.5222	0.13	16.32	16.29	0.08
1221.5048	0.16	16.41	16.38	0.08
1276.3443	0.11	16.50	16.47	0.08
1279.4181	0.13	16.33	16.30	0.08
1286.4067	0.14	16.36	16.33	0.08
1310.3377	0.12	16.51	16.48	0.08
1486.5895	0.15	16.52	16.49	0.08
1494.6009	0.13	16.49	16.46	0.08
1521.6349	0.13	16.60	16.57	0.08
1523.6032	0.08	16.56	16.53	0.08
1532.6334	0.12	16.54	16.51	0.08
1551.5656	0.13	16.47	16.44	0.08
1583.6054	0.12	16.50	16.47	0.08
1586.5511	0.13	16.50	16.47	0.08

Appendix B7.1-Continued

1	2	3	4	5
1723.2827	0.13	16.89	16.86	0.09
2072.2992	0.10	16.86	16.83	0.10
2072.3019	0.09	16.81	16.78	0.08
2237.5545	0.10	16.64	16.61	0.08
2299.6010	0.13	16.86	16.83	0.10
2299.6035	0.09	16.86	16.83	0.08
2299.606	0.12	16.82	16.79	0.08
2299.6085	0.13	16.77	16.74	0.08
2299.6134	0.12	16.80	16.77	0.08
2299.6158	0.11	16.82	16.79	0.08
2299.6193	0.12	16.79	16.76	0.08
2299.6234	0.07	16.84	16.81	0.08
2299.6261	0.13	16.82	16.79	0.08
2299.6293	0.11	16.80	16.77	0.08
2299.6334	0.10	16.80	16.77	0.08
2299.6360	0.09	16.89	16.86	0.08
2299.6385	0.11	16.8	16.77	0.08
2299.6410	0.12	16.84	16.81	0.08
2367.4081	0.10	16.54	16.51	0.08
2367.4106	0.07	16.59	16.56	0.08
2367.4131	0.11	16.49	16.46	0.08
2367.4156	0.08	16.52	16.49	0.08
2369.3477	0.11	16.63	16.60	0.08
2375.2683	0.12	16.49	16.46	0.08
2375.2702	0.09	16.42	16.39	0.08
2611.5502	0.11	16.54	16.51	0.08
2611.5565	0.11	16.63	16.60	0.08
2622.6153	0.10	16.70	16.67	0.09
2622.6231	0.12	16.71	16.68	0.08
2650.4475	0.14	16.67	16.64	0.08
2650.4554	0.11	16.70	16.67	0.08
2671.5123	0.15	16.61	16.58	0.08
2671.5177	0.12	16.61	16.58	0.08
2679.5206	0.14	16.50	16.47	0.08
2679.5470	0.14	16.52	16.49	0.08
2682.5469	0.11	16.45	16.42	0.08
2682.5523	0.13	16.45	16.38	0.08
2699.4951	0.12	16.52	16.49	0.08
2699.4991	0.11	16.55	16.52	0.07
2736.4194	0.12	16.59	16.56	0.07
2751.3311	0.11	16.57	16.54	0.07

Appendix B7.1-Continued

1	2	3	4	5
2751.3369	0.13	16.55	16.52	0.08
2758.4137	0.15	16.50	16.47	0.07
2758.4183	0.13	16.55	16.52	0.08
2767.4781	0.13	16.47	16.44	0.08
2767.4834	0.11	16.51	16.48	0.08
2780.3312	0.13	16.53	16.50	0.08
2783.3213	0.14	16.55	16.52	0.08
2783.3259	0.12	16.56	16.53	0.08
2788.3072	0.13	16.58	16.55	0.08
2788.3114	0.11	16.50	16.47	0.08
2812.2706	0.19	16.51	16.48	0.10
2812.2751	0.12	16.5	16.47	0.10
2817.2990	0.13	16.19	16.16	0.08
2817.3044	0.09	16.23	16.29	0.08
2971.6060	0.15	16.48	16.45	0.10
2995.5992	0.12	16.64	16.61	0.08
2995.6033	0.11	16.61	16.58	0.08
2998.5528	0.13	16.65	16.62	0.08
2998.5575	0.13	16.6	16.57	0.08
3023.5884	0.12	16.38	16.35	0.07
3023.5926	0.19	16.44	16.41	0.07
3028.5646	0.12	16.48	16.45	0.08
3028.5685	0.09	16.42	16.39	0.08
3059.5195	0.11	16.5	16.47	0.08
3059.5242	0.19	16.49	16.46	0.08
3159.3483	0.08	16.55	16.52	0.08
3159.3537	0.19	16.53	16.59	0.08
3172.3485	0.14	16.51	16.48	0.08
3172.3526	0.12	16.48	16.45	0.08
3195.2975	0.14	16.52	16.49	0.08
3304.5740	0.12	16.68	16.65	0.08
3304.5787	0.19	16.66	16.63	0.08
3380.5343	0.13	16.67	16.64	0.08
3380.5384	0.12	16.66	16.63	0.08
3386.4191	0.19	16.68	16.65	0.08
3388.5872	0.15	16.69	16.66	0.08
3388.5917	0.14	16.61	16.58	0.08
3405.3660	0.11	16.84	16.81	0.08
3405.3701	0.11	16.75	16.72	0.08
3417.4536	0.12	16.65	16.62	0.08
3417.4581	0.09	16.71	16.68	0.08

Appendix B7.1-Continued

1	2	3	4	5
3443.5010	0.12	16.83	16.89	0.08
3443.5049	0.15	16.82	16.79	0.08
3501.3270	0.12	17.00	16.97	0.09
3501.3310	0.12	17.03	17.00	0.09
3709.5283	0.10	16.66	16.63	0.08
3709.5322	0.13	16.69	16.66	0.08
3709.5362	0.12	16.7	16.67	0.08
3709.5401	0.10	16.72	16.69	0.08
3789.5163	0.13	16.94	16.91	0.09
3789.5204	0.14	16.92	16.89	0.09
3816.2854	0.17	16.93	16.9	0.08
3816.2893	0.15	16.98	16.95	0.08
3816.2932	0.12	16.99	16.96	0.08
3816.2971	0.11	16.95	16.92	0.08
3823.3592	0.16	16.84	16.81	0.08
3823.3631	0.14	16.78	16.75	0.08
3823.3670	0.13	16.77	16.74	0.08
3823.3709	0.15	16.79	16.76	0.08
3880.2627	0.13	16.67	16.64	0.08
3880.2666	0.13	16.69	16.66	0.08
3880.2705	0.11	16.67	16.64	0.08
3880.2744	0.08	16.74	16.71	0.08
4088.5062	0.13	16.31	16.28	0.08
4088.5096	0.12	16.30	16.28	0.08
4088.5131	0.10	16.40	16.37	0.08
4088.5166	0.11	16.37	16.34	0.08
4088.5200	0.17	16.37	16.34	0.08
4088.5235	0.14	16.38	16.35	0.08
4151.3853	0.14	16.46	16.43	0.08
4151.3888	0.12	16.49	16.46	0.08
4151.3923	0.14	16.44	16.41	0.08
4151.3957	0.13	16.45	16.42	0.08
4151.3993	0.15	16.47	16.44	0.08
4151.4027	0.12	16.43	16.40	0.08
4151.4062	0.14	16.44	16.41	0.08
4151.4097	0.12	16.42	16.39	0.08
4171.3633	0.12	16.35	16.32	0.08
4171.3654	0.13	16.32	16.29	0.08
4171.3676	0.10	16.28	16.25	0.08
4236.2637	0.10	16.21	16.18	0.08
4236.3672	0.12	16.23	16.20	0.08

Appendix B7.1-Continued

1	2	3	4	5
4236.3713	0.10	16.21	16.18	0.08
4236.3742	0.09	16.21	16.18	0.08
4236.3778	0.12	16.16	16.13	0.08
4237.3220	0.12	16.22	16.19	0.08
4237.3255	0.12	16.17	16.14	0.08
4237.3288	0.14	16.2	16.17	0.08
4237.3323	0.11	16.18	16.15	0.08
4237.3358	0.13	16.16	16.13	0.08
4238.2717	0.13	16.21	16.18	0.08
4238.2752	0.12	16.18	16.15	0.08
4238.2788	0.14	16.25	16.22	0.08
4238.2823	0.10	16.26	16.23	0.08
4239.2870	0.12	16.26	16.23	0.08
4239.2905	0.15	16.28	16.25	0.08
4239.2940	0.12	16.32	16.29	0.08
4239.2975	0.12	16.31	16.28	0.08
4239.3009	0.11	16.33	16.30	0.08
4239.3044	0.12	16.30	16.27	0.08
4239.3079	0.13	16.34	16.31	0.08
4317.2511	0.12	16.00	15.97	0.07
4317.2532	0.11	16.00	15.97	0.07
4317.2574	0.11	15.97	15.94	0.07
4317.2616	0.13	15.99	15.96	0.07
4317.2637	0.12	15.99	15.96	0.07
4317.2637	0.10	15.98	15.95	0.07
4317.2658	0.13	15.97	15.94	0.07
4320.2321	0.09	15.99	15.96	0.07
4320.2342	0.09	15.97	15.94	0.07
4320.2363	0.11	15.98	15.95	0.07
4320.2384	0.12	15.99	15.86	0.07
4320.2405	0.13	15.97	15.88	0.07
4320.2426	0.14	15.99	15.86	0.07
4320.2448	0.13	15.99	15.87	0.07
4320.2469	0.12	16.01	15.88	0.07
4320.2490	0.14	15.95	15.92	0.07
4320.2511	0.14	15.97	15.94	0.07
4320.2553	0.12	15.94	15.91	0.07
4320.2574	0.13	15.94	15.91	0.07
4320.2616	0.11	15.95	15.92	0.07
4320.2624	0.10	15.99	15.87	0.07
4320.2637	0.12	15.99	15.86	0.07

Appendix B7.1-Continued

1	2	3	4	5
4320.2659	0.11	16.00	15.86	0.07
4320.3783	0.14	15.96	15.89	0.07
4320.3814	0.10	15.98	15.91	0.07
4320.3842	0.13	15.97	15.91	0.07
4320.3871	0.09	15.99	15.87	0.07
4327.2223	0.08	15.96	15.93	0.07
4327.2238	0.11	15.96	15.93	0.07
4327.2262	0.10	16.00	15.97	0.07
4327.2284	0.12	16.01	15.98	0.07
4332.2327	0.12	16.05	16.02	0.07
4332.2371	0.11	16.05	16.02	0.07
4332.2400	0.15	16.04	16.01	0.07
4332.2443	0.12	16.06	16.03	0.07
4332.2472	0.10	16.05	16.02	0.07
4332.2513	0.09	16.07	16.04	0.07
4346.2103	0.12	16.01	15.98	0.07
4346.2142	0.08	15.99	15.96	0.07
4346.2173	0.11	15.98	15.95	0.07
4346.2215	0.14	15.96	15.93	0.07
4422.6305	0.10	16.18	16.15	0.08

B7.2 Color Indices of 1ES 1028+511

JD-2450000 (1)	<i>V</i> (2)	<i>V-R</i> (3)	Error (4)	Observatory (5)
521.44	16.97	0.34	0.04	Torino
570.37	16.89	0.24	0.04	Torino
841.51	16.87	0.29	0.10	Abastumani
845.54	16.88	0.22	0.10	Abastumani
876.49	16.83	0.23	0.10	Abastumani
1160.60	16.75	0.24	0.09	Abastumani
1170.46	16.75	0.27	0.09	Abastumani
1191.55	16.65	0.26	0.09	Abastumani
1193.52	16.64	0.32	0.09	Abastumani
1221.51	16.67	0.26	0.09	Abastumani
1276.35	16.72	0.22	0.09	Abastumani
1279.42	16.60	0.26	0.09	Abastumani
1286.41	16.57	0.21	0.09	Abastumani
1310.34	16.72	0.21	0.09	Abastumani
1486.59	16.79	0.27	0.09	Abastumani
1494.60	16.76	0.27	0.09	Abastumani
1521.64	16.84	0.24	0.10	Abastumani
1523.61	16.57	0.21	0.09	Abastumani
1532.63	16.76	0.22	0.09	Abastumani
1551.57	16.67	0.2	0.09	Abastumani
1583.61	16.75	0.25	0.09	Abastumani
1586.55	16.75	0.25	0.09	Abastumani

B8 *R* Band Data of 1ES 1426+428

JD-2452000 (1)	Ref 5-Ref 4 (2)	<i>R</i> (3)	Error (4)	<i>F</i> (5)	<i>F_{cor}</i> (6)	<i>R_{hs}</i> (7)	<i>R_{hsd}</i> (8)
730.4673	1.26	15.78	0.07	1.51	0.63	16.72	16.69
730.4719	1.24	15.76	0.07	1.53	0.65	16.69	16.65
763.3780	1.29	15.87	0.07	1.39	0.51	16.95	16.92
763.3819	1.27	15.89	0.07	1.36	0.48	17.02	16.98
908.1993	1.29	15.93	0.07	1.31	0.43	17.14	17.10
908.2034	1.27	15.94	0.07	1.30	0.42	17.16	17.13
1024.5260	1.26	15.92	0.07	1.32	0.44	17.11	17.08
1024.5309	1.29	15.90	0.07	1.35	0.47	17.04	17.01
1141.3240	1.27	15.88	0.07	1.37	0.49	16.99	16.96
1148.3563	1.27	15.97	0.07	1.26	0.38	17.27	17.24
1149.3763	1.24	15.95	0.07	1.29	0.41	17.19	17.16
1149.3808	1.26	15.92	0.07	1.32	0.44	17.11	17.08
1191.3030	1.25	15.92	0.07	1.32	0.44	17.11	17.08
1191.3103	1.24	15.93	0.07	1.31	0.43	17.14	17.10
1191.3268	1.26	15.95	0.07	1.29	0.41	17.19	17.16
1194.4290	1.26	16.00	0.07	1.23	0.35	17.36	17.33
1199.3210	1.24	15.95	0.07	1.29	0.41	17.19	17.16
1199.3252	1.22	15.96	0.07	1.28	0.4	17.21	17.18
1202.5143	1.26	15.98	0.07	1.25	0.37	17.30	17.27
1258.2007	1.26	16.06	0.07	1.16	0.28	17.60	17.57
1258.2047	1.28	16.04	0.07	1.19	0.31	17.49	17.46
1262.2176	1.24	16.05	0.07	1.17	0.29	17.56	17.53
1262.2221	1.24	16.04	0.07	1.19	0.31	17.49	17.46
1264.2207	1.25	16.05	0.07	1.17	0.29	17.56	17.53
1264.2249	1.26	16.06	0.07	1.16	0.28	17.60	17.57
1268.2350	1.24	16.07	0.07	1.15	0.27	17.64	17.61
1386.5150	1.27	16.04	0.07	1.19	0.31	17.49	17.46
1386.5185	1.27	16.01	0.07	1.22	0.34	17.39	17.36
1417.4980	1.25	16.05	0.07	1.17	0.29	17.56	17.53
1417.5028	1.27	16.04	0.07	1.19	0.31	17.49	17.46
1444.3670	1.27	16.02	0.07	1.21	0.33	17.42	17.39
1444.3705	1.25	16.00	0.07	1.23	0.35	17.36	17.33
1467.5077	1.25	15.96	0.07	1.28	0.4	17.21	17.18
1467.5142	1.22	15.96	0.07	1.28	0.4	17.21	17.18
1503.4313	1.25	15.93	0.07	1.31	0.43	17.14	17.10
1503.4354	1.24	15.92	0.07	1.32	0.44	17.11	17.08
1518.2923	1.25	15.90	0.07	1.35	0.47	17.04	17.01
1518.2963	1.27	15.89	0.07	1.36	0.48	17.02	16.98

Appendix B8.1-Continued

1	2	3	4	5	6	7	8
1518.3003	1.24	15.90	0.07	1.35	0.47	17.04	17.01
1523.4089	1.24	15.92	0.07	1.32	0.44	17.11	17.08
1523.4130	1.27	15.93	0.07	1.31	0.43	17.14	17.10
1529.3096	1.25	15.91	0.07	1.34	0.46	17.06	17.03
1529.3140	1.25	15.93	0.07	1.31	0.43	17.14	17.10
1559.2940	1.24	15.96	0.07	1.28	0.4	17.21	17.18
1559.2980	1.25	15.94	0.07	1.30	0.42	17.16	17.13
1582.2596	1.24	15.89	0.07	1.36	0.48	17.02	16.98
1582.2637	1.23	15.87	0.07	1.39	0.51	16.95	16.92
1595.3388	1.24	15.89	0.07	1.36	0.48	17.02	16.98
1595.3430	1.26	15.93	0.07	1.31	0.43	17.14	17.10
1606.2328	1.25	15.89	0.07	1.36	0.48	17.02	16.98
1668.1423	1.23	15.92	0.07	1.32	0.44	17.11	17.08
1668.1520	1.23	15.95	0.07	1.29	0.41	17.19	17.16
1668.1567	1.26	15.95	0.07	1.29	0.41	17.19	17.16
1717.5980	1.28	16.00	0.07	1.23	0.35	17.36	17.33
1717.6009	1.25	16.03	0.07	1.20	0.32	17.46	17.42
1717.6048	1.27	16.01	0.07	1.22	0.34	17.39	17.36
1717.6090	1.25	16.03	0.07	1.20	0.32	17.46	17.42
1733.6291	1.23	16.05	0.07	1.17	0.29	17.56	17.53
1733.6330	1.22	16.01	0.07	1.22	0.34	17.39	17.36
1733.6369	1.24	16.04	0.07	1.19	0.31	17.49	17.46
1787.3451	1.26	16.00	0.07	1.23	0.35	17.36	17.33
1798.4353	1.23	15.98	0.07	1.25	0.37	17.30	17.27
1799.4910	1.27	15.95	0.07	1.29	0.41	17.19	17.16
1799.5144	1.25	15.92	0.07	1.32	0.44	17.11	17.08
1800.3759	1.26	15.98	0.07	1.25	0.37	17.30	17.27
1800.3868	1.24	15.97	0.07	1.26	0.38	17.27	17.24
1801.4622	1.26	15.93	0.07	1.31	0.43	17.14	17.10
1801.4661	1.25	15.90	0.07	1.35	0.47	17.04	17.01
1801.4700	1.23	15.91	0.07	1.34	0.46	17.06	17.03
1801.4738	1.26	15.91	0.07	1.34	0.46	17.06	17.03
1801.4832	1.27	15.92	0.07	1.32	0.44	17.11	17.08
1801.4871	1.24	15.94	0.07	1.30	0.42	17.16	17.13
1801.4910	1.25	15.89	0.07	1.36	0.48	17.02	16.98
1801.4948	1.25	15.92	0.07	1.32	0.44	17.11	17.08
1823.4013	1.23	15.89	0.07	1.36	0.48	17.02	16.98
1823.4093	1.22	15.91	0.07	1.34	0.46	17.06	17.03
1823.4133	1.23	15.92	0.07	1.32	0.44	17.11	17.08
1825.4906	1.24	15.95	0.07	1.29	0.41	17.19	17.16
1825.4941	1.25	15.93	0.07	1.31	0.43	17.14	17.10

Appendix B8.1-Continued

1	2	3	4	5	6	7	8
1825.4980	1.25	15.93	0.07	1.31	0.43	17.14	17.10
1832.4178	1.22	15.92	0.07	1.32	0.44	17.11	17.08
1832.4217	1.24	15.94	0.07	1.30	0.42	17.16	17.13
1832.4256	1.22	15.94	0.07	1.30	0.42	17.16	17.13
1832.4294	1.23	15.95	0.07	1.29	0.41	17.19	17.16
1842.3447	1.24	15.93	0.07	1.31	0.43	17.14	17.10
1852.4021	1.22	15.88	0.06	1.37	0.49	16.99	16.96
1852.4060	1.26	15.90	0.06	1.35	0.47	17.04	17.01
1852.4100	1.25	15.91	0.06	1.34	0.46	17.06	17.03
1852.4137	1.27	15.88	0.06	1.37	0.49	16.99	16.96
1854.3984	1.25	15.94	0.07	1.30	0.42	17.16	17.13
1854.4023	1.23	15.88	0.06	1.37	0.49	16.99	16.96
1854.4062	1.27	15.92	0.07	1.32	0.44	17.11	17.08
1854.4101	1.25	15.94	0.07	1.30	0.42	17.16	17.13
1854.4165	1.29	15.93	0.07	1.31	0.43	17.14	17.10
1854.4704	1.22	15.95	0.07	1.29	0.41	17.19	17.16
1854.4740	1.25	15.92	0.07	1.32	0.44	17.11	17.08
1871.4175	1.24	15.90	0.06	1.35	0.47	17.04	17.01
1871.4210	1.27	15.92	0.07	1.32	0.44	17.11	17.08
1871.4262	1.24	15.85	0.06	1.41	0.53	16.91	16.88
1871.4302	1.25	15.82	0.06	1.45	0.57	16.83	16.80
1871.4380	1.29	15.84	0.06	1.43	0.55	16.87	16.84
1875.3493	1.24	15.82	0.06	1.45	0.57	16.83	16.80
1875.3534	1.24	15.81	0.06	1.47	0.59	16.79	16.76
1877.4171	1.27	15.86	0.06	1.40	0.52	16.93	16.90
1877.4211	1.25	15.83	0.06	1.44	0.56	16.85	16.82
1879.3852	1.25	15.87	0.06	1.39	0.51	16.95	16.92
1879.3891	1.24	15.89	0.06	1.36	0.48	17.02	16.98
1879.3930	1.25	15.88	0.06	1.37	0.49	16.99	16.96
1879.3969	1.27	15.91	0.06	1.34	0.46	17.06	17.03
1880.3159	1.23	15.90	0.06	1.35	0.47	17.04	17.01
1880.3198	1.24	15.90	0.06	1.35	0.47	17.04	17.01
1880.3237	1.26	15.91	0.06	1.34	0.46	17.06	17.03
1880.3276	1.25	15.89	0.06	1.36	0.48	17.02	16.98
1885.3308	1.22	15.88	0.06	1.37	0.49	16.99	16.96
1885.3347	1.24	15.86	0.06	1.40	0.52	16.93	16.90
1885.3425	1.25	15.87	0.06	1.39	0.51	16.95	16.92
1885.3519	1.27	15.85	0.06	1.41	0.53	16.91	16.88
1885.3559	1.25	15.88	0.06	1.37	0.49	16.99	16.96
1885.3997	1.26	15.86	0.06	1.40	0.52	16.93	16.90
1885.3636	1.24	15.87	0.06	1.39	0.51	16.95	16.92

Appendix B8.1-Continued

1	2	3	4	5	6	7	8
1886.3271	1.26	15.89	0.06	1.36	0.48	17.02	16.98
1886.3310	1.25	15.87	0.06	1.39	0.51	16.95	16.92
1886.3348	1.22	15.88	0.06	1.37	0.49	16.99	16.96
1886.3388	1.26	15.91	0.06	1.34	0.46	17.06	17.03
1887.4506	1.27	15.87	0.06	1.39	0.51	16.95	16.92
1887.4545	1.24	15.87	0.06	1.39	0.51	16.95	16.92
1887.4584	1.25	15.89	0.06	1.36	0.48	17.02	16.98
1888.4541	1.24	15.88	0.06	1.37	0.49	16.99	16.96
1888.4580	1.22	15.88	0.06	1.37	0.49	16.99	16.96
1888.4641	1.28	15.89	0.06	1.36	0.48	17.02	16.98
1888.4680	1.25	15.87	0.06	1.39	0.51	16.95	16.92
1900.3426	1.27	15.93	0.07	1.31	0.43	17.14	17.10
1900.3464	1.25	15.92	0.07	1.32	0.44	17.11	17.08
1900.3504	1.23	15.92	0.07	1.32	0.44	17.11	17.08
1900.3543	1.27	15.91	0.07	1.34	0.46	17.06	17.03
1905.2950	1.25	15.94	0.07	1.30	0.42	17.16	17.13
1905.2989	1.25	15.91	0.07	1.34	0.46	17.06	17.03
1905.3028	1.22	15.91	0.07	1.34	0.46	17.06	17.03
1905.3067	1.25	15.93	0.07	1.31	0.43	17.14	17.10
1907.4021	1.24	15.88	0.06	1.37	0.49	16.99	16.96
1907.4060	1.25	15.90	0.06	1.35	0.47	17.04	17.01
1907.4278	1.29	15.87	0.06	1.39	0.51	16.95	16.92
1907.4318	1.24	15.87	0.06	1.39	0.51	16.95	16.92
1907.4357	1.24	15.88	0.06	1.37	0.49	16.99	16.96
1909.2704	1.27	15.88	0.06	1.37	0.49	16.99	16.96
2088.6044	1.25	16.03	0.07	1.20	0.32	17.46	17.42
2088.6079	1.25	16.00	0.07	1.23	0.35	17.36	17.33
2088.6114	1.24	16.01	0.07	1.22	0.34	17.39	17.36
2088.6148	1.25	16.02	0.07	1.21	0.33	17.42	17.39
2088.6184	1.27	15.99	0.07	1.24	0.36	17.33	17.30
2088.6218	1.23	16.01	0.07	1.22	0.34	17.39	17.36
2125.5914	1.24	15.96	0.07	1.28	0.4	17.21	17.18
2125.5949	1.26	15.94	0.07	1.30	0.42	17.16	17.13
2125.5984	1.25	15.99	0.07	1.24	0.36	17.33	17.30
2125.6019	1.23	15.98	0.07	1.25	0.37	17.30	17.27
2145.5028	1.23	15.92	0.07	1.32	0.44	17.11	17.08
2145.5063	1.26	15.90	0.07	1.35	0.47	17.04	17.01
2145.5133	1.25	15.90	0.07	1.35	0.47	17.04	17.01
2146.4917	1.27	15.95	0.07	1.29	0.41	17.19	17.16
2146.4942	1.25	15.96	0.07	1.28	0.4	17.21	17.18
2146.4979	1.23	15.92	0.07	1.32	0.44	17.11	17.08

Appendix B8.1-Continued

1	2	3	4	5	6	7	8
2146.5012	1.22	15.93	0.07	1.31	0.43	17.14	17.10
2148.4292	1.24	15.94	0.07	1.30	0.42	17.16	17.13
2148.4327	1.26	15.91	0.07	1.34	0.46	17.06	17.03
2148.4343	1.25	15.92	0.07	1.32	0.44	17.11	17.08
2148.4362	1.27	15.92	0.07	1.32	0.44	17.11	17.08
2148.4397	1.25	15.91	0.07	1.34	0.46	17.06	17.03
2148.4432	1.26	15.93	0.07	1.31	0.43	17.14	17.10
2151.5053	1.24	15.93	0.07	1.31	0.43	17.14	17.10
2151.5087	1.26	15.90	0.07	1.35	0.47	17.04	17.01
2151.5123	1.25	15.92	0.07	1.32	0.44	17.11	17.08
2151.5157	1.22	15.91	0.07	1.34	0.46	17.06	17.03
2151.5192	1.26	15.91	0.07	1.34	0.46	17.06	17.03
2151.5227	1.27	15.90	0.07	1.35	0.47	17.04	17.01
2157.5550	1.24	15.87	0.07	1.39	0.51	16.95	16.92
2157.5585	1.25	15.90	0.07	1.35	0.47	17.04	17.01
2157.5620	1.24	15.89	0.07	1.36	0.48	17.02	16.98
2157.5644	1.22	15.91	0.07	1.34	0.46	17.06	17.03
2170.5716	1.28	15.94	0.07	1.30	0.42	17.16	17.13
2170.5750	1.25	15.91	0.07	1.34	0.46	17.06	17.03
2170.5785	1.27	15.91	0.07	1.34	0.46	17.06	17.03
2170.5820	1.25	15.93	0.07	1.31	0.43	17.14	17.10
2171.5131	1.23	15.88	0.07	1.37	0.49	16.99	16.96
2171.5152	1.27	15.88	0.07	1.37	0.49	16.99	16.96
2171.5173	1.25	15.90	0.07	1.35	0.47	17.04	17.01
2171.5215	1.25	15.88	0.07	1.37	0.49	16.99	16.96
2171.5236	1.22	15.87	0.07	1.39	0.51	16.95	16.92
2171.5272	1.25	15.89	0.07	1.36	0.48	17.02	16.98
2179.4514	1.24	15.91	0.07	1.34	0.46	17.06	17.03
2179.4535	1.25	15.88	0.07	1.37	0.49	16.99	16.96
2179.4556	1.29	15.88	0.07	1.37	0.49	16.99	16.96
2179.458	1.24	15.90	0.07	1.35	0.47	17.04	17.01
2180.3598	1.24	15.90	0.07	1.35	0.47	17.04	17.01
2180.3620	1.27	15.89	0.07	1.36	0.48	17.02	16.98
2180.3631	1.25	15.97	0.07	1.26	0.38	17.27	17.24
2180.3652	1.25	15.89	0.07	1.36	0.48	17.02	16.98
2181.5444	1.24	15.89	0.07	1.36	0.48	17.02	16.98
2181.5479	1.27	15.90	0.07	1.35	0.47	17.04	17.01
2181.5553	1.23	15.91	0.07	1.34	0.46	17.06	17.03
2198.3554	1.24	15.83	0.07	1.44	0.56	16.85	16.82
2198.3575	1.26	15.86	0.07	1.40	0.52	16.93	16.90
2198.3596	1.25	15.85	0.07	1.41	0.53	16.91	16.88

Appendix B8.1-Continued

1	2	3	4	5	6	7	8
2198.3613	1.23	15.85	0.07	1.41	0.53	16.91	16.88
2198.3635	1.23	15.84	0.07	1.43	0.55	16.87	16.84
2198.3656	1.26	15.86	0.07	1.40	0.52	16.93	16.90
2212.4346	1.28	15.87	0.07	1.39	0.51	16.95	16.92
2212.4381	1.25	15.84	0.07	1.43	0.55	16.87	16.84
2212.4416	1.27	15.84	0.07	1.43	0.55	16.87	16.84
2212.4450	1.25	15.84	0.07	1.43	0.55	16.87	16.84
2219.4099	1.23	15.86	0.07	1.40	0.52	16.93	16.90
2219.4120	1.22	15.85	0.07	1.41	0.53	16.91	16.88
2219.4141	1.24	15.86	0.07	1.40	0.52	16.93	16.90
2219.4162	1.26	15.87	0.07	1.39	0.51	16.95	16.92
2228.3040	1.25	15.82	0.07	1.45	0.57	16.83	16.80
2228.3075	1.27	15.85	0.07	1.41	0.53	16.91	16.88
2228.3110	1.25	15.84	0.07	1.43	0.55	16.87	16.84
2228.3145	1.26	15.86	0.07	1.40	0.52	16.93	16.90
2228.3180	1.26	15.85	0.07	1.41	0.53	16.91	16.88
2228.3215	1.24	15.84	0.07	1.43	0.55	16.87	16.84
2232.3443	1.27	15.85	0.07	1.41	0.53	16.91	16.88
2232.3477	1.27	15.82	0.07	1.45	0.57	16.83	16.80
2232.3513	1.29	15.83	0.07	1.44	0.56	16.85	16.82
2232.3547	1.27	15.84	0.07	1.43	0.55	16.87	16.84
2232.3582	1.26	15.83	0.07	1.44	0.56	16.85	16.82
2232.3623	1.29	15.86	0.07	1.40	0.52	16.93	16.90
2232.3652	1.27	15.84	0.07	1.43	0.55	16.87	16.84
2232.4368	1.27	15.85	0.07	1.41	0.53	16.91	16.88
2232.4401	1.26	15.82	0.07	1.45	0.57	16.83	16.80
2232.4443	1.26	15.85	0.07	1.41	0.53	16.91	16.88
2232.4482	1.25	15.82	0.07	1.41	0.53	16.91	16.88
2232.4553	1.26	15.84	0.07	1.43	0.55	16.87	16.84
2235.3189	1.26	15.83	0.07	1.44	0.56	16.85	16.82
2235.3224	1.24	15.83	0.07	1.44	0.56	16.85	16.82
2236.3169	1.22	15.81	0.07	1.47	0.59	16.79	16.76
2236.3205	1.26	15.84	0.07	1.43	0.55	16.87	16.84
2236.3240	1.26	15.82	0.07	1.45	0.57	16.83	16.80
2236.3275	1.28	15.82	0.07	1.45	0.57	16.83	16.80
2237.3428	1.24	15.80	0.07	1.48	0.6	16.77	16.74
2237.3463	1.24	15.81	0.07	1.47	0.59	16.79	16.76
2237.3500	1.25	15.82	0.07	1.45	0.57	16.83	16.80
2237.3532	1.26	15.80	0.07	1.48	0.6	16.77	16.74
2238.3537	1.24	15.84	0.07	1.43	0.55	16.87	16.84
2238.3572	1.27	15.85	0.07	1.41	0.53	16.91	16.88

Appendix B8.1-Continued

1	2	3	4	5	6	7	8
2238.3607	1.27	15.84	0.07	1.43	0.55	16.87	16.84
2238.3641	1.25	15.86	0.07	1.40	0.52	16.93	16.90
2239.3672	1.27	15.82	0.07	1.45	0.57	16.83	16.80
2239.3707	1.27	15.79	0.07	1.49	0.61	16.76	16.72
2239.3742	1.25	15.81	0.07	1.47	0.59	16.79	16.76
2239.3777	1.25	15.83	0.07	1.44	0.56	16.85	16.82
2239.2812	1.22	15.81	0.07	1.47	0.59	16.79	16.76
2239.285	1.25	15.82	0.07	1.45	0.57	16.83	16.80
2291.3240	1.24	15.92	0.07	1.32	0.44	17.11	17.08
2291.3281	1.25	15.92	0.07	1.32	0.44	17.11	17.08
2292.2633	1.27	15.99	0.07	1.24	0.36	17.33	17.30
2292.2660	1.24	15.98	0.07	1.25	0.37	17.30	17.27
2294.2668	1.24	15.97	0.07	1.26	0.38	17.27	17.24
2294.2711	1.27	15.99	0.07	1.24	0.36	17.33	17.30
2302.2602	1.25	16.01	0.07	1.22	0.34	17.39	17.36
2302.2643	1.25	16.02	0.07	1.21	0.33	17.42	17.39
2317.2721	1.24	16.01	0.07	1.22	0.34	17.39	17.36
2317.2749	1.25	16.00	0.07	1.23	0.35	17.36	17.33
2318.2733	1.24	15.99	0.07	1.24	0.36	17.33	17.30
2318.2762	1.23	15.97	0.07	1.26	0.38	17.27	17.24
2325.2723	1.24	15.99	0.07	1.24	0.36	17.33	17.30
2332.3021	1.26	15.98	0.07	1.25	0.37	17.30	17.27
2332.3060	1.25	16.00	0.07	1.23	0.35	17.36	17.33
2334.3422	1.23	15.97	0.07	1.26	0.38	17.27	17.24
2334.3451	1.23	15.97	0.07	1.26	0.38	17.27	17.24
2345.5237	1.26	15.97	0.07	1.26	0.38	17.27	17.24
2345.5282	1.28	15.94	0.07	1.30	0.42	17.16	17.13
2345.5313	1.25	15.98	0.07	1.25	0.37	17.30	17.27
2345.5354	1.27	15.97	0.07	1.26	0.38	17.27	17.24
2354.5151	1.25	15.89	0.07	1.36	0.48	17.02	16.98
2354.5192	1.23	15.87	0.07	1.39	0.51	16.95	16.92
2375.2122	1.22	15.95	0.07	1.29	0.41	17.19	17.16
2375.2164	1.24	15.96	0.07	1.28	0.40	17.21	17.18
2383.2133	1.26	15.91	0.07	1.34	0.46	17.06	17.03
2383.2172	1.23	15.91	0.07	1.34	0.46	17.06	17.03

B9.1 *R* Band Data of 1ES 1517+656

JD-2450000 (1)	Ref7-Ref6 (2)	<i>R</i> (3)	<i>R_d</i> (4)	Error (5)
497.6743	-	16.04	15.97	0.03
509.6617	-	16.11	16.04	0.03
512.5892	-	16.11	16.04	0.03
513.5613	-	16.08	16.01	0.03
517.6130	-	16.08	16.01	0.03
520.6658	-	16.08	16.01	0.03
525.5604	-	15.99	15.92	0.03
529.5289	-	16.00	15.93	0.03
536.5002	-	15.95	15.88	0.03
541.5087	-	16.05	15.98	0.03
548.6019	-	16.01	15.94	0.03
562.4509	-	16.10	16.03	0.03
569.5497	-	16.07	16.00	0.03
570.5409	-	16.04	15.97	0.03
577.4531	-	16.06	15.99	0.03
590.4812	-	16.10	16.03	0.05
598.4596	-	16.10	16.03	0.03
1660.481	0.17	16.16	16.09	0.08
1719.2921	0.15	16.11	16.04	0.07
2660.5496	0.13	16.24	16.17	0.07
2660.5578	0.12	16.19	16.12	0.07
2660.5610	0.14	16.21	16.14	0.07
2660.5675	0.19	16.18	16.11	0.07
2729.4959	0.22	16.26	16.19	0.07
2729.5006	0.18	16.18	16.11	0.07
2737.4977	0.20	16.26	16.19	0.06
2737.5022	0.21	16.27	16.20	0.06
2752.3576	0.18	16.18	16.11	0.07
2752.3623	0.15	16.24	16.17	0.07
2758.4676	0.16	16.20	16.13	0.07
2758.4718	0.19	16.27	16.20	0.07
2773.5143	0.16	16.26	16.19	0.08
2773.5188	0.22	16.23	16.16	0.08
2780.3630	0.16	16.23	16.16	0.07
2780.3670	0.18	16.27	16.20	0.07
2783.3381	0.17	16.37	16.30	0.07
2783.3429	0.15	16.38	16.31	0.08

Appendix B9.1-Continued

1	2	3	4	5
2788.4270	0.16	16.41	16.34	0.08
2788.4330	0.13	16.40	16.33	0.07
2794.4133	0.15	16.42	16.35	0.07
2794.4174	0.16	16.45	16.38	0.07
2812.3253	0.17	16.41	16.34	0.07
3025.5059	0.15	16.39	16.32	0.07
3025.5107	0.13	16.45	16.38	0.07
3059.5583	0.14	16.32	16.25	0.07
3059.5780	0.14	16.27	16.20	0.07
3149.3954	0.14	16.46	16.39	0.07
3149.4007	0.16	16.5	16.43	0.07
3168.4196	0.15	16.61	16.54	0.07
3168.4237	0.17	16.64	16.57	0.07
3195.3558	0.15	16.61	16.54	0.07
3195.3614	0.14	16.59	16.52	0.07
3199.3624	0.15	16.58	16.51	0.07
3199.3664	0.17	16.61	16.54	0.07
3206.3026	0.15	16.5	16.43	0.07
3206.3063	0.14	16.46	16.39	0.07
3231.3493	0.16	16.72	16.65	0.07
3231.3558	0.17	16.69	16.62	0.07
3238.2907	0.17	16.70	16.63	0.07
3238.2949	0.19	16.65	16.58	0.07
3250.2307	0.19	16.68	16.61	0.07
3250.2348	0.15	16.65	16.58	0.07
3259.2350	0.14	16.53	16.46	0.07
3259.2400	0.14	16.58	16.51	0.07
3263.2197	0.13	16.60	16.53	0.07
3263.2161	0.18	16.60	16.53	0.07
3267.3419	0.15	16.61	16.54	0.07
3267.3459	0.15	16.56	16.49	0.07
3303.5514	0.19	16.68	16.61	0.07
3384.6111	0.17	16.50	16.43	0.07
3387.3956	0.16	16.40	16.33	0.07
3387.3996	0.16	16.30	16.23	0.07
3406.5340	0.15	16.58	16.51	0.07
3406.5389	0.16	16.52	16.45	0.07
3559.3334	0.10	16.22	16.15	0.07
3559.3374	0.16	16.26	16.19	0.07
3582.3710	0.20	16.20	16.13	0.07
3582.3773	0.13	16.17	16.10	0.07

Appendix B9.1-Continued

1	2	3	4	5
3591.3859	0.18	16.22	16.15	0.07
3591.3901	0.15	16.26	16.19	0.07
3602.4101	0.14	16.28	16.21	0.07
3602.4143	0.13	16.25	16.18	0.07
3614.2882	0.13	16.20	16.13	0.07
3614.2921	0.13	16.24	16.17	0.07
3638.2003	0.11	16.33	16.26	0.07
3638.2043	0.15	16.41	16.34	0.07
3667.1926	0.12	16.23	16.16	0.07
3667.1965	0.11	16.21	16.14	0.07
3667.1926	0.11	16.27	16.20	0.07
3667.2043	0.13	16.29	16.22	0.07
3677.2501	0.14	16.17	16.10	0.07
3677.2541	0.13	16.23	16.16	0.07
3677.2580	0.14	16.22	16.15	0.07
3677.2619	0.22	16.21	16.14	0.07
3823.4276	0.20	16.03	15.96	0.07
3823.4315	0.18	16.00	15.93	0.07
3823.4354	0.17	16.04	15.97	0.07
3823.4393	0.18	16.03	15.96	0.07
3878.3585	0.13	16.08	16.01	0.07
3878.3626	0.19	16.00	15.93	0.07
3878.3665	0.21	16.06	15.99	0.07
3878.3704	0.19	15.96	15.89	0.07
3881.4436	0.14	15.96	15.89	0.06
3881.4475	0.18	16.04	15.97	0.06
3881.4514	0.13	16.01	15.94	0.06
3881.4553	0.09	16.03	15.96	0.06
3890.4781	0.19	15.92	15.85	0.06
3890.4820	0.10	15.89	15.82	0.06
3890.4859	0.18	15.84	15.77	0.06
3890.4898	0.16	15.89	15.82	0.06
3894.48000	0.15	15.91	15.84	0.06
3894.4782	0.18	15.89	15.82	0.06
3894.4917	0.13	15.87	15.80	0.06
3939.2960	0.14	16.12	16.05	0.06
3939.3000	0.16	16.03	15.96	0.06
3939.3039	0.15	16.08	16.01	0.06
3939.3078	0.15	16.00	15.93	0.06
3945.2827	0.13	16.21	16.14	0.07
3945.2862	0.17	16.26	16.19	0.07

Appendix B9.1-Continued

1	2	3	4	5
3945.2901	0.19	16.24	16.17	0.07
3945.2942	0.21	16.22	16.15	0.07
4226.3135	0.18	16.14	16.07	0.07
4226.3182	0.20	16.11	16.04	0.07
4226.3214	0.16	16.09	16.02	0.07
4226.3250	0.21	16.11	16.04	0.07
4325.3681	0.13	16.30	16.23	0.07
4325.3723	0.14	16.26	16.19	0.07
4332.3266	0.14	16.22	16.15	0.07
4332.3213	0.14	16.20	16.13	0.07
4332.3342	0.18	16.22	16.12	0.07
4332.3281	0.15	16.17	16.15	0.07
4332.3314	0.17	16.19	16.12	0.07
4332.3351	0.15	16.23	16.14	0.07
4332.3383	0.14	16.19	16.12	0.07
4332.3442	0.15	16.20	16.13	0.07
4332.3571	0.19	16.25	16.17	0.07
4332.3513	0.15	16.23	16.16	0.07
4345.6222	0.14	16.17	16.10	0.06
4345.6071	0.16	16.18	16.11	0.06
4345.6103	0.17	16.16	16.09	0.06
4345.6142	0.17	16.13	16.06	0.06
4345.6169	0.19	16.16	16.09	0.06
4345.6212	0.19	16.17	16.10	0.06
4345.624	0.15	16.19	16.12	0.06
4352.6012	0.14	16.28	16.21	0.06
4352.6051	0.14	16.25	16.18	0.06
4352.6083	0.13	16.27	16.20	0.06
4364.2990	0.18	16.27	16.20	0.06
4364.3031	0.15	16.26	16.19	0.06
4364.3065	0.15	16.27	16.20	0.06
4364.3104	0.19	16.25	16.18	0.06
4366.3671	0.17	16.28	16.21	0.06
4366.3703	0.12	16.26	16.19	0.06
4366.3773	0.19	16.24	16.17	0.06
4375.1943	0.22	16.28	16.21	0.06
4375.1982	0.18	16.26	16.19	0.06
4375.2013	0.20	16.24	16.17	0.06
4375.2054	0.21	16.27	16.20	0.06
4375.2083	0.18	16.23	16.16	0.06
4383.1962	0.15	16.22	16.15	0.06

Appendix B9.1-Continued

1	2	3	4	5
4383.2003	0.16	16.26	16.19	0.06
4383.2031	0.19	16.28	16.21	0.06
4391.3153	0.16	16.29	16.22	0.07
4391.3172	0.22	16.31	16.24	0.07
4391.3214	0.16	16.29	16.22	0.07
4391.3245	0.18	16.31	16.24	0.07

B9.2 Color Indices of 1ES 1517+656

JD-2450000 (1)	<i>V</i> (2)	<i>V-R</i> (3)	Error (4)	Comment (5)
520.67	16.43	0.35	0.03	Torino
570.45	16.38	0.34	0.03	Torino
1 660.48	16.52	0.36	0.10	Abastumani

B10.1 *R* Band Data of 1ES 1959+650

JD-2450000 (1)	Ref7-Ref4 (2)	<i>R</i> (3)	F (4)	<i>F_{corr}</i> (5)	<i>R_{hs}</i> (6)	<i>R_{hsd}</i> (7)
584.6119	0.70	14.59	4.51	2.81	15.10	14.63
665.5134	0.73	14.58	4.55	2.85	15.08	14.61
672.6659	0.73	14.63	4.35	2.65	15.16	14.69
1020.4440	0.71	14.64	4.31	2.61	15.18	14.71
1020.4527	0.70	14.66	4.23	2.53	15.21	14.74
1039.3061	0.69	14.67	4.19	2.49	15.23	14.76
1039.3147	0.71	14.68	4.15	2.45	15.25	14.77
1041.3964	0.74	14.66	4.23	2.53	15.21	14.74
1041.4048	0.73	14.68	4.15	2.45	15.25	14.77
1055.4056	0.71	14.46	5.08	3.38	14.90	14.42
1068.4006	0.73	14.36	5.57	3.87	14.75	14.28
1068.4021	0.72	14.38	5.47	3.77	14.78	14.31
1068.4036	0.72	14.42	5.27	3.57	14.84	14.37
1068.4051	0.68	14.38	5.47	3.77	14.78	14.31
1071.3497	0.70	14.34	5.67	3.97	14.72	14.25
1071.3582	0.73	14.36	5.57	3.87	14.75	14.28
1074.3587	0.74	14.40	5.37	3.67	14.81	14.34
1074.3673	0.74	14.35	5.62	3.92	14.74	14.26
1083.3213	0.73	14.44	5.18	3.48	14.87	14.39
1083.3297	0.74	14.47	5.04	3.34	14.91	14.44
1110.2560	0.73	14.36	5.57	3.87	14.75	14.28
1110.2639	0.73	14.33	5.73	4.03	14.71	14.23
1141.2124	0.71	14.48	4.99	3.29	14.93	14.45
1141.2202	0.72	14.50	4.90	3.2	14.96	14.48
1142.1468	0.74	14.41	5.32	3.62	14.82	14.35
1142.1549	0.68	14.41	5.32	3.62	14.82	14.35
1160.2318	0.69	14.47	5.04	3.34	14.91	14.44
1160.2400	0.76	14.46	5.08	3.38	14.90	14.42
1279.5142	0.69	14.45	5.13	3.43	14.88	14.41
1283.5232	0.69	14.50	4.90	3.2	14.96	14.48
1348.9161	0.74	14.44	5.18	3.48	14.87	14.39
1373.4292	0.70	14.51	4.85	3.15	14.97	14.50
1375.4848	0.75	14.43	5.23	3.53	14.85	14.38
1377.4324	0.72	14.43	5.23	3.53	14.85	14.38
1399.4406	0.71	14.52	4.81	3.11	14.99	14.52
1402.4810	0.7	14.49	4.94	3.24	14.94	14.47
1403.3272	0.68	14.48	4.99	3.29	14.93	14.45

Appendix B10.1-Continued

1	2	3	4	5	6	7
1405.4351	0.70	14.53	4.76	3.06	15.01	14.53
1407.4241	0.71	14.54	4.72	3.02	15.02	14.55
1410.4046	0.75	14.55	4.68	2.98	15.03	14.56
1412.4584	0.74	14.56	4.63	2.93	15.05	14.58
1433.2781	0.68	14.58	4.55	2.85	15.08	14.61
1438.4428	0.72	14.56	4.63	2.93	15.05	14.58
1439.3127	0.75	14.60	4.47	2.77	15.11	14.64
1439.3149	0.72	14.61	4.43	2.73	15.13	14.66
1439.3171	0.71	14.62	4.39	2.69	15.15	14.67
1439.3194	0.74	14.61	4.43	2.73	15.13	14.66
1439.3238	0.72	14.55	4.68	2.98	15.03	14.56
1439.3260	0.75	14.58	4.55	2.85	15.08	14.61
1439.3348	0.71	14.59	4.51	2.81	15.10	14.63
1439.3415	0.69	14.58	4.55	2.85	15.08	14.61
1439.3437	0.70	14.61	4.43	2.73	15.13	14.66
1439.3503	0.71	14.59	4.51	2.81	15.10	14.63
1439.3614	0.69	14.57	4.59	2.89	15.07	14.59
1439.3702	0.73	14.59	4.51	2.81	15.10	14.63
1439.3746	0.75	14.56	4.63	2.93	15.05	14.58
1439.3813	0.71	14.58	4.55	2.85	15.08	14.61
1439.3909	0.71	14.57	4.59	2.89	15.07	14.59
1439.3931	0.69	14.58	4.55	2.85	15.08	14.61
1439.3998	0.71	14.60	4.63	2.93	15.05	14.58
1439.4042	0.72	14.58	4.55	2.85	15.08	14.61
1440.2709	0.72	14.55	4.68	2.98	15.03	14.56
1440.2731	0.70	14.54	4.72	3.02	15.02	14.55
1440.2753	0.71	14.53	4.76	3.06	15.01	14.53
1440.2776	0.75	14.54	4.72	3.02	15.02	14.55
1440.2798	0.75	14.55	4.68	2.98	15.03	14.56
1440.2820	0.71	14.54	4.72	3.02	15.02	14.55
1440.2842	0.71	14.56	4.63	2.93	15.05	14.58
1440.2864	0.73	14.58	4.55	2.85	15.08	14.61
1440.2908	0.69	14.56	4.63	2.93	15.05	14.58
1440.2930	0.74	14.59	4.51	2.81	15.10	14.63
1440.2952	0.71	14.61	4.43	2.73	15.13	14.66
1440.2974	0.70	14.60	4.63	2.93	15.05	14.58
1440.2997	0.72	14.61	4.43	2.73	15.13	14.66
1440.3041	0.73	14.61	4.43	2.73	15.13	14.66
1440.3063	0.71	14.60	4.63	2.93	15.05	14.58
1440.3107	0.72	14.54	4.72	3.02	15.02	14.55
1440.3129	0.73	14.54	4.72	3.02	15.02	14.55

Appendix B10.1-Continued

1	2	3	4	5	6	7
1440.3151	0.74	14.56	4.63	2.93	15.05	14.58
1440.3173	0.75	14.55	4.68	2.98	15.03	14.56
1440.3195	0.74	14.56	4.63	2.93	15.05	14.58
1440.3217	0.75	14.59	4.51	2.81	15.10	14.63
1440.3240	0.73	14.58	4.55	2.85	15.08	14.61
1440.3262	0.74	14.59	4.51	2.81	15.10	14.63
1440.3284	0.72	14.55	4.68	2.98	15.03	14.56
1440.3306	0.73	14.60	4.63	2.93	15.05	14.58
1440.3438	0.72	14.57	4.59	2.89	15.07	14.59
1440.3723	0.71	14.60	4.63	2.93	15.05	14.58
1440.3811	0.69	14.57	4.59	2.89	15.07	14.59
1440.3833	0.73	14.59	4.51	2.81	15.10	14.63
1440.3855	0.72	14.55	4.68	2.98	15.03	14.56
1440.3878	0.74	14.58	4.55	2.85	15.08	14.61
1440.3900	0.70	14.56	4.63	2.93	15.05	14.58
1440.3922	0.74	14.59	4.51	2.81	15.10	14.63
1440.3944	0.7	14.56	4.63	2.93	15.05	14.58
1440.3966	0.74	14.58	4.55	2.85	15.08	14.61
1440.4010	0.68	14.55	4.68	2.98	15.03	14.56
1440.4032	0.73	14.57	4.59	2.89	15.07	14.59
1440.4054	0.74	14.59	4.51	2.81	15.10	14.63
1440.4076	0.73	14.58	4.55	2.85	15.08	14.61
1440.4099	0.69	14.55	4.68	2.98	15.03	14.56
1440.4121	0.67	14.55	4.68	2.98	15.03	14.56
1440.4143	0.65	14.57	4.59	2.89	15.07	14.59
1440.4165	0.69	14.58	4.55	2.85	15.08	14.61
1440.4209	0.67	14.59	4.51	2.81	15.10	14.63
1440.4231	0.66	14.58	4.55	2.85	15.08	14.61
1440.4253	0.68	14.59	4.51	2.81	15.10	14.63
1440.4275	0.71	14.57	4.59	2.89	15.07	14.59
1440.4298	0.73	14.59	4.51	2.81	15.10	14.63
1440.4320	0.74	14.57	4.59	2.89	15.07	14.59
1440.4342	0.74	14.59	4.51	2.81	15.10	14.63
1440.4364	0.70	14.55	4.68	2.98	15.03	14.56
1440.4408	0.74	14.58	4.55	2.85	15.08	14.61
1440.4430	0.74	14.59	4.51	2.81	15.10	14.63
1440.4452	0.72	14.55	4.68	2.98	15.03	14.56
1440.4474	0.69	14.57	4.59	2.89	15.07	14.59
1440.4496	0.71	14.56	4.63	2.93	15.05	14.58
1440.4541	0.75	14.58	4.55	2.85	15.08	14.61
1440.4463	0.71	14.57	4.59	2.89	15.07	14.59

Appendix B10.1-Continued

1	2	3	4	5	6	7
1452.2947	0.72	14.49	4.94	3.24	14.94	14.47
1455.2869	0.70	14.44	5.18	3.48	14.87	14.39
1455.2891	0.72	14.47	5.04	3.34	14.91	14.44
1455.2913	0.74	14.43	5.23	3.53	14.85	14.38
1455.2935	0.74	14.42	5.27	3.57	14.84	14.37
1455.2958	0.69	14.46	5.08	3.38	14.90	14.42
1455.2980	0.71	14.42	5.27	3.57	14.84	14.37
1455.3002	0.69	14.48	4.99	3.29	14.93	14.45
1455.3024	0.7	14.48	4.99	3.29	14.93	14.45
1455.3415	0.69	14.50	4.90	3.2	14.96	14.48
1455.3459	0.78	14.45	5.13	3.43	14.88	14.41
1455.3482	0.76	14.43	5.23	3.53	14.85	14.38
1455.3570	0.74	14.47	5.04	3.34	14.91	14.44
1455.3614	0.69	14.48	4.99	3.29	14.93	14.45
1455.3636	0.75	14.49	4.94	3.24	14.94	14.47
1455.3680	0.70	14.48	4.99	3.29	14.93	14.45
1455.3703	0.73	14.50	4.90	3.2	14.96	14.48
1455.3747	0.75	14.50	4.90	3.2	14.96	14.48
1455.3769	0.73	14.49	4.94	3.24	14.94	14.47
1455.3791	0.68	14.47	5.04	3.34	14.91	14.44
1455.3813	0.70	14.46	5.08	3.38	14.90	14.42
1455.3835	0.69	14.49	4.94	3.24	14.94	14.47
1455.3976	0.74	14.47	5.04	3.34	14.91	14.44
1455.3998	0.75	14.45	5.13	3.43	14.88	14.41
1458.3187	0.75	14.44	5.18	3.48	14.87	14.39
1461.2525	0.74	14.45	5.13	3.43	14.88	14.41
1466.3505	0.69	14.48	4.99	3.29	14.93	14.45
1485.3581	0.69	14.55	4.68	2.98	15.03	14.56
1493.4416	0.74	14.46	5.08	3.38	14.90	14.42
1585.6141	0.69	14.39	5.42	3.72	14.79	14.32
1589.5958	0.70	14.41	5.32	3.62	14.82	14.35
1693.4463	0.69	14.45	5.13	3.43	14.88	14.41
1699.4050	0.70	14.45	5.13	3.43	14.88	14.41
1719.3047	0.74	14.46	5.08	3.38	14.90	14.42
1719.3072	0.71	14.45	5.13	3.43	14.88	14.41
1719.3097	0.73	14.49	4.94	3.24	14.94	14.47
1719.3148	0.75	14.48	4.99	3.29	14.93	14.45
1719.3198	0.72	14.49	4.94	3.24	14.94	14.47
1719.3223	0.72	14.47	5.04	3.34	14.91	14.44
1719.3272	0.73	14.50	4.90	3.2	14.96	14.48
1719.3297	0.72	14.51	4.85	3.15	14.97	14.50

Appendix B10.1-Continued

1	2	3	4	5	6	7
1719.3347	0.73	14.47	5.04	3.34	14.91	14.44
1719.3372	0.73	14.48	4.99	3.29	14.93	14.45
1719.3402	0.69	14.48	4.99	3.29	14.93	14.45
1719.3673	0.71	14.49	4.94	3.24	14.94	14.47
1719.3722	0.68	14.50	4.90	3.2	14.96	14.48
1719.3747	0.70	14.46	5.08	3.38	14.90	14.42
1719.3772	0.68	14.50	4.90	3.2	14.96	14.48
1719.3797	0.70	14.49	4.94	3.24	14.94	14.47
1719.3822	0.69	14.50	4.90	3.2	14.96	14.48
1719.3847	0.70	14.50	4.90	3.2	14.96	14.48
1719.3873	0.72	14.48	4.99	3.29	14.93	14.45
1719.3972	0.75	14.45	5.13	3.43	14.88	14.41
1719.3997	0.71	14.46	5.08	3.38	14.90	14.42
1719.4722	0.72	14.50	4.90	3.2	14.96	14.48
1719.4871	0.73	14.50	4.90	3.2	14.96	14.48
1720.4207	0.71	14.46	5.08	3.38	14.90	14.42
1720.4282	0.73	14.49	4.94	3.24	14.94	14.47
1720.4432	0.69	14.50	4.90	3.2	14.96	14.48
1720.4507	0.74	14.48	4.99	3.29	14.93	14.45
1720.4607	0.74	14.46	5.08	3.38	14.90	14.42
1720.4632	0.73	14.46	5.08	3.38	14.90	14.42
1720.4657	0.71	14.47	5.04	3.34	14.91	14.44
1722.3540	0.76	14.45	5.13	3.43	14.88	14.41
1722.3565	0.75	14.44	5.18	3.48	14.87	14.39
1722.3590	0.76	14.46	5.08	3.38	14.90	14.42
1722.3616	0.74	14.45	5.13	3.43	14.88	14.41
1722.3641	0.75	14.44	5.18	3.48	14.87	14.39
1722.3666	0.73	14.44	5.18	3.48	14.87	14.39
1722.3691	0.73	14.45	5.13	3.43	14.88	14.41
1722.3716	0.73	14.46	5.08	3.38	14.90	14.42
1722.3765	0.73	14.48	4.99	3.29	14.93	14.45
1722.3790	0.75	14.47	5.04	3.34	14.91	14.44
1722.3815	0.71	14.46	5.08	3.38	14.90	14.42
1722.3841	0.70	14.46	5.08	3.38	14.90	14.42
1722.3866	0.69	14.45	5.13	3.43	14.88	14.41
1722.3891	0.72	14.44	5.18	3.48	14.87	14.39
1722.3916	0.72	14.44	5.18	3.48	14.87	14.39
1722.3941	0.72	14.43	5.23	3.53	14.85	14.38
1722.3990	0.70	14.44	5.18	3.48	14.87	14.39
1722.4015	0.71	14.44	5.18	3.48	14.87	14.39
1722.4040	0.72	14.44	5.18	3.48	14.87	14.39

Appendix B10.1-Continued

1	2	3	4	5	6	7
1722.4091	0.69	14.45	5.13	3.43	14.88	14.41
1722.4116	0.70	14.48	4.99	3.29	14.93	14.45
1722.4141	0.66	14.47	5.04	3.34	14.91	14.44
1722.4166	0.70	14.46	5.08	3.38	14.90	14.42
1722.4215	0.73	14.47	5.04	3.34	14.91	14.44
1722.4241	0.71	14.47	5.04	3.34	14.91	14.44
1722.4265	0.71	14.46	5.08	3.38	14.90	14.42
1722.4290	0.73	14.43	5.23	3.53	14.85	14.38
1722.4316	0.75	14.44	5.18	3.48	14.87	14.39
1722.4341	0.74	14.46	5.08	3.38	14.90	14.42
1722.4366	0.71	14.45	5.13	3.43	14.88	14.41
1722.4391	0.72	14.46	5.08	3.38	14.90	14.42
1722.4440	0.73	14.43	5.23	3.53	14.85	14.38
1722.4465	0.75	14.45	5.13	3.43	14.88	14.41
1722.4490	0.74	14.46	5.08	3.38	14.90	14.42
1722.4515	0.70	14.45	5.13	3.43	14.88	14.41
1722.4541	0.72	14.45	5.13	3.43	14.88	14.41
1722.4566	0.75	14.46	5.08	3.38	14.90	14.42
1722.5909	0.74	14.46	5.08	3.38	14.90	14.42
1722.4616	0.69	14.47	5.04	3.34	14.91	14.44
1722.4665	0.76	14.47	5.04	3.34	14.91	14.44
1722.4690	0.72	14.49	4.94	3.24	14.94	14.47
1722.4715	0.69	14.47	5.04	3.34	14.91	14.44
1722.4740	0.74	14.46	5.08	3.38	14.90	14.42
1722.4766	0.75	14.48	4.99	3.29	14.93	14.45
1722.4791	0.74	14.49	4.94	3.24	14.94	14.47
1722.4816	0.71	14.49	4.94	3.24	14.94	14.47
1722.4841	0.74	14.50	4.90	3.2	14.96	14.48
1722.4890	0.73	14.50	4.90	3.2	14.96	14.48
1722.4915	0.7	14.49	4.94	3.24	14.94	14.47
1722.4940	0.64	14.50	4.90	3.2	14.96	14.48
1722.4966	0.68	14.46	5.08	3.38	14.90	14.42
1722.4991	0.75	14.46	5.08	3.38	14.90	14.42
1722.5016	0.74	14.49	4.94	3.24	14.94	14.47
1722.5041	0.65	14.50	4.90	3.2	14.96	14.48
1722.5066	0.76	14.44	5.18	3.48	14.87	14.39
1722.5115	0.69	14.49	4.94	3.24	14.94	14.47
1722.5140	0.70	14.45	5.13	3.43	14.88	14.41
1725.3311	0.74	14.41	5.32	3.62	14.82	14.35
1725.3336	0.72	14.45	5.13	3.43	14.88	14.41
1725.3362	0.75	14.40	5.37	3.67	14.81	14.34

Appendix B10.1-Continued

1	2	3	4	5	6	7
1725.3412	0.74	14.39	5.42	3.72	14.79	14.32
1725.3437	0.77	14.42	5.27	3.57	14.84	14.37
1725.3462	0.73	14.42	5.27	3.57	14.84	14.37
1725.3488	0.73	14.42	5.27	3.57	14.84	14.37
1725.3536	0.74	14.43	5.23	3.53	14.85	14.38
1725.3561	0.72	14.45	5.13	3.43	14.88	14.41
1725.3586	0.73	14.45	5.13	3.43	14.88	14.41
1725.3612	0.73	14.46	5.08	3.38	14.90	14.42
1725.3637	0.72	14.46	5.08	3.38	14.90	14.42
1725.3562	0.72	14.46	5.08	3.38	14.90	14.42
1725.3587	0.71	14.44	5.18	3.48	14.87	14.39
1725.3712	0.74	14.46	5.08	3.38	14.90	14.42
1725.3761	0.71	14.45	5.13	3.43	14.88	14.41
1725.3786	0.69	14.42	5.27	3.57	14.84	14.37
1725.3811	0.70	14.41	5.32	3.62	14.82	14.35
1725.3837	0.75	14.42	5.27	3.57	14.84	14.37
1725.3862	0.75	14.43	5.23	3.53	14.85	14.38
1725.3882	0.74	14.45	5.13	3.43	14.88	14.41
1725.3912	0.72	14.46	5.08	3.38	14.90	14.42
1725.3937	0.68	14.44	5.18	3.48	14.87	14.39
1725.3986	0.72	14.44	5.18	3.48	14.87	14.39
1725.4011	0.71	14.46	5.08	3.38	14.90	14.42
1725.4036	0.70	14.45	5.13	3.43	14.88	14.41
1725.4061	0.71	14.44	5.18	3.48	14.87	14.39
1725.4087	0.69	14.44	5.18	3.48	14.87	14.39
1725.4112	0.70	14.46	5.08	3.38	14.90	14.42
1725.4137	0.73	14.46	5.08	3.38	14.90	14.42
1725.4162	0.76	14.41	5.32	3.62	14.82	14.35
1725.4211	0.72	14.45	5.13	3.43	14.88	14.41
1732.3379	0.75	14.49	4.94	3.24	14.94	14.47
1732.3404	0.77	14.46	5.08	3.38	14.90	14.42
1732.3429	0.75	14.50	4.90	3.2	14.96	14.48
1732.3505	0.73	14.46	5.08	3.38	14.90	14.42
1732.3530	0.72	14.47	5.04	3.34	14.91	14.44
1733.3498	0.71	14.43	5.23	3.53	14.85	14.38
1733.3524	0.73	14.45	5.13	3.43	14.88	14.41
1733.3549	0.72	14.44	5.18	3.48	14.87	14.39
1733.3574	0.74	14.44	5.18	3.48	14.87	14.39
1733.3599	0.73	14.45	5.13	3.43	14.88	14.41
1733.3624	0.73	14.45	5.13	3.43	14.88	14.41
1733.3649	0.69	14.45	5.13	3.43	14.88	14.41

Appendix B10.1-Continued

1	2	3	4	5	6	7
1733.3723	0.69	14.45	5.13	3.43	14.88	14.41
1733.3748	0.68	14.44	5.18	3.48	14.87	14.39
1733.3774	0.72	14.46	5.08	3.38	14.90	14.42
1733.3799	0.75	14.48	4.99	3.29	14.93	14.45
1733.3824	0.73	14.43	5.23	3.53	14.85	14.38
1733.3848	0.75	14.42	5.27	3.57	14.84	14.37
1733.3874	0.72	14.44	5.18	3.48	14.87	14.39
1733.3899	0.73	14.41	5.32	3.62	14.82	14.35
1733.3948	0.69	14.43	5.23	3.53	14.85	14.38
1733.3973	0.72	14.42	5.27	3.57	14.84	14.37
1733.3999	0.72	14.44	5.18	3.48	14.87	14.39
1733.4024	0.71	14.44	5.18	3.48	14.87	14.39
1733.4049	0.73	14.42	5.27	3.57	14.84	14.37
1733.4074	0.70	14.46	5.08	3.38	14.90	14.42
1733.4124	0.72	14.44	5.18	3.48	14.87	14.39
1733.4173	0.75	14.43	5.23	3.53	14.85	14.38
1733.4198	0.72	14.42	5.27	3.57	14.84	14.37
1733.4224	0.73	14.41	5.32	3.62	14.82	14.35
1733.4249	0.71	14.42	5.27	3.57	14.84	14.37
1733.4274	0.74	14.42	5.27	3.57	14.84	14.37
1733.4299	0.74	14.43	5.23	3.53	14.85	14.38
1733.4324	0.75	14.41	5.32	3.62	14.82	14.35
1733.4149	0.74	14.41	5.32	3.62	14.82	14.35
1733.4398	0.72	14.40	5.37	3.67	14.81	14.34
1733.4423	0.71	14.42	5.27	3.57	14.84	14.37
1734.3224	0.71	14.45	5.13	3.43	14.88	14.41
1734.3249	0.73	14.46	5.08	3.38	14.90	14.42
1734.3274	0.73	14.44	5.18	3.48	14.87	14.39
1734.3299	0.71	14.46	5.08	3.38	14.90	14.42
1734.3375	0.70	14.45	5.13	3.43	14.88	14.41
1734.3400	0.74	14.46	5.08	3.38	14.90	14.42
1734.3449	0.73	14.45	5.13	3.43	14.88	14.41
1734.3474	0.70	14.44	5.18	3.48	14.87	14.39
1734.3499	0.71	14.46	5.08	3.38	14.90	14.42
1734.3524	0.71	14.48	4.99	3.29	14.93	14.45
1734.3550	0.71	14.45	5.13	3.43	14.88	14.41
1734.3575	0.74	14.46	5.08	3.38	14.90	14.42
1734.3600	0.71	14.45	5.13	3.43	14.88	14.41
1734.3625	0.70	14.44	5.18	3.48	14.87	14.39
1734.3674	0.72	14.46	5.08	3.38	14.90	14.42
1734.3699	0.71	14.45	5.13	3.43	14.88	14.41

Appendix B10.1-Continued

1	2	3	4	5	6	7
1734.3725	0.74	14.48	4.99	3.29	14.93	14.45
1734.3749	0.72	14.47	5.04	3.34	14.91	14.44
1734.3775	0.73	14.46	5.08	3.38	14.90	14.42
1734.3800	0.73	14.45	5.13	3.43	14.88	14.41
1734.3825	0.72	14.45	5.13	3.43	14.88	14.41
1734.3850	0.73	14.42	5.27	3.57	14.84	14.37
1734.3899	0.72	14.45	5.13	3.43	14.88	14.41
1734.3924	0.72	14.44	5.18	3.48	14.87	14.39
1734.3949	0.73	14.42	5.27	3.57	14.84	14.37
1734.3974	0.73	14.45	5.13	3.43	14.88	14.41
1734.3999	0.74	14.46	5.08	3.38	14.90	14.42
1734.4025	0.74	14.45	5.13	3.43	14.88	14.41
1734.4050	0.73	14.44	5.18	3.48	14.87	14.39
1734.4075	0.72	14.44	5.18	3.48	14.87	14.39
1735.3245	0.73	14.45	5.13	3.43	14.88	14.41
1735.3271	0.73	14.46	5.08	3.38	14.90	14.42
1735.3296	0.75	14.47	5.04	3.34	14.91	14.44
1735.3321	0.72	14.47	5.04	3.34	14.91	14.44
1735.3346	0.71	14.47	5.04	3.34	14.91	14.44
1735.3371	0.73	14.49	4.94	3.24	14.94	14.47
1735.3396	0.73	14.49	4.94	3.24	14.94	14.47
1735.3422	0.74	14.47	5.04	3.34	14.91	14.44
1735.3470	0.74	14.48	4.99	3.29	14.93	14.45
1735.3496	0.71	14.46	5.08	3.38	14.90	14.42
1735.3521	0.72	14.43	5.23	3.53	14.85	14.38
1735.3546	0.70	14.43	5.23	3.53	14.85	14.38
1735.3571	0.70	14.44	5.18	3.48	14.87	14.39
1735.3796	0.74	14.42	5.27	3.57	14.84	14.37
1735.3621	0.73	14.44	5.18	3.48	14.87	14.39
1735.3646	0.71	14.43	5.23	3.53	14.85	14.38
1735.3695	0.73	14.42	5.27	3.57	14.84	14.37
1735.3720	0.75	14.40	5.37	3.67	14.81	14.34
1735.3746	0.73	14.43	5.23	3.53	14.85	14.38
1735.3768	0.71	14.44	5.18	3.48	14.87	14.39
1735.3796	0.73	14.45	5.13	3.43	14.88	14.41
1736.3278	0.75	14.43	5.23	3.53	14.85	14.38
1736.3303	0.72	14.43	5.23	3.53	14.85	14.38
1736.3328	0.71	14.46	5.08	3.38	14.90	14.42
1736.3353	0.71	14.43	5.23	3.53	14.85	14.38
1736.3379	0.72	14.43	5.23	3.53	14.85	14.38
1736.3404	0.72	14.44	5.18	3.48	14.87	14.39

Appendix B10.1-Continued

1	2	3	4	5	6	7
1736.3454	0.70	14.47	5.04	3.34	14.91	14.44
1736.3503	0.71	14.46	5.08	3.38	14.90	14.42
1736.3528	0.71	14.44	5.18	3.48	14.87	14.39
1736.3553	0.73	14.45	5.13	3.43	14.88	14.41
1736.3578	0.73	14.46	5.08	3.38	14.90	14.42
1736.3604	0.74	14.44	5.18	3.48	14.87	14.39
1736.3629	0.73	14.42	5.27	3.57	14.84	14.37
1736.3654	0.71	14.43	5.23	3.53	14.85	14.38
1736.3679	0.7	14.42	5.27	3.57	14.84	14.37
1736.3728	0.71	14.42	5.27	3.57	14.84	14.37
1736.3753	0.74	14.44	5.18	3.48	14.87	14.39
1736.3778	0.74	14.41	5.32	3.62	14.82	14.35
1736.3804	0.73	14.43	5.23	3.53	14.85	14.38
1736.3829	0.70	14.45	5.13	3.43	14.88	14.41
1736.3854	0.74	14.43	5.23	3.53	14.85	14.38
1736.3879	0.73	14.42	5.27	3.57	14.84	14.37
1736.3904	0.70	14.43	5.23	3.53	14.85	14.38
1736.3953	0.69	14.41	5.32	3.62	14.82	14.35
1736.3978	0.72	14.40	5.37	3.67	14.81	14.34
1736.4003	0.74	14.44	5.18	3.48	14.87	14.39
1736.4029	0.74	14.43	5.23	3.53	14.85	14.38
1736.4054	0.73	14.43	5.23	3.53	14.85	14.38
1736.4079	0.75	14.40	5.37	3.67	14.81	14.34
1736.4104	0.74	14.42	5.27	3.57	14.84	14.37
1736.4129	0.74	14.43	5.23	3.53	14.85	14.38
1738.4884	0.74	14.46	5.08	3.38	14.90	14.42
1779.4183	0.73	14.34	5.67	3.97	14.72	14.25
1786.3861	0.74	14.38	5.47	3.77	14.78	14.31
1790.4092	0.74	14.38	5.47	3.77	14.78	14.31
1792.3182	0.76	14.39	5.42	3.72	14.79	14.32
1833.2801	0.74	14.42	5.27	3.57	14.84	14.37
1833.2826	0.75	14.44	5.18	3.48	14.87	14.39
1833.2851	0.70	14.43	5.23	3.53	14.85	14.38
1833.2876	0.73	14.43	5.23	3.53	14.85	14.38
1833.2901	0.73	14.43	5.23	3.53	14.85	14.38
1833.2926	0.73	14.45	5.13	3.43	14.88	14.41
1833.2975	0.73	14.45	5.13	3.43	14.88	14.41
1833.3000	0.72	14.45	5.13	3.43	14.88	14.41
1833.4144	0.70	14.48	4.99	3.29	14.93	14.45
2113.2505	0.71	14.46	5.08	3.38	14.90	14.42
2113.2531	0.74	14.47	5.04	3.34	14.91	14.44

Appendix B10.1-Continued

1	2	3	4	5	6	7
2113.2581	0.74	14.46	5.08	3.38	14.90	14.42
2113.2630	0.72	14.47	5.04	3.34	14.91	14.44
2113.2656	0.73	14.46	5.08	3.38	14.90	14.42
2113.2681	0.75	14.49	4.94	3.24	14.94	14.47
2113.2706	0.72	14.50	4.90	3.2	14.96	14.48
2113.2755	0.71	14.48	4.99	3.29	14.93	14.45
2113.2780	0.73	14.49	4.94	3.24	14.94	14.47
2113.2806	0.73	14.49	4.94	3.24	14.94	14.47
2113.2831	0.75	14.47	5.04	3.34	14.91	14.44
2113.2877	0.72	14.48	4.99	3.29	14.93	14.45
2113.2905	0.71	14.49	4.94	3.24	14.94	14.47
2113.2931	0.73	14.48	4.99	3.29	14.93	14.45
2113.2956	0.71	14.47	5.04	3.34	14.91	14.44
2113.3005	0.70	14.46	5.08	3.38	14.90	14.42
2113.3030	0.74	14.50	4.90	3.2	14.96	14.48
2113.3055	0.74	14.48	4.99	3.29	14.93	14.45
2113.3080	0.71	14.48	4.99	3.29	14.93	14.45
2113.3130	0.71	14.50	4.90	3.2	14.96	14.48
2113.3155	0.69	14.48	4.99	3.29	14.93	14.45
2113.3180	0.72	14.47	5.04	3.34	14.91	14.44
2113.3206	0.73	14.47	5.04	3.34	14.91	14.44
2113.3255	0.75	14.49	4.94	3.24	14.94	14.47
2113.3280	0.72	14.51	4.85	3.15	14.97	14.50
2113.3305	0.69	14.48	4.99	3.29	14.93	14.45
2113.3330	0.70	14.52	4.81	3.11	14.99	14.52
2113.3379	0.73	14.49	4.94	3.24	14.94	14.47
2113.3405	0.72	14.51	4.85	3.15	14.97	14.50
2113.3430	0.74	14.46	5.08	3.38	14.90	14.42
2113.3455	0.76	14.47	5.04	3.34	14.91	14.44
2113.3504	0.75	14.49	4.94	3.24	14.94	14.47
2113.3530	0.73	14.48	4.99	3.29	14.93	14.45
2113.3555	0.71	14.47	5.04	3.34	14.91	14.44
2113.3580	0.71	14.49	4.94	3.24	14.94	14.47
2113.3629	0.70	14.46	5.08	3.38	14.90	14.42
2113.3654	0.68	14.46	5.08	3.38	14.90	14.42
2113.3680	0.73	14.47	5.04	3.34	14.91	14.44
2113.3705	0.70	14.50	4.90	3.2	14.96	14.48
2113.3754	0.69	14.47	5.04	3.34	14.91	14.44
2113.3779	0.69	14.47	5.04	3.34	14.91	14.44
2113.3805	0.72	14.47	5.04	3.34	14.91	14.44
2113.3830	0.75	14.49	4.94	3.24	14.94	14.47

Appendix B10.1-Continued

1	2	3	4	5	6	7
2113.3905	0.76	14.50	4.90	3.2	14.96	14.48
2113.3929	0.71	14.51	4.85	3.15	14.97	14.50
2113.3955	0.70	14.48	4.99	3.29	14.93	14.45
2114.2524	0.72	14.54	4.72	3.02	15.02	14.55
2114.2549	0.75	14.52	4.81	3.11	14.99	14.52
2114.2574	0.71	14.57	4.59	2.89	15.07	14.59
2114.2600	0.69	14.57	4.59	2.89	15.07	14.59
2114.2649	0.71	14.58	4.55	2.85	15.08	14.61
2114.2674	0.74	14.54	4.72	3.02	15.02	14.55
2114.2699	0.73	14.54	4.72	3.02	15.02	14.55
2114.2725	0.70	14.54	4.72	3.02	15.02	14.55
2114.2777	0.70	14.53	4.76	3.06	15.01	14.53
2114.2799	0.70	14.52	4.81	3.11	14.99	14.52
2114.2824	0.77	14.54	4.72	3.02	15.02	14.55
2114.2850	0.71	14.53	4.76	3.06	15.01	14.53
2114.2899	0.71	14.55	4.68	2.98	15.03	14.56
2114.2924	0.72	14.52	4.81	3.11	14.99	14.52
2114.2949	0.72	14.53	4.76	3.06	15.01	14.53
2114.2974	0.69	14.52	4.81	3.11	14.99	14.52
2114.3026	0.72	14.55	4.68	2.98	15.03	14.56
2114.3049	0.75	14.58	4.55	2.85	15.08	14.61
2114.3074	0.69	14.57	4.59	2.89	15.07	14.59
2114.3099	0.73	14.55	4.68	2.98	15.03	14.56
2114.3148	0.74	14.58	4.55	2.85	15.08	14.61
2114.3174	0.71	14.53	4.76	3.06	15.01	14.53
2114.3199	0.73	14.55	4.68	2.98	15.03	14.56
2114.3224	0.74	14.55	4.68	2.98	15.03	14.56
2114.3273	0.73	14.52	4.81	3.11	14.99	14.52
2114.3298	0.73	14.53	4.76	3.06	15.01	14.53
2114.3324	0.74	14.54	4.72	3.02	15.02	14.55
2114.3349	0.73	14.55	4.68	2.98	15.03	14.56
2114.3398	0.71	14.52	4.81	3.11	14.99	14.52
2114.3423	0.74	14.54	4.72	3.02	15.02	14.55
2114.3449	0.72	14.53	4.76	3.06	15.01	14.53
2114.3474	0.75	14.54	4.72	3.02	15.02	14.55
2114.3523	0.73	14.55	4.68	2.98	15.03	14.56
2114.3548	0.71	14.58	4.55	2.85	15.08	14.61
2114.3574	0.7	14.56	4.63	2.93	15.05	14.58
2114.3599	0.72	14.58	4.55	2.85	15.08	14.61
2114.3648	0.71	14.57	4.59	2.89	15.07	14.59
2114.3673	0.72	14.58	4.55	2.85	15.08	14.61

Appendix B10.1-Continued

1	2	3	4	5	6	7
2114.3724	0.75	14.56	4.63	2.93	15.05	14.58
2114.3773	0.74	14.56	4.63	2.93	15.05	14.58
2114.3798	0.76	14.56	4.63	2.93	15.05	14.58
2114.3823	0.73	14.54	4.72	3.02	15.02	14.55
2114.3849	0.73	14.56	4.63	2.93	15.05	14.58
2114.3898	0.68	14.54	4.72	3.02	15.02	14.55
2114.3923	0.67	14.55	4.68	2.98	15.03	14.56
2115.2421	0.7	14.54	4.72	3.02	15.02	14.55
2115.2446	0.7	14.56	4.63	2.93	15.05	14.58
2115.2472	0.72	14.55	4.68	2.98	15.03	14.56
2115.2497	0.72	14.57	4.59	2.89	15.07	14.59
2115.2546	0.71	14.53	4.76	3.06	15.01	14.53
2115.2571	0.76	14.51	4.85	3.15	14.97	14.50
2115.2597	0.75	14.51	4.85	3.15	14.97	14.50
2115.2622	0.75	14.51	4.85	3.15	14.97	14.50
2115.2671	0.72	14.53	4.76	3.06	15.01	14.53
2115.2696	0.74	14.53	4.76	3.06	15.01	14.53
2115.2721	0.74	14.54	4.72	3.02	15.02	14.55
2115.2747	0.73	14.53	4.76	3.06	15.01	14.53
2115.2794	0.73	14.54	4.72	3.02	15.02	14.55
2115.2820	0.75	14.53	4.76	3.06	15.01	14.53
2115.2846	0.73	14.57	4.59	2.89	15.07	14.59
2115.2872	0.7	14.54	4.72	3.02	15.02	14.55
2115.2921	0.75	14.55	4.68	2.98	15.03	14.56
2115.2946	0.71	14.55	4.68	2.98	15.03	14.56
2115.2971	0.7	14.55	4.68	2.98	15.03	14.56
2115.2996	0.69	14.54	4.72	3.02	15.02	14.55
2115.3045	0.75	14.55	4.68	2.98	15.03	14.56
2115.3071	0.73	14.53	4.76	3.06	15.01	14.53
2115.3096	0.73	14.54	4.72	3.02	15.02	14.55
2115.3114	0.75	14.55	4.68	2.98	15.03	14.56
2115.4180	0.72	14.54	4.72	3.02	15.02	14.55
2115.4229	0.72	14.58	4.55	2.85	15.08	14.61
2115.4254	0.69	14.57	4.59	2.89	15.07	14.59
2115.4279	0.73	14.55	4.68	2.98	15.03	14.56
2115.4305	0.69	14.56	4.63	2.93	15.05	14.58
2115.4354	0.70	14.54	4.72	3.02	15.02	14.55
2115.4379	0.69	14.57	4.59	2.89	15.07	14.59
2115.4404	0.70	14.53	4.76	3.06	15.01	14.53
2115.4429	0.71	14.55	4.68	2.98	15.03	14.56
2115.4478	0.69	14.57	4.59	2.89	15.07	14.59

Appendix B10.1-Continued

1	2	3	4	5	6	7
2115.4529	0.71	14.57	4.59	2.89	15.07	14.59
2115.5454	0.72	14.58	4.55	2.85	15.08	14.61
2115.4603	0.70	14.55	4.68	2.98	15.03	14.56
2115.4629	0.73	14.56	4.63	2.93	15.05	14.58
2115.4654	0.71	14.57	4.59	2.89	15.07	14.59
2115.4679	0.72	14.55	4.68	2.98	15.03	14.56
2115.4728	0.75	14.57	4.59	2.89	15.07	14.59
2115.4754	0.72	14.57	4.59	2.89	15.07	14.59
2115.4779	0.72	14.56	4.63	2.93	15.05	14.58
2115.4805	0.73	14.59	4.51	2.81	15.10	14.63
2116.2372	0.72	14.55	4.68	2.98	15.03	14.56
2116.2397	0.73	14.57	4.59	2.89	15.07	14.59
2116.2423	0.72	14.52	4.81	3.11	14.99	14.52
2116.2448	0.74	14.54	4.72	3.02	15.02	14.55
2116.2497	0.73	14.52	4.81	3.11	14.99	14.52
2116.2522	0.72	14.54	4.72	3.02	15.02	14.55
2116.2548	0.73	14.52	4.81	3.11	14.99	14.52
2116.2573	0.71	14.51	4.85	3.15	14.97	14.50
2116.2622	0.73	14.52	4.81	3.11	14.99	14.52
2116.2647	0.74	14.52	4.81	3.11	14.99	14.52
2116.2673	0.71	14.54	4.72	3.02	15.02	14.55
2116.2698	0.74	14.55	4.68	2.98	15.03	14.56
2116.2747	0.72	14.56	4.63	2.93	15.05	14.58
2116.2772	0.75	14.57	4.59	2.89	15.07	14.59
2116.2798	0.73	14.53	4.76	3.06	15.01	14.53
2116.2823	0.75	14.54	4.72	3.02	15.02	14.55
2116.2872	0.72	14.54	4.72	3.02	15.02	14.55
2116.2897	0.73	14.52	4.81	3.11	14.99	14.52
2116.2922	0.74	14.53	4.76	3.06	15.01	14.53
2116.2948	0.72	14.51	4.85	3.15	14.97	14.50
2116.2997	0.73	14.52	4.81	3.11	14.99	14.52
2116.3022	0.72	14.53	4.76	3.06	15.01	14.53
2116.3047	0.73	14.54	4.72	3.02	15.02	14.55
2116.3073	0.75	14.54	4.72	3.02	15.02	14.55
2116.4152	0.74	14.53	4.76	3.06	15.01	14.53
2116.4203	0.72	14.53	4.76	3.06	15.01	14.53
2116.4228	0.72	14.55	4.68	2.98	15.03	14.56
2116.4254	0.72	14.55	4.68	2.98	15.03	14.56
2116.4279	0.75	14.53	4.76	3.06	15.01	14.53
2116.4328	0.75	14.55	4.68	2.98	15.03	14.56
2116.4453	0.74	14.54	4.72	3.02	15.02	14.55

Appendix B10.1-Continued

1	2	3	4	5	6	7
2116.4503	0.72	14.54	4.72	3.02	15.02	14.55
2116.4529	0.71	14.53	4.76	3.06	15.01	14.53
2116.4578	0.72	14.54	4.72	3.02	15.02	14.55
2116.4603	0.71	14.54	4.72	3.02	15.02	14.55
2116.4628	0.71	14.52	4.81	3.11	14.99	14.52
2116.4654	0.72	14.56	4.63	2.93	15.05	14.58
2116.4703	0.73	14.57	4.59	2.89	15.07	14.59
2116.4728	0.75	14.56	4.63	2.93	15.05	14.58
2116.4753	0.74	14.55	4.68	2.98	15.03	14.56
2116.4779	0.75	14.57	4.59	2.89	15.07	14.59
2124.2708	0.72	14.49	4.94	3.24	14.94	14.47
2124.2734	0.72	14.53	4.76	3.06	15.01	14.53
2124.2759	0.73	14.49	4.94	3.24	14.94	14.47
2124.2788	0.71	14.53	4.76	3.06	15.01	14.53
2124.2833	0.72	14.52	4.81	3.11	14.99	14.52
2124.2859	0.72	14.53	4.76	3.06	15.01	14.53
2124.2884	0.71	14.54	4.72	3.02	15.02	14.55
2124.2910	0.72	14.51	4.85	3.15	14.97	14.50
2124.2958	0.72	14.54	4.72	3.02	15.02	14.55
2124.2984	0.74	14.50	4.90	3.2	14.96	14.48
2124.3009	0.74	14.51	4.85	3.15	14.97	14.50
2124.3035	0.7	14.50	4.90	3.2	14.96	14.48
2126.2599	0.73	14.51	4.85	3.15	14.97	14.50
2126.2624	0.72	14.55	4.68	2.98	15.03	14.56
2126.2649	0.73	14.53	4.76	3.06	15.01	14.53
2126.2675	0.75	14.53	4.76	3.06	15.01	14.53
2126.2724	0.72	14.52	4.81	3.11	14.99	14.52
2126.2749	0.75	14.52	4.81	3.11	14.99	14.52
2126.2774	0.73	14.53	4.76	3.06	15.01	14.53
2126.2800	0.72	14.56	4.63	2.93	15.05	14.58
2126.2849	0.72	14.52	4.81	3.11	14.99	14.52
2126.2874	0.73	14.51	4.85	3.15	14.97	14.50
2126.2899	0.72	14.56	4.63	2.93	15.05	14.58
2126.2925	0.71	14.53	4.76	3.06	15.01	14.53
2127.2376	0.72	14.49	4.94	3.24	14.94	14.47
2127.2401	0.72	14.50	4.90	3.2	14.96	14.48
2127.2451	0.71	14.47	5.04	3.34	14.91	14.44
2127.2501	0.73	14.50	4.90	3.2	14.96	14.48
2127.2526	0.72	14.53	4.76	3.06	15.01	14.53
2127.2551	0.69	14.50	4.90	3.2	14.96	14.48
2127.2577	0.69	14.48	4.99	3.29	14.93	14.45

Appendix B10.1-Continued

1	2	3	4	5	6	7
2127.2626	0.72	14.48	4.99	3.29	14.93	14.45
2127.2651	0.7	14.48	4.99	3.29	14.93	14.45
2127.2676	0.69	14.50	4.90	3.2	14.96	14.48
2127.2702	0.74	14.49	4.94	3.24	14.94	14.47
2127.2751	0.68	14.52	4.81	3.11	14.99	14.52
2127.2776	0.69	14.50	4.90	3.2	14.96	14.48
2127.2801	0.70	14.47	5.04	3.34	14.91	14.44
2127.2827	0.71	14.48	4.99	3.29	14.93	14.45
2127.2876	0.75	14.49	4.94	3.24	14.94	14.47
2127.2901	0.70	14.48	4.99	3.29	14.93	14.45
2127.2926	0.72	14.47	5.04	3.34	14.91	14.44
2127.2952	0.73	14.48	4.99	3.29	14.93	14.45
2127.3001	0.67	14.48	4.99	3.29	14.93	14.45
2127.3026	0.73	14.47	5.04	3.34	14.91	14.44
2127.3051	0.72	14.45	5.13	3.43	14.88	14.41
2127.3077	0.77	14.54	4.72	3.02	15.02	14.55
2127.4218	0.69	14.52	4.81	3.11	14.99	14.52
2127.4243	0.68	14.50	4.90	3.2	14.96	14.48
2127.4269	0.74	14.54	4.72	3.02	15.02	14.55
2127.4264	0.68	14.50	4.90	3.2	14.96	14.48
2127.4343	0.68	14.48	4.99	3.29	14.93	14.45
2127.4368	0.69	14.51	4.85	3.15	14.97	14.50
2127.4394	0.75	14.50	4.90	3.2	14.96	14.48
2127.4419	0.70	14.52	4.81	3.11	14.99	14.52
2127.4468	0.73	14.50	4.90	3.2	14.96	14.48
2127.4493	0.72	14.48	4.99	3.29	14.93	14.45
2127.4519	0.71	14.51	4.85	3.15	14.97	14.50
2127.4544	0.70	14.48	4.99	3.29	14.93	14.45
2127.4593	0.71	14.51	4.85	3.15	14.97	14.50
2127.4618	0.70	14.47	5.04	3.34	14.91	14.44
2127.4644	0.74	14.48	4.99	3.29	14.93	14.45
2127.4669	0.76	14.52	4.81	3.11	14.99	14.52
2127.4718	0.75	14.49	4.94	3.24	14.94	14.47
2127.4743	0.71	14.51	4.85	3.15	14.97	14.50
2127.4769	0.74	14.53	4.76	3.06	15.01	14.53
2127.4794	0.73	14.54	4.72	3.02	15.02	14.55
2131.2368	0.73	14.53	4.76	3.06	15.01	14.53
2131.2418	0.71	14.52	4.81	3.11	14.99	14.52
2131.2444	0.73	14.55	4.68	2.98	15.03	14.56
2131.2493	0.71	14.56	4.63	2.93	15.05	14.58
2131.2518	0.72	14.52	4.81	3.11	14.99	14.52

Appendix B10.1-Continued

1	2	3	4	5	6	7
2131.2543	0.71	14.52	4.81	3.11	14.99	14.52
2131.2643	0.74	14.51	4.85	3.15	14.97	14.50
2131.2668	0.72	14.50	4.90	3.2	14.96	14.48
2131.2693	0.74	14.53	4.76	3.06	15.01	14.53
2131.2742	0.70	14.52	4.81	3.11	14.99	14.52
2131.2767	0.73	14.53	4.76	3.06	15.01	14.53
2131.2793	0.71	14.53	4.76	3.06	15.01	14.53
2131.2817	0.72	14.52	4.81	3.11	14.99	14.52
2131.2867	0.70	14.55	4.68	2.98	15.03	14.56
2131.2892	0.71	14.54	4.72	3.02	15.02	14.55
2131.2917	0.73	14.53	4.76	3.06	15.01	14.53
2131.2943	0.74	14.54	4.72	3.02	15.02	14.55
2132.2439	0.72	14.51	4.85	3.15	14.97	14.50
2132.2464	0.70	14.49	4.94	3.24	14.94	14.47
2132.2489	0.69	14.50	4.90	3.2	14.96	14.48
2132.2515	0.69	14.53	4.76	3.06	15.01	14.53
2132.2564	0.71	14.53	4.76	3.06	15.01	14.53
2132.2589	0.70	14.52	4.81	3.11	14.99	14.52
2132.2614	0.71	14.54	4.72	3.02	15.02	14.55
2132.2640	0.70	14.56	4.63	2.93	15.05	14.58
2132.2688	0.69	14.55	4.68	2.98	15.03	14.56
2132.2714	0.74	14.54	4.72	3.02	15.02	14.55
2132.2739	0.75	14.55	4.68	2.98	15.03	14.56
2132.2764	0.75	14.53	4.76	3.06	15.01	14.53
2132.2813	0.73	14.52	4.81	3.11	14.99	14.52
2132.2839	0.75	14.53	4.76	3.06	15.01	14.53
2132.2864	0.75	14.55	4.68	2.98	15.03	14.56
2132.2889	0.74	14.55	4.68	2.98	15.03	14.56
2132.2938	0.72	14.54	4.72	3.02	15.02	14.55
2132.2963	0.75	14.51	4.85	3.15	14.97	14.50
2132.2989	0.75	14.52	4.81	3.11	14.99	14.52
2132.3014	0.72	14.50	4.90	3.2	14.96	14.48
2132.3063	0.71	14.51	4.85	3.15	14.97	14.50
2132.3088	0.72	14.50	4.90	3.2	14.96	14.48
2132.3114	0.71	14.52	4.81	3.11	14.99	14.52
2132.3137	0.74	14.50	4.90	3.2	14.96	14.48
2132.3188	0.72	14.52	4.81	3.11	14.99	14.52
2132.3213	0.73	14.52	4.81	3.11	14.99	14.52
2132.3238	0.72	14.51	4.85	3.15	14.97	14.50
2132.3264	0.74	14.54	4.72	3.02	15.02	14.55
2132.3314	0.75	14.55	4.68	2.98	15.03	14.56

Appendix B10.1-Continued

1	2	3	4	5	6	7
2132.4339	0.71	14.50	4.90	3.2	14.96	14.48
2132.4365	0.71	14.52	4.81	3.11	14.99	14.52
2132.4390	0.75	14.51	4.85	3.15	14.97	14.50
2132.4439	0.74	14.50	4.90	3.2	14.96	14.48
2132.4464	0.74	14.51	4.85	3.15	14.97	14.50
2132.4490	0.74	14.53	4.76	3.06	15.01	14.53
2132.4515	0.73	14.55	4.68	2.98	15.03	14.56
2132.4564	0.71	14.54	4.72	3.02	15.02	14.55
2132.4589	0.73	14.54	4.72	3.02	15.02	14.55
2132.4614	0.74	14.56	4.63	2.93	15.05	14.58
2132.4640	0.75	14.55	4.68	2.98	15.03	14.56
2132.4689	0.75	14.55	4.68	2.98	15.03	14.56
2132.4714	0.74	14.56	4.63	2.93	15.05	14.58
2132.4739	0.75	14.56	4.63	2.93	15.05	14.58
2132.4765	0.71	14.55	4.68	2.98	15.03	14.56
2132.4813	0.72	14.54	4.72	3.02	15.02	14.55
2132.4839	0.73	14.55	4.68	2.98	15.03	14.56
2132.4864	0.73	14.53	4.76	3.06	15.01	14.53
2132.4889	0.69	14.51	4.85	3.15	14.97	14.50
2132.4938	0.70	14.55	4.68	2.98	15.03	14.56
2132.4964	0.71	14.55	4.68	2.98	15.03	14.56
2132.4989	0.74	14.53	4.76	3.06	15.01	14.53
2132.5014	0.71	14.55	4.68	2.98	15.03	14.56
2133.2391	0.72	14.53	4.76	3.06	15.01	14.53
2133.2417	0.73	14.51	4.85	3.15	14.97	14.50
2133.2442	0.73	14.50	4.90	3.2	14.96	14.48
2133.2467	0.71	14.49	4.94	3.24	14.94	14.47
2133.2516	0.73	14.50	4.90	3.2	14.96	14.48
2133.2541	0.75	14.49	4.94	3.24	14.94	14.47
2133.2567	0.71	14.49	4.94	3.24	14.94	14.47
2133.2592	0.71	14.50	4.90	3.2	14.96	14.48
2133.2526	0.73	14.49	4.94	3.24	14.94	14.47
2133.2666	0.69	14.49	4.94	3.24	14.94	14.47
2133.2692	0.71	14.48	4.99	3.29	14.93	14.45
2133.2717	0.70	14.51	4.85	3.15	14.97	14.50
2133.2766	0.71	14.48	4.99	3.29	14.93	14.45
2133.2791	0.71	14.48	4.99	3.29	14.93	14.45
2133.2816	0.70	14.49	4.94	3.24	14.94	14.47
2133.2842	0.71	14.47	5.04	3.34	14.91	14.44
2133.2891	0.72	14.48	4.99	3.29	14.93	14.45
2133.2941	0.69	14.50	4.90	3.2	14.96	14.48

Appendix B10.1-Continued

1	2	3	4	5	6	7
2133.2967	0.72	14.47	5.04	3.34	14.91	14.44
2133.3016	0.69	14.54	4.72	3.02	15.02	14.55
2133.3041	0.72	14.49	4.94	3.24	14.94	14.47
2133.3067	0.75	14.52	4.81	3.11	14.99	14.52
2133.3091	0.72	14.50	4.90	3.2	14.96	14.48
2133.4062	0.69	14.50	4.90	3.2	14.96	14.48
2133.4088	0.74	14.48	4.99	3.29	14.93	14.45
2133.4113	0.73	14.48	4.99	3.29	14.93	14.45
2133.4138	0.71	14.50	4.90	3.2	14.96	14.48
2133.4187	0.71	14.51	4.85	3.15	14.97	14.50
2133.4212	0.7	14.48	4.99	3.29	14.93	14.45
2133.4238	0.71	14.52	4.81	3.11	14.99	14.52
2133.4263	0.73	14.49	4.94	3.24	14.94	14.47
2133.4312	0.69	14.51	4.85	3.15	14.97	14.50
2133.4337	0.68	14.54	4.72	3.02	15.02	14.55
2133.4362	0.73	14.51	4.85	3.15	14.97	14.50
2133.4388	0.71	14.50	4.90	3.2	14.96	14.48
2133.4437	0.72	14.51	4.85	3.15	14.97	14.50
2133.4462	0.71	14.52	4.81	3.11	14.99	14.52
2133.4487	0.71	14.53	4.76	3.06	15.01	14.53
2133.4512	0.70	14.51	4.85	3.15	14.97	14.50
2133.4561	0.72	14.51	4.85	3.15	14.97	14.50
2133.4589	0.74	14.51	4.85	3.15	14.97	14.50
2133.4612	0.69	14.53	4.76	3.06	15.01	14.53
2133.4637	0.71	14.52	4.81	3.11	14.99	14.52
2133.4686	0.74	14.53	4.76	3.06	15.01	14.53
2134.2308	0.73	14.49	4.94	3.24	14.94	14.47
2134.2333	0.71	14.48	4.99	3.29	14.93	14.45
2134.2358	0.71	14.49	4.94	3.24	14.94	14.47
2134.2384	0.70	14.46	5.08	3.38	14.90	14.42
2134.2433	0.69	14.48	4.99	3.29	14.93	14.45
2134.2458	0.70	14.51	4.85	3.15	14.97	14.50
2134.2483	0.73	14.51	4.85	3.15	14.97	14.50
2134.2508	0.74	14.48	4.99	3.29	14.93	14.45
2138.2429	0.75	14.48	4.99	3.29	14.93	14.45
2142.2241	0.73	14.51	4.85	3.15	14.97	14.50
2142.2266	0.73	14.49	4.94	3.24	14.94	14.47
2142.2291	0.73	14.48	4.99	3.29	14.93	14.45
2142.2316	0.73	14.48	4.99	3.29	14.93	14.45
2142.2366	0.74	14.52	4.81	3.11	14.99	14.52
2142.2416	0.69	14.50	4.90	3.2	14.96	14.48

Appendix B10.1-Continued

1	2	3	4	5	6	7
2142.2441	0.71	14.51	4.85	3.15	14.97	14.50
2142.2490	0.72	14.51	4.85	3.15	14.97	14.50
2142.2516	0.74	14.51	4.85	3.15	14.97	14.50
2142.2541	0.71	14.49	4.94	3.24	14.94	14.47
2142.2566	0.73	14.49	4.94	3.24	14.94	14.47
2142.2615	0.71	14.47	5.04	3.34	14.91	14.44
2142.2640	0.71	14.49	4.94	3.24	14.94	14.47
2142.2666	0.73	14.51	4.85	3.15	14.97	14.50
2142.2691	0.72	14.49	4.94	3.24	14.94	14.47
2142.2740	0.71	14.49	4.94	3.24	14.94	14.47
2150.3502	0.72	14.52	4.81	3.11	14.99	14.52
2150.3527	0.71	14.51	4.85	3.15	14.97	14.50
2150.3553	0.74	14.50	4.90	3.2	14.96	14.48
2150.3578	0.71	14.47	5.04	3.34	14.91	14.44
2150.3627	0.73	14.48	4.99	3.29	14.93	14.45
2150.3652	0.71	14.52	4.81	3.11	14.99	14.52
2150.3678	0.70	14.51	4.85	3.15	14.97	14.50
2150.3703	0.72	14.49	4.94	3.24	14.94	14.47
2150.3752	0.72	14.50	4.90	3.2	14.96	14.48
2150.3777	0.73	14.47	5.04	3.34	14.91	14.44
2150.3802	0.74	14.51	4.85	3.15	14.97	14.50
2150.3828	0.72	14.49	4.94	3.24	14.94	14.47
2150.3877	0.75	14.46	5.08	3.38	14.90	14.42
2150.3902	0.71	14.50	4.90	3.2	14.96	14.48
2150.3927	0.74	14.49	4.94	3.24	14.94	14.47
2150.3953	0.72	14.51	4.85	3.15	14.97	14.50
2150.4002	0.73	14.49	4.94	3.24	14.94	14.47
2150.4027	0.74	14.48	4.99	3.29	14.93	14.45
2150.4052	0.72	14.51	4.85	3.15	14.97	14.50
2150.4077	0.73	14.49	4.94	3.24	14.94	14.47
2150.4126	0.74	14.50	4.90	3.2	14.96	14.48
2150.4152	0.75	14.49	4.94	3.24	14.94	14.47
2150.4177	0.73	14.47	5.04	3.34	14.91	14.44
2150.4202	0.73	14.47	5.04	3.34	14.91	14.44
2150.4251	0.74	14.47	5.04	3.34	14.91	14.44
2150.4276	0.75	14.46	5.08	3.38	14.90	14.42
2164.2650	0.71	14.37	5.52	3.82	14.76	14.29
2164.2676	0.71	14.40	5.37	3.67	14.81	14.34
2164.2701	0.73	14.43	5.23	3.53	14.85	14.38
2164.2726	0.74	14.37	5.52	3.82	14.76	14.29
2164.2775	0.72	14.39	5.42	3.72	14.79	14.32

Appendix B10.1-Continued

1	2	3	4	5	6	7
2164.2826	0.76	14.41	5.32	3.62	14.82	14.35
2164.2851	0.73	14.44	5.18	3.48	14.87	14.39
2164.2900	0.72	14.43	5.23	3.53	14.85	14.38
2164.2925	0.73	14.39	5.42	3.72	14.79	14.32
2164.2951	0.74	14.41	5.32	3.62	14.82	14.35
2164.2976	0.77	14.42	5.27	3.57	14.84	14.37
2164.3025	0.78	14.43	5.23	3.53	14.85	14.38
2164.3050	0.73	14.42	5.27	3.57	14.84	14.37
2164.3076	0.75	14.40	5.37	3.67	14.81	14.34
2164.3101	0.74	14.37	5.52	3.82	14.76	14.29
2164.3150	0.71	14.44	5.18	3.48	14.87	14.39
2164.3175	0.75	14.43	5.23	3.53	14.85	14.38
2164.3200	0.73	14.44	5.18	3.48	14.87	14.39
2164.3226	0.73	14.41	5.32	3.62	14.82	14.35
2164.3275	0.75	14.40	5.37	3.67	14.81	14.34
2164.3300	0.73	14.40	5.37	3.67	14.81	14.34
2164.3325	0.75	14.39	5.42	3.72	14.79	14.32
2164.3351	0.73	14.40	5.37	3.67	14.81	14.34
2164.3399	0.7	14.42	5.27	3.57	14.84	14.37
2164.3425	0.71	14.41	5.32	3.62	14.82	14.35
2164.3450	0.76	14.42	5.27	3.57	14.84	14.37
2164.3475	0.72	14.41	5.32	3.62	14.82	14.35
2164.3524	0.75	14.45	5.13	3.43	14.88	14.41
2164.3550	0.74	14.42	5.27	3.57	14.84	14.37
2164.3575	0.72	14.44	5.18	3.48	14.87	14.39
2164.3600	0.76	14.41	5.32	3.62	14.82	14.35
2164.3649	0.73	14.42	5.27	3.57	14.84	14.37
2164.3674	0.74	14.40	5.37	3.67	14.81	14.34
2164.3700	0.72	14.41	5.32	3.62	14.82	14.35
2164.3725	0.68	14.39	5.42	3.72	14.79	14.32
2164.3774	0.74	14.38	5.47	3.77	14.78	14.31
2164.3799	0.72	14.38	5.47	3.77	14.78	14.31
2164.3824	0.69	14.37	5.52	3.82	14.76	14.29
2164.3850	0.71	14.39	5.42	3.72	14.79	14.32
2164.4056	0.75	14.40	5.37	3.67	14.81	14.34
2164.4081	0.7	14.41	5.32	3.62	14.82	14.35
2164.4107	0.74	14.41	5.32	3.62	14.82	14.35
2172.4565	0.72	14.44	5.18	3.48	14.87	14.39
2192.2965	0.76	14.35	5.62	3.92	14.74	14.26
2206.3536	0.75	14.33	5.73	4.03	14.71	14.23
2224.2298	0.74	14.36	5.57	3.87	14.75	14.28

Appendix B10.1-Continued

1	2	3	4	5	6	7
2415.3243	0.73	14.81	3.68	1.98	15.48	15.01
2415.4042	0.75	14.78	3.78	2.08	15.42	14.95
2415.4970	0.73	14.78	3.78	2.08	15.42	14.95
2415.5009	0.72	14.79	3.75	2.05	15.44	14.97
2415.5049	0.73	14.77	3.82	2.12	15.40	14.93
2416.3857	0.73	14.74	3.93	2.23	15.35	14.88
2416.3897	0.72	14.75	3.89	2.19	15.37	14.90
2416.3976	0.7	14.74	3.93	2.23	15.35	14.88
2416.4094	0.70	14.75	3.89	2.19	15.37	14.90
2416.4133	0.69	14.73	3.96	2.26	15.33	14.86
2416.4173	0.72	14.75	3.89	2.19	15.37	14.90
2416.4219	0.73	14.75	3.89	2.19	15.37	14.90
2416.4251	0.71	14.75	3.89	2.19	15.37	14.90
2416.4291	0.71	14.74	3.93	2.23	15.35	14.88
2416.4330	0.72	14.75	3.89	2.19	15.37	14.90
2416.4369	0.73	14.73	3.96	2.26	15.33	14.86
2416.4409	0.73	14.74	3.93	2.23	15.35	14.88
2416.4448	0.71	14.73	3.96	2.26	15.33	14.86
2416.4488	0.74	14.73	3.96	2.26	15.33	14.86
2417.3162	0.69	14.78	3.78	2.08	15.42	14.95
2417.3202	0.70	14.80	3.71	2.01	15.46	14.99
2417.3241	0.68	14.77	3.82	2.12	15.40	14.93
2417.3280	0.70	14.81	3.68	1.98	15.48	15.01
2417.3319	0.68	14.82	3.65	1.95	15.49	15.02
2417.3358	0.70	14.78	3.78	2.08	15.42	14.95
2417.3398	0.68	14.82	3.65	1.95	15.49	15.02
2417.3437	0.73	14.78	3.78	2.08	15.42	14.95
2417.3514	0.70	14.80	3.71	2.01	15.46	14.99
2417.3553	0.70	14.80	3.71	2.01	15.46	14.99
2417.3592	0.73	14.79	3.75	2.05	15.44	14.97
2417.4432	0.71	14.83	3.61	1.91	15.52	15.04
2417.4471	0.73	14.77	3.82	2.12	15.40	14.93
2417.4511	0.71	14.77	3.82	2.12	15.40	14.93
2417.4550	0.73	14.80	3.71	2.01	15.46	14.99
2417.4590	0.72	14.79	3.75	2.05	15.44	14.97
2417.4629	0.71	14.82	3.65	1.95	15.49	15.02
2417.4669	0.73	14.80	3.71	2.01	15.46	14.99
2417.4708	0.69	14.78	3.78	2.08	15.42	14.95
2417.4787	0.73	14.78	3.78	2.08	15.42	14.95
2417.4826	0.71	14.79	3.75	2.05	15.44	14.97
2417.4866	0.72	14.83	3.61	1.91	15.52	15.04

Appendix B10.1-Continued

1	2	3	4	5	6	7
2429.5025	0.75	14.80	3.71	2.01	15.46	14.99
2429.3686	0.77	14.81	3.68	1.98	15.48	15.01
2429.3723	0.73	14.77	3.82	2.12	15.40	14.93
2429.3802	0.76	14.79	3.75	2.05	15.44	14.97
2429.3841	0.75	14.79	3.75	2.05	15.44	14.97
2430.3867	0.74	14.84	3.58	1.88	15.53	15.06
2430.3907	0.75	14.78	3.78	2.08	15.42	14.95
2430.3947	0.74	14.78	3.78	2.08	15.42	14.95
2430.3986	0.79	14.80	3.71	2.01	15.46	14.99
2430.4024	0.77	14.80	3.71	2.01	15.46	14.99
2433.2635	0.78	14.81	3.68	1.98	15.48	15.01
2433.2667	0.77	14.77	3.82	2.12	15.40	14.93
2433.2699	0.77	14.79	3.75	2.05	15.44	14.97
2433.2732	0.78	14.79	3.75	2.05	15.44	14.97
2433.2764	0.74	14.84	3.58	1.88	15.53	15.06
2433.2796	0.73	14.78	3.78	2.08	15.42	14.95
2433.2828	0.74	14.78	3.78	2.08	15.42	14.95
2434.3213	0.73	14.80	3.71	2.01	15.46	14.99
2434.4080	0.73	14.80	3.71	2.01	15.46	14.99
2434.4890	0.73	14.78	3.78	2.08	15.42	14.95
2434.4929	0.74	14.79	3.75	2.05	15.44	14.97
2435.3407	0.75	14.80	3.71	2.01	15.46	14.99
2435.3446	0.73	14.81	3.68	1.98	15.48	15.01
2435.3486	0.74	14.77	3.82	2.12	15.40	14.93
2435.3525	0.74	14.79	3.75	2.05	15.44	14.97
2435.3936	0.75	14.79	3.75	2.05	15.44	14.97
2435.3975	0.72	14.83	3.61	1.91	15.52	15.04
2435.4014	0.74	14.78	3.78	2.08	15.42	14.95
2435.4054	0.72	14.78	3.78	2.08	15.42	14.95
2435.4130	0.72	14.80	3.71	2.01	15.46	14.99
2435.4957	0.73	14.80	3.71	2.01	15.46	14.99
2436.3486	0.75	14.80	3.71	2.01	15.46	14.99
2436.3524	0.72	14.77	3.82	2.12	15.40	14.93
2436.3565	0.74	14.76	3.85	2.15	15.39	14.92
2436.3605	0.76	14.77	3.82	2.12	15.40	14.93
2436.4358	0.73	14.77	3.82	2.12	15.40	14.93
2436.4398	0.73	14.76	3.85	2.15	15.39	14.92
2436.4437	0.75	14.77	3.82	2.12	15.40	14.93
2436.5034	0.70	14.75	3.89	2.19	15.37	14.90
2436.5074	0.71	14.80	3.71	2.01	15.46	14.99
2437.4664	0.73	14.78	3.78	2.08	15.42	14.95

Appendix B10.1-Continued

1	2	3	4	5	6	7
2437.4686	0.75	14.73	3.96	2.26	15.33	14.86
2437.4726	0.75	14.74	3.93	2.23	15.35	14.88
2437.4805	0.75	14.76	3.85	2.15	15.39	14.92
2437.4865	0.70	14.75	3.89	2.19	15.37	14.90
2439.3080	0.73	14.78	3.78	2.08	15.42	14.95
2439.3120	0.72	14.73	3.96	2.26	15.33	14.86
2439.3160	0.74	14.74	3.93	2.23	15.35	14.88
2439.3199	0.72	14.76	3.85	2.15	15.39	14.92
2439.3239	0.75	14.75	3.89	2.19	15.37	14.90
2439.3278	0.72	14.76	3.85	2.15	15.39	14.92
2439.3937	0.75	14.74	3.93	2.23	15.35	14.88
2439.4017	0.71	14.75	3.89	2.19	15.37	14.90
2439.4056	0.72	14.75	3.89	2.19	15.37	14.90
2439.4095	0.71	14.76	3.85	2.15	15.39	14.92
2445.3653	0.73	14.71	4.04	2.34	15.30	14.82
2445.3688	0.71	14.74	3.93	2.23	15.35	14.88
2445.3728	0.72	14.73	3.96	2.26	15.33	14.86
2445.3767	0.73	14.74	3.93	2.23	15.35	14.88
2445.4475	0.73	14.71	4.04	2.34	15.30	14.82
2445.4515	0.72	14.73	3.96	2.26	15.33	14.86
2445.4554	0.74	14.69	4.11	2.41	15.27	14.79
2445.4594	0.75	14.71	4.04	2.34	15.30	14.82
2447.2800	0.75	14.73	3.96	2.26	15.33	14.86
2447.2839	0.71	14.71	4.04	2.34	15.30	14.82
2447.2918	0.72	14.69	4.11	2.41	15.27	14.79
2447.2958	0.71	14.69	4.11	2.41	15.27	14.79
2447.2997	0.75	14.72	4.00	2.3	15.32	14.84
2447.3037	0.75	14.69	4.11	2.41	15.27	14.79
2448.3071	0.76	14.66	4.23	2.53	15.21	14.74
2448.3110	0.75	14.67	4.19	2.49	15.23	14.76
2448.3149	0.72	14.71	4.04	2.34	15.30	14.82
2448.3188	0.73	14.67	4.19	2.49	15.23	14.76
2448.4312	0.73	14.70	4.08	2.38	15.28	14.81
2448.4351	0.71	14.70	4.08	2.38	15.28	14.81
2448.4390	0.7	14.66	4.23	2.53	15.21	14.74
2448.4429	0.71	14.68	4.15	2.45	15.25	14.77
2457.3789	0.72	14.73	3.96	2.26	15.33	14.86
2457.3829	0.72	14.75	3.89	2.19	15.37	14.90
2457.3868	0.69	14.74	3.93	2.23	15.35	14.88
2457.3908	0.69	14.77	3.82	2.12	15.40	14.93
2461.4348	0.73	14.76	3.85	2.15	15.39	14.92

Appendix B10.1-Continued

1	2	3	4	5	6	7
2461.4427	0.75	14.74	3.93	2.23	15.35	14.88
2461.4466	0.72	14.77	3.82	2.12	15.40	14.93
2462.3161	0.75	14.68	4.15	2.45	15.25	14.77
2462.3201	0.75	14.67	4.19	2.49	15.23	14.76
2462.3240	0.71	14.71	4.04	2.34	15.30	14.82
2462.3279	0.72	14.68	4.15	2.45	15.25	14.77
2463.3876	0.71	14.73	3.96	2.26	15.33	14.86
2463.3901	0.71	14.69	4.11	2.41	15.27	14.79
2463.3927	0.73	14.70	4.08	2.38	15.28	14.81
2463.3952	0.74	14.72	4.00	2.3	15.32	14.84
2463.3977	0.72	14.73	3.96	2.26	15.33	14.86
2463.4002	0.73	14.69	4.11	2.41	15.27	14.79
2463.4028	0.73	14.71	4.04	2.34	15.30	14.82
2463.4053	0.73	14.72	4.00	2.3	15.32	14.84
2463.5129	0.71	14.72	4.00	2.3	15.32	14.84
2463.5154	0.73	14.73	3.96	2.26	15.33	14.86
2463.5179	0.75	14.72	4.00	2.3	15.32	14.84
2463.5205	0.74	14.71	4.04	2.34	15.30	14.82
2463.5230	0.73	14.73	3.96	2.26	15.33	14.86
2475.4629	0.71	14.79	3.75	2.05	15.44	14.97
2475.4654	0.72	14.77	3.82	2.12	15.40	14.93
2483.2848	0.68	14.72	4.00	2.3	15.32	14.84
2483.2883	0.71	14.73	3.96	2.26	15.33	14.86
2489.5247	0.72	14.73	3.96	2.26	15.33	14.86
2489.5272	0.73	14.70	4.08	2.38	15.28	14.81
2491.4815	0.74	14.72	4.00	2.3	15.32	14.84
2505.4593	0.71	14.67	4.19	2.49	15.23	14.76
2505.4636	0.75	14.68	4.15	2.45	15.25	14.77
2507.5288	0.71	14.56	4.63	2.93	15.05	14.58
2511.2315	0.70	14.63	4.35	2.65	15.16	14.69
2511.2358	0.71	14.63	4.35	2.65	15.16	14.69
2517.3238	0.69	14.61	4.43	2.73	15.13	14.66
2519.2378	0.72	14.64	4.31	2.61	15.18	14.71
2519.2418	0.72	14.66	4.23	2.53	15.21	14.74
2519.2457	0.69	14.67	4.19	2.49	15.23	14.76
2519.2497	0.70	14.65	4.27	2.57	15.20	14.72
2519.2536	0.70	14.68	4.15	2.45	15.25	14.77
2519.2615	0.72	14.64	4.31	2.61	15.18	14.71
2519.2655	0.69	14.64	4.31	2.61	15.18	14.71
2520.2598	0.72	14.65	4.27	2.57	15.20	14.72
2520.2638	0.72	14.67	4.19	2.49	15.23	14.76

Appendix B10.1-Continued

1	2	3	4	5	6	7
2520.2677	0.70	14.66	4.23	2.53	15.21	14.74
2520.2717	0.73	14.67	4.19	2.49	15.23	14.76
2520.2756	0.69	14.64	4.31	2.61	15.18	14.71
2522.3644	0.75	14.62	4.39	2.69	15.15	14.67
2522.3684	0.74	14.64	4.31	2.61	15.18	14.71
2522.3723	0.72	14.61	4.43	2.73	15.13	14.66
2522.3763	0.73	14.62	4.39	2.69	15.15	14.67
2522.3802	0.70	14.61	4.43	2.73	15.13	14.66
2522.3842	0.73	14.62	4.39	2.69	15.15	14.67
2522.3882	0.69	14.63	4.35	2.65	15.16	14.69
2522.3921	0.73	14.63	4.35	2.65	15.16	14.69
2524.2804	0.72	14.64	4.31	2.61	15.18	14.71
2524.2844	0.71	14.66	4.23	2.53	15.21	14.74
2524.2883	0.73	14.66	4.23	2.53	15.21	14.74
2524.2962	0.75	14.64	4.31	2.61	15.18	14.71
2524.3002	0.74	14.65	4.27	2.57	15.20	14.72
2524.3041	0.73	14.64	4.31	2.61	15.18	14.71
2524.3080	0.75	14.64	4.31	2.61	15.18	14.71
2531.4485	0.74	14.57	4.59	2.89	15.07	14.59
2531.4525	0.69	14.56	4.63	2.93	15.05	14.58
2531.4564	0.72	14.55	4.68	2.98	15.03	14.56
2531.4604	0.74	14.59	4.51	2.81	15.10	14.63
2531.4647	0.72	14.57	4.59	2.89	15.07	14.59
2531.4687	0.71	14.58	4.55	2.85	15.08	14.61
2531.4726	0.73	14.56	4.63	2.93	15.05	14.58
2531.4765	0.72	14.57	4.59	2.89	15.07	14.59
2532.4673	0.73	14.55	4.68	2.98	15.03	14.56
2532.4716	0.73	14.54	4.72	3.02	15.02	14.55
2532.4758	0.70	14.56	4.63	2.93	15.05	14.58
2532.4799	0.71	14.54	4.72	3.02	15.02	14.55
2532.4908	0.72	14.52	4.81	3.11	14.99	14.52
2532.4948	0.73	14.52	4.81	3.11	14.99	14.52
2532.4988	0.72	14.54	4.72	3.02	15.02	14.55
2532.5027	0.74	14.53	4.76	3.06	15.01	14.53
2534.2820	0.73	14.57	4.59	2.89	15.07	14.59
2534.2859	0.74	14.60	4.63	2.93	15.05	14.58
2543.3019	0.73	14.63	4.35	2.65	15.16	14.69
2543.3055	0.73	14.60	4.63	2.93	15.05	14.58
2543.3095	0.72	14.61	4.43	2.73	15.13	14.66
2543.3134	0.72	14.60	4.63	2.93	15.05	14.58
2547.2478	0.74	14.63	4.35	2.65	15.16	14.69

Appendix B10.1-Continued

1	2	3	4	5	6	7
2547.3594	0.75	14.60	4.63	2.93	15.05	14.58
2547.2633	0.79	14.61	4.43	2.73	15.13	14.66
2549.2196	0.77	14.62	4.39	2.69	15.15	14.67
2549.2314	0.76	14.59	4.51	2.81	15.10	14.63
2552.3379	0.74	14.55	4.68	2.98	15.03	14.56
2552.3419	0.73	14.57	4.59	2.89	15.07	14.59
2552.3458	0.72	14.56	4.63	2.93	15.05	14.58
2552.3498	0.73	14.60	4.63	2.93	15.05	14.58
2553.3321	0.73	14.56	4.63	2.93	15.05	14.58
2553.3389	0.71	14.55	4.68	2.98	15.03	14.56
2553.3436	0.71	14.57	4.59	2.89	15.07	14.59
2553.3479	0.71	14.56	4.63	2.93	15.05	14.58
2554.2318	0.73	14.53	4.76	3.06	15.01	14.53
2554.2359	0.73	14.52	4.81	3.11	14.99	14.52
2557.2320	0.71	14.58	4.55	2.85	15.08	14.61
2557.2399	0.70	14.59	4.51	2.81	15.10	14.63
2557.2439	0.73	14.59	4.51	2.81	15.10	14.63
2557.2478	0.70	14.59	4.51	2.81	15.10	14.63
2557.2512	0.72	14.56	4.63	2.93	15.05	14.58
2557.2551	0.72	14.58	4.55	2.85	15.08	14.61
2558.2298	0.74	14.57	4.59	2.89	15.07	14.59
2558.2377	0.73	14.60	4.63	2.93	15.05	14.58
2558.2417	0.74	14.58	4.55	2.85	15.08	14.61
2558.3997	0.71	14.57	4.59	2.89	15.07	14.59
2558.4036	0.71	14.61	4.43	2.73	15.13	14.66
2558.4076	0.70	14.60	4.63	2.93	15.05	14.58
2558.4115	0.73	14.59	4.51	2.81	15.10	14.63
2559.3230	0.73	14.61	4.43	2.73	15.13	14.66
2559.3269	0.72	14.63	4.35	2.65	15.16	14.69
2559.3308	0.74	14.61	4.43	2.73	15.13	14.66
2559.3348	0.71	14.60	4.63	2.93	15.05	14.58
2560.3104	0.74	14.58	4.55	2.85	15.08	14.61
2560.3223	0.73	14.60	4.63	2.93	15.05	14.58
2561.4020	0.71	14.62	4.39	2.69	15.15	14.67
2561.4060	0.72	14.62	4.39	2.69	15.15	14.67
2561.4099	0.73	14.59	4.51	2.81	15.10	14.63
2561.4139	0.70	14.61	4.43	2.73	15.13	14.66
2562.4374	0.70	14.60	4.63	2.93	15.05	14.58
2562.4414	0.71	14.58	4.55	2.85	15.08	14.61
2562.4492	0.71	14.57	4.59	2.89	15.07	14.59
2576.2991	0.71	14.52	4.81	3.11	14.99	14.52

Appendix B10.1-Continued

1	2	3	4	5	6	7
2576.3030	0.71	14.49	4.94	3.24	14.94	14.47
2576.3069	0.73	14.49	4.94	3.24	14.94	14.47
2576.3109	0.73	14.52	4.81	3.11	14.99	14.52
2576.3148	0.73	14.52	4.81	3.11	14.99	14.52
2576.3186	0.73	14.49	4.94	3.24	14.94	14.47
2581.3169	0.72	14.54	4.72	3.02	15.02	14.55
2581.3206	0.75	14.56	4.63	2.93	15.05	14.58
2581.3248	0.72	14.53	4.76	3.06	15.01	14.53
2581.3287	0.71	14.56	4.63	2.93	15.05	14.58
2582.2505	0.72	14.45	5.13	3.43	14.88	14.41
2582.2551	0.75	14.46	5.08	3.38	14.90	14.42
2582.2596	0.74	14.46	5.08	3.38	14.90	14.42
2584.1905	0.69	14.47	5.04	3.34	14.91	14.44
2584.1944	0.73	14.45	5.13	3.43	14.88	14.41
2584.1988	0.72	14.44	5.18	3.48	14.87	14.39
2584.2023	0.71	14.45	5.13	3.43	14.88	14.41
2588.3202	0.72	14.50	4.90	3.2	14.96	14.48
2588.3242	0.74	14.47	5.04	3.34	14.91	14.44
2588.3281	0.70	14.50	4.90	3.2	14.96	14.48
2588.3320	0.71	14.50	4.90	3.2	14.96	14.48
2610.3515	0.71	14.59	4.51	2.81	15.10	14.63
2610.3562	0.68	14.57	4.59	2.89	15.07	14.59
2610.3608	0.70	14.57	4.59	2.89	15.07	14.59
2661.5835	0.70	14.75	3.89	2.19	15.37	14.90
2661.5969	0.71	14.73	3.96	2.26	15.33	14.86
2661.6023	0.77	14.75	3.89	2.19	15.37	14.90
2662.6097	0.69	14.74	3.93	2.23	15.35	14.88
2662.6164	0.73	14.75	3.89	2.19	15.37	14.90
2662.6258	0.71	14.72	4.00	2.3	15.32	14.84
2670.6234	0.73	14.66	4.23	2.53	15.21	14.74
2670.6312	0.72	14.66	4.23	2.53	15.21	14.74
2675.1767	0.76	14.66	4.23	2.53	15.21	14.74
2675.1806	0.7	14.64	4.31	2.61	15.18	14.71
2675.6123	0.72	14.67	4.19	2.49	15.23	14.76
2678.6069	0.75	14.68	4.15	2.45	15.25	14.77
2678.6107	0.78	14.67	4.19	2.49	15.23	14.76
2699.5421	0.76	14.62	4.39	2.69	15.15	14.67
2699.5460	0.74	14.63	4.35	2.65	15.16	14.69
2704.5770	0.70	14.59	4.51	2.81	15.10	14.63
2704.5817	0.74	14.59	4.51	2.81	15.10	14.63
2727.5660	0.71	14.62	4.39	2.69	15.15	14.67

Appendix B10.1-Continued

1	2	3	4	5	6	7
2727.5686	0.72	14.59	4.51	2.81	15.10	14.63
2730.5356	0.73	14.65	4.27	2.57	15.20	14.72
2730.5401	0.72	14.66	4.23	2.53	15.21	14.74
2736.5345	0.72	14.71	4.04	2.34	15.30	14.82
2736.5390	0.69	14.69	4.11	2.41	15.27	14.79
2741.5684	0.68	14.71	4.04	2.34	15.30	14.82
2751.4067	0.69	14.71	4.04	2.34	15.30	14.82
2751.4121	0.73	14.68	4.15	2.45	15.25	14.77
2768.5410	0.72	14.56	4.63	2.93	15.05	14.58
2769.4778	0.74	14.53	4.76	3.06	15.01	14.53
2769.4819	0.77	14.54	4.72	3.02	15.02	14.55
2770.4566	0.71	14.58	4.55	2.85	15.08	14.61
2772.3717	0.71	14.60	4.63	2.93	15.05	14.58
2772.3756	0.68	14.58	4.55	2.85	15.08	14.61
2772.3795	0.75	14.61	4.43	2.73	15.13	14.66
2772.3834	0.75	14.57	4.59	2.89	15.07	14.59
2780.3898	0.72	14.59	4.51	2.81	15.10	14.63
2780.3998	0.73	14.56	4.63	2.93	15.05	14.58
2783.3676	0.69	14.60	4.63	2.93	15.05	14.58
2783.3720	0.72	14.57	4.59	2.89	15.07	14.59
2792.5133	0.75	14.57	4.59	2.89	15.07	14.59
2792.5166	0.75	14.54	4.72	3.02	15.02	14.55
2798.4424	0.72	14.57	4.59	2.89	15.07	14.59
2798.4465	0.70	14.55	4.68	2.98	15.03	14.56
2799.4721	0.72	14.56	4.63	2.93	15.05	14.58
2799.4768	0.74	14.53	4.76	3.06	15.01	14.53
2800.4555	0.72	14.57	4.59	2.89	15.07	14.59
2800.4594	0.70	14.59	4.51	2.81	15.10	14.63
2806.2677	0.72	14.58	4.55	2.85	15.08	14.61
2806.2719	0.72	14.59	4.51	2.81	15.10	14.63
2809.2739	0.74	14.55	4.68	2.98	15.03	14.56
2809.2778	0.73	14.55	4.68	2.98	15.03	14.56
2810.3426	0.72	14.53	4.76	3.06	15.01	14.53
2816.4128	0.70	14.56	4.63	2.93	15.05	14.58
2816.4158	0.70	14.58	4.55	2.85	15.08	14.61
2817.3977	0.74	14.56	4.63	2.93	15.05	14.58
2817.4017	0.75	14.54	4.72	3.02	15.02	14.55
2832.5073	0.73	14.47	5.04	3.34	14.91	14.44
2832.5119	0.75	14.50	4.90	3.2	14.96	14.48
2847.2886	0.70	14.38	5.47	3.77	14.78	14.31
2847.2925	0.73	14.38	5.47	3.77	14.78	14.31

Appendix B10.1-Continued

1	2	3	4	5	6	7
2854.7046	0.69	14.44	5.18	3.48	14.87	14.39
2854.7087	0.71	14.38	5.47	3.77	14.78	14.31
2859.4887	0.71	14.47	5.04	3.34	14.91	14.44
2859.4926	0.75	14.50	4.90	3.2	14.96	14.48
2859.4965	0.74	14.50	4.90	3.2	14.96	14.48
2860.4939	0.75	14.47	5.04	3.34	14.91	14.44
2860.4988	0.74	14.49	4.94	3.24	14.94	14.47
2872.3986	0.74	14.51	4.85	3.15	14.97	14.50
2872.4015	0.72	14.53	4.76	3.06	15.01	14.53
2876.4413	0.71	14.57	4.59	2.89	15.07	14.59
2876.4439	0.73	14.58	4.55	2.85	15.08	14.61
2886.4112	0.74	14.65	4.27	2.57	15.20	14.72
2886.4137	0.75	14.68	4.15	2.45	15.25	14.77
2904.2541	0.75	14.62	4.39	2.69	15.15	14.67
2904.2607	0.75	14.59	4.51	2.81	15.10	14.63
2906.3046	0.74	14.59	4.51	2.81	15.10	14.63
2906.3093	0.73	14.62	4.39	2.69	15.15	14.67
2907.2713	0.72	14.57	4.59	2.89	15.07	14.59
2907.2740	0.75	14.54	4.72	3.02	15.02	14.55
2908.2454	0.70	14.61	4.43	2.73	15.13	14.66
2908.2500	0.73	14.59	4.51	2.81	15.10	14.63
2909.5046	0.69	14.52	4.81	3.11	14.99	14.52
2909.5072	0.71	14.52	4.81	3.11	14.99	14.52
2912.3419	0.70	14.62	4.39	2.69	15.15	14.67
2912.3466	0.72	14.65	4.27	2.57	15.20	14.72
2913.3820	0.73	14.52	4.81	3.11	14.99	14.52
2913.3847	0.71	14.54	4.72	3.02	15.02	14.55
2918.4065	0.75	14.61	4.43	2.73	15.13	14.66
2918.4100	0.75	14.60	4.63	2.93	15.05	14.58
2919.3009	0.73	14.55	4.68	2.98	15.03	14.56
2919.3137	0.75	14.58	4.55	2.85	15.08	14.61
2934.3444	0.71	14.54	4.72	3.02	15.02	14.55
2934.3484	0.75	14.57	4.59	2.89	15.07	14.59
2934.3562	0.73	14.58	4.55	2.85	15.08	14.61
2936.1760	0.75	14.61	4.43	2.73	15.13	14.66
2968.2317	0.73	14.70	4.08	2.38	15.28	14.81
2968.2362	0.70	14.67	4.19	2.49	15.23	14.76
2996.6107	0.71	14.67	4.19	2.49	15.23	14.76
2996.6147	0.71	14.68	4.15	2.45	15.25	14.77
2997.6381	0.73	14.68	4.15	2.45	15.25	14.77
3024.6195	0.75	14.79	3.75	2.05	15.44	14.97

Appendix B10.1-Continued

1	2	3	4	5	6	7
3024.6240	0.75	14.77	3.82	2.12	15.40	14.93
3026.6195	0.74	14.80	3.71	2.01	15.46	14.99
3026.6240	0.75	14.81	3.68	1.98	15.48	15.01
3033.6176	0.69	14.81	3.68	1.98	15.48	15.01
3033.6220	0.70	14.80	3.71	2.01	15.46	14.99
3050.5884	0.75	14.82	3.65	1.95	15.49	15.02
3050.5929	0.72	14.80	3.71	2.01	15.46	14.99
3084.5424	0.74	14.78	3.78	2.08	15.42	14.95
3084.5467	0.71	14.81	3.68	1.98	15.48	15.01
3122.4862	0.72	14.74	3.93	2.23	15.35	14.88
3122.4908	0.73	14.72	4.00	2.3	15.32	14.84
3122.4947	0.72	14.75	3.89	2.19	15.37	14.90
3124.5049	0.71	14.73	3.96	2.26	15.33	14.86
3124.5090	0.71	14.74	3.93	2.23	15.35	14.88
3137.4949	0.74	14.70	4.08	2.38	15.28	14.81
3137.5032	0.72	14.66	4.23	2.53	15.21	14.74
3137.5077	0.72	14.67	4.19	2.49	15.23	14.76
3170.4134	0.72	14.72	4.00	2.3	15.32	14.84
3170.4176	0.73	14.74	3.93	2.23	15.35	14.88
3172.4763	0.74	14.70	4.08	2.38	15.28	14.81
3172.4804	0.73	14.73	3.96	2.26	15.33	14.86
3193.3344	0.71	14.77	3.82	2.12	15.40	14.93
3193.3392	0.69	14.75	3.89	2.19	15.37	14.90
3195.3730	0.72	14.76	3.85	2.15	15.39	14.92
3195.3774	0.73	14.78	3.78	2.08	15.42	14.95
3199.4418	0.71	14.72	4.00	2.3	15.32	14.84
3199.4446	0.73	14.75	3.89	2.19	15.37	14.90
3209.4639	0.73	14.74	3.93	2.23	15.35	14.88
3209.4678	0.73	14.76	3.85	2.15	15.39	14.92
3209.4756	0.73	14.73	3.96	2.26	15.33	14.86
3225.3375	0.72	14.63	4.35	2.65	15.16	14.69
3225.3416	0.74	14.66	4.23	2.53	15.21	14.74
3228.2980	0.75	14.69	4.11	2.41	15.27	14.79
3235.3209	0.74	14.73	3.96	2.26	15.33	14.86
3235.3250	0.72	14.76	3.85	2.15	15.39	14.92
3237.4051	0.73	14.73	3.96	2.26	15.33	14.86
3237.4091	0.72	14.75	3.89	2.19	15.37	14.90
3241.3533	0.74	14.73	3.96	2.26	15.33	14.86
3256.4003	0.74	14.75	3.89	2.19	15.37	14.90
3256.4043	0.75	14.72	4.00	2.3	15.32	14.84
3262.3125	0.72	14.72	4.00	2.3	15.32	14.84

Appendix B10.1-Continued

1	2	3	4	5	6	7
3262.3174	0.72	14.69	4.11	2.41	15.27	14.79
3265.2855	0.71	14.61	4.43	2.73	15.13	14.66
3265.2910	0.74	14.61	4.43	2.73	15.13	14.66
3268.3106	0.75	14.67	4.19	2.49	15.23	14.76
3268.3151	0.75	14.66	4.23	2.53	15.21	14.74
3270.4062	0.72	14.74	3.93	2.23	15.35	14.88
3270.4102	0.70	14.77	3.82	2.12	15.40	14.93
3284.3129	0.71	14.69	4.11	2.41	15.27	14.79
3284.3135	0.74	14.72	4.00	2.3	15.32	14.84
3289.5257	0.71	14.69	4.11	2.41	15.27	14.79
3289.5297	0.72	14.72	4.00	2.3	15.32	14.84
3297.3666	0.72	14.72	4.00	2.3	15.32	14.84
3297.3707	0.73	14.75	3.89	2.19	15.37	14.90
3310.2781	0.74	14.63	4.35	2.65	15.16	14.69
3310.2807	0.72	14.67	4.19	2.49	15.23	14.76
3316.3088	0.74	14.62	4.39	2.69	15.15	14.67
3316.3129	0.75	14.63	4.35	2.65	15.16	14.69
3318.3810	0.75	14.65	4.27	2.57	15.20	14.72
3324.4906	0.73	14.54	4.72	3.02	15.02	14.55
3324.4949	0.71	14.56	4.63	2.93	15.05	14.58
3329.2613	0.74	14.54	4.72	3.02	15.02	14.55
3329.2643	0.74	14.56	4.63	2.93	15.05	14.58
3347.2781	0.74	14.52	4.81	3.11	14.99	14.52
3347.2825	0.74	14.55	4.68	2.98	15.03	14.56
3368.1354	0.75	14.57	4.59	2.89	15.07	14.59
3368.1399	0.73	14.57	4.59	2.89	15.07	14.59
3368.1446	0.74	14.59	4.51	2.81	15.10	14.63
3380.1488	0.71	14.56	4.63	2.93	15.05	14.58
3380.1533	0.71	14.58	4.55	2.85	15.08	14.61
3384.6263	0.74	14.46	5.08	3.38	14.90	14.42
3384.6319	0.71	14.46	5.08	3.38	14.90	14.42
3388.6258	0.75	14.47	5.04	3.34	14.91	14.44
3388.6355	0.74	14.49	4.94	3.24	14.94	14.47
3405.1796	0.71	14.51	4.85	3.15	14.97	14.50
3417.5836	0.72	14.48	4.99	3.29	14.93	14.45
3417.5920	0.73	14.50	4.90	3.2	14.96	14.48
3467.5421	0.72	14.42	5.27	3.57	14.84	14.37
3467.5465	0.70	14.43	5.23	3.53	14.85	14.38
3475.5536	0.71	14.37	5.52	3.82	14.76	14.29
3475.5576	0.70	14.36	5.57	3.87	14.75	14.28
3496.4396	0.73	14.44	5.18	3.48	14.87	14.39

Appendix B10.1-Continued

1	2	3	4	5	6	7
3496.4436	0.73	14.43	5.23	3.53	14.85	14.38
3496.4475	0.73	14.45	5.13	3.43	14.88	14.41
3496.4515	0.74	14.46	5.08	3.38	14.90	14.42
3496.4603	0.75	14.46	5.08	3.38	14.90	14.42
3496.4642	0.72	14.43	5.23	3.53	14.85	14.38
3496.4682	0.73	14.45	5.13	3.43	14.88	14.41
3496.4721	0.71	14.46	5.08	3.38	14.90	14.42
3496.4838	0.74	14.45	5.13	3.43	14.88	14.41
3496.4877	0.73	14.46	5.08	3.38	14.90	14.42
3496.4916	0.72	14.44	5.18	3.48	14.87	14.39
3496.4956	0.73	14.42	5.27	3.57	14.84	14.37
3508.3729	0.72	14.49	4.94	3.24	14.94	14.47
3508.3754	0.72	14.49	4.94	3.24	14.94	14.47
3508.3780	0.72	14.50	4.90	3.2	14.96	14.48
3508.3806	0.74	14.49	4.94	3.24	14.94	14.47
3508.3991	0.71	14.51	4.85	3.15	14.97	14.50
3508.4017	0.71	14.51	4.85	3.15	14.97	14.50
3508.4043	0.71	14.49	4.94	3.24	14.94	14.47
3508.4069	0.70	14.48	4.99	3.29	14.93	14.45
3508.4166	0.72	14.48	4.99	3.29	14.93	14.45
3508.4186	0.74	14.48	4.99	3.29	14.93	14.45
3508.4211	0.73	14.47	5.04	3.34	14.91	14.44
3508.4238	0.74	14.47	5.04	3.34	14.91	14.44
3519.3637	0.71	14.51	4.85	3.15	14.97	14.50
3519.3662	0.72	14.50	4.90	3.2	14.96	14.48
3519.3688	0.74	14.47	5.04	3.34	14.91	14.44
3519.3713	0.73	14.48	4.99	3.29	14.93	14.45
3519.3763	0.69	14.50	4.90	3.2	14.96	14.48
3519.3788	0.70	14.48	4.99	3.29	14.93	14.45
3519.3814	0.69	14.48	4.99	3.29	14.93	14.45
3529.3446	0.71	14.42	5.27	3.57	14.84	14.37
3529.3546	0.72	14.43	5.23	3.53	14.85	14.38
3529.3591	0.68	14.44	5.18	3.48	14.87	14.39
3529.3635	0.69	14.44	5.18	3.48	14.87	14.39
3563.3070	0.70	14.52	4.81	3.11	14.99	14.52
3563.3095	0.73	14.51	4.85	3.15	14.97	14.50
3563.3120	0.72	14.50	4.90	3.2	14.96	14.48
3563.3145	0.74	14.54	4.72	3.02	15.02	14.55
3581.4426	0.73	14.53	4.76	3.06	15.01	14.53
3581.4466	0.72	14.55	4.68	2.98	15.03	14.56
3581.4506	0.76	14.55	4.68	2.98	15.03	14.56

Appendix B10.1-Continued

1	2	3	4	5	6	7
3588.3067	0.76	14.54	4.72	3.02	15.02	14.55
3588.3107	0.71	14.56	4.63	2.93	15.05	14.58
3588.3146	0.76	14.57	4.59	2.89	15.07	14.59
3588.3186	0.76	14.57	4.59	2.89	15.07	14.59
3591.3688	0.73	14.70	4.08	2.38	15.28	14.81
3591.3713	0.73	14.71	4.04	2.34	15.30	14.82
3591.3738	0.74	14.68	4.15	2.45	15.25	14.77
3591.3763	0.71	14.67	4.19	2.49	15.23	14.76
3598.4858	0.74	14.68	4.15	2.45	15.25	14.77
3598.4899	0.73	14.65	4.27	2.57	15.20	14.72
3607.2944	0.72	14.70	4.08	2.38	15.28	14.81
3607.2969	0.71	14.65	4.27	2.57	15.20	14.72
3607.2994	0.71	14.62	4.39	2.69	15.15	14.67
3607.3019	0.69	14.66	4.23	2.53	15.21	14.74
3614.3591	0.74	14.73	3.96	2.26	15.33	14.86
3614.3631	0.72	14.73	3.96	2.26	15.33	14.86
3614.3670	0.75	14.73	3.96	2.26	15.33	14.86
3614.3710	0.74	14.70	4.08	2.38	15.28	14.81
3621.3037	0.71	14.77	3.82	2.12	15.40	14.93
3621.3074	0.72	14.75	3.89	2.19	15.37	14.90
3621.3124	0.75	14.77	3.82	2.12	15.40	14.93
3621.3164	0.73	14.74	3.93	2.23	15.35	14.88
3637.1886	0.75	14.66	4.23	2.53	15.21	14.74
3637.1926	0.76	14.69	4.11	2.41	15.27	14.79
3637.1965	0.76	14.69	4.11	2.41	15.27	14.79
3637.2004	0.74	14.67	4.19	2.49	15.23	14.76
3641.2485	0.74	14.76	3.85	2.15	15.39	14.92
3641.2525	0.71	14.73	3.96	2.26	15.33	14.86
3641.2564	0.71	14.74	3.93	2.23	15.35	14.88
3645.4506	0.75	14.65	4.27	2.57	15.20	14.72
3645.4550	0.73	14.65	4.27	2.57	15.20	14.72
3653.4650	0.69	14.68	4.15	2.45	15.25	14.77
3653.4692	0.72	14.66	4.23	2.53	15.21	14.74
3656.4535	0.79	14.64	4.31	2.61	15.18	14.71
3656.4574	0.77	14.65	4.27	2.57	15.20	14.72
3656.4614	0.75	14.68	4.15	2.45	15.25	14.77
3656.4613	0.75	14.67	4.19	2.49	15.23	14.76
3666.3200	0.71	14.67	4.19	2.49	15.23	14.76
3666.3232	0.71	14.68	4.15	2.45	15.25	14.77
3668.2599	0.73	14.65	4.27	2.57	15.20	14.72
3668.2639	0.74	14.66	4.23	2.53	15.21	14.74

Appendix B10.1-Continued

1	2	3	4	5	6	7
3668.2717	0.71	14.62	4.39	2.69	15.15	14.67
3670.3254	0.73	14.67	4.19	2.49	15.23	14.76
3670.3293	0.72	14.70	4.08	2.38	15.28	14.81
3670.3333	0.73	14.68	4.15	2.45	15.25	14.77
3670.3371	0.71	14.66	4.23	2.53	15.21	14.74
3677.2240	0.73	14.67	4.19	2.49	15.23	14.76
3677.2319	0.74	14.63	4.35	2.65	15.16	14.69
3677.2358	0.75	14.65	4.27	2.57	15.20	14.72
3693.1661	0.75	14.66	4.23	2.53	15.21	14.74
3693.1686	0.72	14.64	4.31	2.61	15.18	14.71
3693.1711	0.71	14.64	4.31	2.61	15.18	14.71
3693.1737	0.72	14.65	4.27	2.57	15.20	14.72
3698.2240	0.75	14.68	4.15	2.45	15.25	14.77
3698.2279	0.75	14.65	4.27	2.57	15.20	14.72
3698.2319	0.73	14.66	4.23	2.53	15.21	14.74
3698.2358	0.75	14.62	4.39	2.69	15.15	14.67
3699.2288	0.72	14.56	4.63	2.93	15.05	14.58
3699.2327	0.72	14.56	4.63	2.93	15.05	14.58
3699.2366	0.71	14.57	4.59	2.89	15.07	14.59
3699.2406	0.74	14.60	4.63	2.93	15.05	14.58
3699.3176	0.73	14.58	4.55	2.85	15.08	14.61
3699.3215	0.74	14.59	4.51	2.81	15.10	14.63
3699.3254	0.73	14.59	4.51	2.81	15.10	14.63
3709.1544	0.74	14.60	4.63	2.93	15.05	14.58
3709.1584	0.73	14.56	4.63	2.93	15.05	14.58
3709.1623	0.71	14.58	4.55	2.85	15.08	14.61
3709.1662	0.74	14.57	4.59	2.89	15.07	14.59
3711.2772	0.74	14.57	4.59	2.89	15.07	14.59
3711.2812	0.71	14.56	4.63	2.93	15.05	14.58
3711.2851	0.71	14.59	4.51	2.81	15.10	14.63
3713.2544	0.71	14.56	4.63	2.93	15.05	14.58
3713.2583	0.72	14.59	4.51	2.81	15.10	14.63
3714.3031	0.72	14.58	4.55	2.85	15.08	14.61
3714.3056	0.74	14.57	4.59	2.89	15.07	14.59
3714.3081	0.73	14.55	4.68	2.98	15.03	14.56
3714.3106	0.73	14.55	4.68	2.98	15.03	14.56
3714.3155	0.74	14.59	4.51	2.81	15.10	14.63
3714.3180	0.68	14.58	4.55	2.85	15.08	14.61
3714.3205	0.72	14.55	4.68	2.98	15.03	14.56
3714.3230	0.69	14.59	4.51	2.81	15.10	14.63
3718.1426	0.73	14.65	4.27	2.57	15.20	14.72

Appendix B10.1-Continued

1	2	3	4	5	6	7
3718.1400	0.75	14.64	4.31	2.61	15.18	14.71
3718.1476	0.74	14.63	4.35	2.65	15.16	14.69
3718.1501	0.75	14.66	4.23	2.53	15.21	14.74
3718.1556	0.75	14.65	4.27	2.57	15.20	14.72
3718.1581	0.73	14.63	4.35	2.65	15.16	14.69
3718.1606	0.75	14.63	4.35	2.65	15.16	14.69
3718.1631	0.72	14.64	4.31	2.61	15.18	14.71
3724.1852	0.75	14.60	4.63	2.93	15.05	14.58
3724.1891	0.76	14.60	4.63	2.93	15.05	14.58
3724.1930	0.75	14.60	4.63	2.93	15.05	14.58
3724.1970	0.75	14.57	4.59	2.89	15.07	14.59
3733.1852	0.72	14.64	4.31	2.61	15.18	14.71
3733.1891	0.71	14.63	4.35	2.65	15.16	14.69
3733.1930	0.73	14.64	4.31	2.61	15.18	14.71
3733.1969	0.72	14.61	4.43	2.73	15.13	14.66
3787.6055	0.75	14.43	5.23	3.53	14.85	14.38
3823.4543	0.71	14.28	6.00	4.3	14.64	14.16
3823.4582	0.74	14.26	6.11	4.41	14.61	14.14
3823.4621	0.72	14.29	5.94	4.24	14.65	14.18
3823.4660	0.75	14.28	6.00	4.3	14.64	14.16
3832.4527	0.73	14.27	6.05	4.35	14.62	14.15
3832.4566	0.76	14.27	6.05	4.35	14.62	14.15
3842.3938	0.75	14.24	6.23	4.53	14.58	14.11
3842.3956	0.71	14.25	6.17	4.47	14.59	14.12
3842.4027	0.73	14.28	6.00	4.3	14.64	14.16
3842.4045	0.68	14.27	6.05	4.35	14.62	14.15
3852.5227	0.74	14.18	6.58	4.88	14.50	14.03
3852.5252	0.74	14.15	6.76	5.06	14.46	13.99
3852.5277	0.75	14.17	6.64	4.94	14.49	14.01
3852.5302	0.71	14.17	6.64	4.94	14.49	14.01
3852.5357	0.70	14.14	6.82	5.12	14.45	13.97
3852.5383	0.75	14.15	6.76	5.06	14.46	13.99
3852.5408	0.72	14.15	6.76	5.06	14.46	13.99
3852.5433	0.76	14.18	6.58	4.88	14.50	14.03
3854.5286	0.74	14.17	6.64	4.94	14.49	14.01
3854.5311	0.73	14.20	6.46	4.76	14.53	14.05
3854.5336	0.72	14.17	6.64	4.94	14.49	14.01
3854.5466	0.72	14.20	6.46	4.76	14.53	14.05
3854.5495	0.71	14.16	6.70	5	14.47	14.00
3867.4789	0.74	14.22	6.34	4.64	14.55	14.08
3867.4807	0.75	14.24	6.23	4.53	14.58	14.11

Appendix B10.1-Continued

1	2	3	4	5	6	7
3867.4825	0.74	14.23	6.28	4.58	14.57	14.09
3867.4843	0.73	14.23	6.28	4.58	14.57	14.09
3867.4891	0.72	14.24	6.23	4.53	14.58	14.11
3867.4909	0.73	14.22	6.34	4.64	14.55	14.08
3867.4927	0.72	14.20	6.46	4.76	14.53	14.05
3867.4945	0.74	14.23	6.28	4.58	14.57	14.09
3867.5002	0.72	14.24	6.23	4.53	14.58	14.11
3867.5020	0.75	14.25	6.17	4.47	14.59	14.12
3867.5038	0.74	14.25	6.17	4.47	14.59	14.12
3867.5057	0.75	14.22	6.34	4.64	14.55	14.08
3867.5105	0.74	14.21	6.40	4.7	14.54	14.07
3867.5123	0.73	14.25	6.17	4.47	14.59	14.12
3867.5141	0.73	14.24	6.23	4.53	14.58	14.11
3867.5159	0.75	14.23	6.28	4.58	14.57	14.09
3870.5115	0.76	14.31	5.83	4.13	14.68	14.21
3870.5165	0.76	14.32	5.78	4.08	14.69	14.22
3870.5190	0.76	14.32	5.78	4.08	14.69	14.22
3870.5239	0.76	14.29	5.94	4.24	14.65	14.18
3870.5264	0.75	14.30	5.89	4.19	14.66	14.19
3870.5289	0.76	14.29	5.94	4.24	14.65	14.18
3875.4208	0.72	14.29	5.94	4.24	14.65	14.18
3875.5066	0.73	14.31	5.83	4.13	14.68	14.21
3875.5091	0.72	14.29	5.94	4.24	14.65	14.18
3875.5116	0.72	14.30	5.89	4.19	14.66	14.19
3877.4907	0.73	14.33	5.73	4.03	14.71	14.23
3877.4932	0.74	14.29	5.94	4.24	14.65	14.18
3877.4982	0.72	14.31	5.83	4.13	14.68	14.21
3878.4332	0.71	14.31	5.83	4.13	14.68	14.21
3878.4357	0.69	14.33	5.73	4.03	14.71	14.23
3878.4383	0.71	14.33	5.73	4.03	14.71	14.23
3878.4408	0.72	14.31	5.83	4.13	14.68	14.21
3879.4993	0.74	14.31	5.83	4.13	14.68	14.21
3879.5018	0.73	14.30	5.89	4.19	14.66	14.19
3879.5043	0.74	14.34	5.67	3.97	14.72	14.25
3879.5068	0.72	14.33	5.73	4.03	14.71	14.23
3879.5129	0.72	14.30	5.89	4.19	14.66	14.19
3879.5155	0.76	14.28	6.00	4.3	14.64	14.16
3879.5176	0.72	14.33	5.73	4.03	14.71	14.23
3880.4595	0.75	14.34	5.67	3.97	14.72	14.25
3880.4614	0.7	14.36	5.57	3.87	14.75	14.28
3881.4716	0.71	14.29	5.94	4.24	14.65	14.18

Appendix B10.1-Continued

1	2	3	4	5	6	7
3881.4833	0.71	14.29	5.94	4.24	14.65	14.18
3882.4815	0.73	14.23	6.28	4.58	14.57	14.09
3882.4841	0.72	14.24	6.23	4.53	14.58	14.11
3882.4866	0.75	14.24	6.23	4.53	14.58	14.11
3882.4900	0.73	14.26	6.11	4.41	14.61	14.14
3885.4669	0.70	14.25	6.17	4.47	14.59	14.12
3885.4708	0.70	14.24	6.23	4.53	14.58	14.11
3885.4747	0.70	14.24	6.23	4.53	14.58	14.11
3886.4680	0.72	14.17	6.64	4.94	14.49	14.01
3886.4705	0.74	14.15	6.76	5.06	14.46	13.99
3886.4730	0.73	14.20	6.46	4.76	14.53	14.05
3886.4755	0.75	14.18	6.58	4.88	14.50	14.03
3887.4246	0.72	14.20	6.46	4.76	14.53	14.05
3887.4279	0.73	14.17	6.64	4.94	14.49	14.01
3887.4311	0.73	14.20	6.46	4.76	14.53	14.05
3887.4343	0.72	14.18	6.58	4.88	14.50	14.03
3888.4947	0.72	14.18	6.58	4.88	14.50	14.03
3888.4979	0.75	14.16	6.70	5	14.47	14.00
3888.5011	0.76	14.19	6.52	4.82	14.51	14.04
3888.5043	0.76	14.20	6.46	4.76	14.53	14.05
3888.5106	0.73	14.16	6.70	5	14.47	14.00
3888.5138	0.72	14.19	6.52	4.82	14.51	14.04
3889.3961	0.71	14.20	6.46	4.76	14.53	14.05
3889.4008	0.70	14.18	6.58	4.88	14.50	14.03
3889.4048	0.71	14.19	6.52	4.82	14.51	14.04
3889.4087	0.71	14.15	6.76	5.06	14.46	13.99
3889.4699	0.73	14.18	6.58	4.88	14.50	14.03
3889.4739	0.72	14.20	6.46	4.76	14.53	14.05
3889.4778	0.74	14.20	6.46	4.76	14.53	14.05
3889.4962	0.72	14.19	6.52	4.82	14.51	14.04
3889.5001	0.71	14.20	6.46	4.76	14.53	14.05
3889.5040	0.70	14.20	6.46	4.76	14.53	14.05
3889.5078	0.72	14.21	6.40	4.7	14.54	14.07
3890.4291	0.71	14.20	6.46	4.76	14.53	14.05
3891.4575	0.72	14.23	6.28	4.58	14.57	14.09
3891.4614	0.72	14.21	6.40	4.7	14.54	14.07
3896.4902	0.74	14.19	6.52	4.82	14.51	14.04
3896.4953	0.73	14.21	6.40	4.7	14.54	14.07
3896.4978	0.71	14.22	6.34	4.64	14.55	14.08
3897.4399	0.72	14.20	6.46	4.76	14.53	14.05
3897.4424	0.72	14.21	6.40	4.7	14.54	14.07

Appendix B10.1-Continued

1	2	3	4	5	6	7
3897.4449	0.75	14.20	6.46	4.76	14.53	14.05
3899.4089	0.71	14.22	6.34	4.64	14.55	14.08
3899.4114	0.72	14.20	6.46	4.76	14.53	14.05
3899.4139	0.74	14.18	6.58	4.88	14.50	14.03
3899.4187	0.75	14.19	6.52	4.82	14.51	14.04
3899.4212	0.73	14.22	6.34	4.64	14.55	14.08
3899.4237	0.71	14.22	6.34	4.64	14.55	14.08
3899.4263	0.74	14.20	6.46	4.76	14.53	14.05
3899.4288	0.72	14.21	6.40	4.7	14.54	14.07
3900.4094	0.69	14.26	6.11	4.41	14.61	14.14
3900.4119	0.71	14.27	6.05	4.35	14.62	14.15
3900.4144	0.73	14.24	6.23	4.53	14.58	14.11
3900.4169	0.72	14.26	6.11	4.41	14.61	14.14
3900.4218	0.71	14.24	6.23	4.53	14.58	14.11
3900.4243	0.74	14.24	6.23	4.53	14.58	14.11
3900.4268	0.76	14.25	6.17	4.47	14.59	14.12
3902.4523	0.72	14.26	6.11	4.41	14.61	14.14
3902.4549	0.72	14.27	6.05	4.35	14.62	14.15
3902.4574	0.72	14.23	6.28	4.58	14.57	14.09
3902.4699	0.67	14.24	6.23	4.53	14.58	14.11
3902.4724	0.71	14.26	6.11	4.41	14.61	14.14
3902.4749	0.70	14.24	6.23	4.53	14.58	14.11
3902.4823	0.71	14.26	6.11	4.41	14.61	14.14
3902.4849	0.74	14.23	6.28	4.58	14.57	14.09
3902.4874	0.70	14.24	6.23	4.53	14.58	14.11
3902.4899	0.72	14.23	6.28	4.58	14.57	14.09
3907.4523	0.73	14.21	6.40	4.7	14.54	14.07
3907.4549	0.75	14.19	6.52	4.82	14.51	14.04
3907.4599	0.71	14.22	6.34	4.64	14.55	14.08
3909.3799	0.72	14.22	6.34	4.64	14.55	14.08
3909.3913	0.69	14.25	6.17	4.47	14.59	14.12
3921.4683	0.72	14.16	6.70	5	14.47	14.00
3921.4708	0.75	14.16	6.70	5	14.47	14.00
3921.4733	0.75	14.19	6.52	4.82	14.51	14.04
3921.4800	0.72	14.17	6.64	4.94	14.49	14.01
3921.4891	0.71	14.20	6.46	4.76	14.53	14.05
3921.4930	0.72	14.19	6.52	4.82	14.51	14.04
3921.4969	0.73	14.17	6.64	4.94	14.49	14.01
3921.5077	0.72	14.19	6.52	4.82	14.51	14.04
3921.5102	0.73	14.15	6.76	5.06	14.46	13.99
3921.5127	0.73	14.13	6.89	5.19	14.43	13.96

Appendix B10.1-Continued

1	2	3	4	5	6	7
3933.3641	0.74	14.05	7.41	5.71	14.33	13.86
3933.3670	0.72	14.07	7.28	5.58	14.35	13.88
3933.3699	0.70	14.05	7.41	5.71	14.33	13.86
3933.3728	0.73	14.09	7.15	5.45	14.38	13.91
3939.3497	0.71	14.07	7.28	5.58	14.35	13.88
3939.3522	0.71	14.06	7.35	5.65	14.34	13.87
3939.3547	0.69	14.04	7.48	5.78	14.32	13.84
3939.3522	0.70	14.07	7.28	5.58	14.35	13.88
3939.3684	0.71	14.05	7.41	5.71	14.33	13.86
3939.3707	0.73	14.06	7.35	5.65	14.34	13.87
3939.3732	0.72	14.05	7.41	5.71	14.33	13.86
3939.3757	0.74	14.09	7.15	5.45	14.38	13.91
3939.3854	0.73	14.06	7.35	5.65	14.34	13.87
3939.3879	0.71	14.08	7.21	5.51	14.37	13.89
3939.3905	0.72	14.04	7.48	5.78	14.32	13.84
3939.3930	0.73	14.07	7.28	5.58	14.35	13.88
3939.4004	0.69	14.05	7.41	5.71	14.33	13.86
3939.4000	0.73	14.06	7.35	5.65	14.34	13.87
3939.4055	0.73	14.05	7.41	5.71	14.33	13.86
3939.4080	0.74	14.03	7.55	5.85	14.30	13.83
3939.4221	0.71	14.07	7.28	5.58	14.35	13.88
3939.4246	0.73	14.05	7.41	5.71	14.33	13.86
3939.4271	0.70	14.07	7.28	5.58	14.35	13.88
3939.4297	0.73	14.05	7.41	5.71	14.33	13.86
3939.4371	0.69	14.06	7.35	5.65	14.34	13.87
3939.4396	0.72	14.05	7.41	5.71	14.33	13.86
3939.4422	0.72	14.09	7.15	5.45	14.38	13.91
3939.4447	0.69	14.03	7.55	5.85	14.30	13.83
3939.4496	0.70	14.01	7.69	5.99	14.28	13.81
3939.4521	0.72	14.05	7.41	5.71	14.33	13.86
3939.4546	0.71	14.03	7.55	5.85	14.30	13.83
3939.4571	0.74	14.04	7.48	5.78	14.32	13.84
3939.4723	0.73	14.07	7.28	5.58	14.35	13.88
3939.4778	0.74	14.01	7.69	5.99	14.28	13.81
3939.4802	0.75	14.05	7.41	5.71	14.33	13.86
3939.4807	0.74	14.07	7.68	5.58	14.35	13.88
3940.3240	0.72	14.06	7.35	5.65	14.34	13.87
3940.3265	0.70	14.07	7.28	5.58	14.35	13.88
3940.3290	0.72	14.03	7.55	5.85	14.30	13.83
3940.3315	0.70	14.07	14.07	14.07	14.07	14.07
3940.3361	0.71	14.03	7.55	5.85	14.30	13.83

Appendix B10.1-Continued

1	2	3	4	5	6	7
3940.3386	0.69	14.08	7.21	5.51	14.37	13.89
3940.3411	0.73	14.04	7.48	5.78	14.32	13.84
3940.3436	0.71	14.08	7.21	5.51	14.37	13.89
3940.3531	0.73	14.08	7.21	5.51	14.37	13.89
3940.3556	0.73	14.07	7.28	5.58	14.35	13.88
3940.3581	0.72	14.05	7.41	5.71	14.33	13.86
3940.3606	0.72	14.04	7.48	5.78	14.32	13.84
3940.3655	0.72	14.06	7.35	5.65	14.34	13.87
3940.3680	0.73	14.04	7.48	5.78	14.32	13.84
3940.3833	0.74	14.05	7.41	5.71	14.33	13.86
3940.3858	0.70	14.05	7.41	5.71	14.33	13.86
3940.3883	0.72	14.03	7.55	5.85	14.30	13.83
3940.3908	0.73	14.06	7.35	5.65	14.34	13.87
3940.3957	0.71	14.04	7.48	5.78	14.32	13.84
3940.3983	0.73	14.07	7.28	5.58	14.35	13.88
3940.4008	0.70	14.08	7.21	5.51	14.37	13.89
3940.4033	0.72	14.03	7.55	5.85	14.30	13.83
3940.4114	0.71	14.05	7.41	5.71	14.33	13.86
3940.4139	0.73	14.04	7.48	5.78	14.32	13.84
3940.4163	0.74	14.05	7.41	5.71	14.33	13.86
3940.4188	0.73	14.04	7.48	5.78	14.32	13.84
3940.4238	0.73	14.08	7.21	5.51	14.37	13.89
3940.4263	0.74	14.07	7.28	5.58	14.35	13.88
3940.4288	0.74	14.03	7.55	5.85	14.30	13.83
3940.4313	0.72	14.08	7.21	5.51	14.37	13.89
3940.4410	0.73	14.04	7.48	5.78	14.32	13.84
3940.4435	0.74	14.09	7.15	5.45	14.38	13.91
3940.4460	0.72	14.06	7.35	5.65	14.34	13.87
3940.4486	0.71	14.07	7.28	5.58	14.35	13.88
3942.2451	0.71	14.09	7.15	5.45	14.38	13.91
3942.2476	0.71	14.08	7.21	5.51	14.37	13.89
3942.2501	0.70	14.07	7.28	5.58	14.35	13.88
3942.2526	0.73	14.09	7.15	5.45	14.38	13.91
3942.2575	0.70	14.08	7.21	5.51	14.37	13.89
3942.2600	0.72	14.06	7.35	5.65	14.34	13.87
3942.2650	0.73	14.10	7.08	5.38	14.39	13.92
3942.2724	0.70	14.07	7.28	5.58	14.35	13.88
3942.2749	0.73	14.09	7.15	5.45	14.38	13.91
3942.2774	0.72	14.05	7.41	5.71	14.33	13.86
3942.2799	0.74	14.06	7.35	5.65	14.34	13.87
3942.2848	0.72	14.05	7.41	5.71	14.33	13.86

Appendix B10.1-Continued

1	2	3	4	5	6	7
3942.2873	0.73	14.05	7.41	5.71	14.33	13.86
3942.2898	0.75	14.07	7.28	5.58	14.35	13.88
3942.2923	0.73	14.06	7.35	5.65	14.34	13.87
3942.3005	0.75	14.08	7.21	5.51	14.37	13.89
3942.3038	0.71	14.09	7.15	5.45	14.38	13.91
3942.3063	0.70	14.10	7.08	5.38	14.39	13.92
3942.3088	0.72	14.09	7.15	5.45	14.38	13.91
3942.3113	0.71	14.09	7.15	5.45	14.38	13.91
3942.3182	0.70	14.07	7.28	5.58	14.35	13.88
3942.3207	0.73	14.11	7.01	5.31	14.41	13.93
3942.3232	0.70	14.08	7.21	5.51	14.37	13.89
3942.3257	0.69	14.08	7.21	5.51	14.37	13.89
3942.3342	0.69	14.11	7.01	5.31	14.41	13.93
3942.3367	0.72	14.08	7.21	5.51	14.37	13.89
3942.3392	0.71	14.07	7.28	5.58	14.35	13.88
3942.3417	0.73	14.09	7.15	5.45	14.38	13.91
3942.3466	0.73	14.08	7.21	5.51	14.37	13.89
3942.3491	0.70	14.10	7.08	5.38	14.39	13.92
3942.3516	0.72	14.08	7.21	5.51	14.37	13.89
3942.3542	0.72	14.11	7.01	5.31	14.41	13.93
3942.3621	0.73	14.05	7.41	5.71	14.33	13.86
3942.3646	0.74	14.04	7.48	5.78	14.32	13.84
3942.3671	0.73	14.08	7.21	5.51	14.37	13.89
3942.3745	0.72	14.04	7.48	5.78	14.32	13.84
3942.3771	0.71	14.08	7.21	5.51	14.37	13.89
3942.3796	0.74	14.07	7.28	5.58	14.35	13.88
3942.3821	0.74	14.11	7.01	5.31	14.41	13.93
3942.3909	0.71	14.10	7.08	5.38	14.39	13.92
3942.3934	0.70	14.09	7.15	5.45	14.38	13.91
3942.3959	0.73	14.06	7.35	5.65	14.34	13.87
3942.3985	0.74	14.07	7.28	5.58	14.35	13.88
3942.4003	0.73	14.06	7.35	5.65	14.34	13.87
3942.4029	0.73	14.11	7.01	5.31	14.41	13.93
3942.4054	0.71	14.10	7.08	5.38	14.39	13.92
3942.4162	0.71	14.11	7.01	5.31	14.41	13.93
3942.4187	0.72	14.09	7.15	5.45	14.38	13.91
3942.4212	0.72	14.10	7.08	5.38	14.39	13.92
3942.4292	0.70	14.07	7.28	5.58	14.35	13.88
3942.4317	0.73	14.10	7.08	5.38	14.39	13.92
3942.4342	0.71	14.07	7.28	5.58	14.35	13.88
3942.4483	0.72	14.11	7.01	5.31	14.41	13.93

Appendix B10.1-Continued

1	2	3	4	5	6	7
3942.4586	0.73	14.07	7.28	5.58	14.35	13.88
3943.2880	0.74	14.11	7.01	5.31	14.41	13.93
3943.2920	0.71	14.09	7.15	5.45	14.38	13.91
3945.2565	0.72	14.07	7.28	5.58	14.35	13.88
3945.2604	0.71	14.10	7.08	5.38	14.39	13.92
3945.2643	0.75	14.08	7.21	5.51	14.37	13.89
3945.2682	0.71	14.10	7.08	5.38	14.39	13.92
3946.2346	0.72	14.06	7.35	5.65	14.34	13.87
3946.2371	0.75	14.09	7.15	5.45	14.38	13.91
3946.2406	0.75	14.05	7.41	5.71	14.33	13.86
3946.2441	0.75	14.06	7.35	5.65	14.34	13.87
3947.4308	0.75	14.07	7.28	5.58	14.35	13.88
3947.4333	0.73	14.07	7.28	5.58	14.35	13.88
3947.4368	0.73	14.08	7.21	5.51	14.37	13.89
3947.4403	0.72	14.06	7.35	5.65	14.34	13.87
3950.2528	0.71	14.17	6.64	4.94	14.49	14.01
3950.2553	0.69	14.14	6.82	5.12	14.45	13.97
3950.2579	0.73	14.14	6.82	5.12	14.45	13.97
3950.2603	0.69	14.12	6.95	5.25	14.42	13.95
3950.2689	0.69	14.14	6.82	5.12	14.45	13.97
3950.2714	0.74	14.15	6.76	5.06	14.46	13.99
3950.2739	0.70	14.17	6.64	4.94	14.49	14.01
3950.2764	0.71	14.15	6.76	5.06	14.46	13.99
3952.3776	0.70	14.12	6.95	5.25	14.42	13.95
3952.3801	0.71	14.10	7.08	5.38	14.39	13.92
3952.3833	0.68	14.10	7.08	5.38	14.39	13.92
3952.3851	0.70	14.12	6.95	5.25	14.42	13.95
3952.3900	0.76	14.10	7.08	5.38	14.39	13.92
3952.3925	0.75	14.14	6.82	5.12	14.45	13.97
3952.3950	0.71	14.09	7.15	5.45	14.38	13.91
3952.3976	0.74	14.13	6.89	5.19	14.43	13.96
4034.3043	0.73	14.10	7.08	5.38	14.39	13.92
4034.3064	0.72	14.09	7.15	5.45	14.38	13.91
4034.3085	0.74	14.08	7.21	5.51	14.37	13.89
4060.2202	0.75	14.19	6.52	4.82	14.51	14.04
4060.2223	0.74	14.18	6.58	4.88	14.50	14.03
4060.2244	0.73	14.22	6.34	4.64	14.55	14.08
4060.2286	0.69	14.20	6.46	4.76	14.53	14.05
4060.2307	0.71	14.22	6.34	4.64	14.55	14.08
4061.1922	0.72	14.21	6.40	4.7	14.54	14.07
4061.1943	0.7	14.23	6.28	4.58	14.57	14.09

Appendix B10.1-Continued

1	2	3	4	5	6	7
4061.1964	0.75	14.21	6.40	4.7	14.54	14.07
4061.1985	0.73	14.22	6.34	4.64	14.55	14.08
4061.2005	0.73	14.21	6.40	4.7	14.54	14.07
4061.2026	0.7	14.21	6.40	4.7	14.54	14.07
4062.1946	0.72	14.24	6.23	4.53	14.58	14.11
4062.1967	0.73	14.23	6.28	4.58	14.57	14.09
4062.1989	0.74	14.22	6.34	4.64	14.55	14.08
4062.2010	0.72	14.23	6.28	4.58	14.57	14.09
4063.2686	0.73	14.21	6.40	4.7	14.54	14.07
4063.2707	0.70	14.19	6.52	4.82	14.51	14.04
4063.2728	0.71	14.21	6.40	4.7	14.54	14.07
4063.2749	0.74	14.21	6.40	4.7	14.54	14.07
4065.2871	0.74	14.19	6.52	4.82	14.51	14.04
4065.2892	0.71	14.20	6.46	4.76	14.53	14.05
4065.2913	0.73	14.19	6.52	4.82	14.51	14.04
4065.2934	0.73	14.18	6.58	4.88	14.50	14.03
4066.2821	0.75	14.16	6.70	5	14.47	14.00
4066.2842	0.71	14.18	6.58	4.88	14.50	14.03
4066.2863	0.7	14.17	6.64	4.94	14.49	14.01
4066.2884	0.72	14.16	6.70	5	14.47	14.00
4125.6143	0.69	14.39	5.42	3.72	14.79	14.32
4125.6164	0.7	14.39	5.42	3.72	14.79	14.32
4125.6185	0.72	14.35	5.62	3.92	14.74	14.26
4125.6206	0.71	14.37	5.52	3.82	14.76	14.29
4125.6227	0.73	14.36	5.57	3.87	14.75	14.28
4125.6248	0.74	14.33	5.73	4.03	14.71	14.23
4125.6270	0.74	14.33	5.73	4.03	14.71	14.23
4179.5476	0.71	14.49	4.94	3.24	14.94	14.47
4179.5498	0.73	14.44	5.18	3.48	14.87	14.39
4179.5520	0.69	14.45	5.13	3.43	14.88	14.41
4179.5541	0.7	14.44	5.18	3.48	14.87	14.39
4180.5370	0.74	14.53	4.76	3.06	15.01	14.53
4180.5391	0.71	14.52	4.81	3.11	14.99	14.52
4180.5412	0.73	14.51	4.85	3.15	14.97	14.50
4180.5432	0.72	14.49	4.94	3.24	14.94	14.47
4198.4759	0.73	14.53	4.76	3.06	15.01	14.53
4198.4780	0.7	14.52	4.81	3.11	14.99	14.52
4198.4800	0.72	14.55	4.68	2.98	15.03	14.56
4198.4821	0.72	14.52	4.81	3.11	14.99	14.52
4212.5266	0.71	14.55	4.68	2.98	15.03	14.56
4212.5301	0.73	14.57	4.59	2.89	15.07	14.59

Appendix B10.1-Continued

1	2	3	4	5	6	7
4212.5371	0.71	14.57	4.59	2.89	15.07	14.59
4228.5119	0.72	14.61	4.43	2.73	15.13	14.66
4228.5140	0.74	14.58	4.55	2.85	15.08	14.61
4228.5161	0.73	14.59	4.51	2.81	15.10	14.63
4228.5182	0.71	14.59	4.51	2.81	15.10	14.63
4228.5202	0.68	14.59	4.51	2.81	15.10	14.63
4228.5223	0.71	14.57	4.59	2.89	15.07	14.59
4236.4794	0.74	14.52	4.81	3.11	14.99	14.52
4236.4815	0.76	14.52	4.81	3.11	14.99	14.52
4236.4837	0.72	14.54	4.72	3.02	15.02	14.55
4236.4858	0.71	14.53	4.76	3.06	15.01	14.53
4237.4999	0.76	14.52	4.81	3.11	14.99	14.52
4237.5034	0.72	14.52	4.81	3.11	14.99	14.52
4237.5069	0.74	14.55	4.68	2.98	15.03	14.56
4237.5104	0.75	14.55	4.68	2.98	15.03	14.56
4237.5139	0.75	14.55	4.68	2.98	15.03	14.56
4239.4776	0.69	14.59	4.51	2.81	15.10	14.63
4239.4810	0.71	14.58	4.55	2.85	15.08	14.61
4239.4845	0.72	14.59	4.51	2.81	15.10	14.63
4239.4880	0.69	14.56	4.63	2.93	15.05	14.58
4292.4363	0.75	14.61	4.43	2.73	15.13	14.66
4292.4398	0.71	14.64	4.31	2.61	15.18	14.71
4292.4433	0.74	14.64	4.31	2.61	15.18	14.71
4292.4468	0.71	14.63	4.35	2.65	15.16	14.69
4295.3461	0.67	14.68	4.15	2.45	15.25	14.77
4295.3482	0.63	14.66	4.23	2.53	15.21	14.74
4295.3504	0.68	14.68	4.15	2.45	15.25	14.77
4295.3525	0.68	14.69	4.11	2.41	15.27	14.79
4303.4397	0.68	14.62	4.39	2.69	15.15	14.67
4303.4418	0.63	14.64	4.31	2.61	15.18	14.71
4303.4560	0.65	14.66	4.23	2.53	15.21	14.74
4306.4566	0.62	14.65	4.27	2.57	15.20	14.72
4306.4588	0.68	14.62	4.39	2.69	15.15	14.67
4306.4609	0.67	14.63	4.35	2.65	15.16	14.69
4306.4630	0.66	14.61	4.43	2.73	15.13	14.66
4307.4393	0.67	14.62	4.39	2.69	15.15	14.67
4307.4432	0.68	14.64	4.31	2.61	15.18	14.71
4307.4471	0.69	14.64	4.31	2.61	15.18	14.71
4309.3806	0.68	14.60	4.47	2.77	15.11	14.64
4309.3835	0.68	14.59	4.51	2.81	15.10	14.63
4318.2871	0.68	14.51	4.85	3.15	14.97	14.50

Appendix B10.1-Continued

1	2	3	4	5	6	7
4318.2893	0.70	14.53	4.76	3.06	15.01	14.53
4318.2914	0.68	14.52	4.81	3.11	14.99	14.52
4318.2935	0.71	14.49	4.94	3.24	14.94	14.47
4321.4477	0.67	14.50	4.90	3.2	14.96	14.48
4321.4498	0.71	14.47	5.04	3.34	14.91	14.44
4321.4519	0.70	14.48	4.99	3.29	14.93	14.45
4321.4540	0.68	14.46	5.08	3.38	14.90	14.42
4324.4512	0.70	14.52	4.81	3.11	14.99	14.52
4324.4554	0.68	14.48	4.99	3.29	14.93	14.45
4324.4596	0.72	14.53	4.76	3.06	15.01	14.53
4324.4637	0.73	14.51	4.85	3.15	14.97	14.50
4327.3703	0.69	14.49	4.94	3.24	14.94	14.47
4327.3735	0.72	14.49	4.94	3.24	14.94	14.47
4327.3766	0.71	14.53	4.76	3.06	15.01	14.53
4329.286	0.73	14.47	5.04	3.34	14.91	14.44
4329.2891	0.68	14.45	5.13	3.43	14.88	14.41
4329.2922	0.69	14.46	5.08	3.38	14.90	14.42
4329.2953	0.68	14.48	4.99	3.29	14.93	14.45
4332.4483	0.71	14.51	4.85	3.15	14.97	14.50
4332.4518	0.73	14.52	4.81	3.11	14.99	14.52
4332.4553	0.69	14.51	4.85	3.15	14.97	14.50
4332.4588	0.7	14.51	4.85	3.15	14.97	14.50
4334.2013	0.74	14.49	4.94	3.24	14.94	14.47
4334.2048	0.71	14.51	4.85	3.15	14.97	14.50
4334.2083	0.73	14.48	4.99	3.29	14.93	14.45
4334.2123	0.72	14.48	4.99	3.29	14.93	14.45
4347.2029	0.73	14.42	5.27	3.57	14.84	14.37
4347.2064	0.7	14.44	5.18	3.48	14.87	14.39
4347.2099	0.72	14.43	5.23	3.53	14.85	14.38
4347.2134	0.72	14.41	5.32	3.62	14.82	14.35
4352.2487	0.71	14.43	5.23	3.53	14.85	14.38
4352.2522	0.73	14.42	5.27	3.57	14.84	14.37
4356.1923	0.71	14.40	5.37	3.67	14.81	14.34
4356.1958	0.71	14.37	5.52	3.82	14.77	14.30
4356.1993	0.72	14.41	5.32	3.62	14.82	14.35
4356.2027	0.74	14.4	5.37	3.67	14.81	14.34
4364.4889	0.73	14.31	5.83	4.13	14.68	14.21
4364.4924	0.71	14.29	5.94	4.24	14.65	14.18
4364.4994	0.71	14.32	5.78	4.08	14.69	14.22
4366.2167	0.74	14.21	6.40	4.7	14.54	14.07
4366.2202	0.76	14.20	6.46	4.76	14.53	14.05

Appendix B10.1-Continued

1	2	3	4	5	6	7
4375.4123	0.72	14.35	5.62	3.92	14.74	14.26
4375.4158	0.71	14.32	5.78	4.08	14.69	14.22
<i>4375.4193</i>	0.76	14.35	5.62	3.92	14.74	14.26
4375.4228	0.72	14.37	5.52	3.82	14.76	14.29
4377.4912	0.74	14.44	5.18	3.48	14.87	14.39
4377.4947	0.75	14.42	5.27	3.57	14.84	14.37
4379.4865	0.75	14.36	5.57	3.87	14.75	14.28
4379.6900	0.69	14.36	5.57	3.87	14.75	14.28
4383.2421	0.71	14.34	5.67	3.97	14.72	14.25
4383.2456	0.72	14.34	5.67	3.97	14.72	14.25
4383.2491	0.69	14.34	5.67	3.97	14.72	14.25
4383.2526	0.75	14.34	5.67	3.97	14.72	14.25
4383.256	0.71	14.32	5.78	4.08	14.69	14.22
4387.3456	0.74	14.35	5.62	3.92	14.74	14.26
4387.3491	0.71	14.37	5.52	3.82	14.76	14.29
4387.3526	0.67	14.34	5.67	3.97	14.72	14.25
4387.3561	0.63	14.34	5.67	3.97	14.72	14.25
4392.4231	0.68	14.33	5.73	4.03	14.71	14.23
4392.4266	0.68	14.32	5.78	4.08	14.69	14.22
4393.4583	0.68	14.35	5.62	3.92	14.74	14.26
4393.4614	0.63	14.35	5.62	3.92	14.74	14.26
4416.2871	0.65	14.22	6.34	4.64	14.55	14.08
4416.2906	0.62	14.20	6.46	4.76	14.53	14.05
4416.2941	0.68	14.21	6.40	4.7	14.54	14.07
4416.2976	0.67	14.22	6.34	4.64	14.55	14.08

B10.2 Color Indices of 1ES 1959+650

JD-2450000 (1)	<i>V</i> (2)	<i>V-R</i> (3)	Error (4)	<i>V-B(error)</i> (5)	Comment(6)
181.65	15.49	0.45	0.02	1.10(0.05)	Torino
246.55	15.43	0.43	0.02	1.05(0.08)	Torino
376.29	15.00	0.46	0.03	1.04(0.08)	Torino
378.31	15.00	0.44	0.03	1.11(0.09)	Torino
570.63	15.54	0.49	0.02	1.09(0.04)	Torino
577.54	15.49	0.50	0.02	-	Torino
1020.45	15.16	0.49	0.05	-	Abastumani
1039.31	15.17	0.51	0.05	-	Abastumani
1041.40	15.15	0.47	0.05	-	Abastumani
1055.40	14.97	0.51	0.05	-	Abastumani
1068.41	14.85	0.47	0.05	-	Abastumani
1071.35	14.86	0.50	0.05	-	Abastumani
1074.36	14.83	0.48	0.05	-	Abastumani
1083.33	14.93	0.46	0.05	-	Abastumani
1110.26	14.84	0.51	0.05	-	Abastumani
1141.22	14.96	0.46	0.05	-	Abastumani
1142.15	14.93	0.52	0.05	-	Abastumani
1160.23	14.97	0.51	0.05	-	Abastumani
1279.51	14.95	0.50	0.05	-	Abastumani
1375.48	14.91	0.48	0.05	-	Abastumani
1377.43	15.01	0.49	0.04	-	Abastumani
1402.49	14.98	0.49	0.05	-	Abastumani
1403.33	14.98	0.50	0.05	-	Abastumani
1405.43	15.03	0.50	0.05	-	Abastumani
1407.43	14.99	0.45	0.05	-	Abastumani
1410.41	15.04	0.49	0.05	-	Abastumani
1412.45	15.06	0.50	0.05		Abastumani
1433.27	15.08	0.50	0.05	-	Abastumani
1438.45	15.05	0.49	0.05	-	Abastumani
1452.30	14.99	0.50	0.05	-	Abastumani
1455.28	14.95	0.50	0.05	-	Abastumani
1461.26	14.93	0.48	0.05	-	Abastumani
1466.34	14.93	0.47	0.05	-	Abastumani
1485.36	15.02	0.47	0.05	-	Abastumani
1585.61	14.87	0.48	0.05	-	Abastumani
1589.62	14.92	0.51	0.05	-	Abastumani
1693.45	14.91	0.46	0.05	-	Abastumani
1699.40	14.94	0.49	0.05	-	Abastumani

Appendix B10.2-Continued

1	2	3	4	5	6
1734.38	14.94	0.50	0.05	-	Abastumani
1738.49	14.87	0.51	0.05	-	Abastumani
1779.42	14.86	0.52	0.05	-	Abastumani
1786.39	14.84	0.46	0.05	-	Abastumani
1790.41	14.86	0.48	0.05	-	Abastumani
1792.41	14.86	0.47	0.05	-	Abastumani
2113.40	14.97	0.49	0.05	-	Abastumani
2114.39	15.01	0.47	0.05	-	Abastumani
2115.48	15.07	0.48	0.05	-	Abastumani
2116.41	15.08	0.51	0.05	-	Abastumani
2138.24	14.99	0.51	0.05	-	Abastumani
2142.27	14.98	0.50	0.05	-	Abastumani
2164.39	14.92	0.51	0.05	-	Abastumani
2172.46	14.91	0.47	0.05	-	Abastumani
2192.30	14.82	0.47	0.05	-	Abastumani
2206.35	14.81	0.48	0.05	-	Abastumani
2224.23	14.86	0.50	0.05	-	Abastumani
2519.27	15.10	0.46	0.05	-	Abastumani
2520.28	15.05	0.45	0.05	-	Abastumani
2531.40	15.07	0.50	0.05	-	Abastumani
2532.51	15.00	0.47	0.05	-	Abastumani
2534.42	15.05	0.46	0.05	-	Abastumani
2547.30	15.07	0.46	0.05	-	Abastumani
2549.24	15.07	0.48	0.05	-	Abastumani
2552.35	15.06	0.46	0.05	-	Abastumani
2554.24	15.00	0.48	0.05	-	Abastumani
2558.25	15.07	0.47	0.05	-	Abastumani
2559.34	15.06	0.46	0.05	-	Abastumani
2560.33	15.09	0.49	0.05	-	Abastumani
2561.42	15.07	0.47	0.05	-	Abastumani
2562.45	15.07	0.50	0.05	-	Abastumani
2576.32	15.00	0.51	0.05	-	Abastumani
2581.33	15.02	0.46	0.05	-	Abastumani
2582.26	14.92	0.46	0.05	-	Abastumani
2584.20	14.96	0.49	0.05	-	Abastumani
2588.24	15.04	0.45	0.05	-	Abastumani
3467.55	15.00	0.47	0.05	-	Abastumani
3519.39	14.96	0.48	0.05	-	Abastumani
3529.37	14.94	0.50	0.05	-	Abastumani
3588.32	15.04	0.47	0.05	-	Abastumani
3607.30	15.14	0.48	0.05	-	Abastumani

B11.1 *R* Band Data of 1ES 2344+514

JD- 2451000 (1)	C2-C1 (2)	<i>R</i> (3)	\bar{R} (4)	<i>F</i> (5)	F_{corr} (6)	\bar{R}_{corr} (7)	\bar{R}_{corr}^{dered} (8)
21.4270	1.98	14.63					
21.4336	2.00	14.61	14.62	4.39	0.69	16.62	16.05
40.3839	1.99	14.63					
40.3925	1.99	14.60	14.62	4.39	0.69	16.62	16.05
56.4658	1.98	14.62					
56.4742	2.01	14.59	14.61	4.43	0.73	16.56	15.98
68.4807	1.97	14.66					
68.4891	1.98	14.63	14.65	4.27	0.57	16.83	16.25
71.4456	2.02	14.67					
71.4511	1.95	14.66	14.67	4.19	0.49	16.99	16.42
73.4364	2.28	14.65					
73.4413	2.29	14.65	14.65	4.27	0.57	16.83	16.25
76.4370	1.97	14.68	14.68	4.15	0.45	17.09	16.51
84.4050	1.95	14.62					
84.4134	1.96	14.64	14.63	4.35	0.65	16.69	16.11
86.4044	1.99	14.58					
86.4129	1.95	14.56	14.57	4.59	0.89	16.35	15.77
101.3823	2.33	14.62					
101.3887	2.35	14.63	14.63	4.35	0.65	16.69	16.11
117.4078	1.98	14.65					
117.4156	2.00	14.67	14.66	4.35	0.65	16.69	16.11
130.4048	1.95	14.66					
131.4126	2.00	14.64	14.65	4.27	0.57	16.83	16.25
138.2030	2.00	14.64					
138.2108	1.96	14.65	14.65	4.27	0.57	16.83	16.25
376.5161	2.06	14.53	14.53	4.76	1.06	16.16	15.58
399.4504	2.01	14.62	14.62	4.39	0.69	16.62	16.05
402.4739	1.98	14.64		4.35	0.65	16.69	16.11
407.5017	2.01	14.61	14.63	4.39	0.69	16.62	16.05
410.4362	2.00	14.64	14.64	4.31	0.61	16.76	16.18
412.4210	1.98	14.64		4.55	0.85	16.40	16.18
438.498	1.98	14.64	14.64	4.31	0.61	16.76	16.18
440.4864	1.96	14.57	14.57	4.59	0.85	16.40	15.82
454.3160	1.96	14.64	14.64	4.31	0.61	16.76	16.18
457.4629	1.95	14.63	14.63	4.35	0.65	16.69	16.11
458.3880	1.95	14.68					
458.3921	1.97	14.66					
458.4010	2.01	14.66					

Appendix B11.1-Continued

1	2	3	4	5	6	7	8
458.4023	2.01	14.68					
458.4045	1.97	14.67					
458.4089	1.97	14.71					
458.4111	1.99	14.71					
458.4134	2.00	14.70					
458.4200	1.97	14.72					
458.4222	1.98	14.69					
458.4244	1.98	14.71					
458.4399	1.98	14.68					
458.4420	1.99	14.67					
458.4444	2.01	14.65					
458.4487	1.98	14.69					
458.4509	1.97	14.68					
458.4531	1.96	14.69					
458.4598	1.99	14.71					
458.4620	1.99	14.70					
458.4642	1.99	14.69					
458.4686	1.98	14.68					
458.4797	2.00	14.69					
458.4819	2.01	14.67					
458.4841	1.97	14.69					
458.4885	1.97	14.69					
458.4907	1.98	14.70					
458.4930	2.00	14.70					
458.4952	1.98	14.69					
458.4996	1.97	14.70					
458.5062	2.00	14.68					
458.5106	1.99	14.70					
458.5362	1.98	14.71					
458.5384	1.98	14.73					
458.5448	1.99	14.66					
458.5473	1.98	14.72					
458.5584	2.00	14.68	14.69	4.11	0.41	17.19	16.61
489.5194	1.99	14.71	14.71	4.05	0.35	17.36	16.79
496.4776	1.98	14.67	14.67	4.19	0.49	16.99	16.42
521.3921	1.97	14.63	14.63	4.35	0.65	16.69	16.11
523.3661	1.98	14.68	14.66	4.23	0.53	16.91	16.33
723.4502	2.01	14.65					
723.4532	2.00	14.66					
723.4560	1.96	14.67	14.66	4.23	0.53	16.91	16.33
789.50115	1.97	14.69					

Appendix B11.1-Continued

1	2	3	4	5	6	7	8
789.5033	1.99	14.65					
789.5055	1.98	14.68					
789.5099	1.98	14.69					
789.5122	1.98	14.70					
789.5144	1.98	14.65					
789.5166	1.99	14.70					
789.5210	1.98	14.65					
789.5232	1.98	14.68					
789.5254	1.99	14.66					
789.5276	1.96	14.68					
789.5298	1.97	14.64					
789.5320	1.98	14.68					
789.5342	2.01	14.69					
789.53648	2.00	14.70	14.68	4.15	0.45	17.09	16.51
792.4507	1.97	14.72					
792.4705	1.99	14.70					
792.4727	1.96	14.68					
792.5586	2.00	14.71	14.70	4.08	0.38	17.27	16.69
820.2328	2.00	14.61					
820.2354	1.98	14.60					
820.2379	2.00	14.64					
820.2404	2.00	14.65					
820.2429	1.98	14.63					
820.2455	1.98	14.66					
820.2503	1.96	14.66					
820.2529	1.99	14.65					
820.2554	1.97	14.66					
820.2579	1.98	14.65					
820.2604	1.99	14.65					
820.2629	1.97	14.65					
820.2655	1.96	14.65					
820.2680	1.97	14.66					
820.2729	2.00	14.61					
820.2754	1.99	14.63					
820.2779	1.97	14.67					
820.2804	1.97	14.68					
820.2829	1.99	14.68					
820.2855	1.98	14.62					
820.2880	1.99	14.62					
820.2905	1.99	14.63					
820.2954	1.99	14.66					

Appendix B11.1Continued

1	2	3	4	5	6	7	8
820.3004	2.01	14.62					
820.3030	2.01	14.65					
820.3055	1.97	14.65					
820.3080	2.00	14.62	14.64	4.31	0.61	16.76	16.18
820.3105	1.98	14.63					
820.3130	1.99	14.62					
820.3179	1.95	14.61					
820.3204	2.00	14.59					
820.3255	1.98	14.60					
820.3305	1.96	14.62					
820.3330	1.95	14.65					
820.3358	1.97	14.60					
820.3455	1.97	14.65					
820.3480	1.99	14.67					
820.3505	1.99	14.66					
820.3530	1.98	14.65					
820.3555	1.99	14.65					
820.3580	1.98	14.62					
820.3629	1.98	14.66					
820.3654	1.99	14.67					
820.3980	1.96	14.66	14.64	4.31	0.61	16.76	16.18
821.4056	1.96	14.70					
821.4082	1.97	14.68					
821.4107	1.96	14.70					
821.4181	1.97	14.66					
821.4206	1.97	14.67					
821.4231	1.97	14.64					
821.4282	1.97	14.64					
821.4307	1.97	14.65					
821.4332	1.97	14.65					
821.4357	1.97	14.65					
821.4406	1.96	14.67					
821.4431	1.98	14.65					
821.4457	1.97	14.65					
821.4482	1.98	14.64					
821.4507	1.99	14.68					
821.4532	1.97	14.67					
821.4557	2.00	14.66					
821.4583	1.97	14.67					
821.4637	1.99	14.67					
821.4707	1.99	14.68					

Appendix B11.1Continued

1	2	3	4	5	6	7	8
821.4783	1.99	14.65					
821.4808	1.98	14.69	14.67	4.19	0.49	16.99	16.42
822.3990	1.99	14.66					
822.4005	1.98	14.65					
822.4041	1.96	14.66					
822.4066	1.98	14.62					
822.4091	1.99	14.66					
822.4116	1.98	14.66					
822.4141	1.97	14.64					
822.4190	2.00	14.65					
822.4215	1.98	14.68					
822.4241	1.97	14.69					
822.4266	1.99	14.64					
822.4291	1.98	14.66					
822.4316	2.00	14.64					
822.4367	1.98	14.64					
822.4415	1.99	14.64					
822.4441	1.97	14.68					
822.4491	1.99	14.64					
822.4516	1.97	14.69					
822.4541	1.97	14.68					
822.4562	1.99	14.69					
822.4592	1.97	14.65					
822.4641	1.99	14.63					
822.4691	1.99	14.61					
822.4742	1.97	14.63					
822.4767	1.99	14.63	14.65	4.27	0.57	16.83	16.25
824.3000	1.98	14.66					
824.3026	2.00	14.63					
824.3051	1.98	14.62					
824.3100	1.98	14.63					
824.3125	1.99	14.64					
824.3157	1.97	14.66					
824.3175	1.98	14.68					
824.3200	1.98	14.64					
824.3375	1.98	14.67					
824.3401	1.99	14.66					
824.3451	1.98	14.58	14.65	4.27	0.57	16.83	16.25
825.3930	1.99	14.61					
825.3955	1.99	14.65					
825.3981	1.99	14.62					

Appendix B11.1-Continued

1	2	3	4	5	6	7	8
825.4006	1.97	14.67					
825.4055	1.96	14.65					
825.4080	1.94	14.67					
825.4105	1.97	14.66					
825.4155	1.99	14.67					
825.4181	1.95	14.66					
825.4206	1.98	14.68					
825.4280	1.99	14.66					
825.4305	2.01	14.63					
825.4355	1.98	14.66					
825.4380	2.01	14.69					
825.4406	2.01	14.68					
825.4431	1.98	14.67					
825.4456	1.99	14.65					
825.4505	1.96	14.69					
825.4530	1.99	14.65					
825.4555	2.01	14.64					
825.4580	1.96	14.66					
825.4631	1.98	14.67					
825.4906	1.99	14.65					
825.5037	1.98	14.64	14.66	4.23	0.53	16.91	16.33
827.5513	1.98	14.70					
827.5538	1.96	14.68					
827.5563	1.97	14.67					
827.5589	1.98	14.69					
827.5688	1.97	14.70	14.69	4.11	0.41	17.19	16.61
830.3392	1.95	14.67					
830.3575	2.03	14.63					
830.3600	1.99	14.64					
830.3626	2.03	14.65					
830.3651	2.02	14.67					
830.3727	2.00	14.68	14.66	4.23	0.53	16.91	16.33
830.3554	1.97	14.67					
830.3579	1.99	14.64					
830.3604	1.99	14.67					
830.3629	1.98	14.69					
830.3655	1.98	14.64					
830.5075	1.97	14.65					
830.5126	1.99	14.66	14.66	4.23	0.53	16.91	16.33
1203.3530	2.00	14.65					
1203.3556	1.96	14.66					

Appendix B11.1Continued

1	2	3	4	5	6	7	8
1203.3581	1.98	14.62					
1203.3606	1.98	14.63					
1203.3655	1.98	14.67					
1203.3681	1.98	14.67					
1203.3706	1.96	14.65					
1203.3741	1.98	14.63					
1203.3780	1.99	14.64					
1203.3806	1.96	14.65					
1203.3841	1.99	14.66					
1203.3880	1.97	14.63					
1203.3905	1.98	14.64					
1203.3931	1.97	14.66					
1203.3956	1.99	14.66					
1203.4030	1.97	14.68					
1203.4056	1.99	14.66					
1203.4081	1.98	14.63					
1203.4106	1.98	14.64	14.65	4.27	0.57	16.83	16.25
1221.3255	1.98	14.62					
1221.3280	1.98	14.65					
1221.3306	2.00	14.60					
1221.3380	2.03	14.64					
1221.3405	2.00	14.65					
1221.3431	1.98	14.64					
1221.3456	1.98	14.65					
1221.3502	2.01	14.61					
1221.3530	1.92	14.62					
1221.3581	1.91	14.65					
1221.3630	1.96	14.63					
1221.3655	1.98	14.62					
1221.3680	1.97	14.61					
1221.3755	2.00	14.61					
1221.3780	1.95	14.63					
1221.3805	1.96	14.66					
1221.3830	1.98	14.64	14.63	4.35	0.65	16.69	16.11
1484.3141	2.00	14.63					
1484.3176	1.98	14.62	14.63	4.35	0.65	16.69	16.11
1488.4745	1.96	14.63					
1488.4771	2.00	14.66	14.65	4.27	0.57	16.83	16.25
1505.4886	1.98	14.65					
1505.4928	1.96	14.64	14.65	4.27	0.57	16.83	16.25
1519.3995	1.98	14.63					

Appendix B11.1-Continued

1	2	3	4	5	6	7	8
1515.4037	2.12	14.62	14.63	4.35	0.65	16.69	16.11
1524.3688	2.01	14.62					
1524.3763	1.98	14.64	14.63	4.35	0.65	16.69	16.11
1530.3846	1.98	14.63	14.63	4.35	0.65	16.69	16.11
1534.4522	1.94	14.64					
1534.4549	1.98	14.66	14.65	4.27	0.57	16.83	16.25
1553.3972	1.97	14.62	14.64	4.31	0.61	16.76	16.18
1554.4006	1.99	14.63					
1554.4123	2.00	14.67	14.65	4.27	0.57	16.83	16.25
1560.3934	1.96	14.70					
1560.3960	2.01	14.66	14.68	4.15	0.45	17.09	16.51
1584.2793	2.03	14.62	14.62	4.39	0.69	16.62	16.05
1592.4123	2.21	14.71					
1592.4164	2.18	14.69	14.70	4.08	0.38	17.27	16.69
1610.4118	2.01	14.63					
1610.4169	1.99	14.65	14.64	4.31	0.61	16.76	16.18
1730.5553	2.00	14.64					
1730.5628	1.97	14.62	14.63	4.35	0.65	16.69	16.11
1770.5177	1.98	14.66	14.66	4.23	0.53	16.91	16.33
1772.4606	1.98	14.67					
1772.4632	1.97	14.63	14.65	4.27	0.57	16.83	16.25
1780.3958	1.96	14.63					
1780.4210	1.94	14.65	14.64	4.31	0.61	16.76	16.18
1783.3960	1.98	14.60					
1873.4000	1.99	14.59	14.60	4.47	0.77	16.50	15.93
1788.4560	1.99	14.62					
1788.4605	2.00	14.66	14.64	4.31	0.61	16.76	16.18
1798.4676	2.00	14.68					
1798.4778	1.99	14.64	14.66	4.23	0.53	16.91	16.33
1800.4949	1.95	14.62	14.62	4.39	0.69	16.62	16.05
1816.4309	2.03	14.64					
1816.4435	2.02	14.65	14.65	4.27	0.57	16.83	16.25
1832.4952	1.98	14.65	14.65	4.27	0.57	16.83	16.25
1828.4846	2.26	14.66					
1828.4896	2.26	14.64	14.65	4.27	0.57	16.83	16.25
1832.4978	1.97	14.63	14.63	4.35	0.65	16.69	16.11
1859.5361	1.99	14.64					
1859.5418	1.98	14.60	14.62	4.39	0.69	16.62	16.05
1886.4331	1.98	14.63	14.63	4.35	0.65	16.69	16.11
1887.2744	1.95	14.61					
1887.2796	2.07	14.65	14.63	4.35	0.65	16.69	16.11

Appendix B11.1-Continued

1	2	3	4	5	6	7	8
1906.3185	2.01	14.61					
1906.3259	1.98	14.61	14.61	4.43	0.73	16.56	15.98
1909.5231	2.02	14.60					
1909.5256	2.00	14.58	14.59	4.51	0.81	16.45	15.87
1918.4722	1.99	14.62					
1918.4752	1.99	14.62	14.62	4.39	0.69	16.62	16.05
1920.4428	2.01	14.63	14.63	4.35	0.65	16.69	16.11
1934.4102	2.01	14.61					
1934.4149	2.01	14.60	14.61	4.43	0.73	16.56	15.98
1968.3220	2.07	14.62					
1968.3259	1.96	14.58	14.60	4.47	0.77	16.50	15.93
2043.1981	2.15	14.57					
2043.2032	2.17	14.59	14.58	4.55	0.85	16.40	15.82
2122.5424	1.97	14.51	14.51	4.85	1.15	16.07	15.49
2137.5250	2.01	14.56	14.56	4.63	0.93	16.30	15.72
2198.4680	1.96	14.61					
2198.4706	1.98	14.58	14.60	4.47	0.77	16.50	15.93
2214.4550	1.97	14.59	14.59	4.51	0.81	16.45	15.87
2215.5096	2.03	14.53					
2215.5136	1.96	14.56	14.55	4.67	0.97	16.25	15.68
2237.3481	1.97	14.59					
2237.3524	1.99	14.58	14.59	4.51	0.81	16.45	15.87
2241.3903	2.01	14.56					
2241.3947	1.99	14.60	14.58	4.55	0.85	16.40	15.82
2263.3307	1.97	14.60					
2263.3348	1.99	14.61	14.61	4.43	0.73	16.56	15.98
2267.5235	1.99	14.55					
2267.5275	1.99	14.55	14.55	4.67	0.97	16.25	15.68
2270.5150	2.09	14.62					
2270.5215	2.10	14.62	14.56	4.63	0.93	16.30	15.72
2274.5707	1.97	14.50	14.54	4.76	1.06	16.16	15.58
2289.5711	2.08	14.56	14.53	4.81	1.11	16.11	15.53
2316.3799	1.90	14.52					
2316.3838	1.94	14.53	14.53	4.81	1.11	16.11	15.53
2323.2890	1.96	14.59					
2323.2926	1.96	14.60					
2323.2890	1.94	14.59					
2323.2924	1.96	14.60	14.60	4.47	0.77	16.50	15.93
2346.3745	1.97	14.58					
2346.2542	2.00	14.57					
2346.2582	1.99	14.56	14.58	4.43	0.73	16.56	15.98

Appendix B11.1-Continued

1	2	3	4	5	6	7	8
2357.3110	2.00	14.60					
2357.3180	1.99	14.61	14.61	4.47	0.77	16.50	15.93
2380.1615	1.98						
2380.1656	1.97	14.60	14.60	4.47	0.77	16.50	15.93
2384.2352	1.97	14.60	14.60	4.47	0.77	16.50	15.93
2385.2825	1.96	14.56					
2385.2855	1.97	14.59	16.59	4.31	0.61	16.76	16.18
2521.4487	1.99	14.64	14.64				
2521.4519	1.96	14.65					
2521.4551	1.97	14.65	14.65	4.27	0.57	16.83	16.25
2529.4895	1.96	14.62					
2529.4951	1.96	14.61	14.62	4.39	0.69	16.62	16.05
2559.3841	1.97	14.62					
2559.3881	1.96	14.62	14.62	4.39	0.69	16.62	16.05
2588.4754	1.81	14.63					
2588.4794	1.78	14.64	14.64	4.31	0.61	16.76	16.18
2591.4564	1.97	14.58					
2591.4628	1.96	14.61	14.60	4.47	0.77	16.50	15.93
2598.5466	2.01	14.60					
2598.5507	2.00	14.63					
2598.5589	1.95	14.61	14.61	4.43	0.73	16.56	15.98
2621.4700	1.98	14.62					
2621.4740	2.05	14.65					
2621.4780	1.96	14.62					
2621.4820	1.96	14.62	14.63	4.35	0.65	16.69	16.11
2637.2636	1.91	14.61	14.61				
2637.2676	1.95	14.61	14.61	4.43	0.73	16.56	15.98
2641.3228	1.97	14.62					
2641.3267	2.02	14.58		4.43	0.73	16.56	15.98
2641.3307	2.01	14.59					
2641.3346	1.95	14.63	14.61	4.43	0.73	16.56	15.98
2645.5296	1.97	14.61					
26455334	1.97	14.63	14.62	4.39	0.69	16.62	16.05
2653.3859	2.05	14.62					
2653.3898	1.89	14.57					
2653.4020	1.95	14.61					
2653.4161	2.01	14.62	14.60	4.47	0.77	16.50	15.93
2656.4990	1.97	14.62					
2656.4976	1.96	14.58					
2656.5001	2.00	14.63					
2656.5055	1.95	14.61					

Appendix B11.1-Continued

1	2	3	4	5	6	7	8
2656.5080	1.99	14.59					
2656.5106	1.97	14.62					
2656.5131	1.98	14.59	14.60	4.47	0.77	16.50	15.93
2666.4353	1.99	14.62					
2666.4449	1.98	14.60					
2666.4528	1.98	14.63					
2666.4604	1.99	14.63					
2666.4718	2.00	14.61					
2666.4743	2.01	14.61	14.61	4.43	0.73	16.56	15.98
2678.2781	2.07	14.65					
2678.2820	2.06	14.62	14.64	4.31	0.61	16.76	16.18
2688.2045	2.00	14.59					
2688.2085	1.98	14.63					
2688.2124	1.99	14.63	14.62	4.39	0.69	16.62	16.05
2693.1828	2.02	14.58					
2693.1854	2.00	14.55					
2693.1879	1.94	14.58					
2693.1903	2.04	14.55	14.57	4.59	0.89	16.35	15.77
2699.2633	2.16	14.58					
2699.2668	2.18	14.58	14.58	4.55	0.85	16.40	15.82
2711.3611	1.99	14.61					
2711.3650	1.98	14.61					
2711.3690	1.97	14.58	14.60	4.47	0.77	16.50	15.93
2732.1791	1.97	14.60					
2732.1823	1.99	14.60	14.60	4.47	0.77	16.50	15.93
2734.2447	2.02	14.65					
2734.2486	1.99	14.61	14.63	4.35	0.65	16.69	16.11
2748.2560	1.95	14.57					
2748.2591	1.96	14.57					
2748.2616	1.96	14.58	14.57	4.59	0.89	16.35	15.77
2754.2660	2.14	14.59					
2748.2695	2.15	14.61	14.60	4.47	0.77	16.50	15.93
2875.5160	1.94	14.60					
2875.9280	1.91	14.61					
2875.5225	1.94	14.57	14.59	4.51	0.81	16.45	15.87
2878.4904	1.97	14.59					
2878.5022	1.99	14.61	14.60	4.47	0.77	16.50	15.93
2881.5064	1.95	14.58					
2881.5103	1.94	14.60	14.59	4.51	0.81	16.45	15.87
2886.4911	2.02	14.57					
2886.4944	1.96	14.60					

Appendix B11.1-Continued

1	2	3	4	5	6	7	8
2886.4976	1.98	14.59	14.59	4.51	0.81	16.45	15.87
2909.4663	1.98	14.62					
2909.4702	1.97	14.61					
2909.4741	1.96	14.62	14.62	4.39	0.69	16.62	16.05
3034.3245	1.95	14.50					
3034.3266	1.97	14.49					
3034.3288	1.96	14.53					
3034.3309	1.96	14.49	14.50	4.9	1.2	16.02	15.45
3061.2839	1.97	15.61					
3061.2898	1.97	14.62					
3061.2933	1.99	14.61					
3061.2867	1.95	14.61	14.61	4.43	0.73	16.56	15.98
3062.3195	1.96	14.61					
3062.3230	1.96	14.62					
3062.3265	1.96	14.60					
3062.3300	1.94	14.62	14.61	4.43	0.73	16.56	15.98
3063.3463	1.99	14.58					
3063.3298	1.97	14.59					
3063.3332	1.95	14.57					
3063.3367	1.95	14.59	14.58	4.55	0.85	16.40	15.82
3066.3885	1.98	14.61					
3066.3906	1.98	14.60					
3066.3927	1.98	14.62					
3066.3948	1.99	14.62	14.61	4.43	0.73	16.56	15.98
3081.3690	1.95	14.56					
3081.3711	1.98	14.57					
3081.3732	1.98	14.55					
3081.3753	1.97	14.58	14.57	4.59	0.89	16.35	15.77
3082.3935	2.00	14.60					
3082.3956	1.95	14.61					
3082.3976	1.95	14.59					
3082.3987	1.95	14.60	14.60	4.47	0.77	16.50	15.93
3088.3320	1.97	14.52					
3088.3355	1.97	14.56					
3088.3390	1.98	14.54					
3088.3425	1.94	14.53	14.54	4.76	1.06	16.16	15.58
3110.3095	1.97	14.55					
3110.3138	1.96	14.53					
3110.3159	1.94	14.54	14.55	4.67	0.97	16.25	15.68
3303.4612	1.76	14.62					
3303.4637	1.74	14.62	14.62	4.39	0.69	16.62	16.05

Appendix B11.1-Continued

1	2	3	4	5	6	7	8
3324.5180	1.65	14.66					
3324.5215	1.63	14.66	14.66	4.23	0.53	16.91	16.33
3329.3431	1.60	14.62					
3329.3501	1.60	14.61	14.62	4.39	0.69	16.62	16.05
3332.5570	1.88	14.58					
3332.5627	1.76	14.60	14.59	4.51	0.81	16.45	15.87
3334.5774	2.04	14.59					
3334.5830	2.00	14.60	14.60	4.47	0.77	16.50	15.93
3346.5758	1.66	14.63					
3346.5866	1.66	14.62	14.63	4.35	0.65	16.69	16.11
3351.6025	1.76	14.61					
3351.6095	1.77	14.62	14.62	4.39	0.69	16.62	16.05
3356.6028	1.70	14.64					
3356.6063	1.71	14.64	14.64	4.31	0.61	16.76	16.18
3364.3439	1.46	14.60					
3364.3544	1.39	14.58	14.60	4.51	0.81	16.45	15.87
3367.5351	1.86	14.62					
3367.5487	1.90	14.61					
3367.5556	1.90	14.61	14.61	4.43	0.73	16.56	15.98
3374.4142	1.82	14.62	14.62	4.39	0.69	16.62	16.05
3376.5012	1.88	14.60					
3376.5033	1.85	14.59					
3376.5055	1.83	14.59	14.59	4.51	0.81	16.45	15.87
3378.5404	1.62	14.61					
3378.5512	1.62	14.62	14.62	4.39	0.69	16.62	16.05
3381.5294	1.75	14.63					
3381.5329	1.76	14.64	14.64	4.31	0.61	16.76	16.18
3383.3014	1.53	14.61					
3383.3112	1.49	14.61	14.61	4.43	0.73	16.56	15.98
3387.3906	1.78	14.59					
3387.3976	1.77	14.61	14.60	4.47	0.77	16.50	15.93
3392.4745	1.80	14.58					
3392.4850	1.76	14.59	14.59	4.51	0.81	16.45	15.87
3415.3289	1.89	14.62					
3415.3304	1.87	14.65					
3415.3374	1.84	14.63	14.63	4.35	0.65	16.69	16.11
3418.2421	1.91	14.62					
3418.2456	1.89	14.64	14.63	4.35	0.65	16.69	16.11

B11.2 Color Indices of 1ES 2344+514

JD-2451000 (1)	<i>V</i> (2)	<i>V-R</i> (3)	Error (4)
21.44	15.23	0.62	0.05
40.39	15.21	0.61	0.05
56.48	15.23	0.64	0.05
68.49	15.25	0.62	0.05
71.45	15.27	0.61	0.05
73.44	15.27	0.62	0.05
76.44	15.26	0.58	0.05
84.41	15.27	0.64	0.05
86.41	15.22	0.66	0.05
117.42	15.27	0.61	0.05
130.41	15.29	0.65	0.05
138.21	15.31	0.66	0.05
376.52	15.18	0.65	0.05
399.46	15.28	0.66	0.05
402.48	15.31	0.67	0.05
407.51	15.26	0.65	0.05
410.44	15.30	0.66	0.05
412.42	15.24	0.60	0.05
438.50	15.29	0.65	0.05
440.49	15.24	0.66	0.05
457.47	15.27	0.64	0.05
458.56	15.31	0.63	0.05
489.52	15.35	0.64	0.05
496.48	15.28	0.61	0.05
521.39	15.22	0.59	0.05
523.37	15.31	0.63	0.05
723.46	15.28	0.61	0.05